CITY UNIVERSITY LONDON

EST 1894

Femtosecond Lasers in Corneal and Refractive Surgery

A thesis submitted by

Jodhbir Singh Mehta

For the Degree of

Doctor of Philosophy - by Prior Publication

September 2017

Centre for Applied Vision Research
School of Health Sciences
City, University of London

Femtosecond Lasers in Corneal and Refractive Surgery

Submitted

Supervised by:

Chris C Hull
Professor of Optics and Vision
Associate Dean for Research and Enterprise
School of Health Sciences
City, University of London

Members of the Examination Committee:

TABLE OF CONTENTS

CHAPTERS

LIST OF TABLES

LIST OF FIGURES

the periphery in and from the periphery in. Pattern D: Laser was fired from the centre out and from the periphery in. B: The corneas under the suction cone during the creation of posterior and anterior surfaces of the refractive lenticule. 120

Figure 4.2 Illustrations of intrastromal incision permitted by VisuMax Circle option (Carl Zeiss Medited, Jena, Germany). A. The circle option permits the creation of three basic components; a side cut with hinge, a lamellar ring and a junction cut. B. Cross-sectional view showing the adjustable femtosecond laser parameters to create the intrastromal incision. C. Front view showing the user-selectable parameters to create the intrastromal incision. OD= Outer diameter, JD= Junction diameter, SD= Side cut depth, SA= Side cut angle, HA= Hinge angle, JU = Junction upper depth, JL= Junction lower depth. 132

Figure 4.3 Illustrations of the tested VisuMax Circle patterns (Carl Zeiss Meditec, Jena, Germany) and the incision parameters selected for respective pattern. Pattern A creates a side cut within the cap cut (CC; in blue). Pattern B creates a lamellar ring posterior to the cap cut. Pattern C creates a lamellar ring anterior to the cap cut. Pattern D creates a lamellar ring adjacent to the cap cut. The parametric settings of the patterns tested in the current study can be found in Table 4.2. (OD = outer diameter; JD = junction diameter; SD = side cut depth; SA = side cut angle; HA = hinge angle; JU = junction upper depth; JL = junction lower depth). 134

Figure 4.4 The corneal stroma treated with different laser firing patterns during refractive lenticule extraction. A: Top panel shows the stromal layer directly anterior to the lenticule's anterior surface. The stromal layer at the keratotomy site of the lenticule's anterior plane is shown in the middle panel and the lenticule's posterior plane is shown in the bottom panel (in vivo confocal micrographs). B: Relative reflectivity level of the

circumference than the flap side cut. Prelenticule extraction where the lenticule was still intact exhibits circular perforations and tissue bridges along the lenticule side cut, which could be due to the effect of cavitation bubbles created from FS photodisruption. Lenticule side cut of the post lenticule extraction stromal bed shows a ridge indicating the platform where lenticule had been removed. 174

Figure 4.20. Visualization of the incision created by VisuMax Circle patterns (Carl Zeiss Meditec, Jena, Germany). Images were obtained after the incision and before flap lifting, using anterior segment optical coherence tomography (AS-OCT). Lamellar ring (a'rrowheads) was characterized by light reflective layer, indicative of femtosecond laser disrupted lamellae. The original refractive lenticule extraction small incision lenticule extraction (SMILE) cap cuts were not visible on AS-OCT by day 28 after SMILE. The presumed cap cut was marked in blue. (A) Pattern A created a side cut within the cap cut. (B) Pattern B created a lamellar ring at a measured depth of 127 microns, placing it posterior to the cap cut. (C) Pattern C created a lamellar ring at a depth of 115 microns,, placing it anterior to the cap cut. (D) Pattern D created a lamellar ring adjacent to the cap cut, which depth was measured at 124microns. Arrows indicate the side cut created by patterns A, B, C, and D. In vivo confocal micrographs of the intrastromal cuts appeared similar in all treatment groups. (E) The appearance of side cut at the depth of 34 microns from the superficial epithelium. (F) The junction between side cut and the lamellar ring at the depth of 114microns. The femtosecond laser disrupted layer of lamellar ring is discernible by its light reflective layer. (G) The junction between the junction cut and the lamellar ring. (H) The junction between the cap cut (blue in illustration) and the junction cut. 176

Figure 4.21. Transmission electron micrographs (TEM) of stromal lenticule showing keratocytes. A, C: Fresh lenticule. B, D: Cryopreserved lenticule. A, B: Apoptotic

illumination photographs (bottom panel) of the cornea before ReLEx and on week 8 and 16 after ReLEx and refractive lenticule re-implantation. (B) Temporal AS-OCT images of postoperative corneas shows thinning of the cornea after ReLEx and restoration of corneal thickness after lenticule re-implantation. (C) Mean corneal thickness before ReLEx and 8 and 16 weeks after ReLEx and lenticule re-implantation. (D) Post-reimplantation corneal haze graded based on observation of the slit lamp photographs found in Figure S3. Corneal clarity or haze was graded on a scale of 0–4 (from 0 being completely clear to 4 being completely obscured). Statistical significance was obtained by comparing post-operative to pre-operative corneal clarity. Error bars in the bar graphs represent standard deviation. PR: post-ReLEx, PLR: post-lenticule re-implantation. 195

Figure 4.34 In vivo confocal micrographs of pre- and post-operative corneas. (A) Horizontal surgical plane between the flap and stromal bed on week 8 and 16 after ReLEx. This region is normally indicated by a relatively higher light reflective layer. Keratocyte repopulation could be observed on week 8 and 16. (B) The top panel shows the anterior interface of the re-implanted lenticule. The middle panel shows the presence of keratocytes within the lamellae of the lenticule and the bottom panel shows the posterior interface of the lenticule. Keratocyte repopulation of anterior and posterior borders of the lenticule occurred by week 8 after lenticule re-implantation. (C) Mean reflectivity level of the laser incision site on day 3, and 2, 4, 8 and 16 weeks after ReLEx. The representative in vivo confocal images of the cornea at the stated time point can be found in Figure S4A. (D) Mean reflectivity level of the re-implanted lenticule's anterior interface on day 3, and 2, 4, 8 and 16 weeks. (E) Mean reflectivity level of the lenticule's posterior interface post-reimplantation. The representative in vivo confocal images of the cornea at the stated time point in panes D and E can be found in Figure

Figure 4.37 Expression of a-smooth muscle actin (a-SMA) in the post-operative central corneas and peripheral flaps. (A–D) a-SMA (green), a marker of myofibroblasts, was not present in the central corneas on week 8 and 16 after both ReLEx and refractive lenticule re-implantation. (E–H) a-SMA (green) was expressed at the flap periphery and co-localized with F-actin (red) subepithelially on week 8 post-ReLEx and lenticule reimplantation, but was absent 16 weeks after both surgical procedures. In pane A–H, a-SMA (green) was double immunostained with F-actin marker (red), phalloidin. Nuclei were counterstained using DAPI (blue). Arrowheads indicate the location of the laser incision site or lenticular interface. PR: post-ReLEx, PLR: post-lenticule reimplantation. Scale bar: 50 mm. 203

ACKNOWLEDGEMENT

There are many people, to acknowledge for the development of this work. First I would like to thank Mr M Sharr, my first consultant and with whom I wrote my first 5 papers. He started my interest in research. I would also like to acknowledge all the consultants I had the chance to work under during my 7 years at Moorfields Eye Hospital. They taught me the value of research and also gave me many opportunities to conduct research in several subspecialties. I would also like to thank Prof D Tan and Prof R Beuerman, who helped co-ordinate my fellowship to bring me to Singapore, where I gained a wide experience in both laboratory and clinical work. I was one of the PI's of the initial Translational Clinical Research (TCR) grant that was awarded to SNEC and SERI in 2008. This enabled me to develop my interest in femtosecond lasers which forms the bases of this work. I have had the opportunity to develop and lead a fantastic Tissue Engineering and Stem Cell group, members of which have contributed to the development of this thesis. I would also like to thank the support of Prof C Hull for taking me on under his supervision, to complete this project, and for his patience and support throughout this endeavour. Last but not least I dedicate this work to my deceased parents. My dad for his influence about the importance of education, and my mother for her support in all endeavours of my life and the belief that anything is possible if you try your best.

DECLARATION

I grant the power of discretion to the University Librarian to allow this thesis to be copied in whole or in part without further reference to me. This permission covers only single copies made for study purposes, subject to normal conditions of acknowledgment.

ABSTRACT

Femtosecond lasers were introduced in ophthalmology initially for flap creation for LASIK. This thesis describes a body of work undertaken by the author exploring the possibility of using these lasers in corneal and refractive surgery. The use of the femtosecond laser in corneal and refractive surgery offered the prospect of better precision with respect to their accuracy in depth cut, and the smoothest of lamellar interface. The development of multiple laser platforms allowed us to perform comparative studies in both ex vivo/animal and clinical studies and to explore the prospect of a new refractive procedure, lenticule extraction and also lenticule re-implantation. The laser proved to be accurate in its vertical depth cutting and following optimization was able to cut a smoothe lamellar interface. The clinical study showed the laser to be safe and effective. The comparative studies showed the superiority of the lower energy femtosecond laser on IOP rise, without compromising on clinical outcomes, which were the same for both lasers. Femtosecond laser lenticule creation was optimised in animal models and then shown to be safe and efficacious in a clinical study. The wound healing benefits of an ‘all in one’ femtosecond laser procedure were evident, in both animal as well clinical studies. Lenticule reimplantation was shown to be effective in both the rabbit and monkey models. The use of the femtosecond laser is set to increase in ophthalmology. The work in this thesis has provided fundmental ex vivo, animal and clinical benefits on the the use of femtosecond lasers in corneal and refractive surgery. It has also envisioned a concept of lenticule re-implantation for future clinical use.

CHAPTER 1

1.0 INTRODUCTION

Lasers are used widely in medicine, and none more so than ophthalmology. They are used for multiple purposes from refractive to retinal surgery. Over the last decade there has been a significant increase in the use of femtosecond lasers specifically. In order to understand the benefits and limitations of these devices it is important to obtain a fundamental understanding of the lasers themselves and how they interact with biological tissue.

1.1 BACKGROUND

Femto-chemistry is the study of biological changes at a fundamental time scale of molecular vibrations: the actual nuclear motions (1). Time resolution chemistry/biology has evolved over the last 150 years. In the last century it was known that electric sparks could have a response time as short as 10 nanoseconds. Eigen developed a method of disturbing the equilibrium of a solution by either a rapid change in temperature, pressure or an electric field (2). Following the disturbance, the system returned to a steady state and the kinetics could be followed during this equilibration. In his Nobel lecture, Eigen described the changes as ‘immeasurably fast.’

The first ruby laser, was demonstrated in 1960, and soon after that, giant and short pulsed lasers were developed. Different pulse energies were obtained by modulating the laser

with techniques such as Q-switching to generate nanosecond pulses and mode-locking to obtain picosecond pulses. In the 1970's dye lasers were developed that could produce sub-picosecond pulses (3) and in 1991, following the discovery of self-mode locking, femtosecond pulse generation was demonstrated in a solid-state Ti:sapphire laser (4) rapidly replacing many of the dye lasers. The early femtosecond lasers typically had pulse characteristics of 750-850nm wavelength, 50fs pulse width, 0.7 mJ energy and 1kHz repetition rate. Improvements in the laser system improved the pulse characteristics to a pulse width of 120fs, 3 mJ energy and 1kHz repetition rate. The laser pulses themselves, in the newer lasers were generated by an all solid state (no gas) oscillation system.

1.2 LASER-TISSUE INTERACTIONS

Lasers have a long history of use in ophthalmology especially for the cornea. Excimer lasers, operating at 193nm, have received the most attention, (5-8) but the use of pulsed infrared lasers, (9,10) has also been investigated. The advantage of both these lasers is that they can produce corneal excisions of high quality with little damage to adjacent tissues. This is because the energy can be absorbed by a small volume, hence little energy would reach the surrounding tissue. Visible and near-infrared lasers can also be used for corneal ablation provided the beam is focused to produce a high enough irradiance (and the tissue is transparent). When the fluence (energy/area) of the laser focus reaches the threshold required, the tissue is photo-ionized in a process that produces laser-induced plasma formation (5). The plasma is a 'soup' of free electrons and ions (11). Plasma-induced photoablation takes place when light is focused to power densities in the range of 10^{11}-10^{12} W/cm^2 (12). Pulsed lasers attain high power density by concentrating light

energy into a short duration (11). At these intensities transparent material will be ionized by multiphoton absorption (13).

Plasma generation with nanosecond or longer pulses is accompanied by photodisruption, which can cause shock waves, bubble jetting and cavitation bubbles that cause unwanted damage. With the use of picosecond and femtosecond laser pulses, it is possible to reduce and therefore control the extent of these photodisruptive effects. (14). One advantage of plasma-induced photoablation is that the thermal damage is minimal, hence it is possible to ablate transparent tissue and to cut close to tissue that must not be damaged. This is because the high absorption of the plasma has a shielding effect. Plasma shielding, where free electrons can absorb any wavelength and convert it into kinetic energy, can be used advantageously in certain situations, for example, to prevent potentially damaging light from reaching the retina during capsulotomy (14). As the plasma expands, a pressure wave is produced. The magnitude of the wave depends on the pressure and temperature in the plasma which is related to the energy density; the shock wave will be of greater amplitude for longer pulses where more energy is applied. Cavitation is a vapour bubble which forms around the plasma; the cavitation bubble will grow to a critical size and then collapse, sending out another shock wave. This is accompanied by a rapid increase in temperature and pressure, the size of which are determined by the focal spot size (15). If the cavitation is close to a solid surface it can form a jet of ejecting plasma as it collapses.

1.3 FEMTOSECOND LASERS - INTERACTION WITH THE CORNEA

In a comparative study of nanosecond, picosecond and femtosecond laser photodisruption of the cornea, the picosecond (ps) and femtosecond (fs) laser pulses were

shown to be ultra-structurally superior to those of the nanosecond (ns) laser (5). The pulses were generated by mode locked ring dye lasers to produce femtosecond (100 and 65fs), picosecond (30ps) and nanosecond (8ns) pulses (5).

The energy to produce photodisruption varied with pulse duration: for the nanosecond pulses the threshold for disruption was 500 μJ, and the ablation depth per pulse was 1 μm; with the picosecond pulses the threshold energy for disruption was 50 μJ, and this was reduced further with a decrease in pulse duration to 10 μJ at 1ps and 2.5 μJ at 100fs; with a 65fs pulse duration the disruption threshold was 0.8 μJ with an absorption length per pulse of <0.001 μm. The threshold energy for disruption varied approximately as the square root of the pulse duration and the efficiency of the lasers was superior for shorter pulses than longer ones. The Nd:YLF laser produced pulses in the 30 to 60 picosecond range and hence caused less collateral damage than conventional Nd:YAG lasers. They were the first lasers to be used for intra-stromal photo-disruption (16) and by using a scanning laser at a high repetition rate, adjacent photo-disruptions were able to create a near-contiguous cut. Despite optimization of the laser delivery, pulse energy, spot size and spot separation, clinical utility was limited by the inability to produce fully contiguous intrastromal photo-disruption (17,18).

The advantage of using a femtosecond laser pulse lies in the ability to control the photodisruption effect. It is interesting to note that femtosecond lasers in corneal tissue caused shock-wave damage that was not seen with the picosecond laser (5). The first step in the process is the formation of a plasma. The size of the plasma is largely dependent on the focal spot diameter of the delivery system. It is ideally created from the smallest spot diameter possible, since this requires the lowest energy to exceed the intensity

threshold for plasma generation. Procedure time and mechanical limitations impose constraints on how small the spot size can be and how fast it can be scanned. At a fixed spot size (e.g. 5-10 μm), the predictive final cavitation bubble size is approximately 12 microns. For picosecond lasers this value was 25 microns (14). The smaller cavitation bubble size allowed the closer (contiguous) placement of femtosecond pluses and also improved the predictability of the plasma threshold (19). Hence reducing the focal spot size and the pulse duration reduces the energy required for laser induced optical breakdown. However, spot size diameter will be limited by the focusing optics of the laser, laser wavelength and propagation effects.

The plasma created in this way initially expands with hypersonic velocity as a result of plasma pressure and temperature (14). A shock-wave is emitted when the plasma expansion decreases to subsonic velocity (20). Further expansion of the plasma results in the creation of a cavitation bubble (21, 22). This is followed by implosion of the bubble which may create secondary radially propagating acoustic waves (23). The collateral damage caused by the shock waves and cavitation bubble is dependent on the energy of the lasers used. In a study examining the effect of shock wave emission and cavitation bubble formation following femtosecond photo-disruption in bovine cornea and water, Juhasz et al. (23) noted a rapid decay of shock waves in both materials. The threshold fluences in the cornea and water were 1.3 J/cm^2 and 0.87 J/cm^2 respectively. The threshold fluence in the stroma was only slightly higher than that measured on the corneal surface (24). The shock wave dynamics in water and bovine cornea (albeit at different fluences of 9 J/cm^2 and 15 J/cm^2), were similar. As the shock wave propagated through the media there was a loss of energy and eventually it decayed to a harmless acoustic wave that propagated with the velocity of sound (14). The pressure at the closest observable point to the optical breakdown was approximately 8 x 10^8 Pa (8Kbar). This dissipated to near

zero within a radius of approximately 20 μm from the optical breakdown. The cavitation bubbles reached their maximum size within 650ns in corneal tissue and 2.7μs in water. The maximum bubble radius was 23 μm in the cornea and approximately 27μm in water. In the cornea a small bubble remains in the tissue for approximately 5μs, requiring 15-30 seconds for full disappearance. Since the bubble consists mainly of CO_2, N_2 and H_2O, these are all diffusible through normal mechanisms.

The decay of a shockwave was faster with femtosecond optical breakdown compared with picosecond. The shockwave radius decreased exponentially with increasing shock wave velocity with smaller radii formed at higher velocities. The shock wave radius reached a minimum at 15 microns and 1500m/s velocity (25). Likewise shock wave radius decreases exponentially with increasing shock wave pressure with smaller radii associated with higher pressure. The shock wave radius reaches a minimum of 20 microns for a shock wave pressure of 0.5 $x10^8$ Pa (25). The volume of tissue affected by the shock wave can be calculated from the volume of a sphere with a radius equal to the range of the shock wave. The results indicate that the volume of tissue affected by the shockwave is 1000 times less with a femtosecond than a picosecond laser (14). Likewise the size of the cavitation bubbles was also reduced from approximately 14μm with a femtosecond laser compared to 80 μm diameter with picosecond lasers after 1ms (25).

The control of the formation of cavitation bubbles is important if isolated intra-stromal ablation is required (11). If the cavitation bubble generated by the subsequent laser pulse coincides with the preceding cavitation bubble, it can produce unwanted effects. Specifically, if the impact of the pulse occurs inside an existing cavitation bubble it does not remove tissue but increases the size of the original cavitation bubble through

heat transfer to the gas in the bubble (14). To avoid this reheating of gas, the next pulse must impact the tissue outside the cavitation bubble. In an optimal scenario the ratio of the cavitation diameter at the moment of arrival of the next pulse (D_c) and the pulse diameter (D_p) should approach unity so that successive cavitation bubbles are contiguous without causing this unwanted side effect.

1.4 Ex Vivo Models and Early Clinical Use

The advances in ultrafast laser design and the development of powerful laser diodes has made low cost reliable diode-pumped femtosecond laser systems possible (26). In combination with scanning delivery patterns this allowed the development of a number of potential laser corneal procedures e.g. flap cutting, laser keratomileusis, implant placement and intrastromal keratectomy (11).

Interestingly there were significant differences noted in the behaviour of laser interactions with porcine and human tissue (17, 18). This is an important consideration when performing ex vivo work with potential translational applications. In a study examining the effect of intrastromal femtosecond ablation in rabbit eyes, the safety of the procedure was established by the return of corneal transparency by 3 days, no inflammation noted on slit lamp examination and greater stability of refractive change compared to excimer laser (27). The accuracy of the pulse with respect to collateral damage was estimated to be 1 μm or below in porcine eyes (12). Hence using pulse energies of 1-2 μJ Lubatschowski et al were able to prepare corneal flaps and lenticules (12). Further refinement of the pulse energy and of the scanning profiles culminated in the first patients undergoing femtosecond laser flap creation with the IntraLase 600c in

2001 (13). There were no significant complications in the clinical series and the ability to customize the flap creation with respect to thickness of flap, diameter and hinge location/angle and side cut architecture was evident. This initial report on amblyopic and partially sighted eyes with a prototype machine was followed up, following FDA clearance, with a series of 208 procedures at two US clinical sites in patients undergoing routine LASIK (28). The laser used was the IntraLase Pulsion FS Beta Series laser and no postoperative complications were noted in any treated eye, although 4 eyes experienced suction loss during the procedure.

Early experience with the IntraLase Femtosecond laser showed distinct differences in the wound healing response compared to conventional microkeratome flap creation (29). Even though clinical outcomes were good (30, 31), greater postoperative inflammation was often observed clinically (32) and with immunohistochemistry (33), especially at the flap edge and in the central interface. Previous studies had shown that stromal cell death after femtosecond laser flap creation was mediated by necrosis even though it was detected by TUNEL (33). This was shown in a rabbit study looking at wound healing responses, at three different energy levels for lamellar cuts (2.7 μJ,1.6 μJ and 0.5 μJ), using a 60kHz IntraLase laser. There was significantly more apoptosis (TUNEL-positive cells) in the high energy group compared to intermediate and low energy groups (29). The authors also noted greater corneal inflammatory cell infiltration with higher energy femtosecond laser energy levels.

1.5 AIMS OF THESIS

The aim of this thesis is to draw together the work reported in 17 papers on the application of femtosecond lasers to refractive and corneal surgery. With the introduction of femtosecond lasers clinically for the creation of flaps with LASIK in 2003, several companies started investigating this technology. In 2006 there were two commercially available femtosecond lasers: the 60kHz IntraLase and the 10/40kHz Femtec (20/10 Prefect Vision, Heidelberg, Germany). The technology offered much promise not only for refractive surgery but also corneal surgery. My first project was to assess the use of femtosecond lasers in corneal surgery. In order to assess the efficacy of the laser we initially performed ex vivo studies on human cornea-scleral rims to assess the accuracy of depth of cutting and smoothness of the lamellar interface. Following our initial ex vivo studies we performed a prospective clinical interventional case series with the Femtec laser. The studies pertaining to this topic are described in chapter 2.

In 2007 we purchased the IntraLase for clinical use and in 2008 we purchased the VisuMax both for clinical and research studies. The opportunity of having two different commercially available femtosecond lasers put us in the unique position of performing some interesting clinical and research comparative studies. The studies pertaining to these comparative studies are in chapter 3.

In 2009 we were one of the first centres to have the software for refractive lenticule extraction. This allowed us to perform both clinical and translational research projects. The studies pertaining to this are detailed in chapter 4.

CHAPTER 2

2.0 STUDIES ON THE USE OF FEMTOSECOND LASERS FOR CORNEAL SURGERY

2.1 INTRODUCTION

Femtosecond lasers were originally introduced to create corneal flaps for LASIK. In order to increase their range of use, optimization of the lasers was required for corneal surgery. In this chapter, the aim of the group of papers that form the basis of the work (Appendix A), was to perform a series of experiments to optimise the laser for use in corneal transplantation surgery. Corneal transplantation has undergone many advancements in the last decade, hence the introduction of a laser could potentially improve the accuracy in performing anterior lamellar surgery, as well as improve the consistency in obtaining thin tissue for endothelial keratoplasty.

2.2 METHODS

2.2.1 FEMTOSECOND LASER NOMOGRAM SELECTION

A 40-kHz femtosecond laser (FEMTEC; 20/10 Perfect Vision, Heidelberg, Germany) was used to achieve the resection of the posterior stromal tissue. With no known standardized software nomograms for deep stromal ablation, we started with the standard ablation parameters recommended for superficial LASIK flaps; energy of 2.8 μJ, line separation of 5 μm, and spot separation of 8 μm. The angle of the vertical rim cuts was set at 90° to the Descemet membrane. The laser was programmed to create an expected posterior lamellar dissection at 150 μm from the Descemet membrane,

measured from the central corneal surface with ultrasonic pachymetry.

2.2.2 Donor Tissue Mount for Femtosecond Laser Ablation

Human donor corneoscleral buttons (n = 70) unsuitable for clinical transplantation were procured from the Singapore Eye Bank and stored in Optisol-GS solution. The mean death-to-experimentation time of the corneas was 3.14 ± 0.86 days (range, 2–4 days). The corneas were mounted onto an artificial anterior chamber (AAC; Coronet Network Medical Products, UK) and with Viscoat (Alcon, Ft. Worth, TX) instilled over the endothelial surface before placement of the corneoscleral rims. Other artificial chambers (eg, Moria Hanna Trephine System; Moria, Antony, France
and the Barron Artificial Chamber; Katena, Denville, NJ) were also suitable. An infusion bottle using a 3-way tap was attached to the AAC, and bottle height was raised to maintain a pressure of 60–65 mm Hg, confirmed by a Barraquer tonometer.
The epithelium was mechanically removed, and the central corneal thickness (CCT), determined by ultrasound pachymetry with measurements repeated three times (CorneoGage Plus; Sonogage, Cleveland, OH).

2.2.3 Deep Posterior Stromal Laser Ablation

The mean CCT was programmed into the laser to calculate the effective depth of laser ablation. To produce a 150 μm-thick endo-stromal corneal lenticule, the laser was first programed to perform the peripheral vertical rim cut, starting at an ablation depth of 1100 μm (ie, within the anterior chamber proceeding upward through the Descemet membrane into the posterior stroma up to 230 μm—this depth was selected to have an overlap between the rim cut and the stromal lamellar ablation to ensure complete detachment of the lenticule). Deep stromal lamellar ablation was performed, aiming for a depth of 150 μm from the Descemet membrane at the central cornea (by subtracting

150 μm from the CCT measurement for each cornea). With this technique, it was also expected that the peripheral thickness would be greater, because of the increase in peripheral thickness in the normal cornea. To calculate the ablation diameter, the laser software converted the programed chord length value to an appropriate arc length. We tested ablation diameters with chord lengths varying from 6.3 to 8.5 mm. The equivalent arc length values were 6.5–8.7 mm. We examined the effect of different laser passes (single, double, and triple) on ease of posterior donor tissue separation and the effect of single, double, or triple pass rim cuts on the endothelium. Hydration of the cornea will affect the quality of the laser ablation in deep stromal tissue. To assess the effects of different laser ablation passes within the same quality of stromal tissue, we assessed the effects of different masking procedures on laser ablation on 1 donor. A series of different masks were used and assessed with respect to their efficacy (Figure 2.1). The masks were fashioned from sterile plastic drape material and were inserted into the applanation interface. The effects of single, double, and triple laser ablations on the endothelium during the vertical rim cut were likewise assessed by performing all 3 ablations in the same cornea by varying the diameter for the rim ablation, again to reduce intercorneal variations.

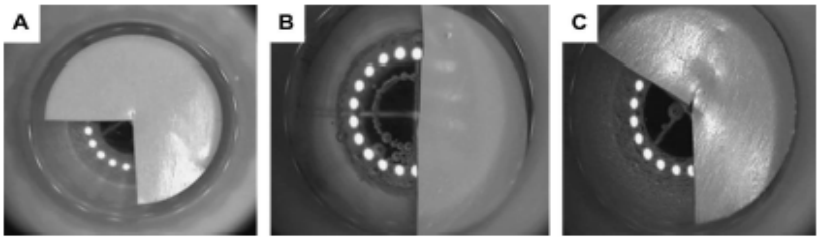

Figure 2.1 Different mask designs used in the study. A, Quadrant B, Half C, Triangle (Courtesy of Mehta et al. (158)).

By performing all the vertical rim ablations in the same cornea with masking of half of the endothelium, the same corneal tissue acted as an internal control. After the

laser procedure, the corneoscleral rim was turned endothelium side up onto a Hanna trephine block (Moria) with a modified high-vacuum teflon block. The block was connected to a vacuum suction machine (Eschmenn, Lancing, UK) (Figure 2.2).

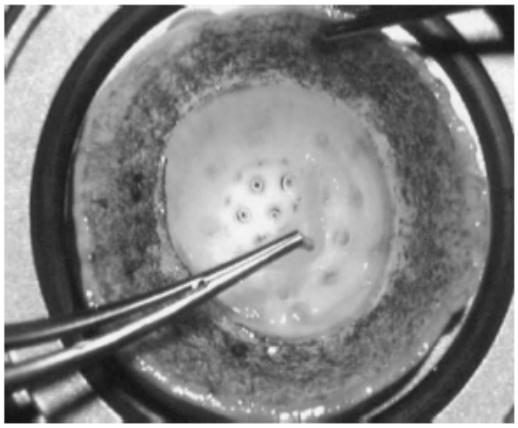

Figure 2.2 Modified high-vacuum Teflon block allowed stabilization of the corneoscleral rim before peeling of lasered donor lenticule. (Courtesy of Mehta et al. (158)).

The extra suction enables the posterior donor button to be removed without destabilizing the corneoscleral rim. The quality of the vertical rim cuts was first assessed by passing a Sinskey hook around the rim to break any residual tissue bridges. The quality of the cut was graded subjectively from 1 (poor) to 4 (excellent) (Table 2.1) depending on the ease of passage of the Sinskey hook and any intervening tissue ‘‘tags’’.

Grading	Quality
1	**Rim tags present greater than ½ clock hour and require surgical scissors to complete the incision**
2	**Rim tags less than ½ clock hour but incision completed with a Sinskey hook**

3	**Few rim tags present, broken by Sinskey hook**
4	**No rim tags present**

Table 2.1 Subjective Grading of Quality of the Rim (Courtesy of Mehta et al. (158)).

If there were excessive tags, they were excised with Vannas scissors. After removal of all tags, the donor tissue was carefully peeled apart using toothed forceps. The ease of removal and the surface regularity of the excised corneal lenticule was graded from 1 (poor) to 4 (excellent).

To measure the corneal disc thickness, 2 microscope coverslips were attached to a microcaliper (resolution, 1 micron; Mahr EX 40; Carl Mahr Holding, Germany). The donor lenticule was placed between the coverslips, and thickness was measured. Five of the corneas were macroscopically photographed. The buttons were placed in fixative (3% glutaraldehyde, 2% paraformaldehyde in 0.1 M sodium cacodylate buffer; pH 7.4) for processing. Statistical analysis was performed by using SPSS v9.0 (SPSS, Chicago, IL). Comparison of means among different groups was performed by using the Mann–Whitney U -test. Significance level was $P < 0.05$.

2.2.4 Measuring Ablation Thickness and Diameter

After the laser procedure, the corneoscleral rim was moved to an operating microscope. The quality of the vertical rim cuts was first assessed by passing a Sinskey hook around the rim to break any residual tissue bridges. After residual ‘‘tags’’ were removed, the anterior donor cap was carefully peeled from the posterior stroma using a toothed

forceps. The remaining corneoscleral rim on the AAC was photographed by digital camera and placed in an independent viewing chamber (IVC, Bausch & Lomb Surgical) full of Optisol-GS fluid. Anterior segment OCT was repeated to ascertain the depth of the resection (Figure 2.3).

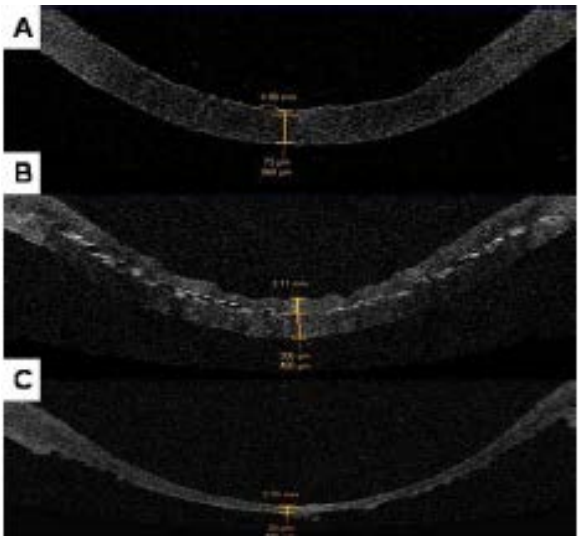

Figure 2.3 Anterior Segment OCT of donor corneoscleral rim placed in a viewing chamber A. Before ablation – to calculate mean CCT B. After femtosecond laser. Discrete white line indicates level of lamellar ablation. C. After peeling of the anterior lamellae. (Courtesy of Mehta et al. (159)).

The circularity was assessed by measuring the diameter of the resected tissue in the digital photograph in 2 planes, horizontal and vertical, with Image J software (NIH imaging). The ASOCT assessment and Image J measurement of the diameter were performed by an independent masked observer. Statistical analysis was performed by SPSS v9.0. Comparison of means among different groups was performed by analysis of variance (ANOVA). Correlation was assessed using Spearman rank correlation. The significance level was $P < .05$.

2.2.5 Histologic and Scanning Electron Microscopy

Tissues were secondary fixed in a mixed aldehyde solution and washed overnight before placing in 1% osmium tetroxide (FMB, Singapore). After dehydration, the samples were dried, mounted, and sputter-coated with gold. Specimens were examined with a JEOL scanning electron microscope (JSM-T220A; JEOL, Tokyo, Japan). Images of the stromal surface were taken at x18, x50, and x100 magnification in a preselected pattern (2 centrally and 1 in each quadrant at the periphery; ie, 6 fields/cornea). Images of the endothelium were taken at a magnification of x350 around the vertical rim cuts. The paraformaldehyde-fixed specimens were processed by dehydration and embedded in a paraffin block for sectioning. Five-micrometer sections were cut and stained with hematoxylin–eosin according to standard protocol and observed with a Zeiss Axioplan 2 microscope (Carl Zeiss, Germany).

2.2.6 Patients (Clinical Trial)

Patients requiring PK were recruited from the cornea clinic at the Singapore National Eye Centre. After informed consent was obtained, patients underwent surgery as follows. The study was approved by the Singapore Eye Research Institute Ethics Committee. All patients were provided with comprehensive information about the study, which conformed to the tenets of the Declaration of Helsinki. The Femtec femtosecond laser was used to trephine both recipient and donor corneas. This was a prototype machine with a repetition rate of 10 kHz, and it was programmed to deliver pulses in a circular pattern at 90 degrees to the corneal surfaces, aiming to achieve a straight, smooth perpendicular trephination. Laser settings used were as follows: energy, 4800 nJ; spot spacing, 3 μm; line spacing, 5 μm; and initial trephination depth, 1100 μm. A donor corneoscleral rim was first placed on a Hanna artificial anterior chamber (Moria, Antony, France). This was then trephined by the laser, commencing from the

anterior chamber and progressing anteriorly until the epithelium was breached. Remaining tissue bridges were severed with a DK Barrett Nucleus Divider and Chopper (Duckworth and Kent, Herts, United Kingdom) and the donor button was set aside. The recipient cornea was then trephined in a similar manner. In most cases, the donor was trephined to a diameter between 0.25 and 0.50 mm larger than the recipient. The donor button was then placed on the recipient eye and sutured in place with either continuous double running 10-0 nylon sutures or 16 interrupted 10-0 nylon sutures if significant vascularization was present. Postoperatively, patients were commenced on G PredForte (Allergan; Irvine, California, USA) G Tobrex (Alcon; Fort Worth, Texas, USA) both instilled one drop three hourly.

2.3 RESULTS

2.3.1 LASER ABLATION PARAMETERS

The mean corneal thickness before laser ablation after epithelial debridement was 574 +/- 74.5 μm (mean +/- SD; range, 480–680 μm). The laser ablation required 19–25 seconds to perform a rim pass and 36–63 seconds to perform a lamellar ablation, depending on the diameter and the number of passes. High-quality vertical laser trephinations were achieved in all corneas, with a minimum energy of 3.2 μJ, line separation of 3 μm, and spot separation of 6 μm. Lamellar laser ablations were achieved with lower energy because of the inherently looser fibrillar configuration of deep stroma. We were able to achieve lamellar cuts with energy setting of 1.3 μm, line separation of 5 μm and spot separation of 5 μm.

2.3.2 ASSESSMENT OF MASKS AND MULTIPLE ABLATION PASSES

The first mask we used was a simple colored cosmetic contact lens. We found this completely ineffective as a shield because the laser beam was able to ablate the cornea

beneath the colored part of the lens. Subsequently, we used masks that were cut in different shapes (e.g. a quadrant shape allowed 3 different ablation passes and a remaining quadrant as a negative control; Figure 2.1). However, although ablations were easily achievable with this technique, subsequent sectioning and separation of tissue quadrants was technically difficult and often resulted in torn tissue fibres.
We therefore opted to assess just 2 different ablation passes in 1 cornea by using a bullseye pattern. In this technique, after a vertical ablation, a standard lamellar ablation was performed, but ablation was aborted when 50% complete, leaving a central circle annulus of untreated tissue. Manual abortion was performed either once or twice depending on experimental protocol. Subsequent laser passes were performed at the same depth as the previous ones. For the last ablation pass, the lamellar ablation was performed all the way to the centre. With this technique, we were able to achieve lamellar laser dissections that had a double pass in the periphery and single centrally, triple ablation in the periphery, and double ablation centrally, etc.

2.3.3 Qualitative Rim Quality Assessment

The effect of different ablation passes on the quality of the vertical rim cuts was assessed in 30 human corneas. There were 10 corneas for each pass. The mean for the rim score of the single-pass ablation was 2.6 +/- 0.5, double-pass ablation was 2.5 +/- 0.8, and triple-pass ablation was 2.7 +/- 0.9. There was no significant difference in rim scores between the 3 groups (single pass vs. double pass, $P = 0.81$; double pass vs. triple pass, $P = 0.63$; single pass vs. triple pass, $P = 0.93$).

2.3.4 Qualitative Assessment of Lenticule Peeling

Peeling of donor lenticules was performed on 3 groups of 5 human corneas. The mean peel score of the single-pass ablation was 1.4 +/- 0.5, double-pass ablation was 3.4 +/-

0.8, and triple-pass ablation was 3.9 +/- 0.31. There was no significant difference in peel scores between the triple- and double-pass ablations (P = 0.196). Both double- and triple pass ablations had significantly higher peel scores than single pass ablation (double vs. single, P = 0.001; triple vs. single, P = 0.0001).

2.3.5 Macroscopic light Microscopy Findings

Rim cuts could easily be identified on light microscopy irrespective of whether a single-, double-, or triple-pass vertical ablation was performed. In corneas that had had multiple lamellar pass ablations, the different effects of stromal ablation could be seen; after single-pass ablation, fine multiple cavitation bubbles were visible, separated by residual tissue tags. After double- and triple-pass ablations, the cavitation bubbles had coalesced with fewer intervening tags (Figure 2.4).

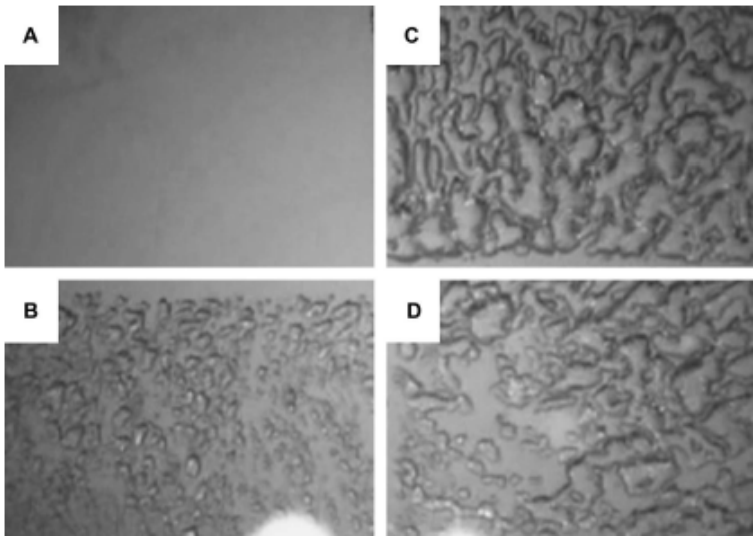

Figure 2.4 Quadrant mask used in 1 cornea before lenticule peeling. A, control-no ablation. B, One-pass ablation C, Double-pass ablation D, Triple-pass ablation. (Courtesy of Mehta et al. (158)).

2.3.6 Histology

Three remnant corneoscleral rims after posterior lenticule removal were processed by paraffin section. The sections showed that the vertical trephination cuts produced precise 90° configurations (Figure 2.5). There was no apparent thermal distortion or alteration of adjacent tissue. There was minimal fraying of collagen fibres at the cut edge both in the remnant corneoscleral rim and also in the cut edge of the donor lenticule. The anterior surface of the posterior donor lenticule after a double-pass ablation was smooth and regular, with minimal evidence of stromal bridges (Figure 2.5). The Descemet membrane was seen to be cleanly severed with the laser parameters described above.

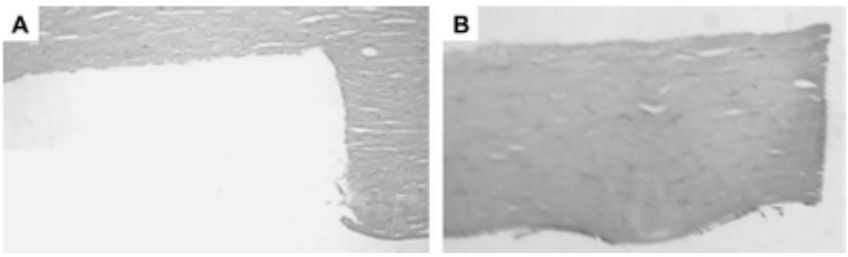

Figure 2.5 Histology section (x20) of A. Corneoscleral rim showing 90° angle of vertical rim cuts, with minimal fraying of the collagen fibres at the cut edge, and B. lenticule surface of donor cornea after double-pass ablation. (Courtesy of Mehta et al. (158)).

2.3.7 Electron Microscopic Findings

Qualitative assessment of the vertical rim cut showed that the Descemet membrane was severed in most cases. There were some areas where residual tags could be seen, but they were only in small contiguous areas (Figure 2.6 A,B). There was no qualitative difference in the amount of residual tags with different ablation passes. Images of the

corneoscleral rim after single, double, and triple passes were consistent with our histologic findings, confirming accurate 90° edges in the vertical rim cuts. Collagen lamellae were noted to have clean and precise separations with minimal adjacent lamellar distortion and few residual tissue bridges. Vertical rim cut ablation through the Descemet membrane showed only minor collateral morphologic damage or disruption to adjacent endothelial cells. There was no qualitative difference in the amount of collateral damage to the endothelial cells with different laser ablation passes (Figure 2.6B).

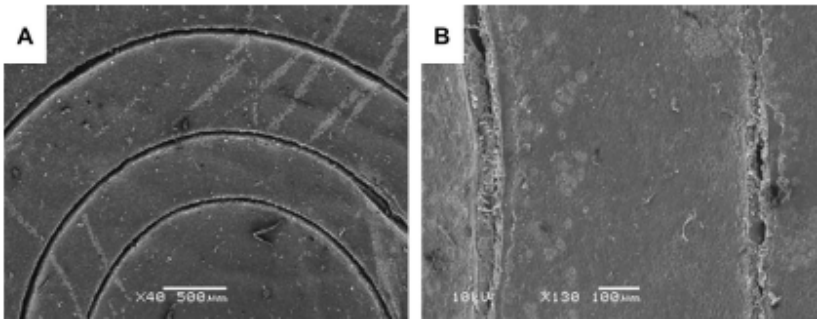

Figure 2.6 SEM of vertical rim cuts. A. Single pass in centre, double pass in middle and triple pass in periphery (x40). B. High-power (x100) view of single (left) and double (right) rim cuts showing residual tissue bridges and minimal collateral endothelial cell damage adjacent to vertical rim cut. (Courtesy of Mehta et al. (158)).

Low-power scanning electron microscopy (SEM) images did not show any evidence of ridges on the stromal surface irrespective of the number of laser ablation passes. Lenticules that underwent ablation with the bullseye configuration showed a clear margin between different ablation passes. Double- and triple-pass ablations gave consistently smoother surfaces than did single-pass ablations (Figure 2.7). The smoothness or roughness of the ablation was consistent throughout the donor lenticule surface. Single-pass ablations produced several areas where the surface was uneven because of residual stromal tags.

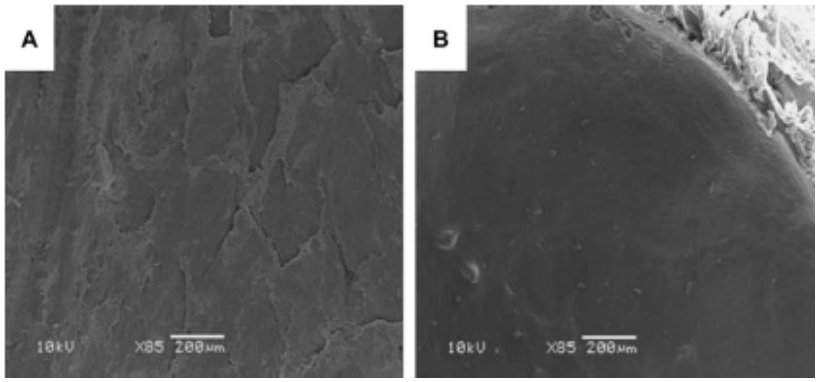

Figure 2.7 SEM of Stromal lamellar bed (x85) qualitative comparison. A. Single pass lamellar ablation B. Double-pass lamellar ablation. (Courtesy of Mehta et al. (158)).

2.3.8 THICKNESS MEASUREMENTS

The mean corneal thickness before femtosecond laser ablation (following epithelial debridement) was 558 μm +/- 72.5 (mean +/- SD; range 410 to 690 μm). The femtosecond incisional parameters were as follows: mean attempted resection depth, 383 +/- 63 μm (range 260 to 540 μm); mean thickness of the cornea posterior lenticule, 204 +/- 54 μm (range 100 to 350 μm). After laser ablation, the mean corneal thickness on ASOCT was 354 +/- 93 μm (range 150 to 545 μm). The mean deviation from the attempted laser ablation was 15 +/- 14 μm (range 0 to 58 μm). There was no significant difference between ablation depth after single-pass, double-pass, or triple-pass ablation ($P = 0.2$). There was a highly significant correlation between the attempted and achieved ablation depths (Figure 2.8) ($r^2 = 0.93$, $P = 0.0001$) but no significant correlation between the preoperative corneal thickness and the accuracy of the laser ablation (Figure 2.9) ($r^2 = 0.18$, $P = 0.911$).

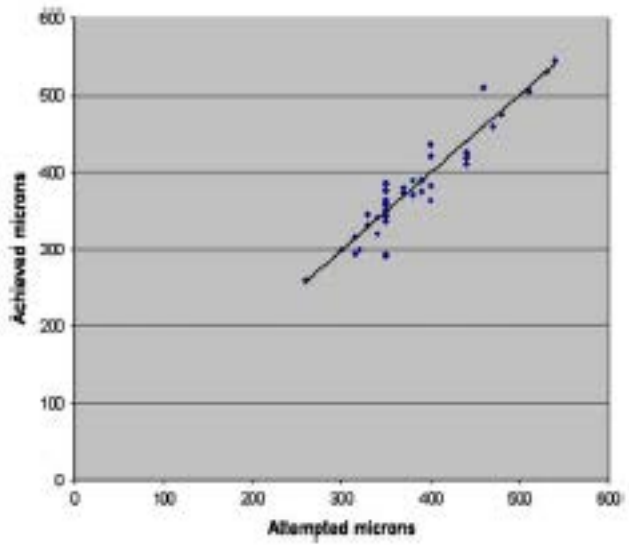

Figure 2.8 Attempted versus achieved ablation depths after femtosecond laser ablation (r^2 = 0.93, P = 0.0001). (Courtesy of Mehta et al. (159)).

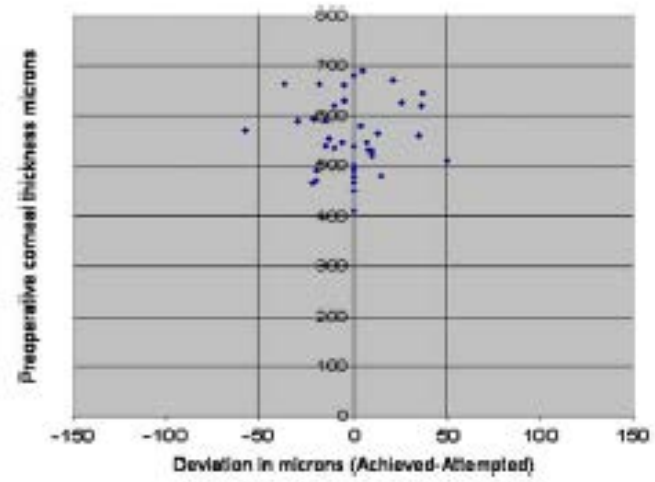

Figure 2.9 Correlation between preoperative corneal thickness and accuracy of laser ablation (r^2 = 0.18, P = 0.911). (Courtesy of Mehta et al. (159)).

2.3.9 Diameter Accuracy

All the obtained corneal vertical ablations were circular (horizontal versus vertical diameter, P = 0.38). The mean deviation from the intended diameter was 0.12+/- 0.15 mm (range 0 to 0.5 mm). The accuracy with different ablation sizes was analyzed.

There was no significant difference in the circularity of the diameter between ablations of 7.0 to 8.0 mm (n = 26), 8.0 to 9.0 mm (n = 7), and larger than 9.0 mm (n = 7) (P = .6). There was a highly significant correlation between the attempted and achieved ablation diameters (Figure 2.10) (r^2= 0.935, P= .001). There was no significant correlation between the preoperative corneal thickness and the accuracy of the horizontal diameter of the laser ablation (r^2= 0.061, P= .757).

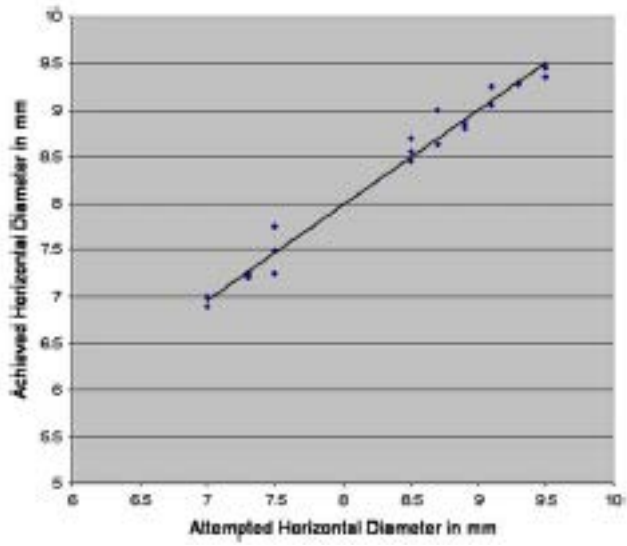

Figure 2.10 Correlation between attempted and achieved horizontal ablation diameter (r^2= 0.935, P= .001). (Courtesy of Mehta et al. (159)).

2.3.10 CLINICAL STUDY

Eight Eyes of eight patients were recruited for this study. All were male and had a mean age of 60.25 years (range, 37 to 75 years). Patients were followed up for a mean of 9.5 months (range, three to 14 months), and surgery was performed for corneal endothelial decompensation (n= 7) from a variety of causes and corneal scarring from herpetic keratitis (n= 1). Table 2.2 summarizes patient information, operative details, and visual outcomes for this series of patients.

Patient No.	Diagnosis	Preoperative BCVA	Suture Type	Donor Diameter (Projected Chord Length)	Recipient Diameter (Projected Chord Length)	Three-month BCVA	Refraction Three Months	Best Vision	Refraction Latest Follow-up
1	BK (trauma)	CF 1 m	16 interrupted	7.75	7.75	20/80	+3.00/−4.00×60	20/60	+1.00/−4.50×60
2	BK (laser PI)	CF 2 m	Double continuous 8 bite	7.75	7.5	20/30	+4.00/−1.50×55	20/30	+5.00/−0.50×55
3	Failed graft (PK for keratoconus)	CF 2 m	Double continuous 8 bite	8.25	8.00	20/70	+3.75/−1.50×160	20/70	+3.75/−1.50×160
4*	BK (Fuchs dystrophy)	HM	16 interrupted	8.25	7.75	CF 2 m	+3.00/−3.50×30	CF 2 m	+2.00/−2.50×20
5	Failed graft	20/400	Double continuous 8 bite	8.50	8.00	20/30	−2.75/−1.00×45	20/30	−3.00/−2.75×35
6†	Pseudophakic BK	CF 3 m	16 interrupted	8.00	8.45	CF 2 m	+3.00/−5.50×60	20/400	PV−4.00×120
7	Herpetic corneal scarring	CF 1 m	16 interrupted	7.75	7.50	20/40	+2.00/−0.50×180	20/20	+3.25/−1.25×145
8	Pseudophakic BK	CF 2 m	Double continuous 8 bite	8.50	8.25	20/80	−0.75/−2.75×160	20/80	−3.00/−3.50×170

BK = bullous keratopathy; BCVA = best-corrected visual acuity; CF = counting fingers; HM = hand motions; PI = peripheral iridotomy; PK = penetrating keratoplasty
*Poor BCVA because of diabetic macular edema.
†Poor BCVA because of epiretinal membrane with macular striae.

Table 2.2 Patient Diagnosis, Operative Details and Outcomes Following Femtosecond Laser-Assisted Penetrating Keratoplasty. (Courtesy of Mehta et al. (160)).

No intraoperative complications were noted. Tissue bridges were more tenacious in the recipient cornea as compared with donor cornea but in most cases could still be separated with the Barrett nucleus divider. In the one case, where blunt separation could not be achieved, Stern scissors were used to complete excision of the recipient corneal button. Postoperatively, best-corrected visual acuity (BCVA) of patients with no ocular comorbidity ranged from 20/20 to 20/80. One patient had vision limited to counting fingers secondary to diabetic macular edema, and another attained BCVA of 20/400 as a result of an epiretinal membrane with retinal striae. Mean cylindrical refractive error at three months was 2.53 diopters [D] (range, 0.50 to 5.50 D) and at last review was 2.56 D (range, 0.50 to 4.00 D). Qualitatively, the donor-host interface was well apposed and very regular in all cases, and this was confirmed with in vivo anterior segment optical coherence tomography (Visante; Carl Zeiss, Jena, Germany) (Figure 2.11).

Figure 2.11 Representative anterior segment optical coherence tomography (ASOCT) image of Patient 7 following femtosecond laser-assisted penetrating keratoplasty, showing perpendicularly cut recipient/donor edges, that are well apposed. (Courtesy of Mehta et al. (160)).

2.4 DISCUSSION

We developed several laser incisional models by using human corneas for studies on the effects of femtosecond laser ablation on corneal stroma, the Descemet membrane, and the corneal endothelium. We established a nomogram for posterior stromal ablation with the FEMTEC 20/10 40-kHz femtosecond laser. Previous studies with this femtosecond laser have been performed by using either rabbit (34), porcine (35,36) eyes or with the previous 10-kHz version (35–37) of this laser. Although animal wetlab results are useful, direct extrapolation of laser parameters to human eyes is not possible. We used fresh research grade corneal tissue (mean death-to-experimentation time, 3.1 days).

Vertical ablation with the laser requires higher energy settings than horizontal lamellae ablation. We first started using vertical cut ablation settings that had been previously described for the 10-kHz femosecond laser (i.e, 4.0 μJ, line separation of 5 μm, and spot separation of 6 μm) (37). Although these settings provide smooth rectilinear cut margins with perpendicular edges, ablation through the Descemet

membrane (an important step in our laser program development) was often incomplete. However, with the new software enhancements on the 40-kHz unit, we were able to use lower energy settings of 3.2 μJ, line separation of 3 μm, and spot separation of 5 μm, which were sufficient to consistently severe the Descemet membrane (38). As expected, lamellar ablations were successfully performed at much lower energy levels (1.3 μJ, line separation of 5 μm, and spot separation of 5 μm).

Studies on deep stromal ablation with the IntraLase have reported the appearance of concentric rings and a more stucco-like texture of the stromal bed (39, 40, 41) whereas a previous report of posterior stromal ablation with the FEMTEC laser, as in our cases, did not document these findings (36). The concentric ridges previously noticed were minimal and could be further smoothed by phototherapeutic keratectomy. It is also interesting that the 60-kHz IntraLase laser has been shown to produce smoother anterior stromal beds than the latest microkeratomes because of lower pulse energies and spot separation settings. (42).

Even though the FEMTEC laser did not produce a stucco texture in the posterior stroma, we were concerned with residual tissue adhesions present during a single-pass ablation. This was noticed during our peeling of the lenticule after single-pass ablation. Because we were already using a close spot and line separation (5/5), we hypothesized whether the remaining tissue bridges could be disrupted by performing a second-pass ablation at the same lamellar depth. This assumption seemed to be correct because, after a double-pass lamellar ablation, we showed there was a significant improvement in the lenticule peel scores. We extrapolated this further to see the effects of a triple-ablation pass. However, even though the triple lamellar pass allowed even easier peeling, this

was not significantly different from the double-pass nomogram. These assumptions were further supported by fewer tissue bridges seen on light microscopy evident by larger cavitation bubbles on stromal tissue that had undergone double- and triple-pass ablation compared with single-pass ablation and on SEM, where double- and triple-pass ablations produced qualitatively smoother stromal beds than single-pass ablations.

We were unable to show a difference in vertical rim quality with multiple ablation passes as assessed by our clinical rim assessment. Even though we were able to show residual tissue adhesions on SEM, our clinical assessment suggested these were of minimal clinical significance because they were easily incised by passage of a Sinskey hook through the rim. This may be because of the close spot and line separation of the nomogram we used for vertical rim cuts. It may be by performing multiple vertical passes that the pulses are too close together; hence, there is minimal improvement in the resection quality.

Our preliminary results, however, indicated an acceptable area of cell loss adjacent to the vertical rim cut. The area of cell loss did not seem to vary with different numbers of ablation passes, showing the local effect of laser cut.

Our results suggest that the double-pass ablation nomogram produced a lenticule that was easier to peel. To achieve this ablation, the laser needs to be programed to perform a vertical rim cut with subsequent programming for the double stromal lamellar pass. A disadvantage of this nomogram is that it needs to be performed as 3 separate laser ablations (1 for vertical and 2 for lamellar).

The second study assessed the circularity and depth of ablation of the Femtec femtosecond laser in performing deep stromal ablations. The mean central corneal depth of ablation was 354 +/- 93 μm (range 150 to 545 μm). The mean deviation from the intended lamellar ablation was 15 +/- 14 μm. We also found there was no correlation between the preoperative donor thickness and the accuracy of the ablation depth.

Accurate deep stromal ablations can be more difficult to achieve because of the loosely packed structure of the posterior collagen layer (43). Our results showed that deep stromal ablation can be achieved accurately with the Femtec laser; the results are comparable to those for LASIK (44). We found no significant difference in accuracy after a single, double, or triple-pass stromal ablation. It was important that the laser applanation pressure via the patient interface was not adjusted during the multiple-pass ablation nomogram.

The graft diameter is an important advantage of endothelial keratoplasty surgery over conventional PKP. The Femtec laser was limited to a maximum arc length diameter of 9.5 mm. Our results showed that the laser was accurate in producing lamellar buttons with arc length diameters ranging from 7.0 to 9.5 mm. There was no significant difference in the accuracy of the circularity of the button between 7.0 to 8.0 mm buttons, 8.0 to 9.0 mm buttons, and more than 9.0 mm buttons (P= .2, P = .3, and P = .6 respectively). One limitation of the Femtec laser was that the deepest lamellar bed dissection that could be programmed was 550 μm. Hence, in corneas thicker than 750 μm, the deepest lamellar dissection possible was 200 μm from Descemet membrane. This may not be seen frequently in clinical-grade Optisol-stored fresh corneal tissue but has been documented following tissue stored in organ cultured medium (45). We have

found that ablation with this laser in corneas thicker than 900 microns often produced inaccurate posterior stromal ablation depths (46).

This study has a few limitations. The tissue used for the femtosecond laser ablation was research-grade corneal tissue. This may have biased the results since research-grade tissue is often more swollen than clinical-grade tissue; the laser may not be accurate. However, there was poor correlation between preoperative corneal thickness and attempted ablation depth, and the mean corneal donor thickness was 558 μm, which was an acceptable thickness for donor tissue. The mean time between death to preservation and experiment for all research-grade tissue was 5 days (range 4 to 6 days).

The clinical study on patients used conventional 90-degree cut angles and a circular trephine configuration with straight edges. Using these parameters we found that the Femtec laser reliably trephined both donor and recipient, providing precisely defined and perpendicular graft edge profiles. In our study, identical settings for dissecting tissue were used for both donor and recipient corneas. We used a DK Barrett Nucleus Divider and Chopper to complete tissue separation after laser trephination. Tissue separation was discernibly more difficult in edematous recipient corneas compared with donor tissue, but it was still possible without sharp cutting instruments in the majority of cases. We theorize that using higher laser energy settings could have improved the quality of cut in these cases, as could future developments in femtosecond laser technology leading to greater repetition rates and closer spot separation settings.

2.5 SUMMARY

We established a nomogram for posterior lamellar ablation with the FEMTEC 40-kHz laser that seemed to deliver consistently high-quality ablation profiles at relatively low-energy settings and minimal adjacent stromal and endothelial morphologic changes. The goal of improving the quality and thickness of the donor lenticule is on the basis of an assumption that a smoother stromal surface and thinner lenticule will provide better visual results. We were also able to show significant improvements in clinical donor peeling with a double-pass ablation compared with a single-pass ablation. Multiple-pass lamellar incisions produced smoother surfaces on SEM.

The Femtec femtosecond laser was able to produce accurate deep posterior stromal ablations. There was no correlation with the preoperative pachymetry, and the laser was accurate in donor corneal thickness up to 690 microns (tested in this study). The diameter of the buttons produced was consistent and circular up to an arc length diameter of 9.5 mm and would be of sufficient diameter to provide donor buttons for DSEK.

For the penetrating keratoplasty, the Femtec laser reliably trephines donor corneas and recipient beds for PK, providing good visual outcomes. Better optimization of laser parameters for different degrees of corneal opacity and edema would increase ease of surgery and possibly improve outcomes. Although both conventional and alternate trephine profiles such as top hat and zig-zag configurations seem to provide good results with low astigmatism, further studies with new trephine patterns may better define the advantages associated with femtosecond laser–assisted PK.

CHAPTER 3

3.0 COMPARATIVE STUDIES ON FEMTOSECOND LASERS

3.1 INTRODUCTION

Following the introduction of the IntraLase femtosecond laser worldwide, there was an increase in femtosecond lasers being made by other companies. IntraLase was still widely regarded as the 'gold' standard laser. However, the new lasers worked on fundamentally different underlining technology, which we wanted to ascertain whether it affected clinical outcomes. The series of experiments in this chapter are the first published papers comparing two different femtosecond lasers, the IntraLase and VisuMax. In order to show differences we did a comprehensive set of studies from animal experimentation, to ex vivo wetlab corneas and finally a clinical trial.

3.2 METHODS

3.2.1 IN VIVO REAL-TIME IOP VARIATION DURING LASIK FLAP CREATION

3.2.1.1 ANIMALS

Thirteen New Zealand White rabbits (weight range, 2–2.5 kg) were procured from the animal holding unit of the National University of Singapore. Rabbits were housed individually at 25°C on a 12-hour light/12-hour dark cycle, with rabbit pellets and water available ad libitum. Approval was obtained from the SingHealth Institutional Animal Care and Use Committee, and all procedures performed in this study complied with the ARVO Statement for the Use of Animals in Ophthalmic and Vision Research. Rabbits

were anesthetized with a combination of ketamine and xylazine (ketamine 40 mg/kg; xylazine 20 mg/kg, administered intramuscularly), and topical anesthesia proparacaine drops were used during surgery.

3.2.1.2 LASIK Flap Creation

This was a paired eye study using a rabbit experimental model of LASIK. All procedures were performed by the same surgeon (JSM - the author). One eye underwent creation of a LASIK flap with a 200-kHz femtosecond laser (VisuMax; Carl Zeiss Meditec, Jena, Germany), and the contralateral eye underwent flap creation with a mechanical microkeratome (M2; Moria, Antony, France). Femtosecond corneal flaps were always made first before treating the other eye with a microkeratome. IOP was evaluated prospectively from application of the suction through to the end of the creation of the LASIK flap in both groups. Each rabbit eye underwent surgery with a new blade in the microkeratome group. To create the flap with the femtosecond laser, the laser parameters were 100 μm estimated flap thickness, 7.9-mm estimated flap diameter, 200-nJ power, and a spot distance and tracking spacing both of 5 μm for lamellar cut and 2 μm for rim cut. A small (S) curved interface cone was used in all cases based on the white-to-white diameter of the rabbit eye. The eyelids were held apart with a paediatric wire speculum. The cannula for IOP measurement was inserted into the limbus before application of the cone. The cone was centred on the pupil with the aid of the internal fixation light, and suction was applied (Figure. 3.1).

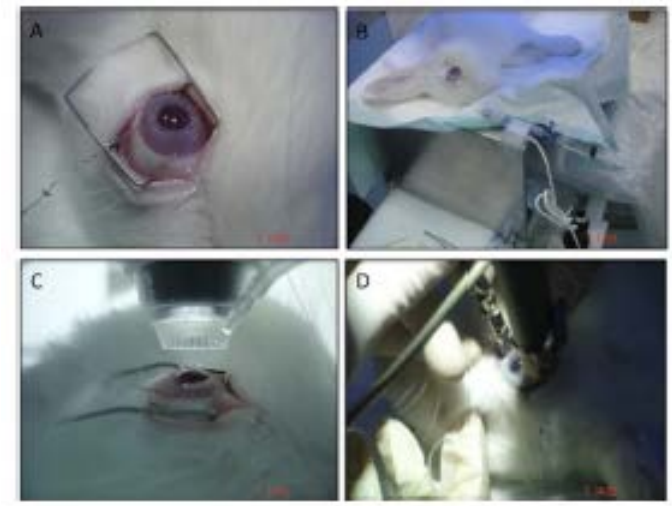

Figure 3.1 Corneal Flap creation and measurement of IOP in rabbits using a femtosecond laser or a microkeratome. A. Insertion of a 30-gauge needle through the limbus into the anterior chamber B. Set up for the IOP recording to the transducer C. Corneal flap created with the femtosecond laser D. Microkeratome blade setting for corneal flap creation with needle inserted into the anterior chamber. (Courtesy of Chaurasia et al. (161)).

Ablation commenced when full suction was achieved and the IOP readings had stabilized. After LASIK flap creation, the cone was elevated, and the flap was examined under the microscope. Microkeratome dissection was performed in a similar fashion. The choice of microkeratome ring size was determined by pre-operative keratometry. Rings used varied from +3 to +1 and were chosen by data supplied by Moria (Antony, France). The stop on the rings was adjusted to obtain the largest flaps possible (range, 8.8–9 mm. A 110-μm microkeratome head was used in all cases to create the flap. After cannulation of the anterior chamber, the ring was placed on the eye, and adequate suction was confirmed by a sudden and constant rise in IOP as measured by our intracameral device. Microkeratome dissection was performed with the microkeratome

by one surgeon (JSM-the author) using forward and reverse pedals. After flap formation, the vacuum was released, and the ring was removed. The flap was then inspected under the microscope but not lifted.

3.2.1.3 Intraocular Pressure Measurements

IOP was measured in the anterior chamber using a 30-gauge winged infusion cannula that was inserted through the limbus so that the suction ring could be applied over the sclera without dislodging the cannula. Pressure measurements were obtained with a transducer. The transducer was prepared according to the instructions of the manufacturer to ensure that the seal was tight and that all air was flushed from the system. The transducer was calibrated before each flap creation to ensure that the IOP was accurate. To ensure the transducer was working accurately, after cannulation of the anterior chamber, IOP measurements were also taken with a tonometer (Tono-Pen; Reichert-Jung, Depew, NY) before the experiment was begun (Figure 3.2). For the microkeratome and femtosecond groups, the suction ring was applied over the sclera after the insertion of the cannula into the anterior chamber of the eye. During the procedure, the IOP was recorded continuously with the amplifier from the time of the application of suction through to the end of the microkeratome pass.

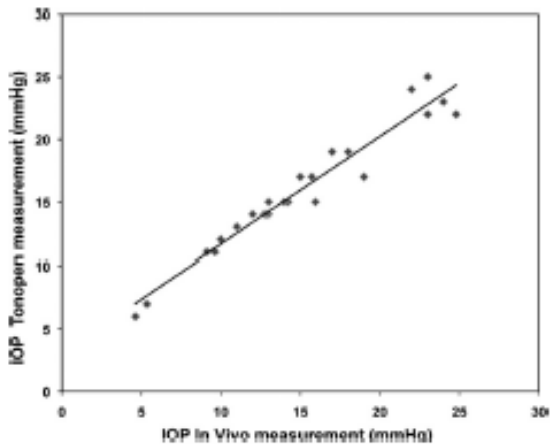

Figure 3.2 Correlation between in vivo IOP and tonometer IOP measurements showing good correlation (r= 0.94) between the two devices before commencement of the flap formation. (Courtesy of Chaurasia et al. (161)).

3.2.1.4 Statistical Analysis

Results were expressed as mean +/- SEM. Statistical comparison of multiple group data was performed using one-way analysis of variance (ANOVA) with Newman-Keuls post hoc adjustment where applicable. Statistical analyses between the microkeratome and femtosecond groups comparing the IOP variations with suction on, globe suction, cutting, and suction off during LASIK flap creation were performed with the Student's t-test. $P < 0.05$ was considered statistically significant.

3.2.2 Nanoscale Helium ION Microscopic Analysis of Collagen Changes following Femtosecond Laser Dissection

3.2.2.1 Intrastromal Ablation Procedure

Intrastromal ablation was investigated using two commercially available femtosecond (FSL) platforms: IntraLase (Abbott Medical Optics) and VisuMax Femtosecond Laser System (Carl Zeiss Meditec). Intrastromal cut with Zyoptix XP microkeratome (Bausch and Lomb, Rochester, NY) was used as a control. The laser parameters (Table 3.1) used for corneal flap creation were selected to correspond to standard LASIK procedures routinely performed at the Singapore National Eye Centre, Singapore.

	Femtosecond Laser Ablation		Microkeratome cut
	IntraLase	VisuMax	Zyoptix XP

Flap diameter (mm)	7.9	7.9	9.0
Flap thickness (μm)	115	115	120
Wavelength (nm)	1040	1040	-
Repetition rate (kHz)	60	500	-
Pulse duration (fs)	>500	220-580	-
Energy (nJ)	950	170	-
Spot size (μm)	3	1	-
Spot/Line separation (μm)	7	4.8	-
Firing pattern	Raster	Spiral	-

Table 3.1 Technical specifications used for corneal flap creation. (Courtesy of Riau et al. (162)).

Fifteen human cadaver corneoscleral buttons aged 55 to 59, unsuitable for transplantation were obtained from Lions Eye Institute (Tampa, FL). The specimens were preserved at 4°C in Optisol-GS (Bausch and Lomb). Mean death to enucleation was 8.2 +/- 7.1 hours and mean death to experiment was 6.67 +/- 0.3 days. Since the time of death to enucleation of the eyes varied significantly, there was a concern that there would possibly be a differential effect on the corneal stromal architecture between eyes that were enucleated earlier than later even before the laser treatment.

To minimize the variability, the samples for each group were selected so that the mean death to enucleation time was similar for all 3 groups (microkeratome group: 8.2+/- 7.7 hours; IntraLase group: 8.4 +/- 8.1 hours; VisuMax group: 8.0 +/- 7.1 hours). The corneoscleral buttons were placed in an artificial anterior chamber (AAC) device (Network Medical Products, Ripon, UK) and the epithelial layer was

mechanically removed. Five corneas were used in each group, i.e., IntraLase, VisuMax and microkeratome groups. All procedures were performed by the same surgeon (JSM-the author). After the lamellar ablation process was completed, three corneas in each group had the flap lifted for topographical analysis, while the flaps of the remaining two corneas were not lifted and processed for cross-sectional analysis. The flap was lifted using a combination of a Price-Sinskey hook (ASICO, Westmont, IL), a Seibel flap lifter (Rhein Medical Inc., Tampa, FL) and a retreatment spatula (Rhein Medical Inc.). After the procedure, the corneoscleral buttons were immediately fixed in 2% glutaraldehyde and 2% paraformaldehyde in 0.1 M sodium cacodylate buffer, pH 7.4 (Electron Microscopy Sciences, Hatfield, PA) overnight at 4°C for further analysis.

3.2.2.2 Scanning Helium Ion Microscopy

Topography analysis was carried out on the lifted flap and bed surfaces with the ORION HeIM (Carl Zeiss). After fixation, the tissues were washed in sodium cacodylate buffer, dehydrated in a graded series of ethanol (increasing from a 25% ethanol to 100% ethanol) and critical point dried (Bal-Tec CPD 030, Balzers, Liechtenstein). The dried samples were mounted on SEM stubs with carbon adhesive tabs and transferred directly into the vacuum chamber of the HeIM with limited atmospheric exposure to minimize water absorption from ambient humidity. All tissue samples imaged with the HeIM did not require any form of conductive overcoat (which would have obscured the fine detail observed in this study). Instead, an electron flood gun, focused to coincide with the position of the helium ion scan field and interlaced in time with the helium ion line scans, was employed to neutralize sample charging. Images of stromal bed surfaces were acquired in secondary electron mode with an acceleration voltage of 35 keV, a beam current of 0.2–0.5 pA and a dwell time of 0.5–

2.0 μs. The electron flood gun dwell time between ion line scans was optimized for maximum sample contrast, and line scan averaging was employed to increase the signal to noise of the images.

3.2.2.3 TRANSMISSION ELECTRON MICROSCOPY (TEM) IMAGING

Cross-sectional analyses of ablated corneas with non-lifted flaps were made with light microscopy (LM) and TEM. After fixation, the tissues were trimmed into smaller pieces before post-fixation in 1% osmium tetroxide and potassium ferricynaide (Electron Microscopy Sciences). After rinsing with sodium cacodylate buffer, the tissues were dehydrated in a graded series of ethanol rinses, and embedded in Araldite (Electron Microscopy Sciences). All semi-thin sections of 0.5–1μm thickness were cut with Reichert-Jung Ultracut E Ultramicrotome (C.Reichert Optische Werke AG, Vienna, Austria), counterstained with toluidine blue/basic fuchsin stain and examined using a Zeiss Axioplan light microscope (Carl Zeiss). All ultra-thin sections, of 60–80 nm thickness, were collected on copper grids, doubled-stained with uranyl acetate and lead citrate for 20 minutes each, then viewed and photographed using a Philips EM 208S Transmission Electron Microscope (FEI Electron Optics BV, Eindhoven, The Netherlands) at 100 kV.

3.2.2.4 IMAGE AND STATISTICAL ANALYSIS

All measurements obtained from images were made using ImageJ version 1.42 (Research Services Branch, National Institutes of Health, Bethesda, MD). Data were expressed as mean+/- standard deviation. The P value was determined using two-tailed Student's t -test with Graph Pad Prism 5 (La Jolla, CA). Data were considered to be statistically significant when $P < 0.05$.

3.2.3 Randomized Controlled Contralateral Eye Study Comparing IntraLase and VisuMax

3.2.3.1 Study Design

Randomized Controlled Trial 1

This prospective clinical trial compared the efficacy, predictability, and stability of femtosecond LASIK using the Visumax femtosecond laser (Group 1) for flap creation in 1 eye versus the Intralase femtosecond laser (Group 2) for flap creation in the other eye. Myopic patients who were suitable for femtosecond LASIK at the Singapore National Eye Centre were invited to participate in this trial. The study was approved by the Singapore Eye Research Institute Ethics Committee. All patients were provided with comprehensive information about the study, which conformed to the tenets of the Declaration of Helsinki. A series of computer-generated randomized numbers was created and placed in an envelope. Based on whether an odd or even number was picked, study participants had LASIK using 1 of the femtosecond lasers in their right eye and with the other femtosecond laser in the other eye. All patients had bilateral LASIK on the same day, and the excimer treatment was performed using the same excimer laser in both eyes. However, the entire LASIK procedure was completed in 1 eye before it was performed in the other eye. The patients were masked as to which femtosecond laser procedure was performed in which eye. All surgeries were performed by certified and experienced users of both femtosecond lasers (the author).

Randomized Controlled Trial 2

This prospective study enrolled patients who had LASIK with femtosecond laser corneal flap creation from April 2008 to September 2009 at Singapore National Eye Centre, Singapore. In this study, the Advanced Control Eye Tracking system

(Bausch & Lomb) was used for iris recognition. It is a dynamic rotational eye tracker that is continuously active to compensate for intraoperative movements, including rotation, during the LASIK ablation. The eye tracker for the Technolas LASIK platform locks onto the eye's iris pattern just before the laser treatment begins and then monitors the pattern throughout the procedure. When rotation of the iris pattern is detected during treatment, the direction of laser pulses is automatically adjusted accordingly. The eye tracker uses an active rotational tracker at a sampling rate of 240 Hz, 50 Hz, and 25 Hz for x-y-z and rotational tracking. The sampling range is 3.0mm x3.0 mmx0.5 mm and +/-15 degrees for x-y-z rotational tracking; x-y is active and z is passive with static and dynamic rotation. The eye tracker recognizes the iris structure and compensates for cyclotorsion by comparing images taken between the upright position and supine position as well as between the dilated pupil and undilated pupil. Once the preoperative iris data are loaded into the excimer laser, the fixation light is centred on the pupil and the dynamic tracker initiated. After initiation and iris recognition, the corneal flap is lifted and laser ablation begun. If iris recognition is not successful, the program can be overridden and laser ablation can be performed without tracking. The surgeon can monitor the x-y and z status and the rotational status of the iris during the treatment; all the values are displayed numerically and graphically. If iris recognition fails during ablation, the last recognized angle is used for the remaining treatment. Microscope and operating room illumination, prevention of corneal dryness, defocusing and waiting for the pupil to dilate to a size of more than 3.5 mm were controlled by the same laser technician before initiation of the eye tracker.

3.2.3.2 PATIENT SELECTION

Male and female patients were eligible for the study if they were older than 21 years and younger than 40 years, had given informed consent to participate in the study, and

were fully agreeable to accept randomized selection of either eye to have flap creation with either femtosecond laser. Before providing consent, all patients were given detailed information regarding each treatment. Patients were required to have stable myopia determined by manifest refraction for at least 6 months, a corrected distance visual acuity (CDVA) of at least 20/20, and stable keratometry after cessation of soft contact lens wear for at least 2 weeks or rigid gas-permeable contact lens wear for at least 3 weeks. The difference in spherical equivalent (SE) between the 2 eyes could not be more than 2.00 diopters (D). Study patients were required to have a minimum corneal thickness of 500 μm measured by pachymetry (Orbscan IIz, Bausch & Lomb). Patients were excluded if they had corneal or anterior segment pathology, any form of retinal degeneration, clinical signs of progressive or unstable myopia, previous ocular surgery, a history of herpes zoster ophthalmicus or herpes simplex keratitis, a history of a steroid-responsive rise in intraocular pressure (IOP) or a preoperative IOP of more than 21 mm Hg in either eye, diabetes mellitus, autoimmune disease, severe dry eye, connective tissue disease, significant atopy, and a corneal thickness that would have resulted in less than 250 μm of remaining posterior corneal thickness below the flap postoperatively. Patients who had keratoconus or were keratoconus suspects, were 1 eyed, were on chronic systemic corticosteroid or immunosuppressive therapy, or opted for monovision were also excluded from the study.

3.2.3.3 Patient Assessment

Preoperative and postoperative examinations included routine slitlamp and dilated fundus evaluations, photopic uncorrected distance logMar visual acuity (UDVA) and CDVA, manifest refraction, and air-puff noncontact tonometry (Nidek NT-3000 Auto Noncontact tonometer). All patients had preoperative imaging (Orbscan IIz). Contrast

sensitivity testing was performed using the Optec 6500P Vision Tester (Stereo Optical Co., Inc.). Contrast sensitivity was tested under photopic (85 candelas Cd/m^2) and mesopic (3 cd/m^2) lighting conditions (without glare) and at spatial frequencies of 1.5 cycles per degree (cpd), 3.0 cpd, 6.0 cpd, 12.0 cpd, and 18.0 cpd. For tear film assessment the outcome measures were comprised of corneal sensitivity, TBUT, Schirmer's test, and corneal fluorescein staining. Measurements for corneal sensitivity were taken preoperatively at 1 month and at 3 months postoperatively, while other outcome measures were collected at each visit, except at 1 day postoperatively. TBUT and corneal staining were evaluated after instillation of fluorescein. TBUT was defined as the time taken (in sec) for the first dark spot to appear on the cornea from the moment of eye opening. The cornea was assessed using fluorescein dye and divided into three horizontal zones (upper, middle, and lower). Positive staining scores were: 0 (no staining), 1 (some staining), 2 (staining in more than half of the area), and 3 (staining in the whole zone). Staining scores were added from each zone, for a total staining score ranging from 0 to 9. Corneal sensitivity was measured in five zones, using the Cochet-Bonnet esthesiometer (Visionix Luneau, Paris, France). The patient was positioned on an ophthalmic chin and brow rest of a slit lamp, and a nylon monofilament of 6.00 cm was perpendicularly advanced to the central cornea. The filament was shortened in 0.50 cm increments, if the patient did not feel the filament. Measurements (in cm) were repeated in the superior, inferior, temporal, and nasal zones. The reduction of corneal sensitivity was equal in all zones, and the average values were reported. Tear production was tested by Schirmer's tests (Sno strips®, Bausch and Lomb), without anesthesia, and the length of wetting (in mm) within 5 minutes was recorded. Postoperatively, all patients were reviewed at 1 day, 1 week, and 1 and 3 months. The trained nurses and optometrists performing the visual acuity

examinations and refractions were masked to the randomization process; that is, they did not know which femtosecond laser had been used in which eye.

3.2.3.4 SURGICAL TECHNIQUE

In Group 1 (Visumax femtosecond laser group), small size cones were used in all eyes, creating a flap diameter of 7.9 mm. Flap thickness was 115 μm in all eyes. All flaps had superior hinges, side-cut angles of 85 degrees, and hinge angles of 70 degrees. The laser bed energy was set at 160 to 165 nJ, spot separations were 1.5 μm (rim) and 4.8 μm (lamellar), and line spot separations were 1.5 μm (rim) and 4.8 μm (lamellar). In Group 2 eyes (Intralase), the flap thickness was 110 μm in all eyes and the flap diameters were between 8.5mm and 9.0 mm. All Group 2 flaps had superior hinges, side-cut angles of 70 degrees, and hinge angles of 50 degrees. The mean laser bed energy was 950 nJ (range 920 to 1080 nJ). Pocket creation was enabled with a pocket width of 0.25 mm, pocket start depth of 230 μm, pocket tangent of 7 mm, and radian spot separations of 6 mm. The Wavelight Allegretto Eye-Q 400 Hz excimer laser system (Wavelight Laser Technologie AG) was used for all excimer laser ablations in RCT1. All patients had the wavefront optimized treatment profile. An optical zone of 6.5 mm was used, and the target refraction was emmetropia. For RCT2 all eyes had LASIK using a Technolas LASIK platform (Technolas Perfect Vision GmbH). In Group A, the corneal flaps were created with a 60kHz IntraLase femtosecond laser (Abbott Medical Optics, Inc.). In Group B, the corneal flaps were created with a 200 kHz VisuMax femtosecond laser (Carl Zeiss Meditec AG). Attempted flap thickness for both lasers was between 90μm and 110 μm. The flap diameter was 8.7 mm in Group A and 7.9 mm in Group B. The limbus was marked at the slitlamp before the ablation to compensate for head position–related static cyclotorsional error. After femtosecond laser ablation, the patient was

transferred to the excimer laser for treatment. There was a 5-minute delay between flap creation and the transfer to the excimer laser. The corneal flap was marked in the usual manner and the eye tracker initiated. Iris recognition with the eye tracker was attempted 3 times, after which no further attempts were made in an effort to prevent further stromal dehydration and overcorrection. Eye tracking was considered a success if the eye movements could be followed during the LASIK procedure in the presence or absence of an OBL. Once the patient was under the eye tracker, the technician switched off the room lights and the aiming lights on the excimer laser; the eye tracker was then initiated. The cornea was kept hydrated to ensure good reflection of the tracking lights. The same laser technician initiated the eye tracker in all cases. After the initiation of eye tracking, the corneal flap was lifted in the usual manner and excimer ablation performed (Zyoptix Tissue Saving). The mean target optical zone was 6.34 mm (range 6.00 to 6.50 mm). Postoperatively, patients were prescribed moxifloxacin hydrochloride 0.5% eyedrops (Vigamox) and dexamethasone 0.1% eyedrops (Maxidex) 4 times a day for 1 week. Artificial tears (Tears Naturale Free) were prescribed after surgery, and the dosage was adjusted based on the patient's symptoms.

3.2.3.5 QUESTIONNAIRE

Postoperatively, patients were asked to complete a standardized questionnaire about their intraoperative experiences, including light perception, ability to fixate, pain scores, and level of fear during the flap-making process. Surgeons reported their experiences and preferences while performing the surgery and described intraoperative and postoperative complications. The standardized questionnaire was modified from a previously published questionnaire comparing femtosecond laser flap creation and microkeratome flap creation in LASIK (47). The modification included additional

questions about intra-operative and postoperative pain.

Patients were asked a series of questions relating to each step of the LASIK procedure in each eye. The patients were masked to which femtosecond laser was used in each eye. Visual experience questions regarding blackout and the clarity of the focus light were asked in a yes or no format. The level of pain experienced at each step of the procedure was recorded on a linear scale of 0 to 10 (0=no pain; 10=worse pain imaginable). The level of fear at each step of the procedure was measured on a linear scale of 0 to 6 (0=no fear; 6=worse fear imaginable). All questions except the 4-hour postoperative level of pain were recorded on the day of surgery. Also, which eye patients preferred or whether they had no preference was recorded at the 1-day visit. The surgeon questionnaire comprised simple yes or no responses about complications recorded intraoperatively and 1 day, 1month, and 3months postoperatively. The occurrence of an opaque bubble layer (OBL) and difficulty lifting the flap were recorded on a linear scale of 1 to 4 (1=no difficulty; 4=extreme difficulty). A question asking whether the surgeon had preference or no preference for a particular femtosecond laser was asked on the day of surgery.

3.2.3.6 Statistical Analysis

RCT 1

Sample-size calculation was performed using previously published LASIK outcomes. The LASIK series, which is from the Singapore National Eye Centre, has shown an efficacy rate of 94% at 3 months and predictability of 75% within +/-0.50 D. Sample sizes of 41 in Group 1 and 41 in Group 2 were required to achieve 80% power to detect a non-inferiority in efficacy outcomes between the groups. The test statistic used was

the 2-sided t test with pooled variance. The significance level of the test was targeted at P<.0500. However, the recruitment number was increased to 45 in case patients dropped out of the study before the study ended. Data analysis was performed using SPSS for Windows software (version 15, SPSS, Inc.). Chi-square tests were used to compare results of categorical data. Paired t tests were used (continuous variables) for within-group and between-group comparisons. Statistical significance was defined as a P value less than 0.05. For the questionnaire data, a Bonferroni correction to account for the possibility of a type I error adjusted the significance level to less than 0.0019. The differences in clinical outcomes over time and between femtosecond platforms at various visits were analyzed with a mixed linear model, using the SPSS package (Version 17.0, IBM, Armonk, NY, USA). The dependent variables were corneal sensitivity, TBUT, Schirmer's test, and corneal staining, while fixed factors included visit, femtosecond laser, and level of myopia. The levels of myopia were defined as low myopia (<−6.00 D) and high myopia (>−6.00 D). The operating surgeon, patient age, and patient gender were included as covariates, to model their influence on each dependent variable. Pearson's correlations were performed, to identify significant interactions between refractive status and clinical measures. A significance level (alpha) of 0.05 was used.

RCT 2

Patients were allocated using a block randomization protocol because not all surgeons in the study were certified to use both femtosecond lasers. Patients presenting for LASIK assessment on Monday or Thursday were allocated to Group B. Those presenting on Tuesday or Wednesday were allocated to Group A. Eye tracking success was analyzed in both groups using a logistic regression analysis model for a univariate and multivariate analysis using the SPSS software (version 17, SPSS, Inc.). The

variables were eye tracking, femtosecond laser used, spherical and cylindrical errors, optical zone, mean rotational tracking degree, and flap-thickness values. A P value less than 0.05 was considered statistically significant. A power calculation using the 88% success rate reported in a previous study of the IntraLase laser with eye tracking showed that to attain an equivalence of 0.2 (20%) between the 2 femtosecond lasers, 42 eyes would be required in each group to have an 80% power for a significance level of 5%. Thus, the present study was powered to allow a 20% difference in tracking rate between the 2 femtosecond lasers. Because the tracking rate in the previous study was high, the study was powered to determine whether the 2 lasers were equivalent in their tracking. The sample size was sufficient to detect whether there was a more than 20% difference between the 2 lasers in tracking, which would mean the 2 lasers were not equivalent. This value was chosen because a difference greater than 20% was considered clinically significant.

3.3 RESULTS

3.3.1 IN VIVO REAL-TIME IOP VARIATION DURING LASIK FLAP CREATION

In vivo real-time IOP profiles were successfully measured intracamerally in all eyes of 13 rabbits during the different stages of LASIK flap creation using either the microkeratome or the femtosecond laser. Under either condition, we observed a steep rise in IOP levels throughout the surgery ($P < 0.001$). No complications were observed with the insertion of the catheter and the suction ring. No postoperative infections were documented. In the microkeratome group, the mean IOP before flap creation (baseline IOP) as measured with an intracameral catheter was 13.45 +/- 1.65 mm Hg, which

increased significantly up to 141.02 +/- 20.46 mm Hg during cutting. Pressure was maintained at a mean high value of 89.30 +/- 12.15 mm Hg until the suction was removed (Figure 3.3). In contrast, the femtosecond group showed a more stable and subtle increase in mean IOP values during the entire LASIK flap creation procedure (Figure 3.3).

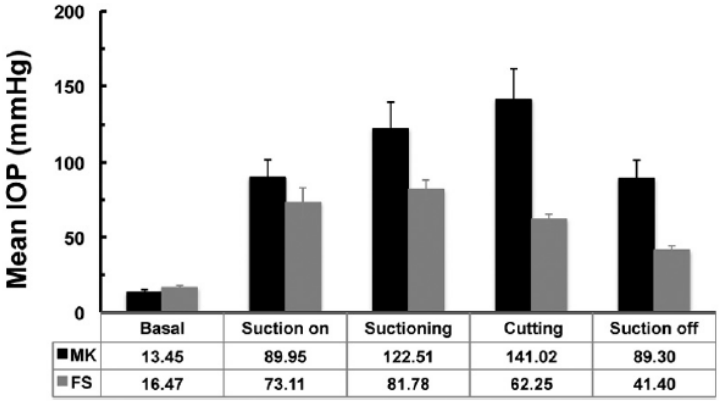

	Basal	Suction on	Suctioning	Cutting	Suction off
MK	13.45	89.95	122.51	141.02	89.30
FS	16.47	73.11	81.78	62.25	41.40

Figure 3.3 In vivo real-time mean IOP recorded during LASIK flap creation using a microkeratome mechanical blade (MK) or a femtosecond laser (FS). Mean IOP values obtained during various stages of surgery (mean ± SEM) (n=13). (Courtesy of Chaurasia et al. (161)).

Mean IOP values at baseline level and during the application of suction were 16.47 +/- 1.27 mm Hg and 73.11 +/- 10.0 mm Hg, respectively. During globe suction and cutting of the corneal flap, IOP levels remained steady (81.78 +/- 6.55 mm Hg and 62.25 +/- 3.28 mm Hg, respectively) and decreased to 41.40 +/- 2.99 mm Hg when the suction was removed. Although the two groups showed similar patterns of fluctuation in the IOP levels recorded in each stage of corneal flap creation, there were clear differences in several respects. Corneal flaps made with the microkeratome showed significantly higher IOP values at globe suction ($P = 0.035$), cutting ($P = 0.0009$), and suction off (P

= 0.0008) stages compared with the femtosecond group. The IOPs recorded in all animal eyes during the study—preoperative, globe suction, cutting, and suction off—in the microkeratome and femtosecond groups are depicted in Figures 3.4A and 3.4B.

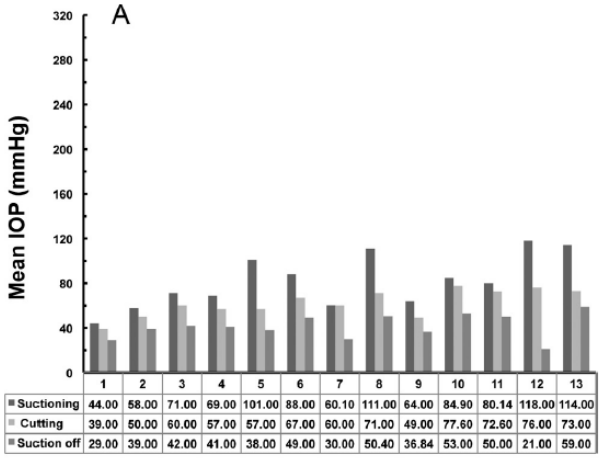

	1	2	3	4	5	6	7	8	9	10	11	12	13
Suctioning	44.00	58.00	71.00	69.00	101.00	88.00	60.10	111.00	64.00	84.90	80.14	118.00	114.00
Cutting	39.00	50.00	60.00	57.00	57.00	67.00	60.00	71.00	49.00	77.60	72.60	76.00	73.00
Suction off	29.00	39.00	42.00	41.00	38.00	49.00	30.00	50.40	36.84	53.00	50.00	21.00	59.00

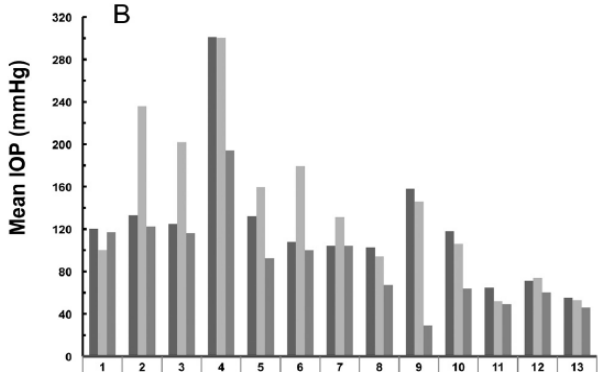

	1	2	3	4	5	6	7	8	9	10	11	12	13
Suctioning	120.00	132.93	125.00	301.00	131.94	108.00	104.00	102.70	158.00	118.00	65.00	71.00	55.00
Cutting	100.13	235.68	202.14	300.49	159.40	179.37	131.00	94.05	146.00	106.00	52.00	74.00	53.00
Suction off	117.00	122.30	116.00	194.13	92.30	100.00	104.00	67.14	29.00	64.00	49.00	60.00	46.00

Figure 3.4 In vivo real-time IOP recorded in all rabbit eyes during the various stages of LASIK flap creation – globe suction, cutting and suction using the A. Femtosecond laser and B. Microkeratome. Individual IOP data recorded from each animal are provided under the figure. (Courtesy of Chaurasia et al. (161)).

Individual IOP changes observed from application of the suction ring to the end of the flap creation ranged from 34 to 53 to 100 to 179 mm Hg in the microkeratome group compared with 21 to 76 to 49 to 126mm Hg in the femtosecond group. The mean total

time required for the corneal flap procedure in the femtosecond group was 38 +/- 2 seconds, approximately two fold higher than the mean time of 19 +/- 2 seconds observed in the microkeratome group (P = 0.0001; Figure 3.5).

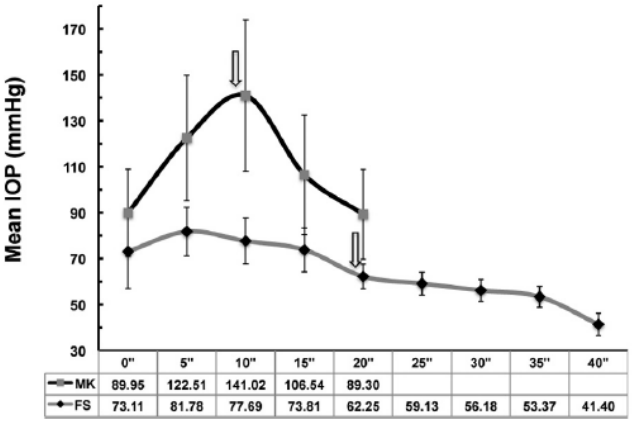

	0"	5"	10"	15"	20"	25"	30"	35"	40"
MK	89.95	122.51	141.02	106.54	89.30				
FS	73.11	81.78	77.69	73.81	62.25	59.13	56.18	53.37	41.40

Figure 3.5 In vivo real-time IOP recorded and time to complete LASIK flap creation using femtosecond laser (FS) and microkeratome (MK). Mean IOP values recorded during the procedure are shown under the figure. Arrows: time at which cutting started. Data are presented as mean +/- SEM (n=13). (Courtesy of Chaurasia et al. (161)).

The mean time required for globe suction was 19 +/- 2 seconds in the femtosecond group, approximately two fold higher than the 10 +/- 2 seconds observed in the microkeratome group (P =0.0009). Similarly, the mean time required for cutting was 19 +/- 2 seconds in the femtosecond group, approximately twofold higher than the 9 +/- 2 seconds observed in the microkeratome group (P = 0.0001).

3.3.2 Nanoscale Helium Ion Microscopic Analysis of Collagen Changes following Femtosecond Laser Dissection

3.3.2.1 Laser Effects

The HeIM images reveal arrays of periodic micro-sized pores resulting from FSL photodisruption, and that the nature of these disruption sites is dependent on the laser pulse and patterning parameters (Figure 3.6). The diameter of the holes correlated with the laser spot size expected from the respective laser/optical configurations, and the pore-to-pore spacing was consistent with the address grid defined by the pattern generator. The diameter of the pores found on IntraLase and VisuMax ablated surfaces was 2.2 +/- 0.73 μm and 0.9 +/- 0.27 μm ($p < 0.05$), respectively. The distance between two adjacent holes was 9.2 +/-1.63 μm on the IntraLase-ablated and 4.1+/- 0.13 μm on VisuMax-ablated corneas ($p < 0.05$). More detailed examination of the individual pores showed craters of irregular shape, which were mainly found on the IntraLase ablated stromal surfaces (Figure 3.6 A, D and G). In contrast, the spots appeared to be relatively annular on VisuMax ablated stromal surfaces (Figure 3.6 B, E and H).

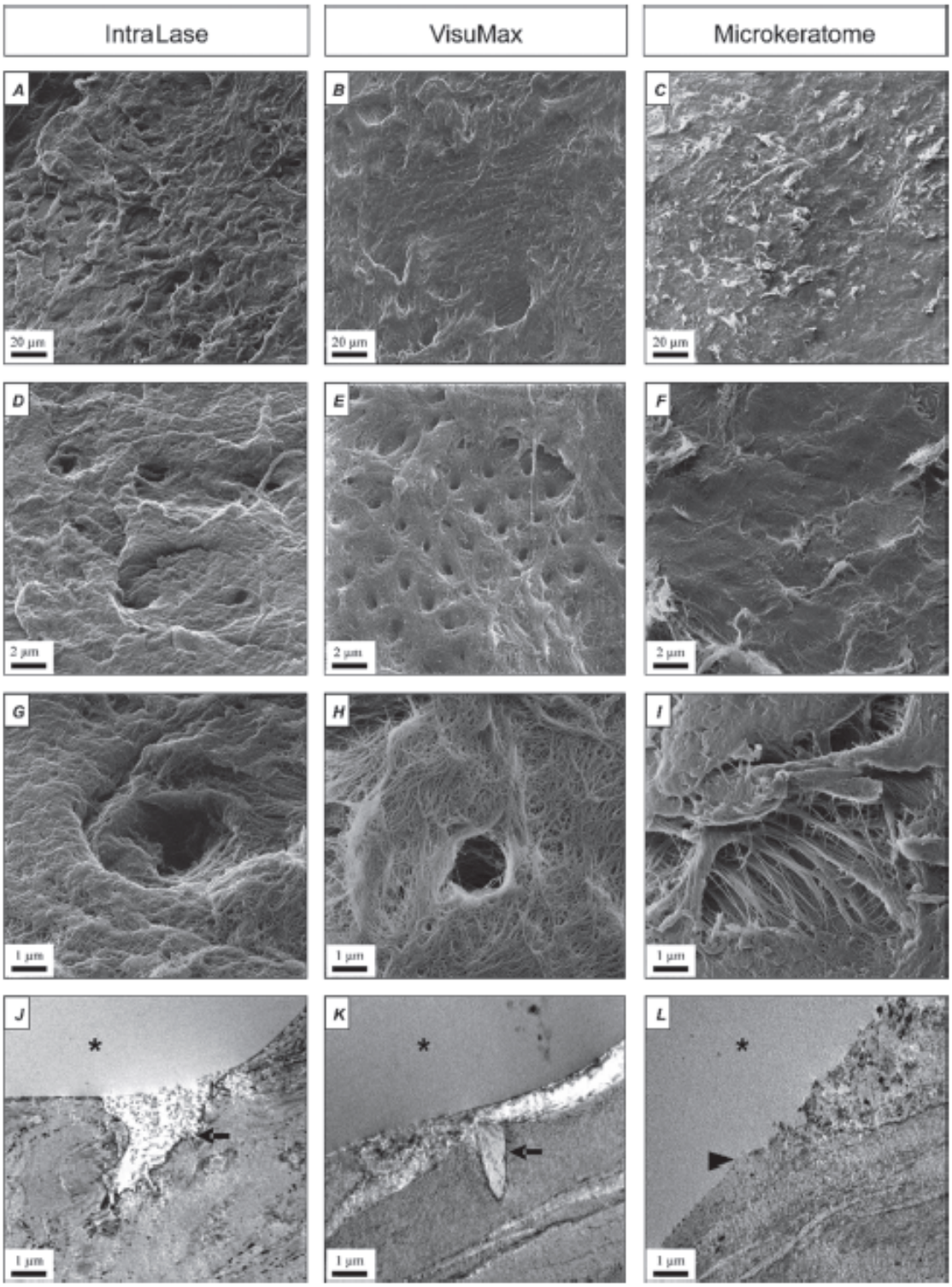
IntraLase
VisuMax
Microkeratome
A
B
C
20 µm
D
E
F
2 µm
G
H
I
1 µm
J
K
L
*
1 µm

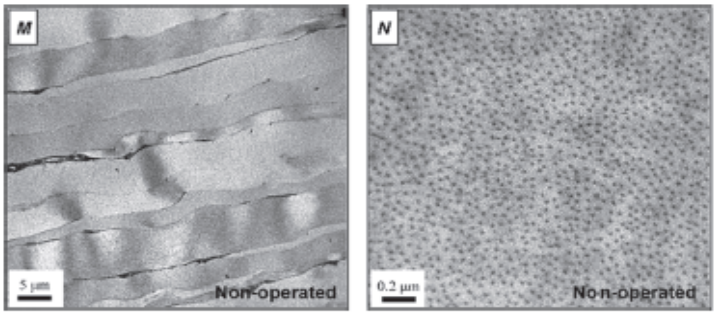

Figure 3.6 Laser etching in stromal tissue resulting from laser disruption. Scanning HeIM of stromal surfaces ablated with IntraLase (A, D, G), VisuMax (B, E, H) and microkeratome cut (C, F, I). At low magnification (A-C), femtosecond laser (FSL) ablation presented smoother bed morphology than microkeratome cut. Higher magnification revealed laser etching by the FSL in the form of arrays of periodic micro-sized pores which are absent on microkeratome cut surface (D, F). Examination of each micro-sized hole showed irregular crater by IntraLase (G) and relatively annulated perforation by VisuMax (H). Cross section morphology showed by TEM (J-L). A typical hollow conical cavity (arrows) was observed in corneas treated with IntraLase (J) and VisuMax (K), with an orifice opening into empty space (asterisks) at the dissection interface. No laser-etched spots were seen in the microkeratome cut (L). Normal cornea sections in M and N. (Courtesy of Riau et al. (162)).

TEM images of the cross section face along the FSL ablation and microkeratome cut were taken, and conical cavities were observed in corneas treated with both FSL platforms, with an orifice opening into empty space at the dissection interface and an apex embedded into the stroma. Each cavity was identified as a single laser-etched spot since the width of the orifice matched the laser spot size. Cavities found in IntraLase samples had structures with oblique angle (Figure 3.6 J) while VisuMax samples had symmetrical sides congruent to the apex (Figure 3.6 K). The length of the cavities was 4.05 +/- 0.97 μm and 2.25 +/- 0.46 μm for IntraLase and

VisuMax ($p < 0.05$), respectively. The microkeratome cut control samples lacked laser-etched cavities (Figure 3.6 C, F and I) as expected. As a comparison, at lower magnification, the non-operated corneal stroma featured orthogonally stacked lamellae, interspersed with quiescent keratocytes (Figure 3.6M). At higher magnification, the healthy corneal stroma presented collagen fibrils with uniform diameter and also highly uniform interfibrillar spaces (Figure 3.6N).

3.3.2.2 CAVITATION BUBBLES AND TISSUE BRIDGES

Topographical analysis showed an isolated laser-etched spot, enclosed in a bubble crater (Figure 3.7A). Cross section examination with TEM complementing the observation showed a cavitation bubble overlaying a laser-etched cavity (Figure 3.7B). The laser-etched cavity joined the overlaying cavitation bubble through an orifice (Figure 3.7C). Some laser etchings do not follow through to generate cavitation bubbles, rendering incomplete photodisruption. Size and shape of the laser-etched cavities and cavitation bubbles were observed to be highly variable.

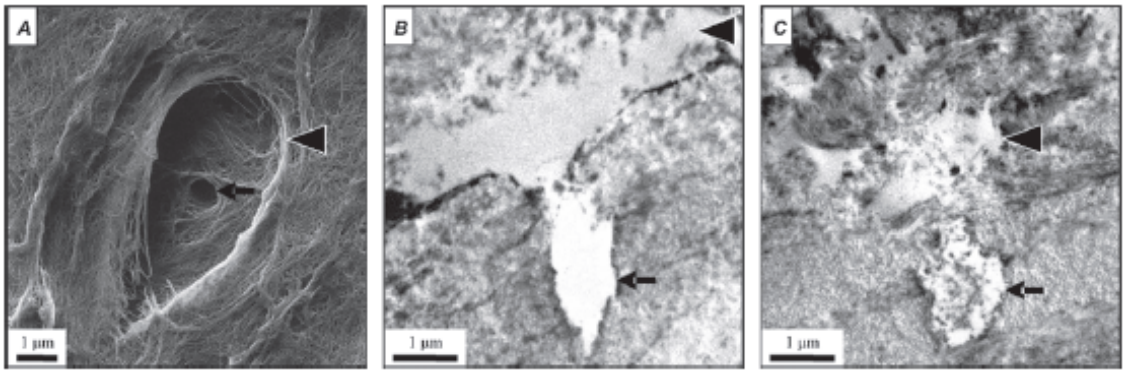

Figure 3.7 Laser effect created by VisuMax FSL system on corneal stromal tissue. Scanning HeIM (A) showing laser-etched spot (arrow) of approx. diameter 1 micron, enclosed in a bubble crater (arrowhead). Cross section examination by TEM imaging

(B), (C) found a cavitation bubble (arrowhead) overlaying the laser-etched cavity with approximate width of 1 micron. (Courtesy of Riau et al. (162).

Collateral damage around the laser-etched cavity was evidently less than that of the overlying cavitation bubble (Figure 3.7 B and C), which could result from the acoustic shock wave produced by the expansion and subsequent collapse of the cavitation bubble. Expansion of cavitation bubbles to separate stromal tissue was shown with histology and results from the scanning HeIM were complementary (Figure 3.8).

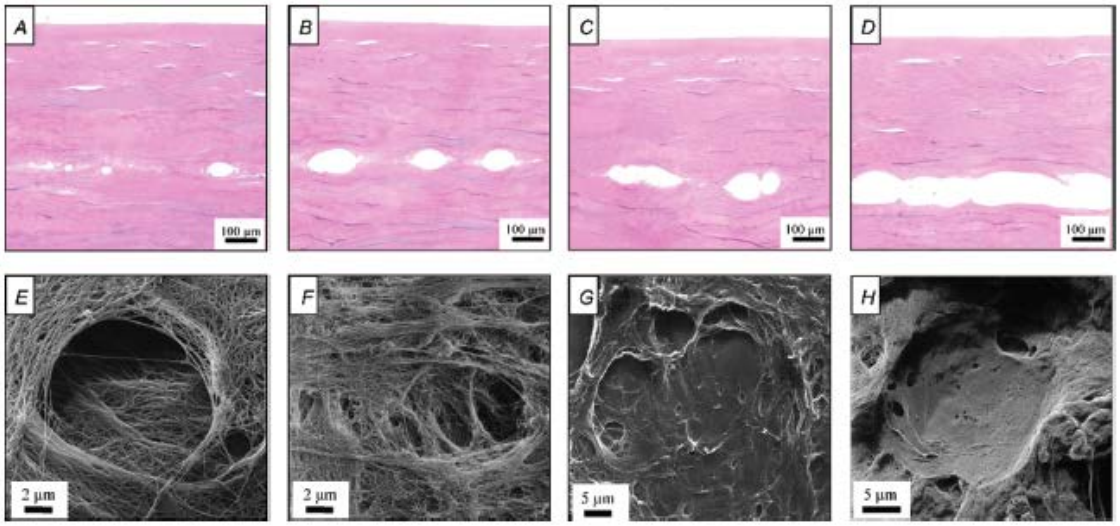

Figure 3.8 Expansion of cavitation bubbles separating corneal stroma tissue. Images are shown by histology (A-D) and scanning HeIM (E-H) examination. Micro-bubbles (A, E) of <5 microns were the smallest detected. The bubbles enlarged in size and moved in close proximity to adjacent bubbles (B, F). Adjacent bubbles had the propensity to coalesce with each other (C, G). A dissection plane was created when successive bubbles coalesce to form a single layer (D, H). (Courtesy of Riau et al. (162).

The smallest bubbles detected were ≤ 5 µm (Figure 3.8 A and E). The bubbles enlarged in size and moved in close proximity to adjacent bubbles (Figure 3.8 B and F).

Neighboring bubbles had the propensity to coalesce with each other (Figure 3.8 C and G). Successive coalescence of bubbles in a single layer creates a dissection in the tissue (Figure 3.8 D and H). We observed that cavitation bubbles near the edge of the ablation zone had a lower frequency of formation, were smaller in size, and existed as segregate bubbles, which did not undergo coalescence since no other bubbles were in the vicinity. Tissue bridges were identified on rough surfaces as loose tissue fragments that were prominent features on the topological landscape in the FSL-treated corneas (Figure 3.9 (A)).

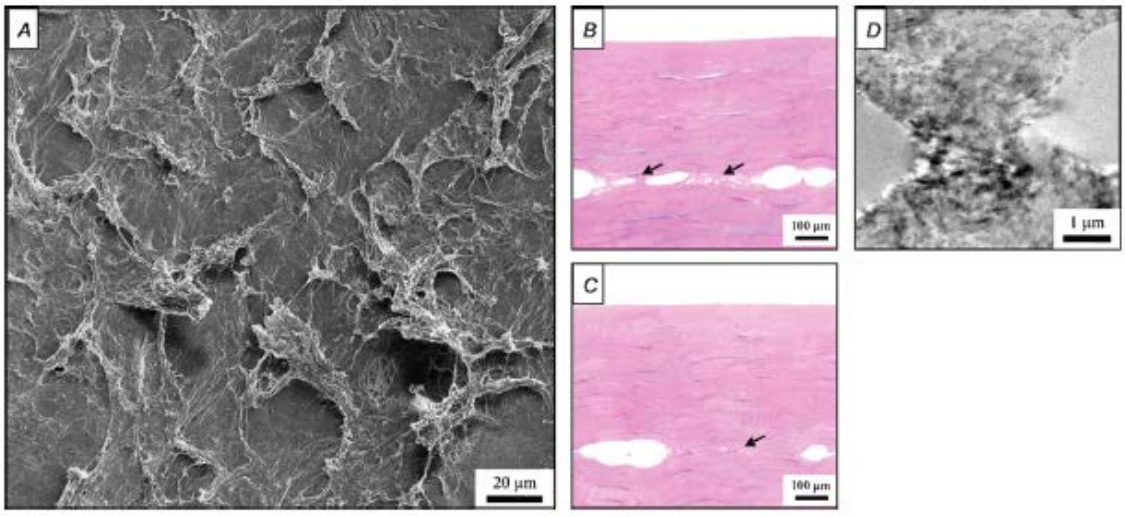

Figure 3.9 Tissue bridges identified on rough stromal bed surfaces. Tissue bridges viewed in scanning HeIM (A), and as incomplete ablation highlighted (arroes) in histology (B,C). TEM on regions of tissue bridges showed uncut stromal tissue between cavitation bubbles (D). (Courtesy of Riau et al. (162).

In histology, the tissue bridges appeared as incomplete dissection where discontinuity in the coalescence of cavitation bubbles occurred (Figure 3.9 B and C). TEM examination showed uncut stromal tissue between cavitation bubbles (Figure 3.9 D).

3.3.2.3 COLLATERAL DAMAGE

Using scanning HeIM, FSL-induced collateral damage to the collagen lamellae was studied (Figure 3.10). Collagen lattice morphology was classified as either intact or collapsed. Intact collagen lattice was found to be tightly packed in orthogonal layers (Figure 3.10 A and B) and tiny clumps of debris were found bound on the collagen fibres at higher magnification (Figure 3.10 B and C).

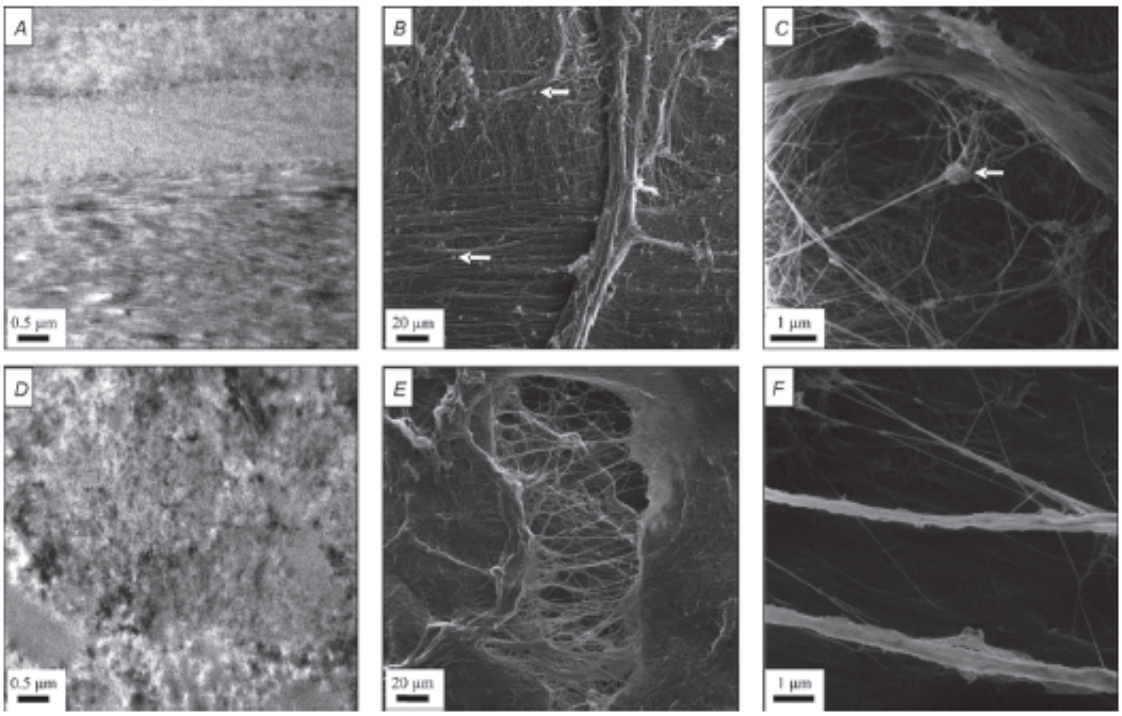

Figure 3.10 FSL induced collateral damage on collagen lamellae. Collagen lattice morphology on the femtosecond laser ablated surfaces can be identified as wither intact or collapsed. Intact collagen lattice shown in TEM (A) and HeIM (B) exhibited typical perpendicular layers. Clumps of debris (arrows) were seen bound on the fibres (B,C). Collapsed collagen lattice showed in TEM (D) and HeIM (E) was found to be disrupted. No banded appearance was see on fibres (E, F). (Courtesy of Riau et al. (162).

Collapsed collagen lattice presented as loosely connected fibres in a disarrayed network with more open spaces in between (Figure 3.10 D and E). We didn't observe any characteristic banded appearance of collagen fibres. Instead, the fibres presented an amorphous surface of irregular diameter (Figure 3.10 E and F). Debris of uniformly-shaped spherical structures was ubiquitously found attached to stromal collagen fibres (Figure 3.11 A).

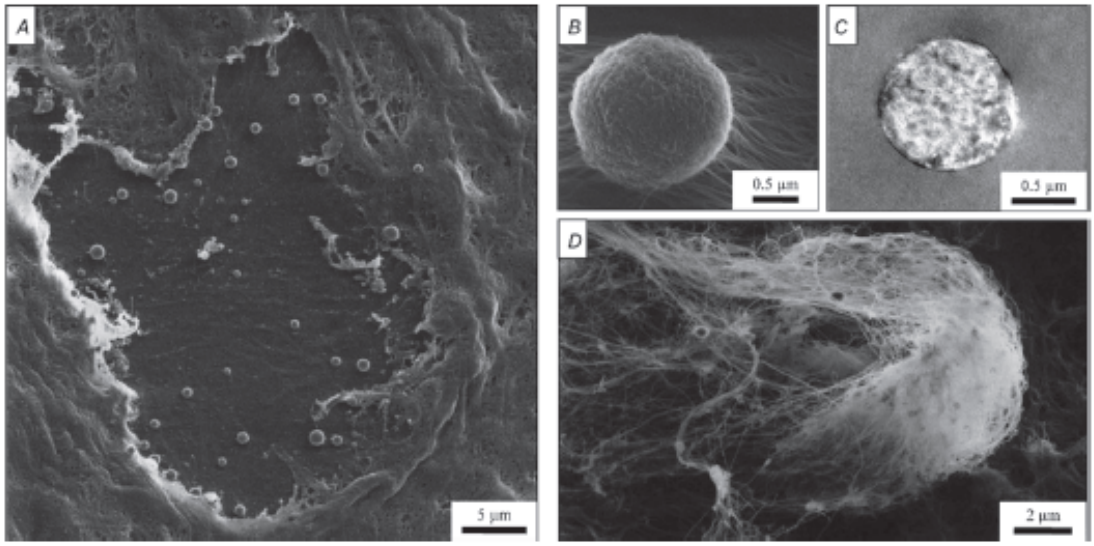

Figure 3.11 Spherical debris was found attached to stromal collagen fibres. Scanning HeIM at low magnification A, showing nano-sized spherical structures scattered on the FSL ablated surface, B at high magnification. TEM, C, demonstrated similar round structures. Masses of collagen fibres bundled up in a loop conformation were also observed in scanning HeIM, D. (Courtesy of Riau et al. (162).

The nano-sized spherical debris was measured at 0.41 µm +/- 0.15 in diameter. Rough texture of the spherical debris was observed under scanning HeIM (Figure 3.11 B). Similar structures that appeared to be composed of stromal material were seen in TEM

(Figure 3.11 C). Masses of collagen fibres bundled up in loop conformation were also observed in scanning HeIM (Figure 3.11 D).

3.3.3 Randomized Controlled Contralateral Eye Study Comparing IntraLase and VisuMax

3.3.3.1 Demographics

Forty-five patients participated in this study. The mean age of the patients was 29 years (range 22 to 39 years), and there were 25 women (55.6%). The preoperative SE in Group 1 and Group 2 was similar (Table 3.2). All 45 patients returned for the first-month postoperative review; 39 patients returned for the third-month postoperative review.

	Spherical Equivalent (D)		
Exam	Group 1	Group 2	*P* Value
Preop (n = 45)			
Mean ± SD	−4.94 ± 2.08	−4.91 ± 2.09	.940
Range	−9.75, −2.13	−11.25, −1.75	
1 mo postop (n = 45)			
Mean ± SD	0.28 ± 0.35	0.21 ± 0.43	.402
Range	−0.50, 1.13	−1.50, 1.00	
3 mo postop (n = 39)			
Mean ± SD	0.12 ± 0.43	0.15 ± 0.38	.729
Range	−1.25, 0.75	−1.00, 1.00	

Table 3.2 Comparison of preoperative and postoperative spherical equivalent refraction. (Courtesy of Rosman et al. (163)).

3.3.3.2 Efficacy

The mean postoperative SE 1 month and 3 months after femtosecond LASIK was similar in both groups (Table 3.2). Figure 3.12 shows the proportion of eyes and the

preoperative and postoperative UDVA. All eyes in both groups achieved a UDVA of 20/40 or better (P= 1.0) 3 months after femtosecond LASIK. At 3 months, 31 eyes (79.5%) in Group 1 and 32 eyes (82.1%) in Group 2 (P= 0.8 achieved a UDVA of 20/20 (Figure 3.12). The mean efficacy index (postoperative UDVA/preoperative CDVA) 1 month after surgery was 0.96 in Group 1 and 0.95 in Group 2 (P= .16). The mean efficacy index 3 months after surgery was 0.97 in Group 1 and 0.98 in Group 2 (P= .735).

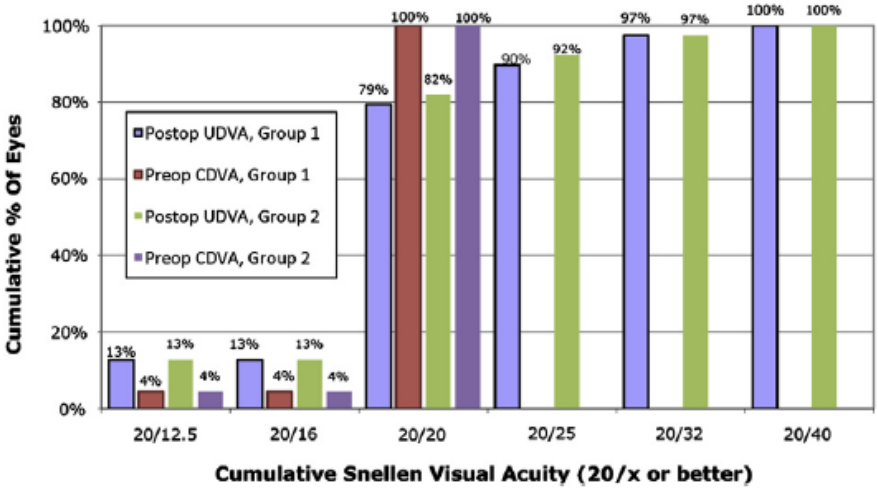

Figure 3.12 Comparison of preoperative and postoperative visual acuity (CDVA= corrected distance visual acuity; UDVA= uncorrected distance visual acuity). (Courtesy of Rosman et al. (163)).

3.3.3.3 PREDICTABILITY

One month after surgery, 45 eyes (100%) in Group 1 and 44 eyes (97.8%) in Group 2 (P= 1.0) were within +/- 1.00 D of emmetropia; 38 eyes (84.4%) and 39 eyes (86.7%), respectively, were within +/- 0.50 D of emmetropia (P= .764). Three months after surgery, 37 eyes (94.9%) in Group 1 and 39 eyes (100%) in Group 2 were within +/- 1.00 D of emmetropia (P= .494); 35 eyes (89.7%) and 33 eyes (84.6%) were within

+/- 0.50 D of emmetropia (P= .498) (Figure 3.13).

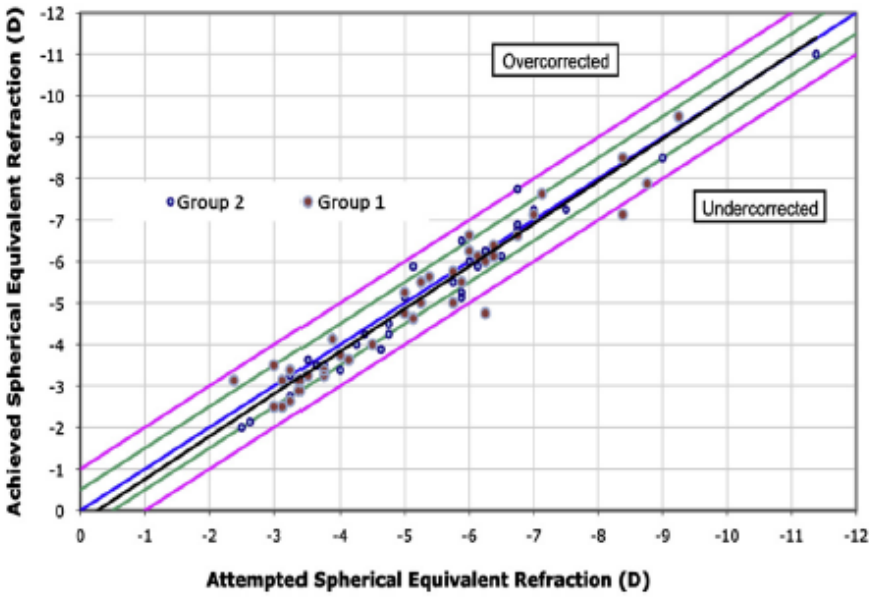

Figure 3.13 Comparison of achieved versus attempted SE at 3 months after surgery. (Courtesy of Rosman et al. (163)).

3.3.3.4 SAFETY

Figure 3.14 shows the change in the 3-month postoperative CDVA compared with the preoperative CDVA. No eye in either group lost more than 2 lines of CDVA. The proportion of eyes that lost 1 line of CDVA and those that gained 1 line of CDVA was similar in both groups. Three months postoperatively, the mean safety index was 1.11 in Group 1 and 1.10 in Group 2 (P= .570).

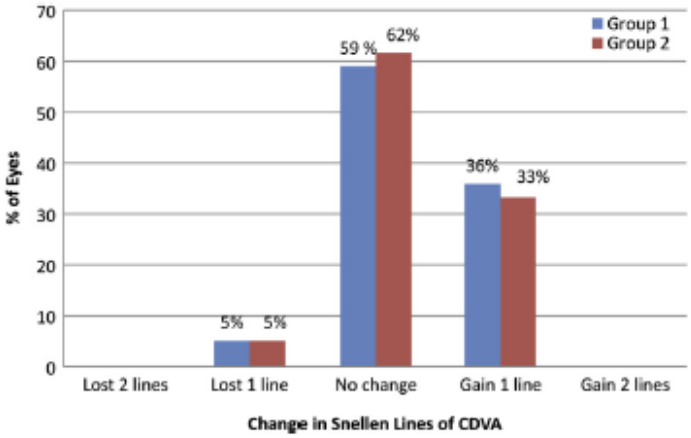

Figure 3.14 Change in CDVA 3 months postoperatively (Group1, 39 eyes; Group 2, 39 eyes) (CDVA =corrected distance visual acuity). (Courtesy of Rosman et al. (163)).

3.3.3.5 CONTRAST SENSITIVITY

The mean preoperative contrast sensitivity values under photopic and mesopic light conditions were similar in both groups. One month after surgery, there was an improvement in the mean photopic contrast sensitivity values at 1.5 cpd, 3.0 cpd, 6.0 cpd, 12.0 cpd, and 18.0 cpd in both groups (Table 3.3). Statistically significant improvements in the mean mesopic contrast sensitivity values were seen at 3.0 cpd, 6.0 cpd, and 12.0 cpd in both groups (Table 3.3 and Figure 3.15). The differences in the mean improvement in contrast sensitivity 1 month postoperatively between the 2 groups were not statistically significant (all P> .05).

Contrast Sensitivity	Group 1			Group 2		
	Preop	1 Mo Postop	*P* Value	Preop	1 Mo Postop	*P* Value
Photopic						
1.5 cpd	60.7 ± 5.9	62.1 ± 6.0	.030	66.5 ± 6.3	66.6 ± 6.2	.141
3.0 cpd	76.4 ± 6.6	96.8 ± 8.7	.264	78.4 ± 6.9	93.8 ± 8.4	.786
6.0 cpd	83.3 ± 7.2	126.9 ± 10.8	.064	92.5 ± 8.5	108.3 ± 9.0	.362
12.0 cpd	53.8 ± 6.3	67.7 ± 6.7	<.001	55.0 ± 5.6	64.6 ± 6.4	.078
18.0 cpd	20.7 ± 3.4	22.8 ± 3.5	.007	21.1 ± 3.1	21.8 ± 2.9	.145
Mesopic						
1.5 cpd	72.8 ± 6.4	63.6 ± 5.5	.297	70.0 ± 5.6	68.4 ± 5.8	.081
3.0 cpd	80.9 ± 7.8	79.6 ± 8.3	.015	83.4 ± 7.7	87.5 ± 8.9	<.001
6.0 cpd	67.3 ± 7.1	73.4 ± 8.2	.031	60.4 ± 6.9	86.5 ± 9.6	.012
12.0 cpd	27.8 ± 4.3	46.9 ± 8.1	<.001	26.0 ± 3.5	49.1 ± 6.7	.003
18.0 cpd	5.3 ± 0.8	6.8 ± 1.8	.002	6.8 ± 1.2	6.6 ± 1.0	.076

cpd = cycles per degree

Table 3.3 Preoperative and Postoperative contrast sensitivity values. (Courtesy of Rosman et al. (163)).

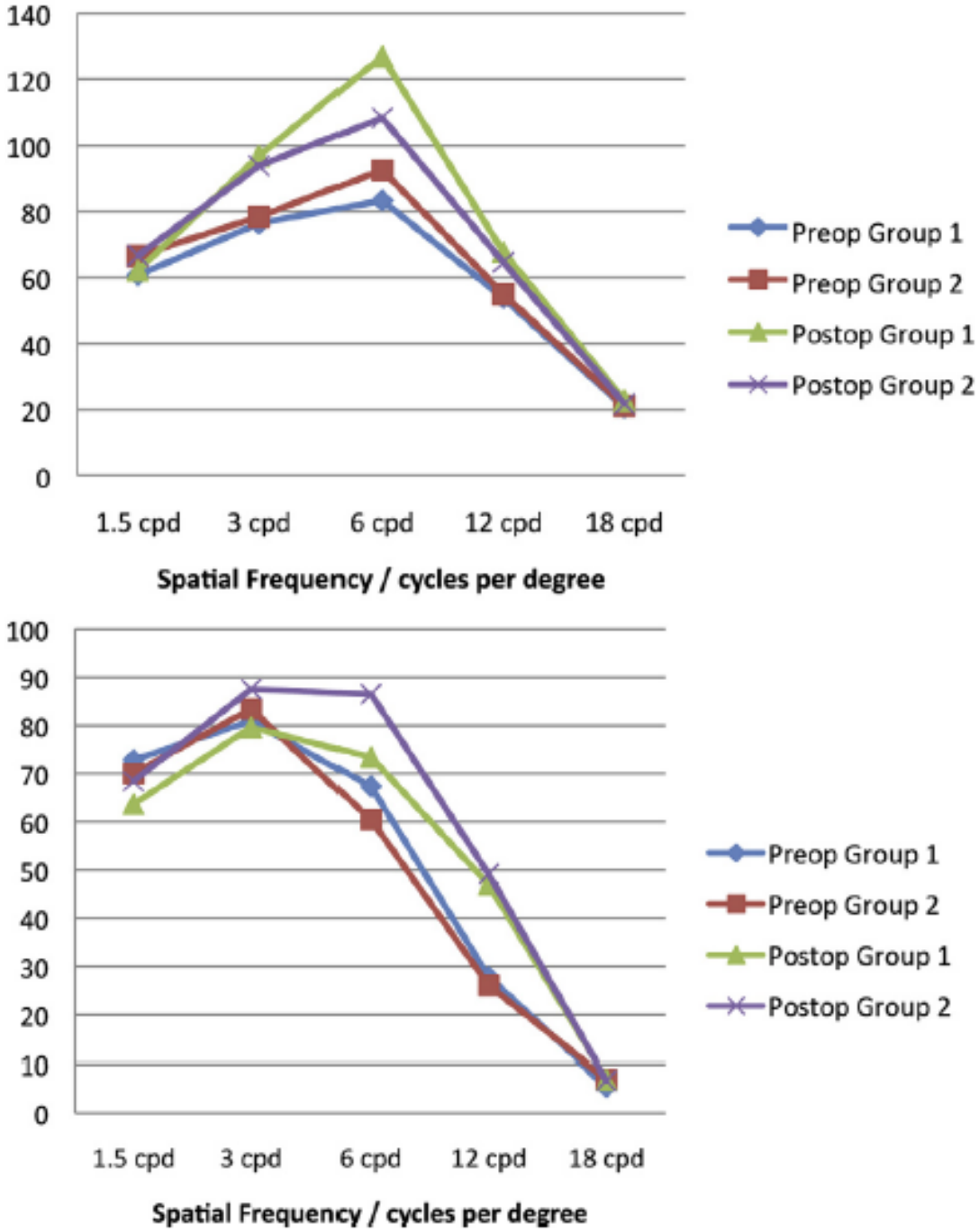

Figure 3.15 Top Preoperative versus 1 month postoperative photoptic contrast sensitivity. Bottom Preoperative versus 1 month postoperative mesopic contrast sensitivity. The y axis describes the contrast senstitivty defined as the reciprocal of the contrast at a measured threshold. (Courtesy of Rosman et al. (163)).

3.3.3.6 COMPLICATIONS

No major intraoperative or postoperative complications that might affect visual outcomes were seen. Intraoperatively, in Group 1, loss of suction occurred in 2 eyes (4.4%) during the femtosecond laser process during lamellar ablation before involvement of the visual axis. In both cases, the docking cones were reapplied and the femtosecond laser procedures were completed. A significant opaque bubble layer (OBL) was observed in 4 eyes (8.9%) in Group 1 and 1 eye (2.2%) in Group 2; however, the presence of the OBLs did not affect the outcomes of the surgery. Thirty-one eyes (68.9%) in Group 2 had a subconjunctival hemorrhage on the first postoperative day. No eye in Group 1 had subconjunctival hemorrhage. No eyes required repositioning of the LASIK flaps.

3.3.3.7. PATIENTS EXPERIENCE

Table 3.4 shows the patients' visual experience responses. Statistically significantly more patients lost perception of light during docking and suction and during laser flap creation with the 60 kHz laser than with the 500 kHz laser (both $P < .0001$). In addition, statistically significantly more patients saw the fixation light during the 500 kHz laser procedure than during the 60 kHz laser procedure ($P < .0001$).

Finding	Number/Total (%)		*P* Value
	60 kHz Laser	500 kHz Laser	
Docking blackout	23/46 (50.0)	0	<.0001
Laser flap creation blackout	29/46 (63.0)	0	<.0001
Focus light seen most procedure	16/46 (34.8)	42/46 (91.3)	<.0001
Focus light blurred throughout	16/24 (66.7)	11/31 (35.5)	.05
Focus light only blurred at end	5/20 (25.0)	31/37 (83.8)	<.0001
Focus light clear throughout	0	1/25 (4.0)	.82

Table 3.4 Patients' visual experience. (Courtesy of Hall et al. (164)).

The fixation light of the femtosecond laser was described as blurred by more patients during the 60 kHz laser procedure than during the 500 kHz laser procedure (P =.05). Significantly more patients described the fixation light as being clear for most of the procedure and blurred only at the end with the 500 kHz laser than with the 60 kHz laser.

Step	Mean ± SD		*P* Value
	60 kHz Laser	500 kHz laser	
Docking-suction	5.0 ± 3.5	1.8 ± 2.4	<.0001
Laser flap creation	3.6 ± 3.3	2.0 ± 2.5	.006
Flap lifting	2.3 ± 2.3	1.6 ± 1.9	.02
Postop 4 hours	3.3 ± 2.9	3.4 ± 3.1	.46

Table 3.5 Patients' pain scores (scale 0 to 10). (Courtesy of Hall et al. (164)).

Table 3.5 shows the differences in the pain scores between the 2 lasers. Statistically significantly more patients found the 60 kHz laser more painful during docking and suction (P < .0001), laser flap creation (P = .006), and flap lifting (P = .02). These were all significant. There was no statistically significant difference in pain scores 4 hours

postoperatively between the 2 lasers (P = .46). Patients described being more fearful during docking and suction with the 60 kHz laser than with the 500 kHz laser (P= .005) (Table 3.6). There was no statistically significant difference in the fear score for flap creation (P = .31), flap lifting (P = .43), laser ablation (P= .17), or flap placement (P = .04) between the 2 lasers (Table 3.6).

	Mean ± SD		
Step	60 kHz Laser	500 kHz laser	*P* Value
Docking–suction	4.4 ± 1.7	3.7 ± 1.8	.005
Blackout	3.0 ± 1.7	N/A	—
Laser flap creation	3.7 ± 1.5	3.8 ± 1.4	.31
Flap lifting	3.7 ± 1.6	3.8 ± 1.4	.44
Laser ablation	3.3 ± 1.8	3.7 ± 1.7	.17
Flap placement	2.3 ± 1.7	2.4 ± 1.7	.38

Table 3.6 Patients' subjective experience of fear (scale 0 to 6). (Courtesy of Hall et al. (164)).

3.3.3.8. SURGEON EXPERIENCE

There was no statistically significant difference in docking difficulties (P = 0.28), suction loss (P = 0.72), or significant OBL (P = 0.48) between the 60 kHz laser and the 500 kHz laser (Table 3.7).

	Number/Total (%)		
Complication	60 kHz Laser	500 kHz laser	*P* Value
Docking difficulty	6/46 (13.0)	0	.28
Suction loss	0	2/46 (4.3)	.72
OBL, significant	1/46 (2.2)	4/46 (8.7)	.48

OBL = opaque bubble layer

Table 3.7 Patients' pain scores (scale 0 to 10). (Courtesy of Hall et al. (164)).

There was also no statistically significant difference in difficulty of flap lifting (P =

.055) in the OBL area (P = .13) or the non-OBL areas (P = .07) between the 2 lasers (Table 3.8).

	Mean ± SD		
Area	60 kHz Laser	500 kHz laser	*P* Value
Non OBL	0.85 ± 0.6	1.02 ± 0.6	.07
OBL	0.52 ± 0.6	0.72 ± 0.8	.13
Overall	0.87 ± 0.5	1.10 ± 0.6	.055

OBL = opaque bubble layer

Table 3.8 Difficulty lifting flap reported by surgeon (grade 1 to 4). (Courtesy of Hall et al. (164)).

One day postoperatively, there were statistically significantly more subconjunctival hemorrhages after the 60 kHz laser procedure than after the 500 kHz laser procedure (P < .0001). There were no cases of chemosis in either laser group (P= .50). There was no statistically significant difference in flap striae (P = .43) or inflammation (P = .43) between the 2 lasers (Table 3.9).

	Number/Total (%)		
Complication	60 kHz Laser	500 kHz laser	*P* Value
Subconjunctival hemorrhage	31/46 (67.4)	1/46 (2.2)	<.0001
Striae	1/46 (2.2)	0	.43
Inflammation	2/46 (4.4)	1/46 (2.2)	.43

Table 3.9 One-day postoperative complications reported by surgeon. (Courtesy of Hall et al. (164)).

3.3.3.9. Patient and Surgeon Preference

Overall the patients preferred the surgical experience more with the 500 kHz laser than

with the 60 kHz laser (P < .0001). The surgeons preferred flap creation and flap lifting using the 60 kHz laser than using the 500 kHz laser (P < .0001) (Table 3.10). However, in more than 40% of cases, the surgeon had no preference for either femtosecond platform.

	Number/Total (%)		
Preference	60 kHz Laser	500 kHz laser	*P* Value
Patient	10/46 (21.7)	36/46 (78.3)	<.0001
Surgeon	23/46 (50.0)	4/46 (8.7)	<.0001

Table 3.10 Patient and surgeon laser preference. (Courtesy of Hall et al. (164)).

3.3.3.10. COMPLICATIONS

No major intraoperative or postoperative complications were observed in any eye. No relifting of the flap was required at any time postoperatively in either group. At the 1-month and 3-month follow-ups, no striae, diffuse lamellar keratitis, epithelial ingrowth, or other complications were observed in either group.

3.3.3.11. OCULAR SURFACE OUTCOMES

Corneal sensitivity following LASIK was not statistically different when both femtosecond platforms were compared (P =0.90). However, corneal sensitivity was dependent on preoperative levels of myopia (P < 0.001). The data was split into high and relatively low myopia. A trend towards greater reduction was observed in IntraLase-operated eyes, with myopia less than −6.00 D at the 1 month postoperative visit (P > 0.05) (Table 3.11).

Preop						1 month					3 months				
Level of myopia	Flap creation	Mean (cm)	95% CI		P	Mean (cm)	95% CI		Change to preop (%)	P	Mean (cm)	95% CI		Change to preop (%)	P
≥–6.00 D	VisuMax	5.9	4.9	6.9	0.434	3.5	2.4	4.6	–40.7	0.335	4.0	2.8	5.1	–32.3	0.468
	IntraLase	5.7	4.5	7.0		3.8	2.4	5.1	–34.3		3.2	1.8	4.6	–43.6	
	Eyes (n)	24				21					18				
<–6.00 D	VisuMax	5.9	5.5	6.3	0.086	5.3	4.9	5.8	–9.7	0.095	5.2	4.7	5.6	–12.5	0.107
	IntraLase	5.8	5.3	6.3		4.8	4.3	5.3	–17.1		4.9	4.4	5.4	–14.8	
	Eyes (n)	63				55					54				

Notes: Estimated mean of corneal sensitivity, lower and upper bound of 95% confidence interval. VisuMax (Carl Zeiss Meditec, Jena, Germany) and IntraLase™ (Abbott Medical Optics Inc, Santa Ana, CA, USA).
Abbreviations: LASIK, laser in situ keratomileusis; CI, confidence interval.

Table 3.11 Changes over time in corneal sensitivity following VisuMax or IntraLase LASIK. (Courtesy of Petznick et al. (165)).

Over time, corneal sensitivity was generally decreased for both techniques at 1 week ($P < 0.04$), 1 month ($P < 0.001$), and 3 months ($P < 0.001$) after surgery. The TBUT and Schirmer's values were significantly reduced at 1 week ($P < 0.05$), but there was no difference between the two femtosecond lasers at any visit ($P > 0.05$) (Tables 3.12 and 3.13).

Preop						1 week					1 month					3 months				
Level of myopia	Flap creation	Mean (sec)	95% CI		P	Mean (sec)	95% CI		Change to preop (%)	P	Mean (sec)	95% CI		Change to preop (%)	P	Mean (sec)	95% CI		Change to preop (%)	P
≥–6.00 D	VisuMax	10.1	8.8	11.4	0.318	8.3	5.8	10.9	–17.4	–	8.6	6.9	10.3	–14.8	–	10.2	8.6	11.9	+1.4	–
	IntraLase	9.5	7.9	11.1		5.3	2.3	8.3	–44.1		7.5	5.6	9.4	–20.8		8.2	5.9	10.4	–14.2	
	Eyes (n)	25				5					13					13				
<–6.00 D	VisuMax	10.5	9.1	11.9	0.377	8.8	6.5	11.0	–16.6	0.211	9.3	7.5	11.1	–11.6	0.981	8.8	7.0	10.6	–16.8	0.892
	IntraLase	10.2	8.9	11.4		7.5	5.9	9.2	–25.9		8.4	6.9	9.8	–17.7		8.0	6.6	9.5	–21.0	
	Eyes (n)	62				19					33					36				

Notes: Estimated mean of TBUT, lower and upper bound of 95% confidence interval. A statistical comparison using the linear mixed model adjusted for surgeon, age, and gender could not be performed for a level of myopia greater than –6.00 D due to small sample size.
Abbreviations: TBUT, tear film break up time; LASIK, laser in situ keratomileusis; CI, confidence interval; D, diopter.

Table 3.12 Reduction of TBUT following VisuMax and IntraLase LASIK. (Courtesy of Petznick et al. (165)).

Preop						1 week					1 month					3 months				
Level of myopia	Flap creation	Mean (cm)	95% CI		P	Mean (cm)	95% CI		Change to preop (%)	P	Mean (cm)	95% CI		Change to preop (%)	P	Mean (cm)	95% CI		Change to preop (%)	P
≥–6.00 D	VisuMax	11.3	7.6	15.0	0.577	8.8	5.1	12.5	–22.1	0.542	10.4	6.6	14.2	–7.8	0.464	10.1	6.1	14.1	–10.5	0.447
	IntraLase	11.7	6.6	16.9		9.2	3.9	14.5	–21.6		12.4	7.1	17.7	+5.8		9.4	3.9	14.8	–20.2	
	Eyes (n)	24				22					21					18				
<–6.00 D	VisuMax	15.2	12.2	18.3	0.316	12.4	9.4	15.3	–18.8	0.233	12.8	9.7	15.9	–16.0	0.956	12.7	9.5	15.9	–16.3	0.069
	IntraLase	13.7	11.0	16.4		10.7	8.0	13.4	–21.9		12.4	9.7	15.2	–9.0		13.7	10.9	16.6	+0.4	
	Eyes (n)	62				62					57					51				

Notes: Estimated mean of Schirmer's, lower and upper bound of 95% confidence interval. VisuMax (Carl Zeiss Meditec, Jena, Germany) and IntraLase™ (Abbott Medical Optics Inc, Santa Ana, CA, USA).
Abbreviations: LASIK, laser in situ keratomileusis; CI, confidence interval; D, diopter.

Table 3.13 Reduction of Schirmer's values following VisuMax and IntraLase LASIK. (Courtesy of Petznick et al. (165)).

Due to a low number of eyes, a statistical comparison for TBUT based on myopia could only be performed in eyes with myopia less than −6.00 D. A consistent, but not significant, tendency for lower TBUT values was observed with the IntraLase (P > 0.05) (Table 3.12). Although there was a general and significant increase in corneal staining after LASIK (P >0.05), the staining between both femtosecond lasers was not statistically different at any visit (P = 0.70) (Table 3.14).

Preop					1 week			1 month			3 months		
Level of myopia	Flap creation	Mean	SE	Incidence rate (%)	Mean	SE	Incidence rate (%)	Mean	SE	Incidence rate (%)	Mean	SE	Incidence rate (%)
≥–6.00 D	VisuMax	0.0	0.0	0	0.5	0.3	38.5	0.4	0.2	30.8	0.3	0.2	18.2
	IntraLase	0.1	0.1	8.3	0.6	0.3	16.7	0.3	0.2	25.0	0.2	0.2	20.0
	Eyes (n)	25			25			25			21		
<–6.00 D	VisuMax	0.0	0.0	3.2	0.7	0.2	35.5	0.1	0.1	6.5	0.2	0.1	21.4
	IntraLase	0.0	0.0	0	0.9	0.2	46.9	0.2	0.1	15.6	0.3	0.1	13.8
	Eyes (n)	65			65			65			57		

Notes: Estimated mean of corneal staining score ± standard error. VisuMax (Carl Zeiss Meditec, Jena, Germany) and IntraLase™ (Abbott Medical Optics Inc, Santa Ana, CA, USA).
Abbreviations: LASIK, laser in situ keratomileusis; SE, standard error; D, diopter.

Table 3.14 Changes over time in corneal fluorescein staining and incidence rates following VisuMax or IntraLase LASIK. (Courtesy of Petznick et al. (165)).

3.3.3.12. RCT2 - Eye Tracking Outcomes

The study enrolled 87 eyes (44 right) of 47 consecutive patients (44 women) with a mean age of 29.42 years (range 20 to 51 years). Preoperatively, the mean manifest sphere was - 5.64 +/- 2.17 D (mean +/-SD; range -9.75 to -0.25 D); the mean manifest

cylinder, 1.65 +/- 1.63 D (range -3.75 to 0.00 D); and the mean K value, 43.48 +/- 1.32 D (range 40.1 to 42.8 D). The mean estimated flap thickness was 109.30 +/- 5.21 μm (range 90 to 115 μm) and the mean optical zone, 6.34+/-0.20 mm (range 5.6 to 7.0 mm). Group A comprised 42 eyes, 38 (90.5%) of which were successfully tracked and 4 (9.5%) of which were not recognized by the eye tracker. The Group B comprised 45 eyes, 43 (95.6%) of which were successfully tracked and 2 (4.4%) of which were not recognized by the eye tracker. The mean intraoperative cyclotorsion movement was -0.40 +/- 3.78 degrees (range -12.00 to 6.50 degrees). Forty-two eyes had incyclotorsion (mean 0.41 +/- 2.91 degrees), and 45 eyes had excyclotorsion (mean 2.51 +/- 1.98 degrees). There was no statistically significant difference in induced torsion between the 2 femtosecond laser groups. The LASIK procedure could be completed in all eyes. Table 3.15 shows the patient data and femtosecond lasers' parameters in eyes with successful tracking and eyes that were not tracked.

			Sex (n)		Eye (n)			Mean (D)				FS Laser (n)			Mean	
Group	Eyes (n)	Mean Age (Y)	M	F	L	R	Pach (μm)	Sphere	Cylinder	OZ (mm)	Mean K (D)	A	B	Est Flap Thickness (μm)	Rotational Tracking (Degrees)	Ablation (μm)
Tracked	81	29.49	38	43	40	41	541	−5.75	−1.64	6.3	43.42	38	43	95	0.4	107.6
Not tracked	6	28.59	5	1	4	2	538	−4.23	−1.77	6.5	44.28	4	2	100	0.8	98
P value	—	.969	.126		.438		.853	.109	.769	.035	.160	.346		.113	.503	.408

Est = estimated; FS = femtosecond; K = keratometry; OZ = optical zone; Pach = pachymetry

Table 3.15 Patient data and femtosecond laser parameters FSL A IntraLase B Visumax. (Courtesy of Gimeno et al. (166)).

The mean magnitude (absolute value) of torsion was 1.02 +/- 3.51 degrees (range -10.5 to 5.6 degrees). In the tracked group, the mean UDVA was 20/200 preoperatively and 20/25 (P<.0001) 3 months postoperatively. In the non-tracked group, the mean UDVA was 20/150 and 20/25, respectively (P<.0001). There were no statistically significant differences in visual acuity between the 2 groups. There was no specific, consistent type of OBL formation with either laser (Figure 3.16).

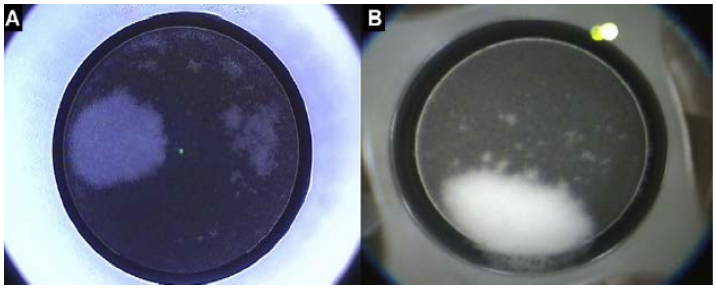

Figure 3.16 OBL after flap creation A. Eye in Group B B. Eye in group A. In both cases the central visual axis was not affected. (Courtesy of Gimeno et al. (166))

Two types of OBL were observed - a deeper (hard) OBL in the posterior or anterior stroma and a more diffuse OBL. The anterior hard OBL was associated with more difficult flap lifting. Despite the development of hard OBL, it did not interfere with the majority of subsequent iris tracking because of its position. The OBL tended to be in the midperipheral part of the cornea in Group B and in the superior flap, near the hinge, in Group A (Figure 3.16). Univariate analysis for the logistic regression model showed a significant correlation between positive tracking and a smaller optical zone (P= .03). The multivariate analysis did not, however, show statistically significant differences when the optical zone was analyzed in a model with age or sex.

3.4 DISCUSSION

During the entire surgical procedure of corneal flap creation, there was an initial surge in IOP levels as the suction ring was applied. A transient increase in IOP induced during globe suction deforms the anterior segment rapidly, which results in anterior-posterior compression and expansion of the globe. These events may cause extreme damage to the eye along the anterior-posterior axis. Complications including retinal

tears, (48) retinal detachments, (49, 50) optic neuropathy, (51) macular holes, (52) and choroidal neovascular membranes (53) have been reported. Nonarthritic ischemic optic neuropathy (54) and visual field loss (55) after LASIK have been attributed to the sudden surge in IOP levels caused by the suction ring placed during surgery.

The maximal IOP differences comparing the two groups were observed during the globe suction and cutting stages; the mechanical microkeratome group showed more than a twofold increase in IOP values than the femtosecond laser group, which theoretically would put eyes that have undergone microkeratome surgery at higher risk for the posterior segment complications described above. We also observed that the corneal flaps made with the femtosecond laser facilitated more stable and lower IOP than with the surge and irregular pattern observed in the microkeratome group.
Two previous studies have investigated the IOP changes during LASIK using animal (56) and human cadaveric eye (57) models. These studies had weaknesses in their designs and in their IOP measurement methods. First, they were performed on enucleated eyes, and IOP was achieved by infusion of a glycosylated solution. Second, the IOP measurements were made by inserting an intravenous pressure sensor into the vitreous cavity through a pars plana incision. Therefore, these studies did not represent actual IOP because the pressure was transmitted in a fluid-filled tube that was dependent on fluid viscosity and thus did not represent the true values based on IOP measured directly in the anterior chamber. Recently, Hernandez-Verdejo et al. (58) reported real-time measurement of IOP changes on enucleated porcine eyes during LASIK flap creation with a reusable blood pressure transducer connected to the anterior chamber by direct cannulation. Although this study added insight into IOP measurements during LASIK, it lacked the response of a living biological system in

vivo during surgery.

The mean procedure time required for globe suction and cutting by femtosecond laser was twice that required for the microkeratome-created flaps. The longer precut suction time can be attributed to the mechanism by which the femtosecond laser achieves suction and can vary depending on the contact between patient interface and corneal surface during surgery.

A limitation of our study was that we used a rabbit model instead of a primate model because the rabbit cornea is biomechanically more unstable and the anterior chamber is shallower than that of the human. (59) Hence, the rabbit cornea may be more susceptible to changes induced by raised IOP. The age of the rabbit will also have an effect on the biomechanical properties of the rabbit cornea. To minimize this effect, we performed a paired eye study so that the effects of age and biomechanical variation were minimized. The present study could have been strengthened if we had been able to make comparisons with other commercially available femtosecond lasers used for LASIK (e.g., Intralase [Abbott Medical Products, Abbott Park, IL], LDV [Ziemer, Port, Switzerland]). However, we did not have access to these lasers for animal experimentation, and the aim of our study was to examine the IOP variations in the new-generation, low-pressure femtosecond lasers.

Using HeIM and TEM, we were able to show the presence of laser etchings, which have cone-shaped structure on the stromal bed along the FSL incision plane. The pores formed arrays, precisely defined on a periodic grid. The creation of the cone-shaped pores was probably a direct result from collagen fibrillar damage caused by the

intense laser beam. At this stage, plasma formation need not be initiated. The laser ablation threshold for corneal collagen is much lower than the threshold of plasma formation. By measuring the depth of the pores from the stromal bed, we found that the IntraLase produced deeper pores than the VisuMax. Although the numerical aperture (NA) of the lens of both laser systems is not disclosed by either manufacturer, the resulting shallow pores are most likely due to the higher NA lens in the VisuMax system. The higher the numerical aperture, the more shallow the pore since the intensity to build up to plasma levels can be achieved in a shorter distance. Utilizing a higher NA laser system can therefore limit the depth of the corneal damage, which translates to a reduced incidence of opaque bubble layer, collateral thermal damage, vertical gas breakthrough and transient light sensitivity after photodisruption.

The higher-energy IntraLase produced greater spacing between spots and supposedly larger cavitation bubbles, because the expanding cavitation bubbles are the primary driving force in the tissue dissection process. However, overly wide spacing can result in excessive tissue bridges and difficulty in lifting the corneal flap. On the other hand, the lower-energy VisuMax laser uses substantially more spots that are smaller in volume and placed closer together because the plasma is the primary driver of the tissue dissection process. The dissection is further enhanced by the smaller cavitation bubbles as the secondary driving force of the cutting process. The advantage of using a low-energy, high-frequency laser system is twofold: First, the lower the total energy delivered to the cornea during the dissection, the less inflammation and cell death the laser would induce. Second, the smaller the cavitation bubbles, the smaller the area of damage inflicted on the surrounding collagen fibrils.

Complex applications of the FSL in corneal surgery, such as in ReLEx, requires accurate spot and line spacing in order to facilitate 3 dimensional cutting of the corneal stroma. After laser excitation, hot electrons and ions trapped proximal to the focal plane explosively expand out of the pore forming a cavitation bubble. Our work was limited to end point observations, but time-resolved imaging performed by other research groups substantiate our findings where they observed the formation of a laser ablation plume on water, gelatin and skin surfaces (60, 61). The ablation plume acquired a mushroom-like shape, exhibiting a ring vortex at its top, a thin stem with a diameter smaller than the ablation spot, and a radial flow component parallel to the surface at the foot of the plume.

The clumping, loss of banded appearance, and irregular diameter of the collagen fibres are most likely caused by the thermal changes generated during the photodisruption process. Using the HeIM, we have observed the abundant presence of spherical structures on the stromal bed. These spherical structures may be formed by the coiling of collagen fibres induced by the heat generated during the photodisruption process. HeIM offers many advantages over conventional SEM for imaging biological specimens. The higher image resolution is produced by the probe that can be focused to approximately 0.25 nm (62) and the much shorter de Broglie wavelength of helium ions (63). Its ability to image nonconductive samples without the application of a metal overcoat and without the need of a background gas has also proven to improve the resolution and hence surface detail. Sample damage is also minimized due to the relatively low mass of the helium ion, allowing the acquisition of real, unaltered information from the sample (64).

The results of femtosecond LASIK are comparable to those of microkeratome LASIK (62, 66–69). However, it has been shown that flaps created by the femtosecond laser are more planar and the thicknesses of the flaps are more consistent and predictable than flaps created with a microkeratome (70,71). The results of femtosecond LASIK in our study were better than the overall LASIK results published by our centre on data up to 2007 (72). In 2007, 72.8% of eyes that had LASIK at our centre achieved a UDVA of 20/20 compared with 79.5% in the Visumax group and 82.1% in the Intralase group in our present study. In 2007, 74.6% of eyes that had LASIK at our centre were within +/- 0.50D of the intended correction compared with 84.4% of eyes in the Visumax group and 86.7% in the Intralase group. The better results in our study compared with our centre's overall results in 2007 could be because the femtosecond LASIK procedures in our study were performed by only 3 LASIK surgeons with greater LASIK experience who were very familiar with the use of both laser platforms.

Blum et al. (73) reported that 91% of eyes that had femtosecond LASIK with the Visumax femtosecond laser platform and the MEL-80 excimer laser achieved a UDVA of 20/20 compared with 79.5% in the Visumax group in our study. The results of femtosecond LASIK with the Visumax femtosecond laser in both studies appear similar. We compared the results of Intralase femtosecond LASIK in our study with the 3-month results in a U.S. Food and Drug Administration (FDA) trial by Stonecipher et al. (74). In the FDA trial using the Intralase femtosecond laser and the Wavelight Allegretto excimer laser with wavefront optimized ablation profiles, 93% of eyes achieved a postoperative UDVA of 20/20 or better and 94% of eyes were within +/- 0.50 D of the intended refraction. The results of LASIK with the Intralase femtosecond laser and Allegretto excimer laser appear similar to the results in our study. Thus, our

study confirmed that femtosecond LASIK with the Intralase femtosecond laser or the Visumax femtosecond laser was efficacious and predictable.

Few studies report on contrast sensitivity after femtosecond LASIK. Fares et al. (75) found improvement in photopic and mesopic contrast sensitivities after LASIK with the Allegretto wave front optimized treatment profile. Chayet and Bains (76) report improvement in photopic and mesopic contrast sensitivities after LASIK with the Nidek CXIII excimer laser. In our study, there was an improvement in the mean 1-month postoperative photopic contrast sensitivity values at 1.5 cpd, 3.0 cpd, 6.0 cpd, 12.0 cpd, and 18.0 cpd in both femtosecond laser groups. However, the improvement was significant at 1.5 cpd (close at 6.0), 12.0 cpd, and 18.0 cpd in the Visumax group and was not significant in the Intralase group. There was also a significant improvement in the mean 1 month postoperative mesopic contrast sensitivity values at 6.0 cpd, 12.0 cpd, and 18.0 cpd in the Visumax group and at 3.0 cpd, 6.0 cpd, and 12.0 cpd in the Intralase group. Montes-Mico at el. (77) also found no significant difference in photopic contrast sensitivity values before and after femtosecond LASIK with the Intralase femtosecond laser. However, in their study, there was a significant reduction in mesopic contrast sensitivity at 12.0 cpd and 18.0 cpd. We believe this may be due to an increase in higher order aberrations after femtosecond LASIK because the optical zone was only 6.0mm and a plano scan ablation was performed with the Visx S2 laser system. In our study, the optical zone was 6.5 mm and a wavefront-optimized ablation profile was used. Another study by Reinstein et al. (78) found a statistical improvement in postoperative mesopic contrast sensitivity at 3.0 cpd and no statistical change at 6.0 cpd, 12.0 cpd, and 18.0 cpd after femtosecond LASIK with the Visumax system.

In our study, statistical analysis showed that the differences in mean improvement in contrast sensitivity 1 month after surgery between the Visumax group and Intralase group were not statistically significant. Thus, our study appears to show that femtosecond LASIK with either system results in similar effects on contrast sensitivity. One of the strengths of our study was that it was prospective and involved a comparison of contralateral eyes. As such, selection bias was greatly reduced and a smaller sample size was required. However, although the rest of the research staff (ie, those measuring visual acuity, refraction, and contrast sensitivity) were masked, it was impossible to mask the procedure from the operating surgeon. Despite the multiple differences between the Intralase and the Visumax femtosecond laser platforms, these differences did not affect the visual or refractive outcomes of femtosecond LASIK. These differences also did not affect the change in contrast sensitivity after LASIK.

We used a questionnaire to assess patient and surgeon experience after femtosecond laser flap creation with 2 platforms. The responses were evaluated for differences and preferences between the 2 femtosecond lasers. Loss of light perception occurred more frequently with the Intralase 60 kHz laser than with the Visumax 500 kHz laser during docking and suction and flap creation. This can be explained by the different corneal applanation and suction application techniques each femtosecond laser uses.

IOP in living eyes may be lower than in enucleated eyes at IOP values above the intraocular systolic blood pressure due to compensation mechanisms, such as choroidal compression and aqueous displacement (79, 80). When the IOP increases above 40mmHg or the ocular perfusion pressure decreases below 50 mm Hg, autoregulation is

overcome and can result in hypoxic optic nerve damage (81, 82). This approaches the estimated diastolic ophthalmic artery pressure, and Doppler sonography has found no central retinal artery blood flow during the suction phase of microkeratome use (M2, Moria) (83).

Patients found the steps of docking and suction and flap creation more painful with the 60 kHz laser than with the 500 kHz laser. Most patients (93%) were of Chinese ethnic origin and had small palpebral apertures. This may have contributed to their discomfort. Other steps of the procedure were comparable; 4 hours postoperatively, there was no difference in pain and discomfort between the 2 lasers. The increased perceived pain could again be explained by higher IOP and direct applanating force on the cornea during this part of the procedure. The fear perceived by patients was significantly higher with the 60 kHz laser during the docking and suction step and during visual blackout. The most frequent complication was subconjunctival hemorrhage, which occurred more often with the 60 kHz laser at 1 day.

More than three quarters of patients preferred LASIK with the 500 kHz laser; less than a quarter preferred the 60 kHz laser. Because of the visual experience with less frequent loss of vision and lower pain scores, it is no surprise that most patients preferred the 500 kHz laser treatment. All patients had a preference and did not perceive both eyes as being equal. Surgeons encountered less OBL and less suction loss with the 60 kHz laser but more docking difficulties with the 60 kHz laser than with the 500 kHz laser. Again, the docking difficulty may have been because most patients were of Chinese ethnic origin and had small palpebral apertures. We did not perform lateral cantholysis in any eye.

The difficulty lifting the flap was rated better with the 60 kHz laser than with the 500 kHz laser in the non-OBL area, in the OBL area, and overall. The difference was not statistically significant; however, a study with more patients may find a difference. This may explain why surgeons preferred the 60 kHz laser over the 500 kHz laser.

The limitations of our study include a possible bias resulting from the surgeons not being masked to each procedure; however, because the 2 machines have different footprints and are located in separate surgical rooms, this was unavoidable. Nursing staff and physicians administering the questionnaire were also not masked because the lasers are in different rooms and the questions were asked after completion of the laser ablation. The same staff member administered all questionnaires to all patients. As in any study using questionnaires, the data are subjective and different patients' perceptions to stimuli can vary. We minimized this with the randomization of each eye and keeping all steps of the procedure standard except the type of femtosecond laser used. The patients were also masked to which femtosecond laser was used, and the analysis of the data was masked. The strength of the study is that it was prospective, randomized, and clinical and used contralateral eyes.

We also assessed, whether newer femtosecond lasers have a greater potential to better preserve tear function. We assessed the effect of VisuMax- and IntraLase-created flaps for corneal sensitivity, tear function, and corneal health in myopic patients over a 3-month period. Results showed that both platforms were not statistically different in terms of clinical outcomes. However, a trend towards greater reduction of corneal sensitivity and TBUT was observed in IntraLase-treated eyes. Overall, a significant reduction in

corneal sensitivity following LASIK persisted for up to 3 months postoperatively, with a larger decrease noted in high myopic eyes. Furthermore, significantly diminished Schirmer's and TBUT values as well as increased corneal staining were recorded for up to 1 week postoperatively.

Naturally, the process of photoablation to correct the desired amount of myopia plays an important role, ie, a higher target correction of myopia required deeper ablation, thereby damaging more corneal nerves. In the current 3-month study, corneal sensitivity did not return to preoperative levels, which concurs with previous investigations that have demonstrated that nerve recovery may take as long as 6 months or even longer. The current study highlighted that a higher level of myopia, corresponding to greater ablation depth, negatively affected corneal sensitivity, which is in agreement with findings of previous studies. (84, 85) A higher amount of necessary correction reduced corneal sensitivity by up to 44%, while a lower amount of correction diminished sensitivity by about 17%.

It has been suggested that larger flap diameters may reduce sensitivity to a higher degree as a result of greater corneal nerve insult (86). A slightly greater, but not significant, loss of corneal sensitivity was noted in relatively low myopic IntraLase-treated eyes at 1 month postoperatively, which may have been derived from the larger flap size. The reason for this insignificant finding may be that the difference in flap diameter of 0.5 mm between both techniques was too small or that the sample size was not sufficient to show a significant effect. However, a similar finding was made in a study that compared eyes with femtosecond laser and microkeratome-created flaps. (87) In that study, the diameter of the microkeratome flaps was generally 0.4 mm larger. The study

did not find differences in sub-basal nerve density or corneal sensitivity between the larger microkeratome and the smaller femtosecond laser flaps (87). Truncation of corneal nerves during flap creation interrupts the neuronal feedback mechanism linking the lacrimal gland and cornea. As a consequence of corneal denervation, a reduction in tear secretion and dry eye symptoms may occur (88, 89). Most studies have confirmed this hypothesis and have reported diminished Schirmer's values for up to 1 week (90, 91) or even 6 months postoperatively (92-95).

The present study did not identify differences between the two femtosecond platforms, but found Schirmer's values that were generally lower 1 week following LASIK as compared with preoperative values. In contrast, some studies found little or no changes in Schirmer's values (89, 96, 97). The reason for this short-term decline in tear secretion is not clear. We observed a decrease in corneal sensitivity for up to 3 months postoperatively, which implies corneal denervation. It may be possible that peripheral and unaffected nerves compensated for the loss of some of the corneal sensation, thereby partially restoring function of the neuronal feedback loop and facilitating lubrication of the ocular surface.

Previous literature is inconsistent in regards to tear film stability following LASIK. It has been reported that TBUT was diminished in both microkeratome- and femtosecond laser–created flaps. (84, 92, 94, 95, 98, 99) Some authors found no significant changes in TBUT, (89, 97) while others noted a slight, but insignificant, increase in TBUT, in particular when using femtosecond lasers (90). The present findings showed that TBUT was significantly reduced 1 week after surgery. In relative contrast to earlier reports that noticed an increased TBUT, we detected TBUT values that appeared

to be slightly, but not significantly, lower in the IntraLase-treated eyes as compared with VisuMax. This finding may be explained by the different suction mechanisms used in both platforms. While the IntraLase system applies suction onto the sclera via a suction ring, the VisuMax system creates suction on the cornea via a curved contact glass. The high level of pressure induced by a suction ring onto the sclera has been shown to reduce the number of goblet cells in the bulbar conjunctiva (100). The tear film stability may therefore directly be affected by a compromised mucin layer, hence resulting in a slightly less stable tear film, as shown in the IntraLase-treated eyes of the current study.

In the present study, corneal staining was elevated at 1 week postoperatively and returned to baseline levels after 1 month. (97, 98) Some studies reported persistent corneal staining for up to 6 months, which may not be explained by a decrease in tear secretion. Specifically, Wilson (96) observed Rose Bengal staining patterns developing 1 to 3 months postoperatively that disappeared 6 months postoperatively, coinciding with the return of corneal sensation (101, 102). Furthermore, Wilson reported no changes in tear secretion, indicating that staining was not a result of decreased tear production (96). He suggested that punctate epithelial erosions after surgery may be attributed to neurotrophic epitheliopathy. Generally, we did not identify significant differences in corneal sensation, tear stability, or corneal health, between VisuMax and IntraLase.

There were a few limitations of the study. This present study was powered for refractive error outcomes, and the sample size may have been too low to show a statistical difference in ocular surface outcomes between the femtosecond laser platforms. Therefore, this study serves as a pilot study to appropriately calculate sample sizes for

future studies. The current study utilized 50-degree and 70-degree hinge angles for the VisuMax and IntraLase flaps, respectively. In our experience, optimal results for each platform have been achieved with the specified hinge angles. A different study tested the effect of 45-degree or 90-degree hinge angles on corneal sensitivity in femtosecond laser flaps, over a 12-month follow up period (97, 98). The authors concluded that overall, hinge position and hinge angles had no effect on corneal sensation and dry eye sensations. In the current study, however, VisuMax and IntraLase hinge angles differed by 20 degrees, an amount that is a lot smaller than the 45-degree difference employed by the previous study

3.5 SUMMARY

In conclusion our first study corroborates our clinical experience with the Carl Zeiss Meditec laser (VisuMax), during which patients do not experience a blackout in vision during flap creation. They are able to fixate for 90% of the procedure, indicating the pressure increase must be lower than the retinal arterial pressure. This is different from microkeratome flap creation in which patients experience a complete blackout. Our present findings suggest that further improvements and studies are required to evaluate the long-term impact of IOP spikes during LASIK, and they highlight the importance of in vivo real-time IOP measurements during developments to improve the safety of contemporary LASIK surgery.

The HeIM assisted observations of the detailed structural changes of collagen fibres induced by photodisruption have provided us important clues for understanding the extent of corneal collagen fibrillar damage on a nanoscale level. This will not only allow us to characterize finer structural details following laser corneal refractive

surgery, but also fine tune the future laser technology with an aim to minimize collateral damage to the collagen fibres and hence, producing better post-operative visual results.

Femtosecond LASIK with the Intralase and the Visumax femtosecond laser platforms were both efficacious and predictable. The majority of patients showed a preference for LASIK with the Visumax 500 kHz laser femtosecond laser. Because the Intralase 60 kHz laser applanates the cornea flat, causing significantly higher IOP that leads to vision loss and increased pain, it was the least preferred laser by patients. It is likely the vision loss and increased pain led to the greater patient fear with this laser. These differences were statistically significantly different. In contrast, the surgeons preferred the Intralase 60 kHz laser because they had less difficulty lifting the flap and there was less suction loss; however, there were more docking difficulties. These differences were not statistically different. The difference between the surgeons' preference and patients' preference is not unexpected given that the surgeons only expressed a preference in half the cases and were equally happy with both lasers in 41.3% of cases. The main reason for the surgeons' preference was the ease of flap lifting, which usually takes only a few seconds with either laser, and that under topical anesthesia, patients are unaware of differences in flap lifting between more adhesive flaps and less adhesive flaps.

Patient satisfaction outcomes at refractive centres are independent of visual acuity results (103, 104). Making LASIK more comfortable and less fearful, and the patient having a better cosmetic appearance 1 day postoperatively, can improve patient satisfaction. Future studies of patients' experiences, such as pain and discomfort, rather than only refractive outcomes would benefit patients who chose to have refractive

surgery.

The present study found that the VisuMax and IntraLase femtosecond lasers did not affect the ocular surface system in a significantly different manner. We noted an ablation depth-dependent reduction in corneal sensitivity that persisted up to 3 months after surgery as well as diminished tear secretion and increased corneal staining at 1 week postoperatively. These findings suggest that the choice of a suitable femtosecond laser for a patient may be based on the surgeon's preference rather than any differential potential to cause dry eyes. However, a trend towards slightly lower reductions in corneal sensitivity and TBUT were observed in the VisuMax-operated eyes, which may be attributed to improved technical specifications.

CHAPTER 4

4.0 REFRACTIVE LENTICULE EXTRACTION

4.1 INTRODUCTION

The VisuMax laser as mentioned in the previous chapter showed equivalent or better results to the IntraLase with respect to pre clinical and clinical outcomes. However, due to firing pattern of the laser, the curved iinterface, and the larger numerical aperture, the laser was also capable of being more accurate in 3-D than just 2-D. Hence the possibility existed of creating a 3D shape in the stroma. This allowed the development of a new refractive procedure called ReLEx – refractive lenticule extraction. The fundamental difference between ReLEx and LASIK is that in the former, only one femtosecond laser is used for the complete refractive treatment, and the 'by' product of the procedure is the refractive lenticule that is removed from the cornea. For any new refractive procedure, it is important to compare it to the 'gold standard' which we would consider is LASIK. This chapter outlines how the laser was optimised to create a lenticule shape and then our initial clinical trial prior to introducing the concept of reversible laser refractive surgery. ReLEx has two versions – FLEX where the lenticule is removed under a LASIK-like flap and SMILE where the lenticule is removed through a small incision.

4.2 METHODS

4.2.1 EFFECT OF DIFFERENT FIRING PATTERNS ON COLLAGEN DISRUPTION

Before undertaking lenticule creation in the cornea, it was important to understand the effects of different firing patterns on lenticule creation. In this study we examined the effects of different firing sequence on lenticule creation.

4.2.1.1 ANIMALS

Twelve- to 15-week-old New Zealand white rabbits (3 to 4 kg body weight) were housed under standard laboratory conditions. Animals were anesthetized with xylazine hydrochloride (5 mg/kg intramuscularly) and ketamine hydrochloride (50 mg/kg intramuscularly). The rabbits were killed humanely under anesthesia 24 hours after surgery by an overdose intracardiac injection of sodium pentobarbital. Corneas were excised from the globe and divided; 1 half was used for immunofluorescent staining and the other for TEM. All animals were treated according to the guidelines of the Association for Research in Vision and Ophthalmology's Statement for the Use of Animals in Ophthalmic and Vision Research. The protocol was approved by the Institutional Animal Care and Use Committee, SingHealth, Singapore.

4.2.1.2 SURGICAL TECHNIQUE

Refractive lenticule extraction was performed using the Visumax femtosecond laser; however, the flap was not lifted, as described previously. The laser energy delivered was slightly higher (175 nJ) than that used by Shah et al. (105) in their clinical study (160 nJ). All rabbits had a -6.00 diopter (D) correction performed in both eyes. Once the globe suction was applied, the main refractive and nonrefractive femtosecond incisions were performed. The animals were divided into 4 groups of eyes that had incisions created by the firing patterns shown in Table 4.1.

Pattern	Lenticule's Posterior Interface	Lenticule's Anterior Interface
A	Spiral in from the periphery to the center	Spiral out from the center to the periphery
B	Spiral out from the center to the periphery	Spiral out from the center to the periphery
C	Spiral in from the periphery to the center	Spiral in from the periphery to the center
D	Spiral out from the center to the periphery	Spiral in from the periphery to the center

Table 4.1 Different laser firing patterns tested in the study. (Courtesy of Riau et al. (167)).

Figure 4.1, A and B, show the laser firing patterns and snapshots of the procedure under the corneal suction cone, respectively.

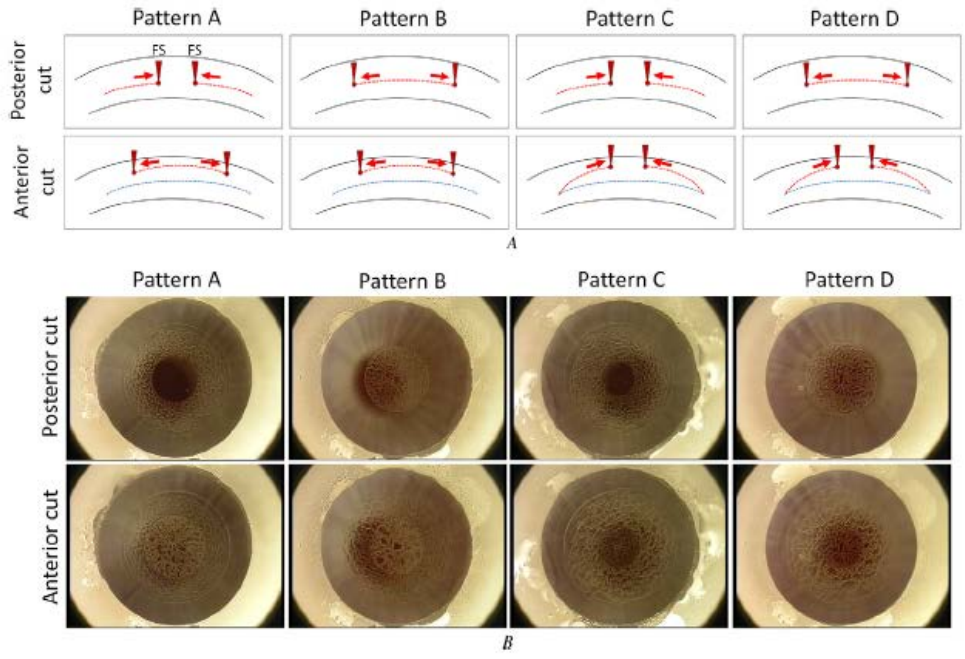

Figure 4.1 Tested laser-firing patterns during refractive lenticule extraction. A: The 4 laser-firing patterns. Pattern A: Laser was fired from the periphery in (lenticule's posterior surface) and from the centre out (lenticule's anterior surface). Pattern B: Laser was fired from the centre out and from the centre out. Pattern C: Laser was fired from

the periphery in and from the periphery in. Pattern D: Laser was fired from the centre out and from the periphery in. B: The corneas under the suction cone during the creation of posterior and anterior surfaces of the refractive lenticule (FS - femtosecond laser). (Courtesy of Riau et al. (167))

The femtosecond laser parameters were the same for all firing patterns: 120 μm flap thickness, 7.5 mm flap diameter, 175 nJ power for the lenticule, and 160 nJ for the flap, with side-cut angles at 90 degrees. The spot distance and tracking spacing were set at 3 μm/3 μm for the lenticule, 2 μm/2 μm for lenticule border, 3 μm /3 μm for the flap, and 2 μm/2 μm for the flap side cut. To study the effect of the femtosecond laser delivery on the stromal layers, the corneal flap was not lifted. Displacing the flap required manipulation of the corneal tissue and may have affected the roughness of the flap interface. In addition, it may have introduced other experimental variables, such as possible flap dislocation, epithelial ingrowth, inflammation, and microbial infection.

4.2.1.3 In Vivo Confocal Microscopy

In vivo confocal microscopy was performed 24 hours after surgery using the HRT3 retinal tomographer (Heidelberg Engineering GmbH). A carbomer gel (Vidisic, Mann Pharma) was used as the immersion fluid. All corneas were examined centrally with at least 3 z-axis scans through from epithelium to endothelium. In vivo confocal micrographs were analyzed with Heidelberg Eye Explorer software (version 1.5.1, Heidelberg Engineering GmbH). Semi-quantitative analysis of the reflectivity level of the lenticule's interface was performed by measuring the mean gray value of the reflective particles using Image J software (NIH, Bethesda, MD; available at http://rsb.info.nih.gov/ij/index.html).

4.2.1.4 Tissue Fixation and Sectioning

For immunofluorescent staining, corneas were embedded in optimum cutting temperature cryocompound (Leica Microsystems). Frozen tissue blocks were stored at -80°C until sectioning. Serial sagittal corneal sections (8 microns) were cut using a Microm HM550 cryostat. Sections were placed on polylysine-coated glass slides and air dried for 15 minutes.

4.2.1.5 Immunofluorescent Staining

Sections were fixed with 4% paraformaldehyde (Sigma-Aldrich Co.) for 15 minutes, washed with 1X phosphate buffered solution (PBS), blocked with 4% bovine serum albumin (Sigma-Aldrich Co.) in 1X PBS–0.15% Triton X-100 (Sigma-Aldrich Co.) for 1 hour, and incubated with mouse monoclonal antibody against cellular fibronectin (Millipore Corp.) diluted 1:400, mouse monoclonal antibody against CD11b (cluster of differentiation 11b; BD Pharmingen) diluted 1:100, or mouse monoclonal antibody against collagen type I (Sigma-Aldrich Co.) diluted 1:150 in the blocking solution at 4°C overnight. After being washed with 1X PBS, the sections were incubated with goat anti-mouse Alexa Fluor 488-conjugated secondary antibody (Invitrogen Corp.) diluted 1:1000 at room temperature for 1 hour. Slides were then mounted with Ultracruz mounting medium containing 40,6-Diamidino-2phenylindole, dihydrochloride (DAPI) (Santa Cruz Biotechnology). For negative controls, nonimmune serum was used in place of the specific primary antibody. Sections were viewed and imaged with an Axioplan 2 fluorescence microscope (Carl Zeiss Meditec AG).

4.2.1.6 Transmission Electron microscopy

A 1.5 mm x1.5 mm section was excised from the central cornea and fixed with a cold mixture of 2% paraformaldehyde and 2% glutaraldehyde in 0.1 M sodium cacodylate

buffer (pH 7.4) (Electron Microscopy Sciences) at 4°C overnight. Tissues were washed in sodium cacodylate buffer and rinsed with distilled water. Tissues were then postfixed in 1% osmium tetroxide and potassium ferrocyanide (Electron Microscopy Sciences) to enhance membrane contrast. After extensive rinsing with distilled water, tissues were dehydrated in an increasing concentration of ethanol and embedded in Araldite (Electron Microscopy Sciences). Ultrathin sections of 80 to 100 nm thickness were cut with Reichert-Jung Ultracut E Ultramicrotome (C. Reichert Optische Werke AG) and collected on copper grids, stained with uranyl acetate for 8 minutes, and then viewed and photographed using a JEM 1010 electron microscope (JEOL Ltd.) at 100 kV.

4.2.1.7 Statistical Analysis

Data are expressed as the mean ± standard deviation (SD). The P value was determined using the 2-tailed Student t test calculated using Excel 2007 software (Microsoft Corp.). Data were considered statistically significant if the P value was less than 0.05.

4.2.2 Early Wound Healing and Inflammatory Response after ReLEx

Following optimal lenticule creation, we wanted to examine the early inflammatory response in ReLEx compared to conventional refractive surgery i.e. LASIK. A rabbit model is the most commonly used for such studies.

4.2.2.1 Animals

Thirty-six 12- to 15-week-old New Zealand White rabbits (3– 4 kg body weight) were obtained from National University of Singapore and housed under standard laboratory conditions. Eighteen eyes from eighteen rabbits were subjected to ReLEx (group 1) or LASIK (group 2). The eye chosen for surgery was selected at random. Both groups

(ReLEx and LASIK) were divided into three subgroups consisting of six rabbits that underwent either - 3.00 D, -6.00 D or -9.00 D refractive corrections. In each subgroup, three contralateral eyes were used as unoperated controls and the other three contralateral eyes underwent ReLEx with the corneal flap left intact (not lifted). ReLEx with lenticule extraction and LASIK could not be performed in the same rabbit, since both eyes need a temporary tarsoorraphy after the procedure. Animals were anesthetized with xylazine hydrochloride (5 mg/kg intramuscularly; Troy Laboratories, Smithfield, Australia) and ketamine hydrochloride (50 mg/kg intramuscularly; Parnell Laboratories, Alexandria, Australia). The rabbits were euthanatized under anesthesia 1 day after the surgery by overdose intracardiac injection of sodium pentobarbital. All animals were treated according to the guidelines of the Association for Research in Vision and Ophthalmology Statement for the Use of Animals in Ophthalmic and Vision Research. The protocol was approved by the Institutional Animal Care and Use Committee of SingHealth.

4.2.2.2 Femtosecond LASIK Procedure

Our rabbit experimental model for LASIK was used as previously described in 3.2.1.2.

4.2.2.3 Refractive Lenticule Extraction (ReLEx)

ReLEx was performed using a femtosecond laser (Visumax; Carl Zeiss Meditec) as in 4.2.1.2 but using the optimal lenticule creation i.e. Pattern A. After completion of the laser sequence, a Siebel spatula was inserted under the flap near the hinge and the flap was lifted, the refractive lenticule was then grasped with forceps and extracted. The flap was then repositioned. A bandage contact lens was placed over the flap and the eyelid was closed with a temporary tarsorraphy. Three contralateral eyes in each group underwent the same ReLEx procedure using the settings as described, however the flaps

were not lifted and hence, no tarsorraphy was done.

4.2.2.4 Slit Lamp Photography, Optical Coherence Tomography and Corneal topography Refractive Lenticule Extraction (ReLEx)

Slit lamp photographs and anterior segment optical coherence tomography scans (AS-OCT) were captured before surgery and on Day 1 after surgery. Slit lamp photographs were taken with a zoom photo slit lamp (Nikon FS-3V; Nikon, Tokyo, Japan). Corneal cross-sectional visualization was performed using an AS-OCT (Visante; Carl Zeiss Meditec) and corneal topography was captured by using a hand-held videokeratographer (Oculus, Lynnwood, WA).

4.2.2.5 In Vivo Confocal microscopy

As described above 4.2.1.3.

4.2.2.6 Tissue Fixation and Sectioning

As described above 4.2.1.4.

4.2.2.7 Immunofluorescent Staining

Sections were fixed and incubated with either mouse monoclonal antibody against cellular fibronectin (Millipore, Billerica, MA) diluted 1:400, mouse monoclonal antibody against CD11b (BD Pharmingen, Franklin Lakes, NJ) diluted 1:100 in the blocking solution, or with prediluted mouse monoclonal antibody against Ki-67 (Invitrogen, Carlsbad, CA) at 4°C overnight. After washing with 1X PBS, the sections were incubated with goat anti-mouse Alexa Fluor 488-conjugated secondary antibody (Invitrogen) at room temperature for 1 hour. Slides were then mounted with medium

containing DAPI (UltraCruz Mounting Medium; Santa Cruz Biotechnology, Santa Cruz, CA). For negative controls, nonimmune serum was used in place of the specific primary antibody. Sections were observed and imaged with a fluorescence microscope (Zeiss Axioplan 2; Zeiss, Oberkochen, Germany). To detect apoptotic cells, a fluorescence-based TUNEL assay (In Situ Cell Death Detection Kit; Roche Applied Science, Indianapolis, IN) was used according to the manufacturer's instructions.

4.2.2.8 Statistical Analysis

Data were expressed as mean +/- standard deviation (SD) where appropriate. The P value was determined using the two-tailed Student's t-test (Excel 2007; Microsoft). Data were considered to be statistically significant when $P < 0.05$.

4.2.3 FLEx: Clinical Results, Interface Evaluation and IOP Variation

Following our initial animal studies we started a clinical trial. We also evaluated some of the critical steps of the procedure with further work on human cadaver eyes.

4.2.3.1 Prospective Clinical Study

We conducted a prospective, noncomparative clinical trial of FLEx at the Singapore National Eye Centre (SNEC) over a 10 month period in 2010. This study followed the principles of the Declaration of Helsinki, with ethics approval obtained from the SingHealth Institutional Review Board. Inclusion criteria for the study were as follows: spherical myopia between -1.00 diopters (D) and -9.00 D and myopic astigmatism less than 3.00 D; minimum age of 21 years, corneal thickness >500 μm with calculated residual stromal bed after treatment >300 μm; stable refractive error for 12 months

before surgery; normal peripheral retina or after prophylactic treatment with photocoagulation; with no previous ocular surgery, corneal diseases, glaucoma, or history of ocular trauma. Exclusion criteria were keratoconus or forme fruste keratoconus diagnosed on corneal topography; and active ocular or systemic diseases likely to affect corneal wound healing. Preoperative evaluations with a topographer (Orbscan II; Bausch & Lomb, Orbtek Inc., Salt Lake City, UT) and ultrasound pachymetry (AC Master; Carl Zeiss Meditec AG) were performed to exclude forme fruste keratoconus and other topographic abnormalities. After FLEx, all patients underwent postoperative examinations at 1 day, 1 week, 1 month, and 3 months after the initial procedure. We evaluated both uncorrected and best-corrected visual acuity (UCVA and BCVA) using a standard Snellen acuity chart at 6m; manifest refraction, slit-lamp biomicroscopy, fundoscopy, and cycloplegic refraction. Ocular wavefront analysis was performed pre and postoperatively at 3 months using an aberrometer system (Technolas Zywave with Zywave software version 4.45, ZYOPTIX Diagnostic Workstation; Bausch & Lomb). Patients' vision was evaluated by independent examiners at each follow-up. After application of topical anesthesia, standard sterile draping and insertion of the speculum, the patient's eye was centred and docked with the curved interface cone before application of suction fixation. The laser treatment started with the posterior surface of the refractive lenticule (spiral in) before the lenticule border was created. A vertical 15 μm lenticule side cut at the outer border of lamellar dissection was then created to outline the edge of the lenticule. The anterior surface of the refractive lenticule (spiral out) was then formed which extended beyond the posterior lenticule diameter by 0.5 mm to form the anterior flap, followed by a surface rim cut. We used the following FS laser parameters: 120 μm flap thickness, 7.5 mm flap diameter, 6.5 mm optical zone of lenticule, 145 nJ of power with side cut

angles at 90°. A superior hinge, 50 ° in chordal length, was made in all cases. The spot distance and tracking spacing were 3/3 μm for the lenticule, 2.5 /2.5 μm for the lenticule side cut, 3/3 μm for the flap, and 2/2 μm for the flap side cut. After the suction was released, a spatula (Seibel; Rhein Medical, Heidelberg, Germany) was inserted under the flap near the hinge before the flap was separated and reflected. The edge of the refractive lenticule was separated from the stromal bed with a Sinsky hook and the posterior border of the lenticule gently separated with the spatula (Seibel; Rhein Medical). The lenticule was then grasped with non-toothed serrated forceps and removed, after which the flap was repositioned. The postoperative regimen consisted of topical preservative-free dexamethasone and moxifloxacin, each four times a day for 1 week. Subsequently, only the lubricating drops were used up to 3 months as needed.

4.2.3.2 In Vivo Real-Time IOP Study

Forty female New Zealand White rabbits underwent FLEx procedure (40 eyes) and femtosecond flap creation (FS-LASIK) (40 eyes). We obtained approval from the SingHealth Institute Animal Care and Use Committee and all procedures were performed in accordance with the ARVO Statement for the Use of Animals in Ophthalmic and Vision Research. In vivo real-time IOP in the rabbit eyes was measured using a previously described and validated technique as in 3.2.1.3 for each procedure (FLEx see section 4.2.1.2 and FS-LASIK see section 3.2.1.2).

4.2.3.3 Ex Vivo Study of FLEx using Scanning Electron Microscopy

Human cadaveric corneas were used to study the ultrastructure of the corneal stromal bed and the posterior surface of the corneal flap. Human eyes stored in corneal storage medium (Optisol; Chiron Ophthalmics, Irvine, CA) were obtained from the Lions Eye

Bank (Tampa, FL); mean age, 60 +/-10 years (range, 48 to 74 years); death to tissue harvest time, 1 day; mean death to experiment time, 10 +/- 5 days (range, 5 to 17 days). We performed FLEx procedures on 12 human corneoscleral rims (JSM) using the VisuMax as described in 4.2.3.1. Briefly, the corneoscleral buttons were mounted on an artificial anterior chamber (ACC; Coronet Network Medical Products, Yorkshire, UK) that was attached to an infusion bottle via a three-way tap to maintain physiological pressure. The VisuMax FS laser was programmed for a refractive correction of three different magnitudes of myopia, treatment groups: A, <-5.0 D [n = 4]; B, > -5.00 D and <-9.00 D [n =4]; and C, >-9.0 D [n=4]. After lenticule extraction the residual stromal bed was immediately fixed overnight in a mixture of cold 2.0% glutaraldehyde, 2% paraformaldehyde, and 0.1 M sodium cocodylate buffer, pH 7.4 (Electron Microscopy Sciences, Fort Washington, PA) at 4°C. The tissues were then washed in buffer and secondarily fixed in 1% osmium tetroxide (Electron Microscopy Sciences) before being dehydrated, critical point dried, and mounted on SEM stubs. Specimens were sputter coated with 10 nm of gold and examined with a scanning electron microscope (JSM-5600; JEOL, Tokyo, Japan) at 10 kV. We used an established scoring system to evaluate the surface morphology of the stromal bed and corneal flap. Essentially, this was based on four criteria to evaluate the surface relief (two points), regularity of the surface structure (three points), extent of surface irregularities (three points), and the position of the irregular area (three points). The total score was 11 points with a higher score indicating a smoother surface, and images were scored at magnification x18 and x50. To reduce subjectivity, two independent observers (MA, JSM) graded the images in a masked fashion.

4.2.3.4 Statistical Analysis

Statistical analysis included descriptive statistics. Mean and SD were calculated for continuous variables; while frequency distribution and percentages were used for categorical variables. Comparisons between categorical variables were conducted by Fisher's exact test. One-way ANOVA was used for means. We compared the IOP variations and surface irregularity indices from each group using the Student's t-test, and intraclass correlation was used to compare interobserver agreement between graders. Alpha was set at a significance level of 5%. All analyses were performed using statistical software (STATA version 11; StataCorp LP, College Station, TX).

4.2.4 Comparison of Four Circle patterns for Flap Creation after SMILE

Having initiated our clinical ReLEx programme, we started to perform small incision lenticule extraction (SMILE) which is a small incision form of ReLEx. The issue with SMILE is that because there is no flap creation, enhancement following the procedure could be more problematic. In order to circumvent this issue we examined the possibility of converting the SMILE pocket to a flap.

4.2.4.1 Animals

Six 12- to 15-week-old New Zealand White rabbits (3 to 4 kg body weight) were divided into four groups consisting of 3 eyes each that underwent either Circle pattern A, B, C, or D**.** Temporary tarsorraphy was not performed in any eye after SMILE; hence, the procedure was performed bilaterally. Anesthesia, recovery from sedation, and euthanasia of the rabbits were performed as described previously. All animals were treated according to the guidelines of the Association for Research in Vision and Ophthalmology's Statement for the Use

of Animals in Ophthalmic and Vision Research. The protocol was approved by the Institutional Animal Care and Use Committee of SingHealth, Singapore.

4.2.4.2 RELEX SMILE PROCEDURE

SMILE was first performed using the VisuMax femtosecond laser system (Carl Zeiss Meditec). All rabbits underwent a -6.00 diopter (D) spherical correction. Once suction was applied, the main refractive and non-refractive femtosecond incisions were performed in the following automated sequence: the posterior surface of the lenticule (spiral in pattern) and the anterior surface of the lenticule (spiral out pattern), followed by a 3-mm vertical incision to the corneal surface placed superiorly. The diameter and depth of the cap were set at 7.5 mm and 120 microns, respectively. The diameter of the lenticule (equating to the optical zone) was 6.5 mm. This set-up resulted in a 0.5 mm-wide clearance zone on each side (zone between the circumference of corneal cap and optical zone). The following femtosecond laser parameters were used: 200 nJ power for lenticule, lenticule side cut, cap and cap side cut, and side cut angle of 90 degrees. The spot distance and tracking spacing were set at 3/3 microns for the lenticule, 2/2 micron for the lenticule side cut, 3/3 microns for the cap, and 2/2 microns for the cap side cut. Following completion of the laser sequence, a Seibel spatula (Rhein Medical Inc., Petersburg, FL) was inserted into the vertical pocket incision to access the lamellar plane of dissection. A proprietary lamellar dissector (Asico, Westmont, IL), which we designed for SMILE lamellar dissection, was used to separate first the anterior portion of the lenticule from the overlying stroma and then the posterior surface of the lenticule from the underlying stroma. Once the lenticule was free from both surfaces, a co-axial DSAEK forceps (Asico) was used to grasp the lenticule and

extract it from within the cornea. Finally, a 24-gauge cannula was used to flush the pocket insertion with balanced salt solution.

4.2.4.3 Flap Creation After SMILE

Flap creation was performed 28 days after the initial SMILE procedure in all rabbits, which allowed for sufficient corneal wound healing to occur prior to flap creation. Four different VisuMax Circle patterns were studied. The Circle option permits the creation of three basic components: lamellar ring, side cut with hinge, and junction cut (Figure 4.2). The user selectable femtosecond laser parameters (Figures 4.2B and 4.2C) to produce these three basic components are adjustable.

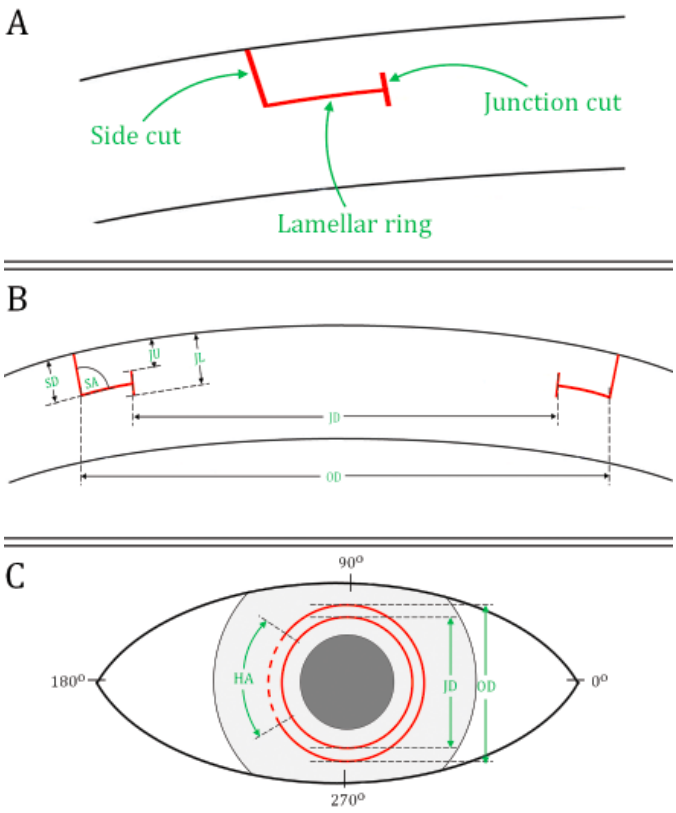

Figure 4.2 Illustrations of intrastromal incision permitted by VisuMax Circle option (Carl Zeiss Medited, Jena, Germany). A. The circle option permits the creation of three

basic components; a side cut with hinge, a lamellar ring and a junction cut. B. Cross-sectional view showing the adjustable femtosecond laser parameters to create the intrastromal incision. C. Front view showing the user-selectable parameters to create the intrastromal incision. OD= Outer diameter, JD= Junction diameter, SD= Side cut depth, SA= Side cut angle, HA= Hinge angle, JU = Junction upper depth, JL= Junction lower depth. (Courtesy of Riau et al. (170))

The laser energy level to perform the circle pattern has been preset by the manufacturer and therefore is not user adjustable. Pattern A creates a side cut to meet the cap cut within the clearance zone (outside of the optical zone); pattern B creates a lamellar ring posterior to the cap to meet the cap cut in the clearance zone with the help of a junction cut; pattern C produces a lamellar ring anterior to the cap to meet the cap cut in the clearance zone with the help of a junction cut; and pattern D creates a lamellar ring at the same depth as the cap to meet the cap cut in the clearance zone with the help of a junction cut. The cross-sectional and front views of the incisions are illustrated in Figure 4.3.

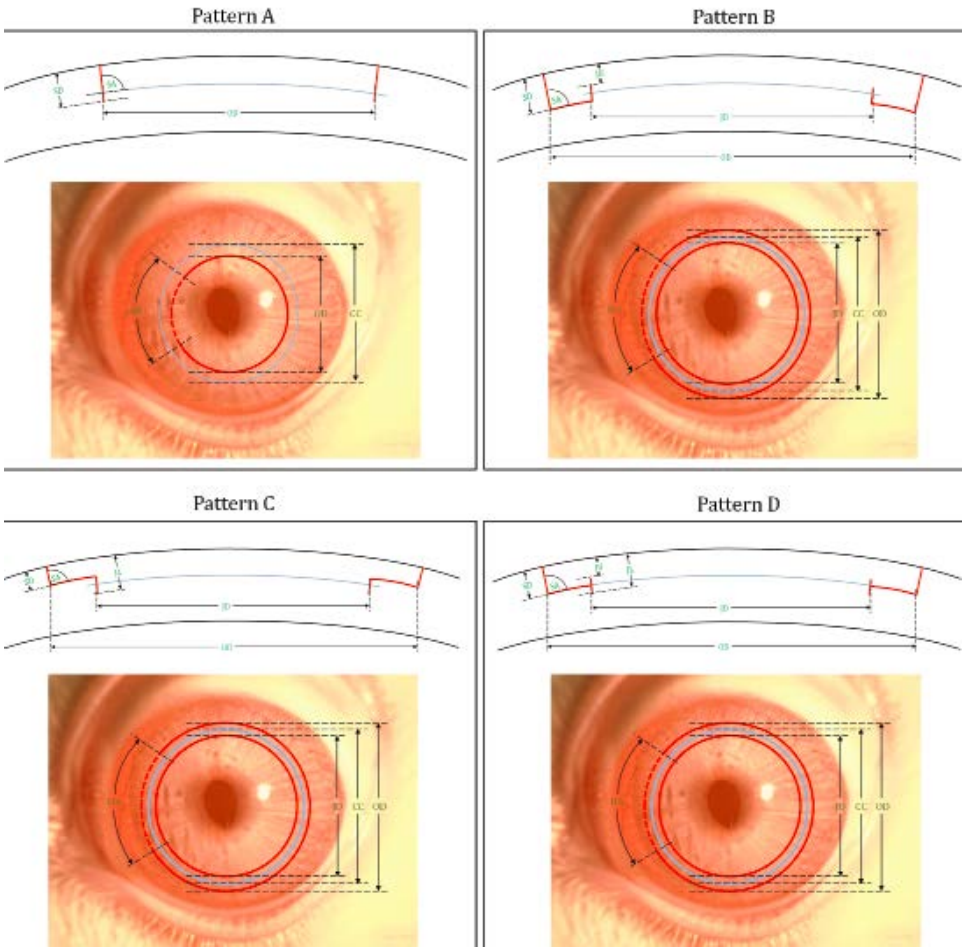

Figure 4.3 Illustrations of the tested VisuMax Circle patterns (Carl Zeiss Meditec, Jena, Germany) and the incision parameters selected for respective pattern. Pattern A creates a side cut within the cap cut (CC; in blue). Pattern B creates a lamellar ring posterior to the cap cut. Pattern C creates a lamellar ring anterior to the cap cut. Pattern D creates a lamellar ring adjacent to the cap cut. The parametric settings of the patterns tested in the current study can be found in Table 4.2. (OD = outer diameter; JD = junction diameter; SD = side cut depth; SA = side cut angle; HA = hinge angle; JU = junction upper depth; JL = junction lower depth). (Courtesy of Riau et al. (170))

	Lamellar and Side Cut				Junction Cut		
Pattern	Outer Diameter (mm)	Side Cut Depth (μm)	Side Cut Angle	Hinge Position	Junction Diameter (mm)	Junction Upper Depth (μm)	Junction Lower Depth (μm)
A	7.0	130	90°	Nasal	NA	NA	NA
B	7.9	130	90°	Nasal	7.0	100	NA
C	7.9	110	90°	Nasal	7.0	NA	130
D	7.9	120	90°	Nasal	7.0	100	130

NA = not applicable.

Table 4.2 Femtosecond Laser Parameters used in the VisuMax Circle patterns tested in the current study. (Courtesy of Riau et al. (170))

Following completion of the laser sequence and subsequent corneal imaging, a Sinskey hook (Rhein Medical Inc.) was used to create a small incision along the furrow of the flap side cut near the hinge. A Seibel spatula (Rhein Medical Inc.) was inserted under the flap edge through the incision to create access from the lamellar ring to the original cap-stromal bed interface. A lamellar dissector (Asico) was then inserted through the intrastromal tunnel to gently release the flap-bed and remaining flap-lamellar ring adhesions. A Seibel spatula was re-inserted under the flap, flap adhesions were released completely by sweeping under the flap, and the flap was finally lifted.

4.2.4.4 ASOCT AND CONFOCAL MICROSCOPY

AS-OCT was performed using the RTVue Fourier-domain OCT (Optovue, Fremont, CA) prior to flap creation to measure the depth of the laser resection. After the intrastromal circle incision was made and before the flap was lifted, the cross-section images of the side cut and lamellar ring were visualized. The depth of the lamellar ring was measured using standard measurement tools provided by the Optovue software. En-f8ace images of the side cut, lamellar ring, and junction cut were captured using an in vivo confocal microscope as

described above (section 4.2.1.3).

4.2.4.5 Scanning Electron Microscopy

After the flap was lifted and the rabbits were sacrificed, the cornea was excised from the whole globe. The quality of the exposed stromal bed was anlyzed by SEM. Corneas were fixed in 2% paraformaldehyde (Sigma, St. Louis, MO}, 2% glutaraldehyde (Sigma), and 0.1M sodium cacodylate (pH 7.4) overnight at 4°C. The corneas were then washed twice in distilled water for 10 minutes each before being immersed in 1% osmium tetraoxide (FMB, Singapore) for 2 hours at room temperature. Following this, the samples were dehydrated in 25%, 50%, 75%, 95%, and 100% ethanol, with 95% and 100% concentrations being performed twice. The samples were then dried in a critical point dryer (Bal-Tec, Balzers, Liechtenstein) and mounted on stubs using carbon adhesive tabs. They were then sputter coated with a 10nm thick layer of gold (Bal- Tec) and examined with a JSM-5600 scanning electron microscope (JEOL, Tokyo, Japan).

4.2.4.6 Grading of Difficulty of Flap Lift

Flap lifting was performed and graded by a senior corneal surgeon experienced in LASIK, SMILE, and anterior lamellar corneal transplantation surgery (JSM). The treatment groups were not masked from the surgeon when evaluating the difficulty of flap lift. The difficulty of flap lift was graded on a scale of 1 to 5: grade 1 was the easiest and similar to a microkeratome created flap lift, grade 2 was graded as similar to a normal femtosecond laser-created flap lift, grade 3 had at least two areas of adhesion, grade 4 had at least three areas, and grade 5 was the most difficult and almost impossible to lift flap, with a sticky

interface due to excessive remnant tissue bridges

4.2.5 Lenticule Viability and Integrity

One of the interesting facts about ReLEx was the fact that as opposed to LASIK, where the refractive tissue is vapourized, in ReLEx, the extracted refractive lenticule maybe used for other purposes. In order to establish its use the first point would be to understand the viability of the removed lenticule.

4.2.5.1 Human Cornea Samples

Twelve human cadaveric corneas stored in Optisol medium were obtained from the Lions Eye bank (Tampa, FL). The mean donor age was 60±10 years (range: 48–74); the death-to-tissue harvest time was 24 h or less in all cases and the mean time from death to surgery was 10±5 days (range: 5–17). All studies related to human tissues were approved by the Institutional Review Board of Singapore Eye Research Institute and Singapore National Eye Centre. The flow diagram for the detailed experimental plan is described in Table 4.3 below. Briefly, ReLEx-FLEx surgery was performed on 12 corneas with a −9.0 diopters spherical treatment and the extracted stromal lenticules divided into two groups of 6 lenticules each. One group was analyzed immediately after extraction (fresh group) and the other group was cryopreserved for a period of one month (cryopreserved group). Three lenticules from each group were used for cell culture to analyze gene expression of isolated cells using reverse transcription-polymerase chain reaction (RT–PCR). The three remaining lenticules from each group were subsequently cut into half. One half was used for transmission electron microscopy (TEM) and other was used for terminal deoxynucleotidyl transferase-

mediated nick end labeling (TUNEL) assay.

4.2.5.2 Refractive Lenticule Extraction (ReLEx) Procedure

ReLEx procedure (FLEx technique) was performed as described above 4.2.3.3. Briefly, the corneoscleral buttons were mounted on an artificial anterior chamber (AAC; Coronet Network Medical Products, Yorkshire, UK) and attached to an infusion bottle via a 3-way tap to maintain physiologic pressure. The edge of the refractive lenticule was separated from the stromal bed with a Sinsky hook and the posterior border of the lenticule gently separated with the Siebel spatula. The lenticule was grasped and removed with traumatic serrated forceps and the flap was repositioned. The extracted lenticule was either processed immediately or processed for cryopreservation (Table 4.3).

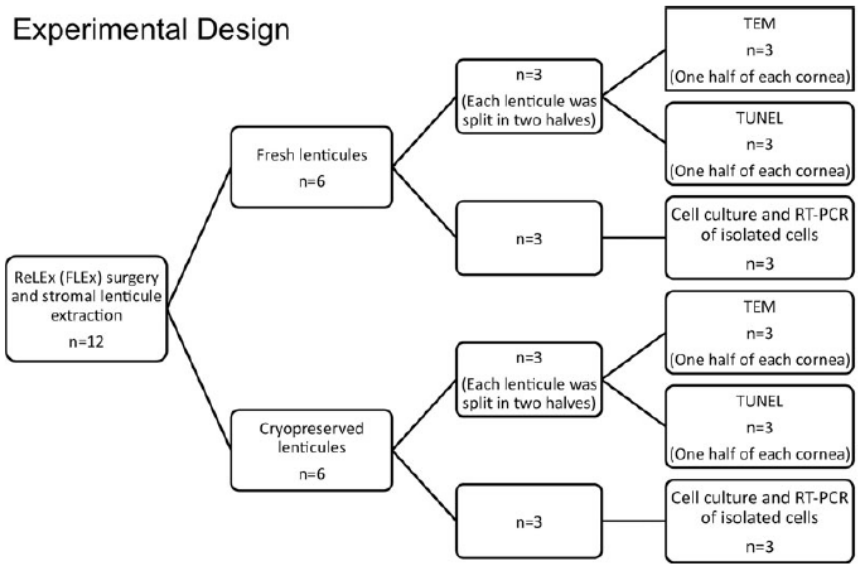

Table 4.3 Flow Diagram showing the experimental design. ReLEx: Refractive lenticule extraction. FLEx: Femtosecond lenticule extraction. Rt-PCR: reverse transcription-polymerase chain reaction. TEM: transmission electron microscopy. TUNEL: Deoxynucleotidyl transferase-mediated nick end labeling assay. (Courtesy of Noriega et

al. (171))

4.2.5.3 Cryopreservation and Thawing of Stromal Lenticules

Extracted lenticules were washed twice (10 min each) in a PBS buffered antibiotic/antimycotic solution. The lenticules were then transferred into a cryovial and resuspended in 500 µl medium containing 10% FBS. A stock freezing solution containing 10% FBS and 20% dimethyl sulfoxide (DMSO; Sigma, St. Louis, MO.) was added slowly in a drop wise manner to an equal volume ratio, to make a final volume of 1 ml freezing solution containing 10% FBS and 10% DMSO. Freezing of the cryovial containing the stromal lenticule was performed at a controlled cooling rate with a cryo-container ("Mr. Frosty"; Thermo Fisher Scientific, Roskilde, Denmark) in a −80 °C freezer overnight, and transferred into liquid nitrogen the following day for long-term storage (one month). After one month of cryopreservation, the vial containing the frozen stromal lenticule was rapidly thawed in a water bath at 37 °C and rinsed twice in a PBS solution to remove cryoprotectant agents. Thawed lenticules were either enzymatically digested for cell culture and gene expression or fixed for TEM analysis and TUNEL assay.

4.2.5.4 Ultrastructural Analysis – Transmission Electron Microscopy

TEM was performed in fresh (n=3) and cryopreserved (n=3) groups for the analysis of keratocyte viability and collagen architecture. The TEM procedure was as described in 4.2.1.6. To compare collagen fibril density (CFD) between fresh and cryopreserved groups, we analyzed for each group 3 randomly selected transversal section images of collagen fibrils at a magnification of 50,000×. Every image was analyzed with Image J software to obtain the number of collagen fibrils and the corresponding area fraction

(%) of the collagen fibrils to represent the CFD value.

4.2.5.5 Apoptosis Detection

TUNEL assay was performed on fresh (n=3) and cryopreserved (n=3) lenticules. The lenticules were immersed in an optimum cutting temperature (OCT) cryocompound (Leica Microsystems, Nussloch, Germany) and frozen at −80 °C until sectioning. Seven-micron thick sections were cut using a MicromHM550 cryostat (Microm, Walldorf, Germany). The TUNEL assay was performed according to manufacturer's instructions (In Situ Cell Death Detection Kit; Roche Applied Science, Indianapolis, IN). Slides were then mounted with UltraCruz mounting medium containing 4',6-diamidino-2-phenylindole (DAPI; Santa Cruz
Biotechnology, Santa Cruz, CA) for nuclear staining. Sections were observed and imaged with Zeiss Axioplan 2 fluorescence microscope (Carl Zeiss, Oberkochen, Germany). The positive TUNEL and DAPI stained cells were manually counted on the peripheral and central area of the lenticules in seven randomly selected fields of each sample using a magnification of 200×.

4.2.5.6 In Vitro Cell Viability

Cornea stroma lenticules of fresh (n=3) and cryopreserved (n=3) groups were washed twice in a phosphate-buffered saline (PBS), buffered antibiotic/antimycotic solution and enzymatically digested in serum supplemented culture medium containing collagenase A (2 mg/ml; Roche, Mannhein, Germany) for at least 2 h. Stromal keratocytes were rinsed twice and seeded onto cell culture dishes coated with Cell Attachment Reagent (FNC Coating Mix, BRFF AF-10; US Biologic, Swampscott, MA). The cells were cultured in Ham's F12 and M199 (1:1 ratio) medium supplemented with 5% fetal bovine serum (FBS; Invitrogen, Carlsbad, CA), 1× ITS (insulin, transferrin, selenium),

1× antibiotic/antimycotic (all from Invitrogen), 20 µg/ml ascorbic acid (Sigma), and 10 ng/ml bFGF (R&D Systems, Minneapolis, MN). Culture medium was refreshed every two days. All cultures and incubations were performed at 37 °C in a humidified incubator (Binder, Bohemia, NY) at 5% CO2.

4.2.5.7 Gene Expression Analysis

RT–PCR was performed for specific keratocyte markers on cells isolated from fresh and cryopreserved lenticules. Briefly, keratocytes were isolated immediately after washing twice (10 min each) with a PBS buffered antibiotic/antimycotic solution, supplemented with 5% FBS and digested with collagenase A (2 mg/ml; Roche) overnight. Cell pellets were rinsed once, snap frozen and stored at −80 °C before use. Total RNA was extracted using a RNeasy kit (Qiagen, Hilden, Germany) and the sample was treated with a DNase and purified using Turbo DNAfree (Ambion, Austin, TX) according to the manufacturers' instructions. The RNA sample was reverse-transcribed into cDNA using superscript first-strand synthesis system (Invitrogen). PCR was performed for the expression of human aldehyde dehydrogenase 3A1 (ALDH3A1) and Keratocan (KERA). For the ALDH3A1 gene the following primer was used: F=5′-ACT CAG CAG GAC GAG CTC TAC-3′, R=5′-GGG TCA CAG AGG ATG TAG TC-3′ (GenBank NM_001135168.1; Size: 495 bp) (106). For the KERA gene the following primer was used: F=5′-ATC TGCAGC ACC TTC ACC TT-3′, R=5′-CAT TGG AAT TGG TGG TTT GA-3′ (GenBank NM_007035; Size: 167 bp). PCR was performed alongside a ubiquitously expressed housekeeping gene, Glyceraldehyde 3-phosphate dehydrogenase (GAPDH) using the following primer: F=5′-GCC AAG GTC ATC CAT GAC AAC-3′, R=5′-GTC CAC CAC CCT GTT GCT GTA-3′ (GenBank NM_002046.3; Size: 498 bp). PCR reactions were performed on a thermal cycler

(C1000; Bio-Rad Laboratories, Hercules, CA) and followed denaturation at 94 °C for 30 s, primer annealing at 50–60 °C for 30 s, and template elongation at 72 °C for 1 min for 34 cycles, with a final template extension at 72 °C for 5 min. The annealing temperatures used were 58 °C, 52 °C, and 55 °C for ALDH3A1, KERA, and GAPDH primers, respectively. The PCR products were validated via gel electrophoresis on a 1% agarose gel stained with ethidium bromide, and visualized using a Kodak Image Station 4000R (Kodak, Rochester, NY) under ultraviolet light.

4.2.5.8 Statistical Analysis

All categorical data were analyzed by a two-tailed Pearson χ^2 test. Continuous data were analyzed by a two-tailed independent t -test. For same specimen stains, a binominal test was used to test whether it was equally proportioned. Statistics were performed in IBM SPSS v.19 (IBM Corporation, Armonk, NY) software program. Statistically significant data was consider when $P<0.05$.

4.2.6 Lenticule Re-Implantation Proof of Concept-Rabbit Study

Given that the lenticule showed viable cells both fresh and following cryopreservation, we subsequently experimented with the effect of re-implantation.

4.2.6.1 Animals

Six 12- to 15-week-old New Zealand White rabbits (3–4 kg in weight) were obtained from the National University of Singapore and housed under standard laboratory conditions. The rabbits underwent -6.00 D ReLEx (FLEx) correction in one eye that was selected at random. Contralateral eyes were used as unoperated controls. Extracted lenticules were stored at -80°C for 28 days, after which autologous re-implantation of

the stromal lenticule was performed. Animals were anesthetized with xylazine hydrochloride (5 mg/kg intramuscularly; Troy Laboratories, Smithfield, Australia) and ketamine hydrochloride (50 mg/kg intramuscularly; Parnell Laboratories, Alexandria, Australia) during both ReLEx (FLEx) and the re-implantation procedure. The rabbits were euthanized under anesthesia 28 days after the reimplantation procedure by overdose intracardiac injection of sodium pentobarbital. All animals were treated according to the guidelines of the ARVO Statement for the Use of Animals in Ophthalmic and Vision Research. The study protocol was approved by the Institutional Animal Care and Use Committee of SingHealth (Singapore).

4.2.6.2 Refractive Lenticule Extraction (FLEx)

Refractive Lenticule Extraction (FLEx) Procedure ReLEx (FLEx) was performed using the Visumax FSL as previously described in 4.2.2.3.

4.2.6.3 Storage and Re-Implantation of Stromal Lenticules

Stromal lenticules were carefully transferred on to rigid gas permeable (RGP) contact lenses (Bausch & Lomb) with careful attention to maintaining anatomical lenticular orientation. A marking at the 12 o'clock position was made on the RGP lens to indicate the corresponding anatomical position of the lenticule on the cornea before extraction. The contact lens was placed in a lens case and the well was filled with a stock freezing solution containing 10% fetal bovine serum (FBS; Sigma, St. Louis, MO) and 20% dimethyl sulfoxide (DMSO; Sigma). Freezing of the RGP and contact lens case containing the stromal lenticule was carried out at a controlled cooling rate within a cryocontainer (Mr. Frosty; Thermo Fisher Scientific, Roskilde, Denmark) in a -80°C freezer overnight, and transferred into liquid nitrogen the following day for long term

storage. The re-implantation of the lenticule was performed 28 days after the initial ReLEx (FLEx) procedure. The lenticule/RGP was allowed to warm to room temperature and then washed with balanced salt solution (BSS-Plus; Alcon, Forth Worth, TX). Rabbits were anesthetized and a Seibel spatula was inserted under the ReLEx (FLEx) flap near the hinge. Flap adhesions were released by sweeping under the flap and the flap was then lifted. The lenticule was transferred directly onto the exposed stromal bed by sliding it from the RGP contact lens. The 12 o'clock orientation of the lenticule on the stromal bed was carefully observed during re-implantation. The flap was then replaced and a bandage contact lens (Bausch & Lomb) was placed over the cornea and the eyelid was closed with a temporary tarsorrhaphy for 3 days. Gentamicin sulphate (40 mg/ml; Shin Poong Pharmaceutical, Seoul, South Korea) and Dexamethasone sodium phosphate (4 mg/ml; Hospira, Lake Forest, IL) of 1 mL each were injected subconjunctivally following the re-implantation procedure. Prednisolone acetate (1%; Allergan, Irvine, CA) and Tobramycin (0.3%; Alcon) drops were administered four times a day for 1 week.

4.2.6.4 Corneal Imaging: Slit Lamp Photography, ASOCT, Corneal Topography

Slit lamp photographs, corneal topography, and anterior segment optical coherence tomography (AS-OCT) scans were taken before ReLEx (FLEx), 28 days after ReLEx (FLEx), and at 3, 14, and 28 days after lenticule re-implantation. Slit lamp photographs were taken with a Zoom Slit Lamp NS-2D (Righton, Tokyo, Japan). Post re-implantation corneal clarity was assessed by adopting a grading method reported by Fantes et al. (107). Corneal cross-sectional visualization was performed by using the Visante AS-OCT (Carl Zeiss Meditec) and corneal topography was captured by using a handheld videokeratographer (Oculus, Lynnwood, WA).

4.2.6.5 In Vivo Confocal Microscopy

In vivo confocal microscopy was performed before ReLEx (FLEx), 28 days after ReLEx (FLEx), and at 3, 14, and 28 days after lenticule reimplantation, using the Heidelberg retinal tomography HRT3 with Rostock corneal module (Heidelberg Engineering GmbH, Heidelberg, Germany) as described in 4.2.1.3.

4.2.6.6 Tissue Fixation and Sectioning

After euthanization, the rabbit corneas were excised from the globe and embedded in an optimum cutting temperature (OCT) cryocompound (Leica Microsystems, Nussloch, Germany) as described above 4.2.1.4.

4.2.6.7 Immunofluorescent Staining

Sections were fixed with 4% paraformaldehyde (Sigma) for 15 minutes, and incubated with either mouse monoclonal antibody against cellular fibronectin (catalog no. MAB1940; Millipore, Billerica, MA) diluted 1:400, tenascin-C (ab88280; Abcam, Cambridge, UK) diluted 1:200, CD18 (NB100- 65,303; Novus Biologicals, Littleton, CO) diluted 1:100, a-smooth muscle actin (a-SMA; N1584; Dako Cytomation, Glostrup, Denmark) diluted 1:50, Thy-1/CD90 (sc-53116; Santa Cruz Biotechnology, Santa Cruz, CA) diluted 1:50 in the blocking solution, or with prediluted mouse monoclonal antibody against Ki67 (08-0156; Invitrogen, Carlsbad, CA) at 48°C overnight. A probe (Alexa Fluor 488 phalloidin; Invitrogen) was used to detect filamentous actin. After washing with 1X PBS, the sections were incubated with goat anti-mouse Alexa Fluor 488 conjugated secondary antibody (Invitrogen) at room temperature for 1 hour. Slides were then mounted with UltraCruz Mounting Medium

containing 40,6-diamidino-2-phenylindole (DAPI; Santa Cruz Biotechnology). For negative controls, nonimmune serum was used in place of the specific primary antibody. Sections were observed and imaged with a fluorescence microscope (Zeiss Axioplan 2; Zeiss, Oberkochen, Germany). To detect apoptotic cells, a fluorescence-based TUNEL assay (In Situ Cell Death Detection Kit; Roche Applied Science, Indianapolis, IN) was used according to the manufacturer's instructions.

4.2.6.8 Statistical Analysis

Data were expressed as mean +/- SD where appropriate. The P value was determined using the two-tailed Student's t-test with Microsoft Excel 2007 software (Microsoft, Redmond, WA). Data were considered to be statistically significant when P was less than 0.05.

4.2.7 Lenticule Re-Implantation Proof of Value Non-human Primate (NHP) Study

The rabbit results showed the utility of stromal volume replacement. However, the assessment of true refractive correction was only possible with a Non-human primate model. This is because refractive assessment is extremely difficult in rabbits and there is a higher degree of variability compared to NHP. We felt it was manadatory to assess the results in a NHP model before any clinical human trials.

4.2.7.1 Animals

Twelve adult monkeys (Macaca fascicularis) underwent FLEx as detailed above in 4.2.2.3. Animals were housed in adjoining individual stainless steel monkey cages allowing social interactions. The cages were equipped with automatic watering systems.

The room environment was continuously controlled for temperature (24+/-2°C), humidity (50+/- 20%), light cycle (12 hours light:12 hours dark), and air change (10 to 15 air changes/hour). Food was withdrawn overnight prior to any anesthesia. Continuous clinical care (24 hours/7 days) was provided throughout the study to ensure prompt intervention when needed. Animals were anesthetized with 0.5 ml of ketamine hydrochloride (100 mg/ml intramuscularly; Parnell Laboratories, Alexandria, Australia) and 0.1 ml of medetomidine hydrochloride (1 mg/ml subcutaneously; Pfizer Animal Health, New York, NY) during ReLEx and lenticule re-implantation procedure, as well as during pre- and postoperative eye examinations. The monkeys were sacrificed under sedation at different time points by overdose intravenous injection of sodium pentobarbitone (Jurox, Rutherford, Australia). At the conclusion of the study, a total of 8 eyes were used to study long-term effect of ReLEx (4 eyes for 8 weeks post-surgical study and the other 4 eyes for 16 weeks post-surgical study) and a total of 14 eyes were collected to study long-term effect of RL re-implantation (7 eyes for 8 weeks post-reimplantation study and the other 7 eyes for 16 weeks post-reimplantation study). The remaining unoperated eyes (n= 2) were used as controls for immunohistochemical analysis. All animals were treated according to the guidelines of the Association for Research in Vision and Ophthalmology's Statement for the Use of Animals in Ophthalmic and Vision Research. The study protocol was approved by the Institutional Animal Care and Use Committee of SingHealth, Singapore.

4.2.7.2 Refractive Lenticule Extraction (ReLEx Procedure)

ReLEx was performed using a VisuMax femtosecond laser system (Carl Zeiss Meditec) as described in 4.2.2.3. All experimental eyes underwent a spherical -6.00D myopia correction.

4.2.7.3 Storage and Re-Implantation of Intrastromal Lenticule

The storage and cryopreservation of the extracted lenticule was conducted as described earlier 4.2.6.3.

4.2.7.4 Corneal Imaging: Slit Lamp Photography and Anterior Segment optical Coherence Tomography

Slit lamp photographs and AS-OCT scans were obtained pre-ReLEx and 3 days, and 2, 4, 8 and 16 weeks after ReLEx surgery as described in 4.2.6.4.

4.2.7.5 Corneal Curvature and Spherical Error Measurement

Measurements of corneal curvature (keratometry) and spherical error (refractometry) were obtained pre-ReLEx, 8 and 16 weeks post-ReLEx and similarly followed for RL re-implantation. Keratometric values and spherical errors were measured using a Nidek ARK-30 Autorefractor/Keratometer (Hiroishi, Japan).

4.2.7.6 In Vivo Confocal Microscopy

In vivo confocal microscopy was performed pre-ReLEx, 3 days, and 2, 4, 8 and 16 weeks after ReLEx and lenticule reimplantation surgeries, using a Heidelberg retinal tomograph HRT3 with Rostock corneal module (Heidelberg Engineering GmbH, Heidelberg, Germany) as described in 4.2.1.3.

4.2.7.7 Immunohistochemistry

After euthanization, the corneas were excised from the globe and embedded in Optimal Cutting Temperature (OCT) cryocompound (Leica Microsystems, Nussloch, Germany). Frozen tissue blocks were stored at -80 ^{o}C until sectioning. Serial sagittal

corneal 10 mm sections were cut using a Microm HM550 cryostat (Microm, Walldorf, Germany). Sections were placed on polylysine-coated glass slides and air dried for 15 minutes. Immunohistochemical staining was performed as described previously. The following primary antibodies and the corresponding working dilution factor were used: mouse monoclonal antibody against cellular fibronectin (Millipore, Billerica, MA) diluted 1:400; tenascin-C (Abcam, Cambridge, UK) diluted 1:200; collagen type I (Sigma) diluted 1:100; and CD18 (Novus Biologicals, Littleton, CO) diluted 1:100 in the blocking solution. After washing with 1X PBS, the sections were incubated with goat anti-mouse Alexa Fluor 488-conjugated secondary antibody (Invitrogen) at room temperature for 1 hour. Slides were then mounted with UltraCruz Mounting Medium containing DAPI (Santa Cruz Biotechnology) and were observed and imaged with a Zeiss AxioImager Z1 fluorescence microscope (Carl Zeiss, Oberkochen, Germany). Double immunohistochemical staining was performed as described previously, with minor modifications. Tissue sections were incubated with mouse monoclonal antibody against α-smooth muscle actin (α-SMA, Dako Cytomation, Glostrup, Denmark) diluted 1:50 in the blocking solution, or with pre-diluted mouse monoclonal antibody against Ki-67 (Invitrogen, Carlsbad, CA) at 4C overnight. On the following day, the sections were incubated with Alexa Fluor 488-conjugated secondary antibody (Invitrogen) at room temperature for 1 hour. After washing with 1X PBS, the sections were double stained with an Alexa Fluor 568-conjugated phalloidin probe (Invitrogen) at room temperature for 30 minutes. Slides were subsequently mounted with UltraCruz Mounting Medium containing DAPI (Santa Cruz Biotechnology) and observed with the Zeiss AxioImager Z1 microscope (Carl Zeiss). To detect apoptotic cells, a fluorescence-based TUNEL assay (In Situ Cell Death Detection Kit, Roche Applied Science, Indianapolis, IN) was used according to the manufacturer's instructions. Double

staining with Alexa Fluor 568-conjugated phalloidin probe (Invitrogen) was then performed as described in the preceding sub-section.

4.2.7.8 Statistical Analysis

Data were expressed as mean +/- standard deviation. The P value was determined using the two-tailed Student's t-test with GraphPad Prism 5 (La Jolla, CA). Data were considered to be statistically significant when $P<0.05$.

4.1 Results

4.3.1 Effect of Firing Pattern on Collagen Disruption

4.3.1.1 In Vivo Confocal Microscopy

Stromal layers directly anterior to the front surface of the lenticule showed an increase in highly reflective keratocytes after laser photodisruption. These keratocytes were observed in similar density in all corneas regardless of the laser-firing pattern (Figure 4.4, A, top panel). The anterior surface of the lenticule had a layer of increased light reflectivity and visible keratocytes (Figure 4.4, A, middle panel). A similar appearance could be seen at the posterior interface of the lenticule (Figure 4.4, A, bottom panel). No significant difference in the pattern of the reflectivity level of the anterior incision surface (Figure 4.4, B) and posterior incision surface (Figure 4.4, C) was detected in all treated corneas.

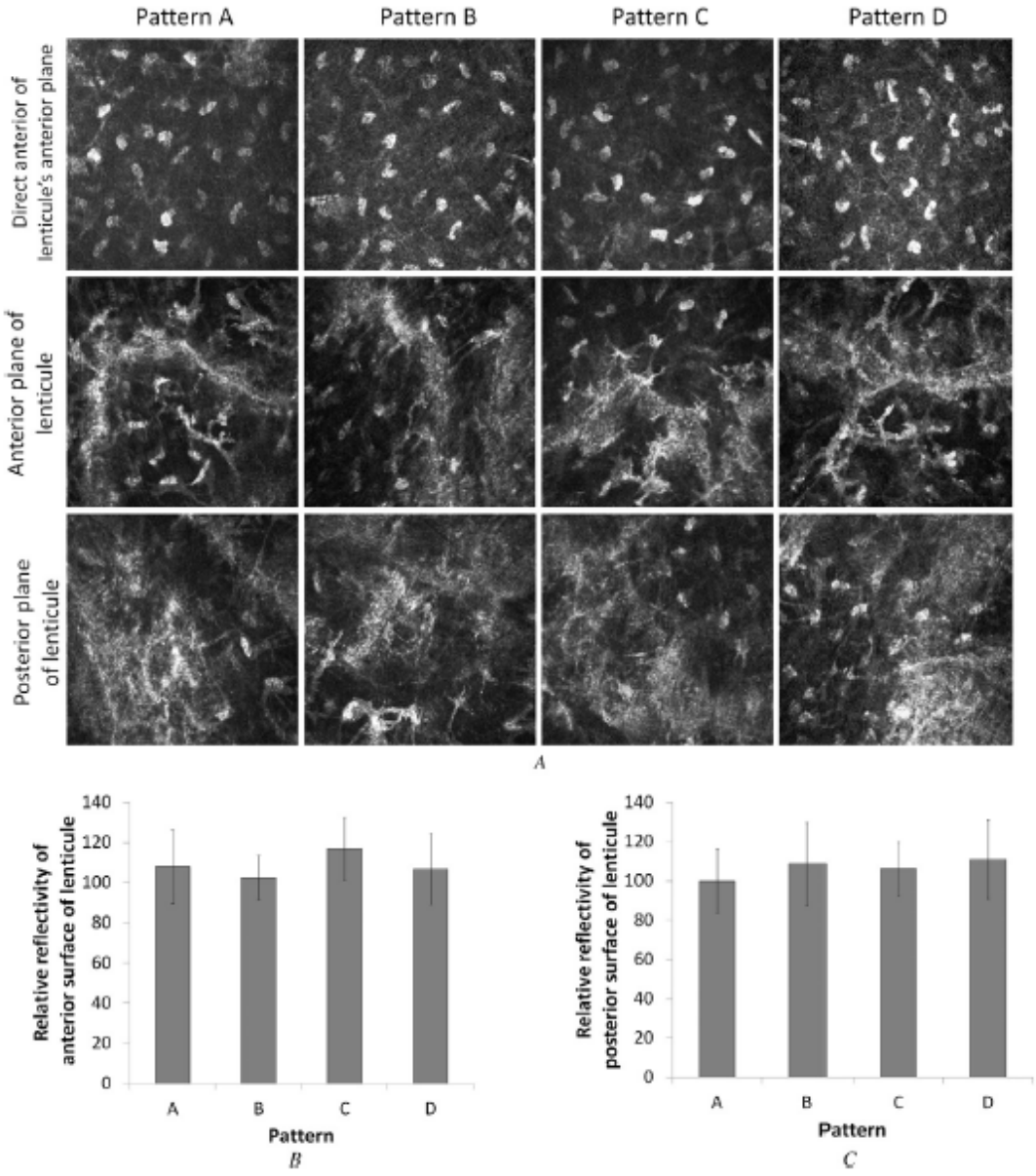

Figure 4.4 The corneal stroma treated with different laser firing patterns during refractive lenticule extraction. A: Top panel shows the stromal layer directly anterior to the lenticule's anterior surface. The stromal layer at the keratotomy site of the lenticule's anterior plane is shown in the middle panel and the lenticule's posterior plane is shown in the bottom panel (in vivo confocal micrographs). B: Relative reflectivity level of the anterior surface of the lenticule. C: Relative reflectivity level of the posterior surface of the lenticule. Error bars denote the SD. (Courtesy of Riau et al. (167))

4.3.1.2 IMMUNOHISTOCHEMISTRY

Expression of fibronectin appeared in the central cornea of all treated eyes. The expression was distinct and consistent along the anterior and posterior interfaces of the lenticule. There was no significant difference in intensity and staining pattern of the

corneas regardless of the firing pattern used (Figure 4.5, A to D). Early inflammation, which can be detected by the presence of CD11b-positive cells, was not observed in corneas that were treated with firing pattern A, B, C, or D (Figure 4.5, E to H). Collagen type I was expressed in the full thickness of the corneal stroma of all treated eyes. A uniform expression pattern throughout the full thickness of the corneal stroma was observed in the eyes that were treated with pattern A, B, or C (Figure 4.5, I to K). In contrast, a fine, discontinuous and relatively stronger expression of collagen type I was seen along the anterior interface incision of the lenticule in the corneas treated with pattern D (Figure 4.5, L).

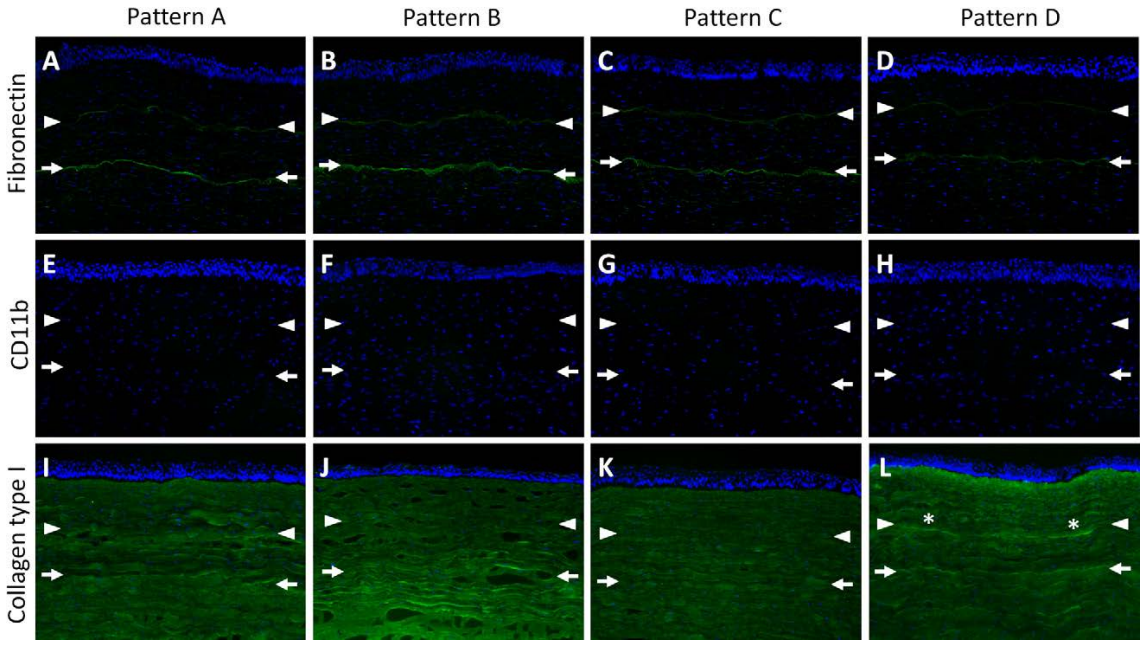

Figure 4.5 Expression of fibronectin (A to D), CD11b (E to H), and collagen type I (I to L) in the corneas treated with different laser-firing patterns during refractive lenticule extraction. Arrowheads and arrows indicate the position of the anterior surface and posterior surface of the intrastromal lenticule, respectively. Asterisks show the discontinuous and intense expression of collagen type I along the lenticule's anterior plane. Nuclei were counterstained with DAPI (blue). All images were captured at 100×

magnification. (Courtesy of Riau et al. (167)).

4.3.1.3 Transmission Electron Microscopy

The anterior incision plane was delineated by electron-dense and dark areas. In corneas treated with pattern A, the appearance of the electron-dense surface was uniform along the incision site. The boundary between the laser affected area and undisrupted collagen fibrils was easily discernible (Figure 4.6, A and B). The laser incision area of the corneas that were treated with pattern B showed a similar appearance as those that were treated with pattern A (Figure 4.6, C and D). A relatively more disrupted collagen arrangement could be seen in the corneas treated with pattern C. The border between the laser disrupted tissue and unaffected collagen fibrils became more difficult to discern (Figure 4.6, E and F). In the corneas after pattern D treatment, the collagen fibrils appeared even more deranged. The border between the disrupted and undisrupted tissue had become completely indiscernible. In addition, collagen fibrils that were located directly anterior to the anterior incision plane were affected by the photodisruption process (Figure 4.6, G and H).

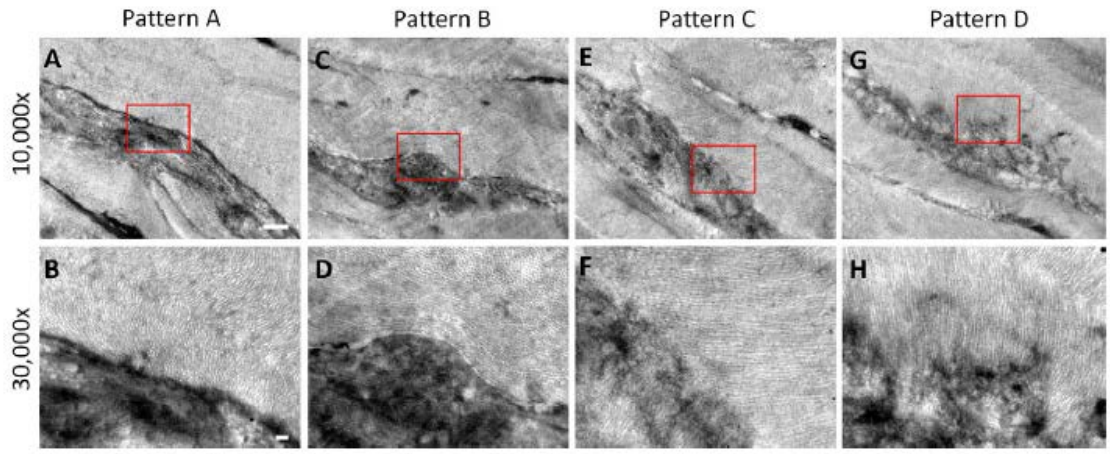

Figure 4.6 Anterior surface of the intrastromal lenticule after treatment with different femtosecond laser-firing patterns (TEM images). The separation between the laser affected area, which was marked by the appearance of an electron-dense surface and the undisrupted collagen fibres, was easily discernible in corneas treated with firing-pattern A (A and B) and pattern B (C and D). In pattern C–treated corneas, the border between the laser-disrupted tissue and unaffected collagen fibres became more difficult to discern due to increased disruption of the fibrils (E and F). In pattern D–treated corneas, the border between the disrupted and undisrupted tissue was completely indiscernible and collagen fibres that were located directly anterior to the anterior incision plane were also affected by the photodisruption process (G and H). Figure in bottom panel (B, D, F, and H) shows the enlarged image within the red rectangle found on the top panel (A, C, E, and G). Original magnification: 10 000 (top panel), 30 000 (bottom panel). Scale bars: 1 μm (top panel), 0.2 μm (bottom panel). (Courtesy of Riau et al. (167)).

4.3.2 Early Wound Healing and Inflammatory Response after ReLEx

4.3.2.1 Slit Lamp and AS-OCT

One day after the surgery, the central cornea of all rabbits in either ReLEx or LASIK groups remained clear on slit lamp examination (Figure 4.7A). The flap side cut outline could be seen on Day 1 after both surgical techniques. In both groups, increasing the degree of refractive correction did not seem to affect the clarity of the centre of the cornea. In the post-ReLEx corneas with no flap separation, the flap side cut was difficult to visualize. On AS-OCT examination (Figure 4.7B), an increase in reflectivity could be seen at the flap interface of both post-ReLEx and LASIK eyes. Differences in the reflectivity level were not discernible in corneas that underwent -3.00 D and -6.00 D

of refractive correction; however, a relatively more intense reflective band was observed in the central corneal flap interface after -9.00D LASIK in comparison with -9.00D ReLEx. In the corneas that underwent ReLEx with flap left intact, the posterior and anterior incision plane of the lenticule was discernible, particularly in those that underwent -9.00D correction (Figure 4.7C).

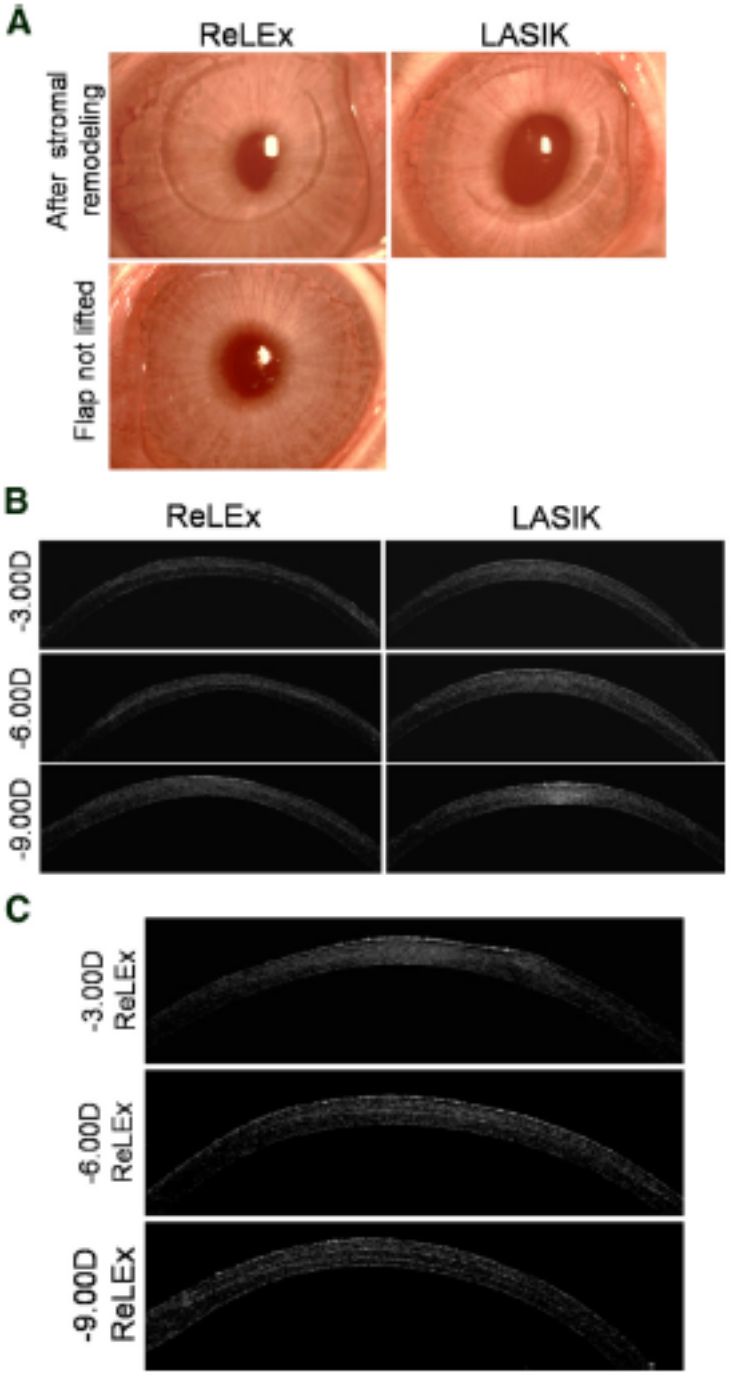

Figure 4.7 Slit lamp microscopy and anterior segment optical AS-OCT of the corneas 1 day after ReLEx and LASIK. Each group was subjected to a different degree of correction: 3.00 D, 6.00 D, and 9.00 D. (A) Slit lamp photographs represent the cornea that underwent a 6.00 D correction. The top panel shows the cornea after stromal ablation by excimer laser in LASIK, and after removal of lenticule in ReLEx. The bottom panel shows the post-ReLEx cornea with the flap not lifted. (B) Cross-sectional visualization of postoperative corneas using AS-OCT. (C) AS-OCT of the corneas with intact flap. (Courtesy of Riau et al. (168))

4.3.2.2 In vivo Confocal Microscopy

One day after ReLEx and LASIK, a few highly reflective keratocytes could be seen in the stromal layer directly anterior to the interface. These keratocytes were observed in similar density in all corneas that underwent -3.00 D, -6.00 D, and -9.00 D refractive correction (Figure 4.8A). In nonoperated corneas, the keratocytes only showed moderate light-scattering (Figure 4.8A, control). The flap interface itself was acellular and characterized by light-scattering particles. More intense and abundant reflective particles were observed in the corneas that underwent LASIK compared with those that underwent ReLEx, particularly in the corneas that had -6.00 D and -9.00 D correction (Figure 4.8B). Semi-quantitative analysis of the intensity of the reflectivity at the flap interface is depicted in a bar graph (Figure 4.8C). In corneas that underwent ReLEx with the flap left intact, the reflective particles could be seen at the posterior and anterior incisions of the lenticule (Figure 4.8D). The density and intensity were comparable to those in the corneas where the lenticule was removed. Keratocytes with moderate light-scattering nuclei were present in the lenticule's lamellae of the undisturbed ReLEx procedure (Figure 4.8D).

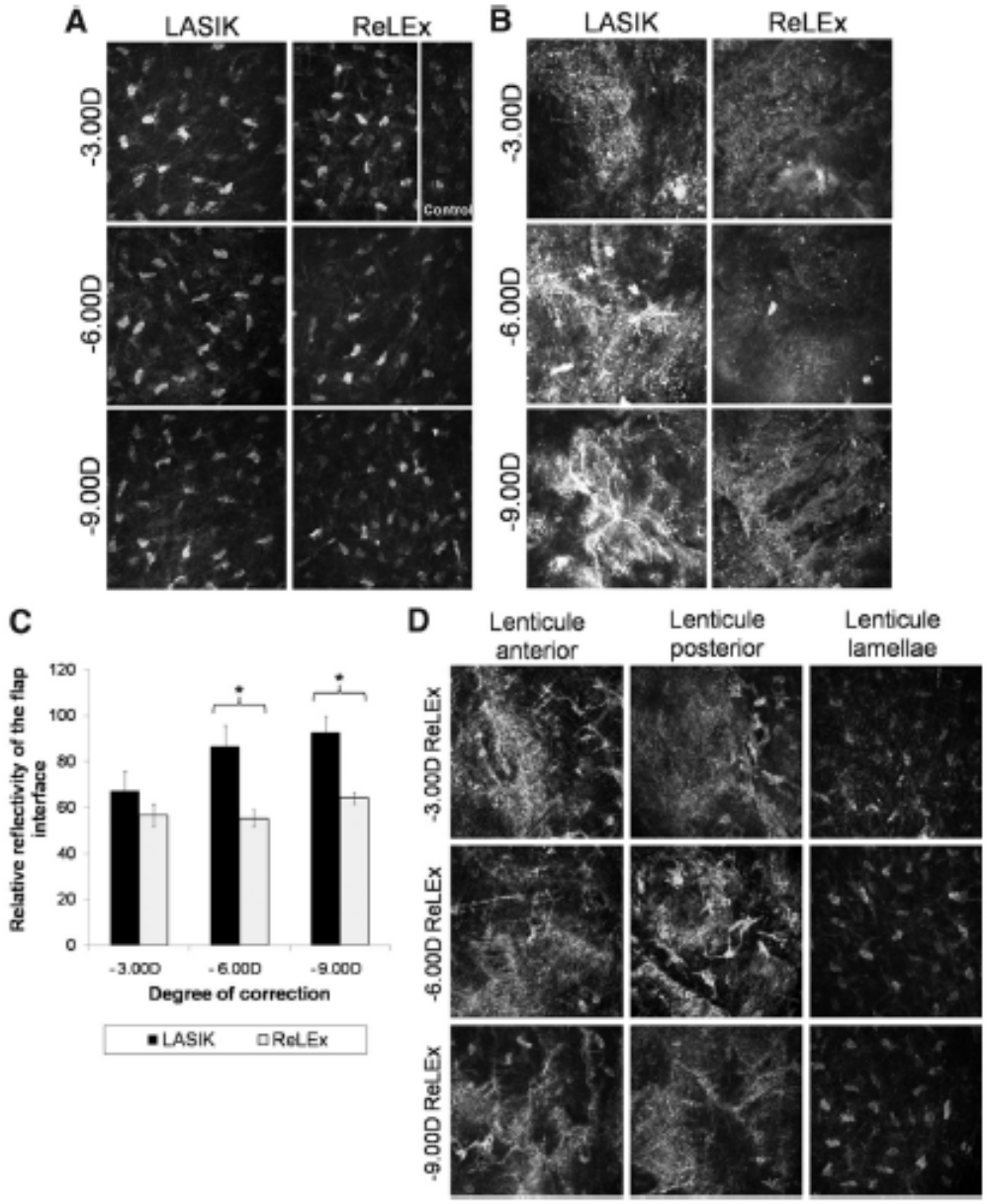

Figure 4.8 In vivo confocal micrographs of the corneas 1 day after ReLEx and LASIK. Each group was subjected to a different degree of correction: 3.00 D, 6.00 D, and 9.00 D. (A) A few highly reflective activated keratocytes could be seen directly anterior to the laser ablated zone. (B) The keratotomy site itself was acellular and light reflective. (C) Bar graph showing the relative intensity of the reflectivity at the laser treated zone. Reflectivity level was analyzed (ImageJ software). Error bars represent SD and asterisks (*) indicate that P 0.05. (D) The flap was left intact (not lifted) in some corneas. Light

reflective particles were observed at the lenticule's posterior and anterior incisions after ReLEx. The presence of quiescent keratocytes could be detected within the lenticule's lamellae. (Courtesy of Riau et al. (168))

4.3.2.3 CORNEAL TOPOGRAPHY

As expected with myopic correction, flattening of the central corneas could be seen in the both post-LASIK and – ReLEx corneas. The average K of the non-operated corneas was 44.7 +/- 1.2 D. Keratometric changes were similar in the corneas that underwent -3.00 D LASIK and ReLEx; Kmin and Kmax after LASIK were 39.2 +/- 3.3 D and 39.6 +/-1.9 D, respectively compared with 38.6 +/- 1.1 D and 40.0 +/- 1.2 D, respectively after ReLEx. The average K was 39.4 +/- 2.3 D after LASIK and 39.3 +/- 0.5 D after ReLEx (P = 0.916). (Table 4.4)

Procedure	K_{min}	K_{max}	Average K	P
Control	43.8 ± 1.3	45.7 ± 1.2	44.7 ± 1.2	
−3.00 D LASIK	39.2 ± 3.3	39.6 ± 1.9	39.4 ± 2.3	0.916
−3.00 D ReLEx	38.6 ± 1.1	40.0 ± 1.2	39.3 ± 0.5	
−6.00 D LASIK	37.6 ± 3.1	38.0 ± 2.0	37.8 ± 2.0	0.196
−6.00 D ReLEx	37.9 ± 2.1	41.0 ± 2.9	39.5 ± 2.2	
−9.00 D LASIK	34.3 ± 4.0	35.5 ± 2.1	34.9 ± 2.9	0.097
−9.00 D ReLEx	35.6 ± 0.4	38.9 ± 2.2	37.3 ± 1.2	

Table 4.4 Keratometric (K) Changes 1 Day after ReLEx and LASIK. (Courtesy of Riau et al. (168)).

The difference in keratometric measurements became more evident as we increased the power of refractive correction. When the degree of correction was increased to -6.00 D, the K_{min} and K_{max} after LASIK were 37.6 +/- 3.1 D and 38.0 +/- 2.0D, respectively, compared with 37.9 +/- 2.1 D and 41.0 +/- 2.9 D, respectively, after ReLEx. The average K was 37.8 +/- 2.0 D after LASIK and 39.5 +/- 2.2 D after ReLEx (P = 0.196). After -9.00 D correction, the K_{min} and K_{max} post-LASIK were 34.3 +/- 4.0

D and 35.5 +/- 2.1 D, respectively, compared with 35.6 +/- 0.4 D and 38.9 +/- 2.2 D, respectively, after ReLEx. The average K was 34.9 +/- 2.9 D after LASIK and 37.3 +/- 1.2 D after ReLEx (P = 0.097). The keratometric changes were depicted by the corneal topography. As the degree of refractive correction was increased, we could clearly see a more flattened zone (blue zone on topography) on corneas after LASIK compared with ReLEx (Figure 4.9).

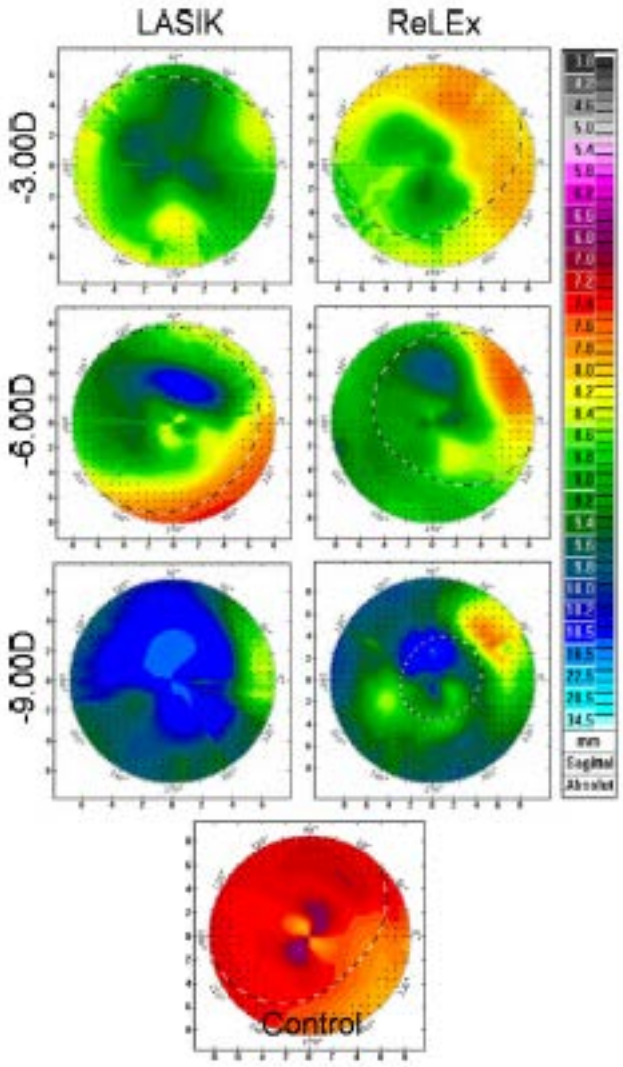

Figure 4.9. Corneal topography of the corneas 1 day after ReLEx and LASIK. Each group was subjected to a different degree of refractive correction: 3.00 D, 6.00 D, and

9.00 D. Preoperative topography is depicted at the bottom (control). (Courtesy of Riau et al. (168)).

4.3.2.3 IMMUNOHISTOCHEMISTRY

Expression of fibronectin appeared in the central cornea on day 1 after ReLEx and LASIK surgery. The expression was distinct and consistent along the laser injury site. We observed a marginal difference in the staining intensity between the corneas that underwent -3.00 D ReLEx and -3.00 D LASIK. However, the difference became more marked when the degree of correction was increased to -6.00 D and -9.00 D. Fibronectin expression was relatively stronger at the site of laser injury and more apparent at the stromal bed after LASIK, in comparison with that after ReLEx (Figure 4.10A). Similar features were also seen in the peripheral flap area (Figure 4.10B). In the corneas that did not undergo flap elevation, weak expression of fibronectin was observed along the posterior and anterior dissection plane of the lenticule after the ReLEx procedure (Figure 4.10C). Similar staining intensity could be found atthe peripheral flap (Figure 4.10D).

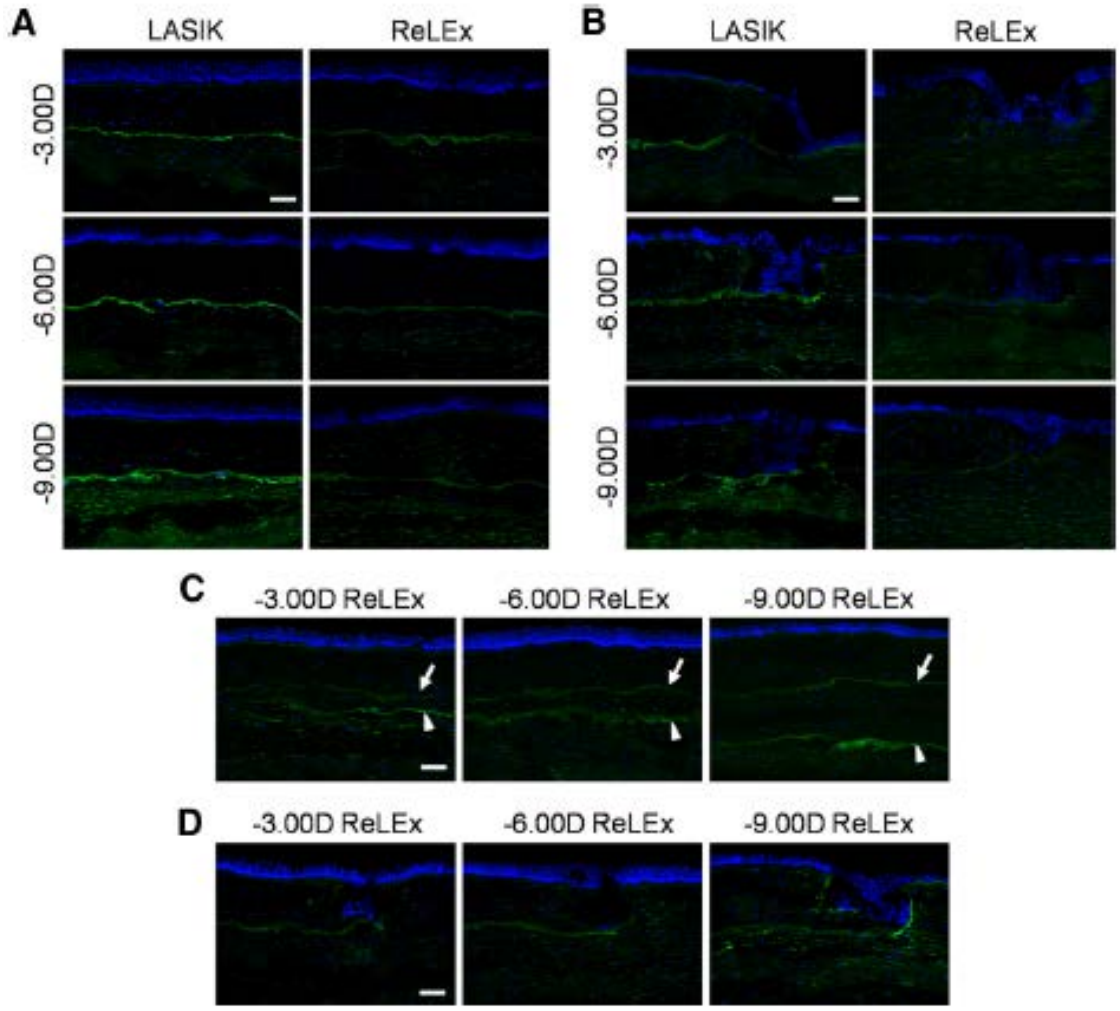

Figure 4.10. Expression of cellular fibronectin in the corneas on Day 1 after ReLEx and LASIK. Each group was subjected to a different degree of correction: 3.00 D, 6.00 D, and 9.00 D. Fibronectin was detected along the incision line in (A) the cornea centre and (B) the periphery of flap. In the post-ReLEx corneas with flap not elevated, fibronectin was also expressed along the incision line at (C) the flap centre and (D) the flap margin. Arrowheads show the lenticule's posterior incision line and arrows show the lenticule's anterior/flap interface incision line. Sections were counterstained with DAPI, which stained the nuclei (blue). Scale bars, 50 microns. (Courtesy of Riau et al. (168)).

Immunostaining of CD11b, an early inflammatory marker, showed a distinct difference

between post-ReLEx and post-LASIK eyes, primarily in the central cornea. There was little to no CD11b-positive cells detected in the central cornea after -3.00 D ReLEx and only a little was seen after -3.00D LASIK. However, there was a significant elevation of the number of cells expressing CD11b in the post-LASIK corneas when the power of correction was increased to -6.00 D and -9.00 D. Whereas in the post-ReLEx corneas, the CD11b positive cells remained low even when higher power of correction was performed (Figure 4.11A). There was an elevated number of cells expressing CD11b in the peripheral area of the flap compared with that in the central, probably representing peripheral recruitment and migration of inflammatory cells. This observation applied to both post-ReLEx and post-LASIK eyes. Lowering or increasing the power of correction did not seem to affect the number of the inflammatory cells after ReLEx (Figure 4.11B). Quantification of CD11b positive cells is depicted in a bar graph (Figure 4.11C). When the corneal flap was not lifted after ReLEx, there were no inflammatory cells seen in either the cornea centre (Figure 4.11D) or the flap margin (Figure 4.11E).

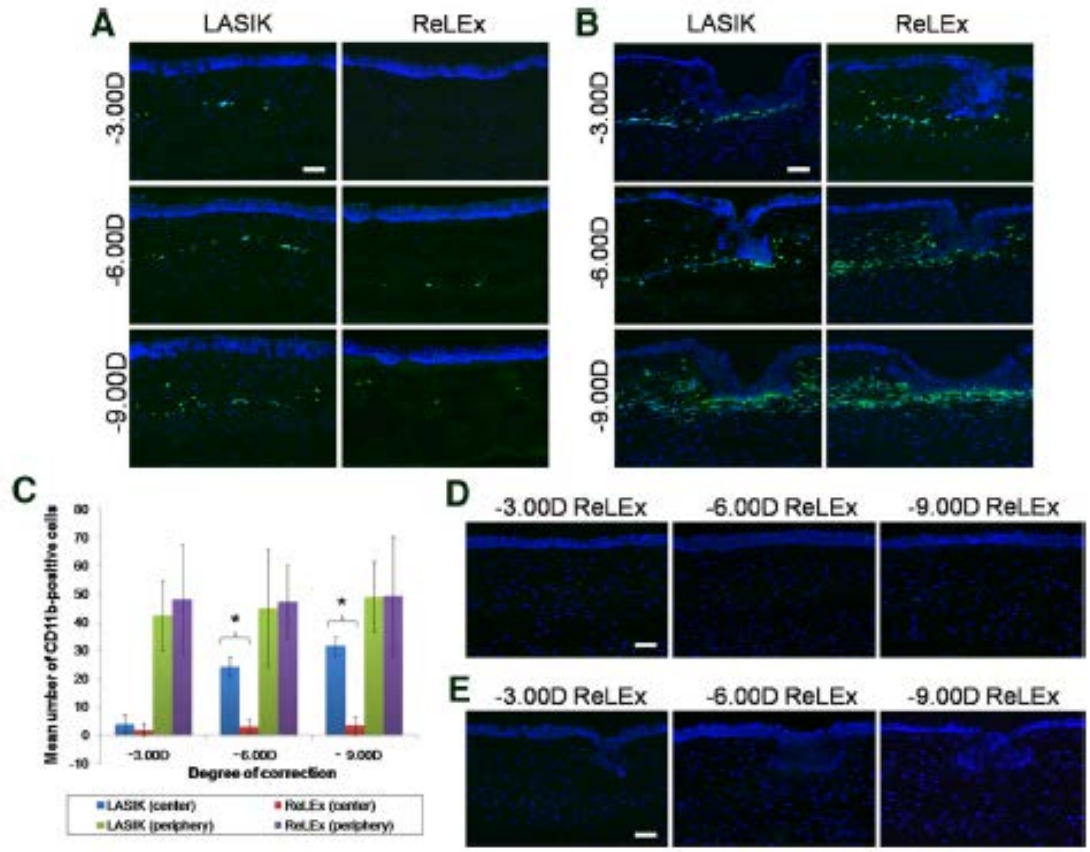

Figure 4.11. Expression of CD11b in the corneas on Day 1 after ReLEx and LASIK. Each group was subjected to a different degree of correction: 3.00 D, 6.00 D, and 9.00 D. CD11b-positive cells was observed along the incision line in (A) the cornea centre and (B) the periphery of the flap. (C) Mean number of CD11bpositive cells in the flap centre and periphery depicted in the bar graph. Error bars represent SD and asterisks (*) indicate that P 0.05. In the post-ReLEx corneas with intact flap, there were no CD11b-positive cells seen along the incision line at either (D) the flap centre or (E) the flap margin. Sections were counterstained with DAPI, which stained the nuclei (blue). Scale bars, 50 microns. (Courtesy of Riau et al. (168))

4.3.2.4 Cell Proliferation and Cell death

Ki-67 staining was observed in some cells on day 1 after both LASIK and ReLEx. We did not observe much difference in the number of cells expressing this proliferation

marker after both surgeries and after increasing the degree of correction. There were very few cells expressing Ki-67 in the central flap (Figure 4.12). The expression was mainly restricted to the epithelial cells at the peripheral site of the corneal flap (Figure 4.12B). A similar observation could be made on the corneas with intact flaps (Figure 4.12C and 4.11D). Ki-67 was also primarily present in the epithelial cells of the flap margin.

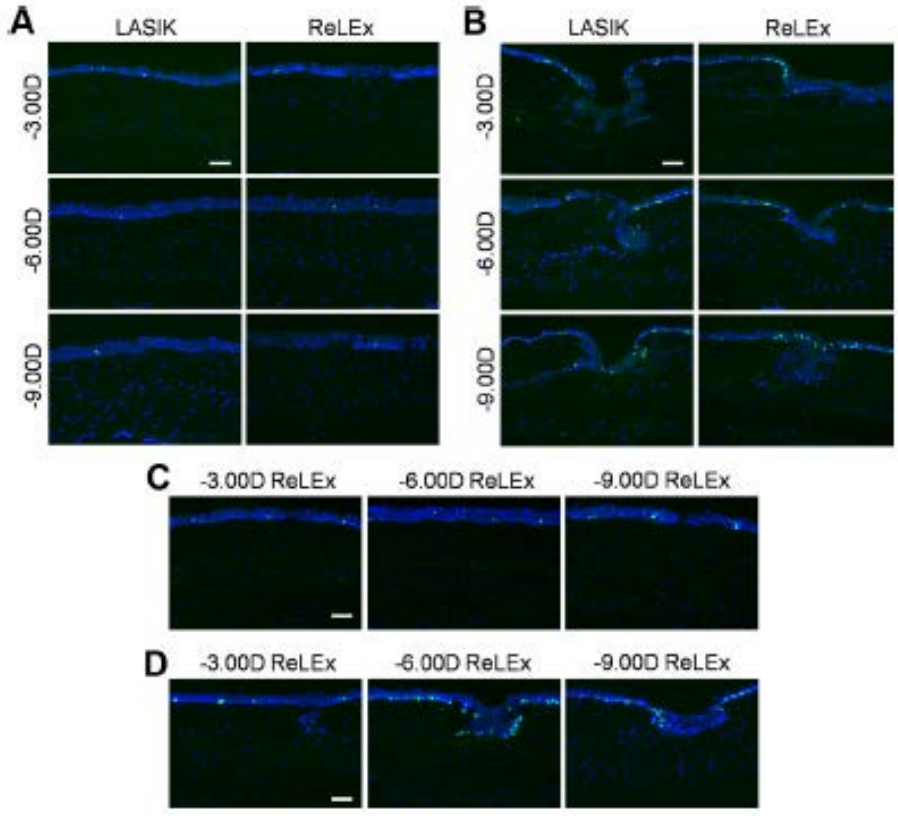

Figure 4.12. Expression of Ki-67 in the corneas on Day 1 after ReLEx and LASIK. Each group was subjected to a different degree of correction: 3.00 D, 6.00 D, and 9.00 D. (A) Only a few Ki-67-positive cells were detected in the epithelium of the cornea centre. (B) In contrast, Ki-67-positive cells were relatively abundant in the epithelium of the flap edge. Similar Ki-67 staining pattern could be observed in the post-ReLEx corneas with intact flap at (C) the flap centre or (D) the flap margin. Sections were

counterstained with DAPI, which stained the nuclei (blue). Scale bars, 50 microns. (Courtesy of Riau et al. (168)).

TUNEL assay detected DNA fragmentation adjacent to the keratotomy site in the central flap (Figure 4.13A), as well as peripheral flap (Figure 4.13B). An increased number of apoptotic cells in the flap periphery in comparison with the flap centre could be observed after ReLEx and LASIK. However, there was no significant disparity in the number of apoptotic cells after both procedures, even after elevating the power of refractive correction. Quantification of TUNEL-positive cells is depicted in a graph (Figure 4.13C). Cell death was also detected in the corneas with intact flaps, adjacent to the laser incision in the cornea centre (Figure 4.13D) and the flap margin (Figure 4.13E). DNA fragmentation was distinct along the posterior and anterior aspects of the lenticule incisions after the ReLEx procedure.

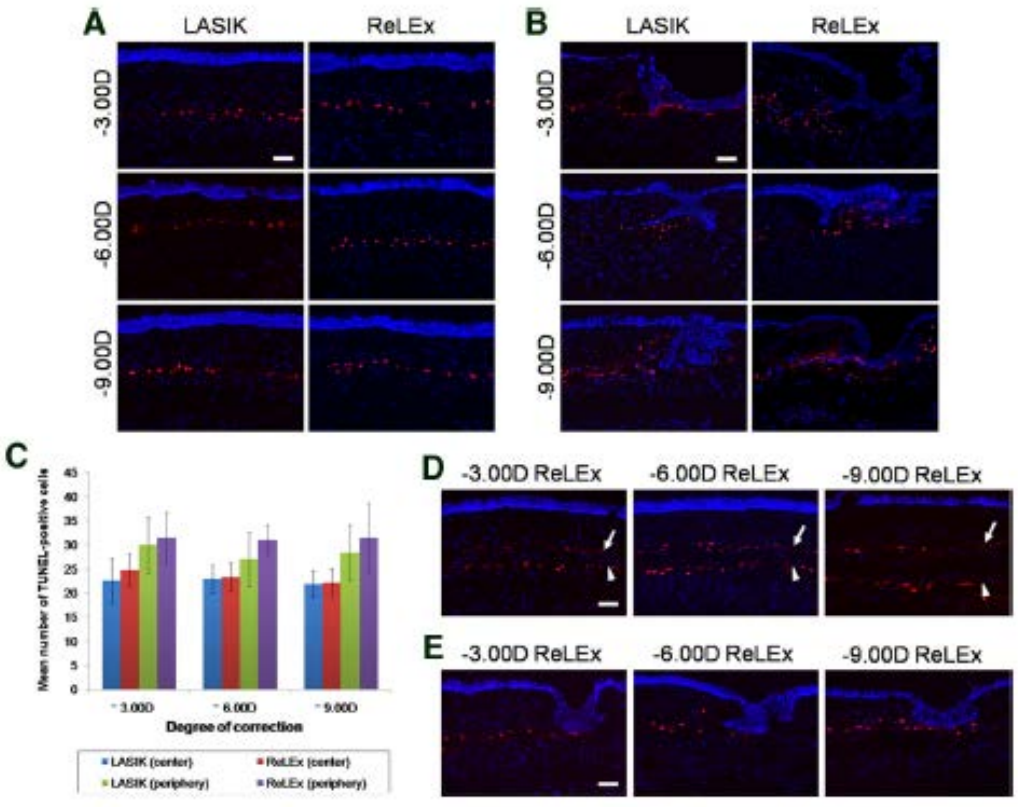

Figure 4.13. DNA fragmentation detection by TUNEL assay in the corneas 1 day after

ReLEx and LASIK. Each group was subjected to a different degree of correction: 3.00 D, 6.00 D, and 9.00 D. Cell death was detected along the incision line in (A) the cornea centre and (B) the periphery of flap. (C) Mean number of TUNEL-positive cells in the flap centre and periphery depicted in the bar graph. Error bars represent +/- 1SD. In the post-ReLEx corneas with flap not elevated, cell death was also observed along the incision line at (D) the flap centre and (E) the flap margin. Arrowheads show the lenticule's posterior incision line and arrows show the lenticule's anterior/flap interface incision line after ReLEx. Sections were counterstained with DAPI, which stained the nuclei (blue). Scale bars, 50 microns. (Courtesy of Riau et al. (168))

4.3.3 FLEx: Clinical Results, Interface Evaluation and IOP Variation

Refractive Results

4.3.3.1 Clinical Trial

We enrolled 22 female (67%) and 11 male patients (33%) that underwent FLEx in both eyes (total of 66 eyes). The mean age was 32 years (range, 21 to 46 years). Preoperative UCVA was 0.05 +/- 0.01 with mean spherical equivalent (SE) of -5.77 +/- 2.04 D, mean sphere -5.28 +/- 2.05 D, and mean myopic astigmatism of -1.03 +/- 0.72 D.

Postoperative results at 1 and 3 months are described in Table 4.5.

Parameters	Mean ± SD	Range
Preoperative		
MR SE	−5.77 D ± 2.04 D	−1.38 D to −9.75 D
MR sphere	−5.28 D ± 2.05 D	−0.50 D to −9.00 D
MR cylinder	−1.03 D ± 0.72 D	Up to −3.00 D
Postoperative 1 Month **(n = *44 Eyes*)**		
MR SE	0.19 D ± 0.64 D	1.75 D to −1.63 D
MR sphere	0.39 D ± 0.57 D	2.00 D to −0.50 D
MR cylinder	−0.41 D ± 0.45 D	Up to −2.25 D
Postoperative 3 Months **(n = *40 Eyes*)**		
MR SE	0.14 D ± 0.53 D	1.75 D to −1.00 D
MR sphere	0.33 D ± 0.50 D	2.00 D to −0.25 D
MR cylinder	−0.38 D ± 0.43 D	Up to −2.00 D

MR, manifest refraction.

Table 4.5 Preoperative and Postoperative Refraction. (Courtesy of Ang et al. (169))

Predictability was high at 1 month postoperatively (Figure 4.14). At the 3-month follow-up, 81.8% of eyes (36/44 eyes) were within -0.5 D and 95.5% (42/44 eyes) within +/-1.0 D of the intended refractive target.

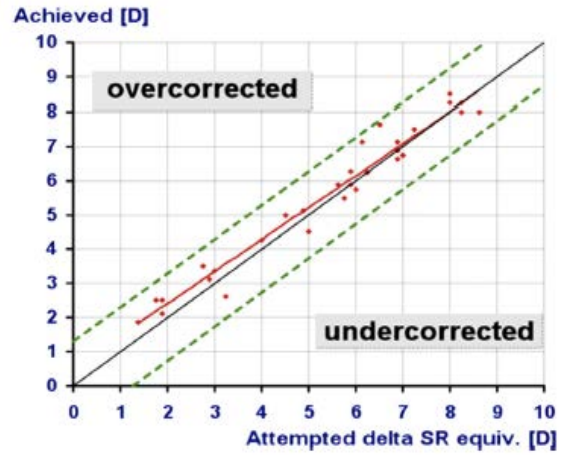

Figure 4.14. Clinical results: predictability. Scatterplot of the attempted SE refractive change plotted against the achieved SE refractive change at 3 months (44 eyes). (Courtesy of Ang et al. (169)).

Figure 4.14 illustrates the regression line plot within the plot of the actual correction achieved versus the attempted refractive correction 3 months postoperatively. There was a slight hyperopic shift in the eyes (mean SE 0.14+/- 0.53 D) at 3 months postoperatively, with mean sphere 0.33 +/- 0.50 D. Mean induced myopic astigmatism was -0.38 +/- 0.43D at 3 months (Figure 4.15).

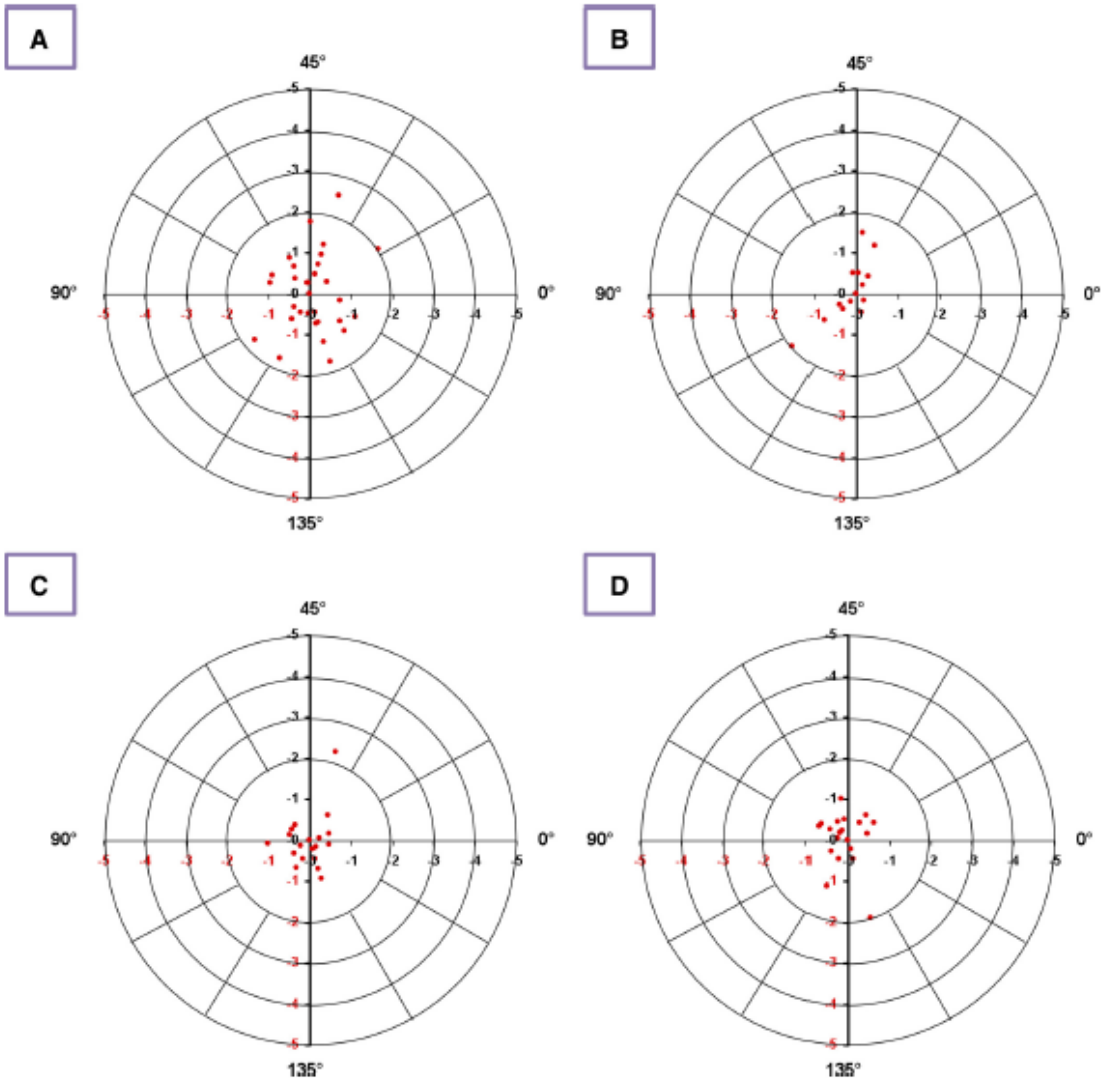

Figure 4.15. Preoperative (A), 1 week (B), 1 month (C), and 3 months postoperative (D) normalized double-angle minus-cylinder scatterplots. (Courtesy of Ang et al. (169)).

On the first few postoperative days, the eyes were undercorrected. The refraction stabilized by the 1-week follow-up. The postoperative refraction appears to be stable within 1 week after surgery, as seen in the plot of the mean refraction (SE) and range of refraction against time (Figure 4.16).

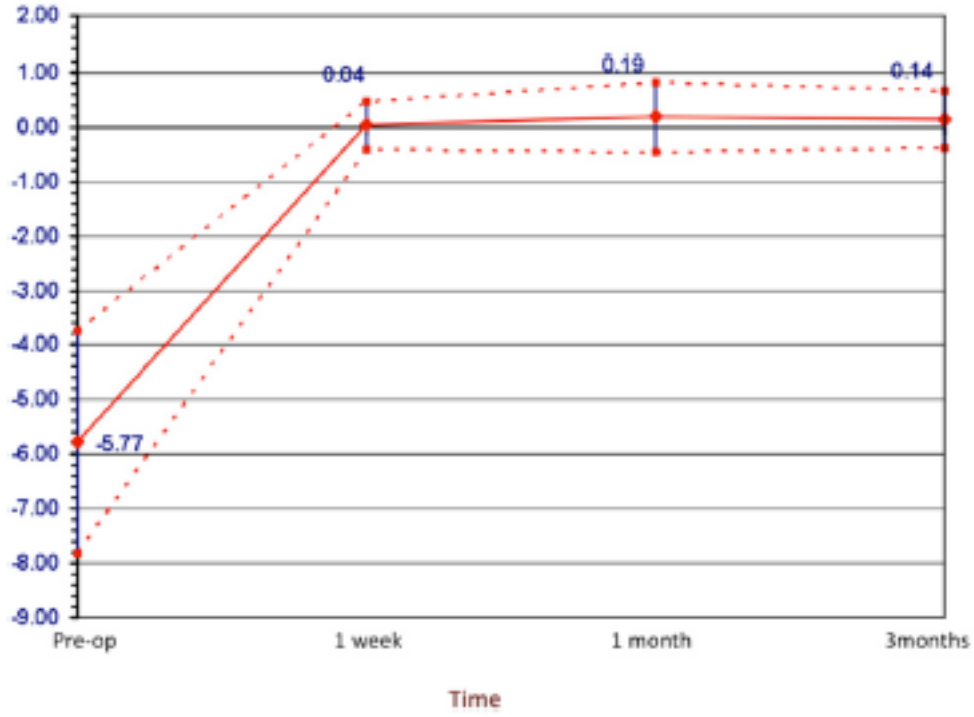

Figure 4.16. Clinical results: stability. Mean SE plotted as a function of time postoperatively. (Courtesy of Ang et al. (169)).

There was no statistically significant difference in the SE refraction between 1 month and 3 months (P = 0.05, Wilcoxon test). UCVA was >= 20/20 in 46%, 52%, and 65% of eyes at 1 week, 1 month, and 3 months postoperatively. BCVA was >=20/20 in 88% and 94% of eyes at 1 month and 3 months postoperatively. UCVA was >=20/25 in 88% and BCVA was >=20/25 in 100% of eyes at 3 months postoperatively. Eighty-one percent of eyes were within +/-0.50 D of intended refraction at 1 week and 83% at 1 month postoperatively, while 95% were within +/- 1.00 D of intended refractive target at 3 months postoperatively. We compared aberration data in 50 eyes pre- and postoperatively at 3 months. The mean mesopic pupil diameter was 6.0 +/- 0.8 mm. There was a significant increase in the root mean square (RMS) higher order aberrations (HOAs) of 0.26 +/- 0.02μm preoperatively compared with 0.38 +/- 0.02μm postoperatively (P < 0.001) (Table 4.6).

	Lower Order Error (D)			RMS (μm)		
Parameter	Spherical	Cylindrical	Coma	Trefoil	Spherical	Total Higher Order
Preoperative mean (SD)	−5.6 (1.9)	−1.0 (0.7)	0.07 (0.07)	0.07 (0.01)	0.06 (0.01)	0.26 (0.02)
Postoperative mean (SD)	0.3 (0.6)	−0.4 (0.3)	0.14 (0.013)	0.08 (0.01)	0.17 (0.02)	0.38 (0.02)
P Value	0.001	0.001	0.01	0.27	0.001	0.001

Table 4.6 Preoperative and Postoperative Aberrometry Data. (Courtesy of Ang et al. (169)).

At 1 month postoperatively, 82% of eyes did not lose any lines of UCVA; increasing to 97% of eyes at 3 months postoperatively (Figure 4.17).

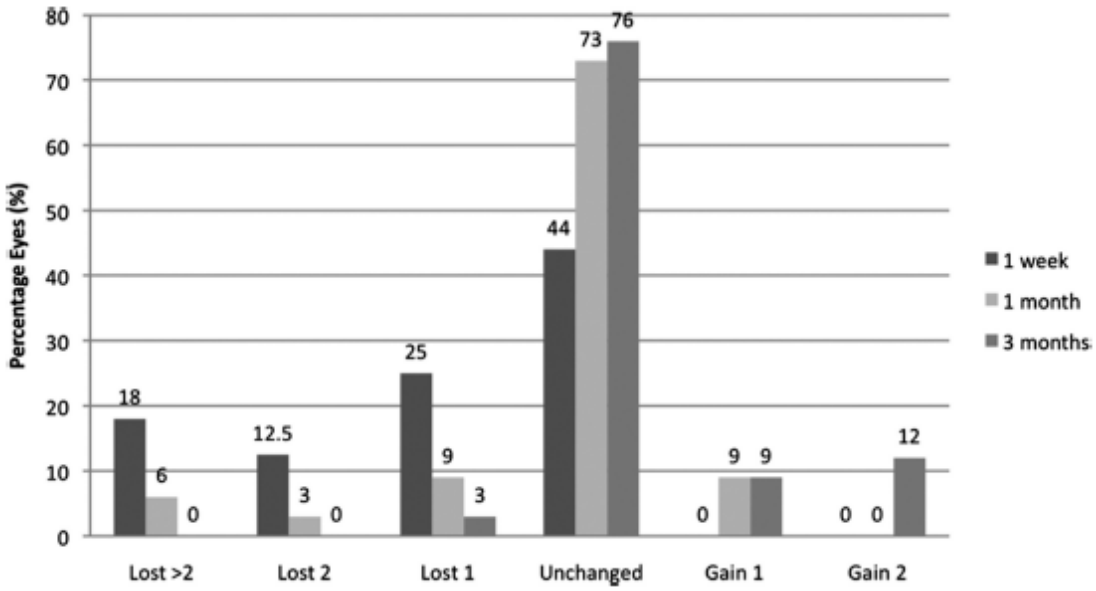

Figure 4.17. Clinical results: safety. The percentage of eyes (y-axis) in which there was a gain/loss of specified number of Snellen BCVA lines (x-axis) for different postoperative periods. (Courtesy of Ang et al. (169)).

At 3-month follow-up, 3% of eyes lost 1 line of BCVA. There were no significant side effects such as diffuse lamellar keratitis, transient light sensitivity syndrome, subconjunctival hemorrhage, interface debris, or corneal ectasia in any of the cases during the period of the study. There was 1 case of suction loss during lenticule cutting where >10% was completed. We restarted and completed the procedure as recommended at the time, and the patient had a UCVA of 20/60 and BCVA of 20/25 with -2.0 D of induced astigmatism at 1 month postoperatively. Thus, this patient

underwent subsequent enhancement with LASIK and the patient achieved UCVA of 20/25 on 1 day postoperatively and remained stable at 3 months postoperatively.

4.3.3.2 Real Time IOP

We successfully measured real time IOP in 78 eyes of 39 rabbits for both FLEx (n= 40) and FS-LASIK (n = 38) procedures. Incomplete data were obtained from one rabbit due to malfunction of the pressure transducer and were excluded from the analysis. There were no significant differences between all baseline calibration IOP measurements with the tonometer (Tono-pen XL; Reichert Ophthalmic Instruments) and our device (8.56 +/- 1.8 mm Hg vs. 9.14 +/- 1.6 mm Hg; P = 0.190). No complications occurred during intraocular cannulation. We did not observe any procedural or postoperative complications. There was no significant difference between the mean baseline IOP in the rabbit eyes in the FS-LASIK group and the FLEx group (9.03 +/- 2.1 mm Hg vs. 8.90 +/- 2.4 mm Hg; P = 0.204). There was a significant increase in mean IOP in both FS-LASIK (mean increase in IOP: 26.8 +/- 1.2mm Hg; P < 0.001) and FLEx procedures (mean increase in IOP, 27.2 +/- 1.5 mm Hg; P < 0.001) compared with the baseline IOP. However, there was no significant difference in mean increase in IOP between both procedures (P = 0.203); and mean difference between baseline and peak IOP (FS-LASIK 30.0 +/- 1.6 mm Hg vs. FLEx 30.2 +/-1.4 mm Hg; P = 0.559). We also compared real-time in vivo IOP measurements at specific stages of each procedure (Figure 4.18A, 4.18B).

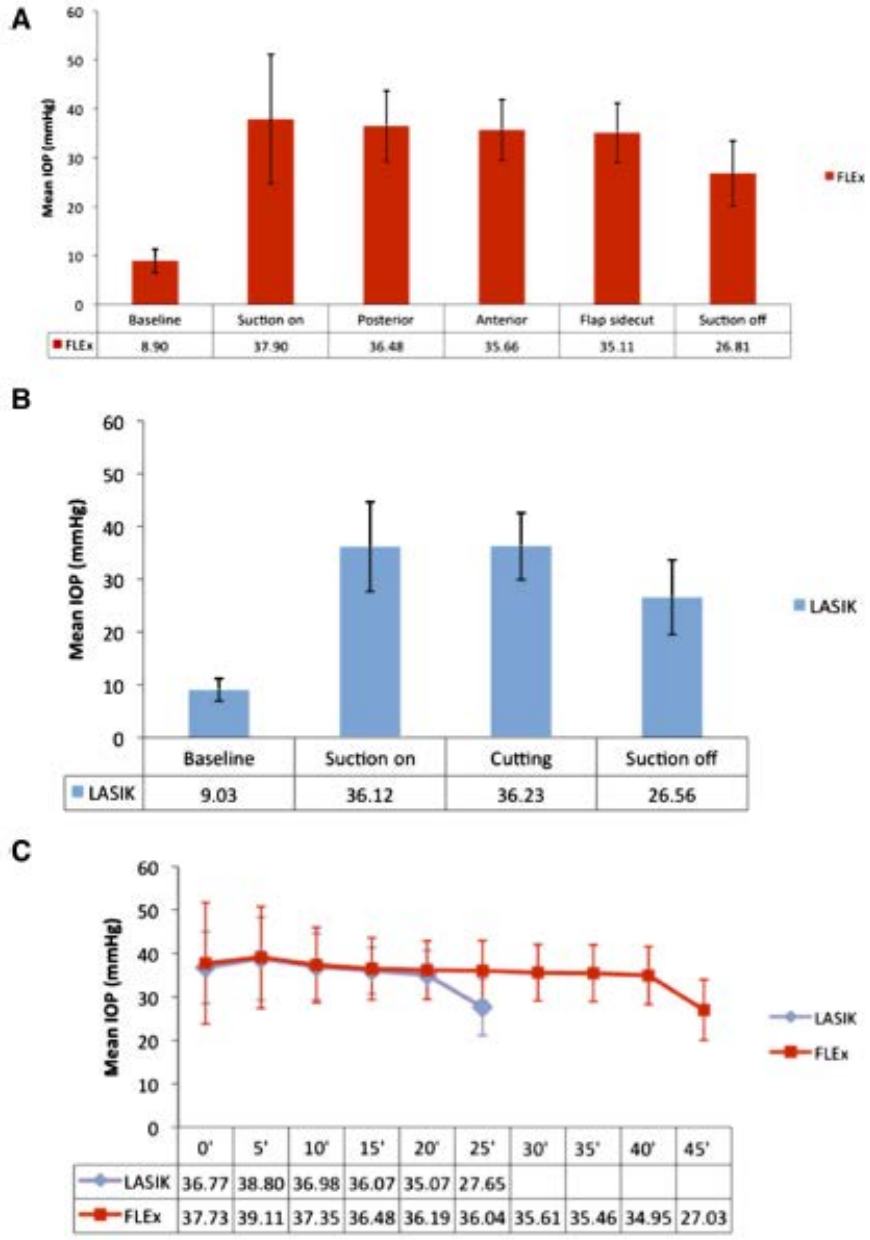

Figure 4.18. In vivo real-time mean IOP measurements during LASIK (A) and FLEx (B) procedures. Mean IOP values obtained during the various stages of the surgery are provided below the figure. Data are presented as mean standard error of the mean (n=38 for LASIK and n=40 for FLEx). P 0.05 was considered significant. One-way analysis of variance (ANOVA) indicated a statistical significant difference in all the groups compared with the basal levels in both the techniques used. (C) Comparison of in vivo real-time mean IOP levels and time required during LASIK and FLEx procedures. Mean IOP values recorded during the each procedure are shown below the figure. Data are presented as mean standard error of the mean (n=38 for LASIK and n=40 for FLEx). P 0.05 was considered significant. (Courtesy of Ang et al. (169)).

We found no significant differences in mean IOP of the eyes undergoing the FLEx or FS-LASIK during the procedure comparing mean IOP for suction on (P =

0.803), cutting (P = 0.487) and suction off (P =0.433) stages. Overall, the FLEx procedures took significantly longer to perform than the FS-LASIK procedures (mean overall duration of procedure: 46.1 +/- 3.5 vs. 25.5 +/- 2.7 seconds; P < 0.001), thereby subjecting each eye undergoing FLEx to a longer duration of increased IOP (Figure 4.18C).

4.3.3.3 Ultra-structural Analysis of FLEx

The human corneal flap beds analyzed with SEM appeared similar for both FS-LASIK (Figure 4.19A) and FLEx (Figure 4.19B, 4.19C) treated groups. There were minimal differences observed on high power images of the surfaces of the beds created by FS-LASIK (Figure 4.19D) and pre-lenticule extraction FLEx (Figure 4.19E). Cavitation bubbles generated by laser photodisruption in the prelenticule-extracted FLEx group can be easily seen demarcating a circumferential groove on the stromal surface before lenticule extraction (Figure 4.19E, 4.19F). We used a previously described grading system with a maximal score of 11 (smoothest) to grade the flap surfaces.

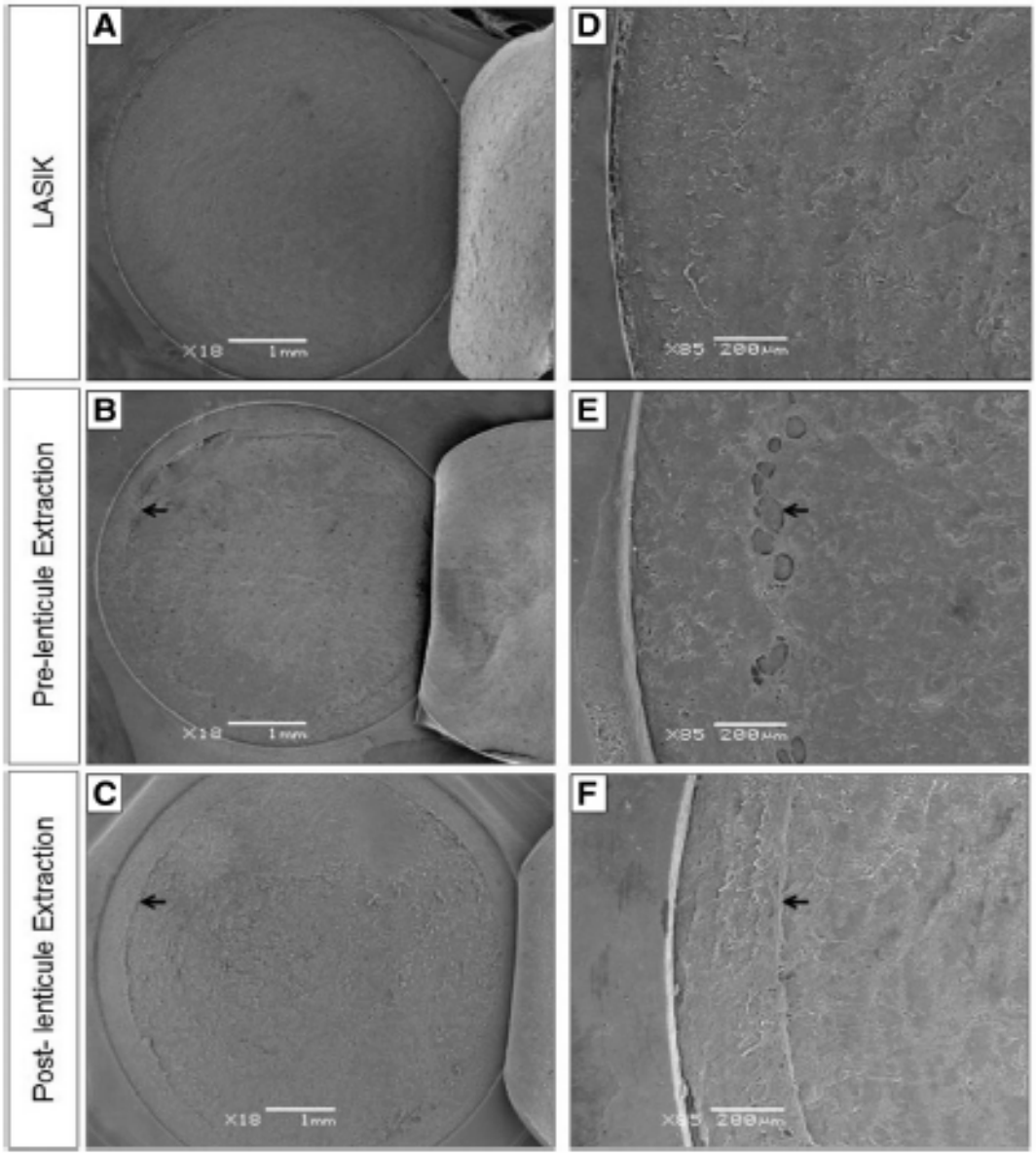

Figure 4.19. Scanning electron micrographs showing the surface topographical analysis of the residual corneal stromal bed. The topography of LASIK-treated (A, D) stromal bed serves as control. FLEx-treated stromal beds were divided into pre- (B, E) and post- (C, F) lenticule extraction. Lenticule side cut (arrow) can be seen delineating a smaller circumference than the flap side cut. Prelenticule extraction where the lenticule was still intact exhibits circular perforations and tissue bridges along the lenticule side cut, which could be due to the effect of cavitation bubbles created from FS photodisruption. Lenticule side cut of the post lenticule extraction stromal bed shows a ridge indicating the platform where lenticule had been removed. (Courtesy of Ang et al. (169)).

There was good agreement between the independent, masked observers for each treatment group (intraclass coefficient, 0.8). We found no significant difference between

the mean irregularity scores comparing treatment groups A, B, and C of the stromal bed after lenticule extraction (8.8 +/- 0.6, 10.3 +/- 0.4, and 8.7 +/- 0.6, respectively; P = 0.88), which suggests that the smoothness of the stromal bed does not depend on the dioptric power of the lenticule extracted. There was also no significant difference in smoothness of the corneal flaps between all 3 groups (10.8 +/- 0.8, 10.6 +/- 0.4, and 9.8 +/- 0.8, respectively; P = 0.33).

4.3.4 Comparison of Four Circle patterns for Flap Creation after SMILE

4.3.4.1 ASOCT

The previously performed cap-stromal bed interface was barely detectable by AS-OCT 28 days after the SMILE procedure. In pattern A treated corneas, only the side cut was visible (Figure 4.20A). In pattern B treated corneas, a lamellar ring with an average depth of 131.33 ± 4.04 microns and a side cut could be observed (Figure 4.20B). A lamellar ring with a depth of 113.67 ± 3. 21 microns and a side cut were seen in pattern C treated corneas (Figure 4.20C). In pattern D treated corneas, a lamellar ring with a depth of 122.00 ± 3.46 microns and a side cut were visible (Figure 4.20D). The junction cut created by all patterns was not detectable on AS-OCT.

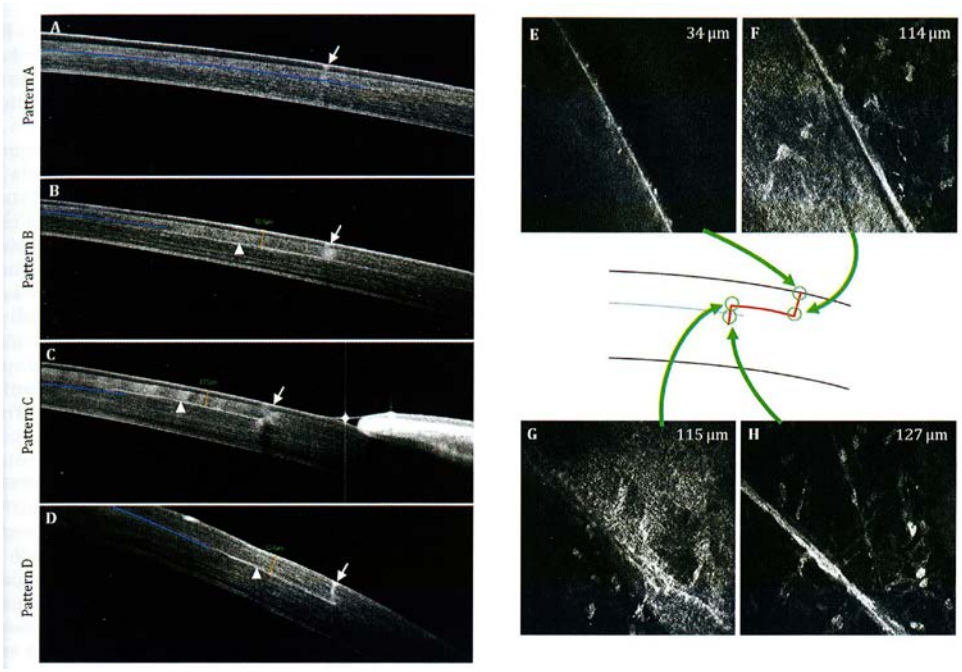

Figure 4.20. Visualization of the incision created by VisuMax Circle patterns (Carl Zeiss Meditec, Jena, Germany). Images were obtained after the incision and before flap lifting, using anterior segment optical coherence tomography (AS-OCT). Lamellar ring (arrowheads) was characterized by light reflective layer, indicative of femtosecond laser disrupted lamellae. The original refractive lenticule extraction small incision lenticule extraction (SMILE) cap cuts were not visible on AS-OCT by day 28 after SMILE. The presumed cap cut was marked in blue. (A) Pattern A created a side cut within the cap cut. (B) Pattern B created a lamellar ring at a measured depth of 127 *microns*, placing it posterior to the cap cut. (C) Pattern C created a lamellar ring at a depth of 115 microns,, placing it anterior to the cap cut. (D) Pattern D created a lamellar ring adjacent to the cap cut, which depth was measured at 124microns. Arrows indicate the side cut created by patterns A, B, C, and D. In vivo confocal micrographs of the intrastromal cuts appeared similar in all treatment groups. (E) The appearance of side cut at the depth of 34 microns from the superficial epithelium. (F) The junction between side cut and the lamellar ring at the depth of 114microns. The femtosecond laser disrupted layer of lamellar ring is discernible by its light reflective layer. (G) The junction between the junction cut and the lamellar ring. (H) The junction between the cap cut (blue in illustration) and the junction cut. (Courtesy of Riau et al. (170)).

The appearance of intrastromal cuts and lamellar ring was similar on in vivo confocal micrographs in all treatment groups. Therefore, we selected the images from pattern C-treated corneas to represent the in vivo confocal microscopy results. En-face images showed the side cut through the anterior cornea (Figure 4.20 E) and the junction between the side cut and the lamellar ring at the depth of 114 microns (Figure 4.20 F). The femtosecond laser-

disrupted lamellar ring was marked by a light reflective layer. In vivo confocal images also showed the intersection between the junction cut and lamellar ring (Figure 4.20 G) and between the junction cut and cap interface (Figure 4.20 H).

4.3.4.2 Scanning electron Microscopy and Flap Lift

PATTERN A

SEM showed the vertical side cut after the flap was lifted and the undisrupted collagen fibrils at the centre of the flap bed. The difficulty of flap lift was grade 2 for all 3 eyes, similar to the difficulty of femtosecond laser-created flap lift.

PATTERN B

Following AS-OCT, we attempted to lift the flap by inserting a Seibel spatula under the flap edge near the hinge to create access from the lamellar ring to the original cap-stromal bed interface. Because the lamellar ring was placed posterior to the cap cut, we had difficulty in accessing the intended plane and inadvertently damaged the lamellae under the edge of the optical zone during the intrastromal manipulation with the spatula, as illustrated and revealed by the SEM image. Once the correct plane (cap cut) was reached, the flap lift was straightforward and no further significant tissue damage was observed at the opposite quadrant of the optical zone**.** An approximately 10μm elevation could be seen from the lamellar ring to the cap cut**.** SEM also revealed the vertical side cut and the undisrupted central corneal flap bed**.** Due to the difficulty in accessing the original cap-stromal bed interface and resultant tissue damage, the difficulty of flap lift was grade 4 for all 3 eyes treated with pattern B.

PATTERN C

SEM images showed no lamellar damage in pattern C-treated corneas. The

slight depression (arrow) from the lamellar ring to the cap-stromal bed interface was barely visible. The difficulty of flap lift was grade 3 in all 3 eyes because there was a minor resistance when attempting to access the original cap cut, most probably due to the difference in depth between the lamellar ring and the cap cut.

PATTERN D

The transition between the lamellar ring and the optical zone was not discernible in the SEM image. Similar to corneas treated with patterns A, B, and C, the central corneal flap bed created by pattern D was also undisrupted after flap lifting. The difficulty of flap lift after pattern D treatment was grade 2 in all 3 eyes, similar to the difficulty in lifting a standard femtosecond laser-created LASIK flap.

4.3.5 Lenticule Viability and Integrity

4.3.5.1 Transmission Electron Microscopy (TEM)

The ultrastructural analysis of fresh (n=3) and cryopreserved (n=3) lenticules with TEM showed apoptotic, necrotic and normal quiescent keratocytes. We observed more necrotic than apoptotic keratocytes, which were mostly located at the periphery of the lenticule (Figure 4.21).

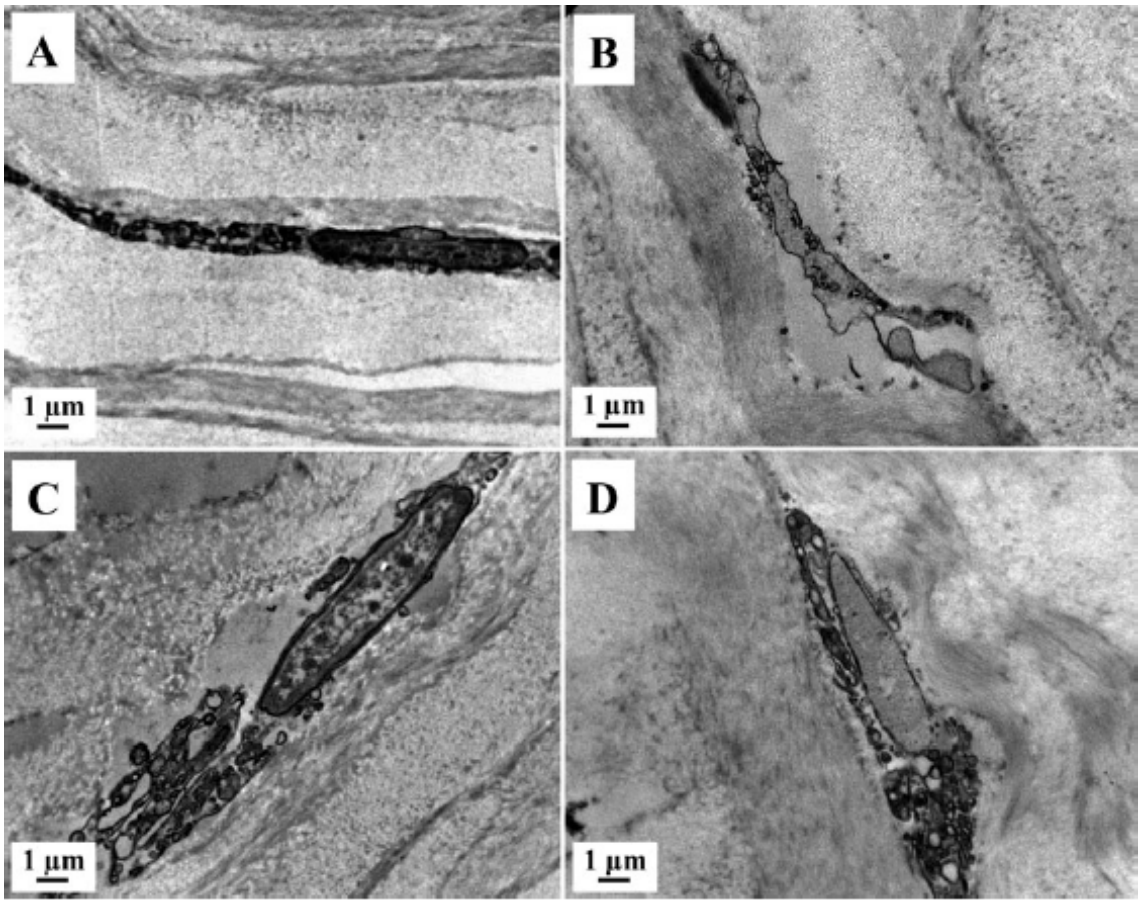

Figure 4.21. Transmission electron micrographs (TEM) of stromal lenticule showing keratocytes. A, C: Fresh lenticule. B, D: Cryopreserved lenticule. A, B: Apoptotic keratocytes with cromatin condensation and fragmentation, apoptotic bodies, loss of cytoplasm and cell shrinkage. C, D: Necrotic keratocyte, with incomplete nuclear membrane and vacuoles in the cytoplasm. Magnification, 8900×. (Courtesy of Noriega et al. (171)).

The normal quiescent keratocytes were defined as those with large nuclei with peripheral heterochromatin and thin cytoplasm with complete cellular and nuclear membrane without visible mitochondria or extensive rough endoplasmic reticulum. Apoptotic keratocytes were defined as having chromatin condensation and fragmentation, shrinkage of nucleus and cell, apoptotic bodies, and/or loss of cytoplasm. Necrotic keratocytes were defined as those having incomplete nuclei and cell membrane, cytoplasmic vacuoles, dispersed chromatin with irregular clumpings, and/or swelling and a vacuolated nucleus. Lenticule collagen fibril architecture in both groups was relatively well preserved after ReLEx and after cryopreservation. There were no

fragmented fibrils or areas of collagen disruption; as well as no change in fibrils diameter (Figure 4.22).

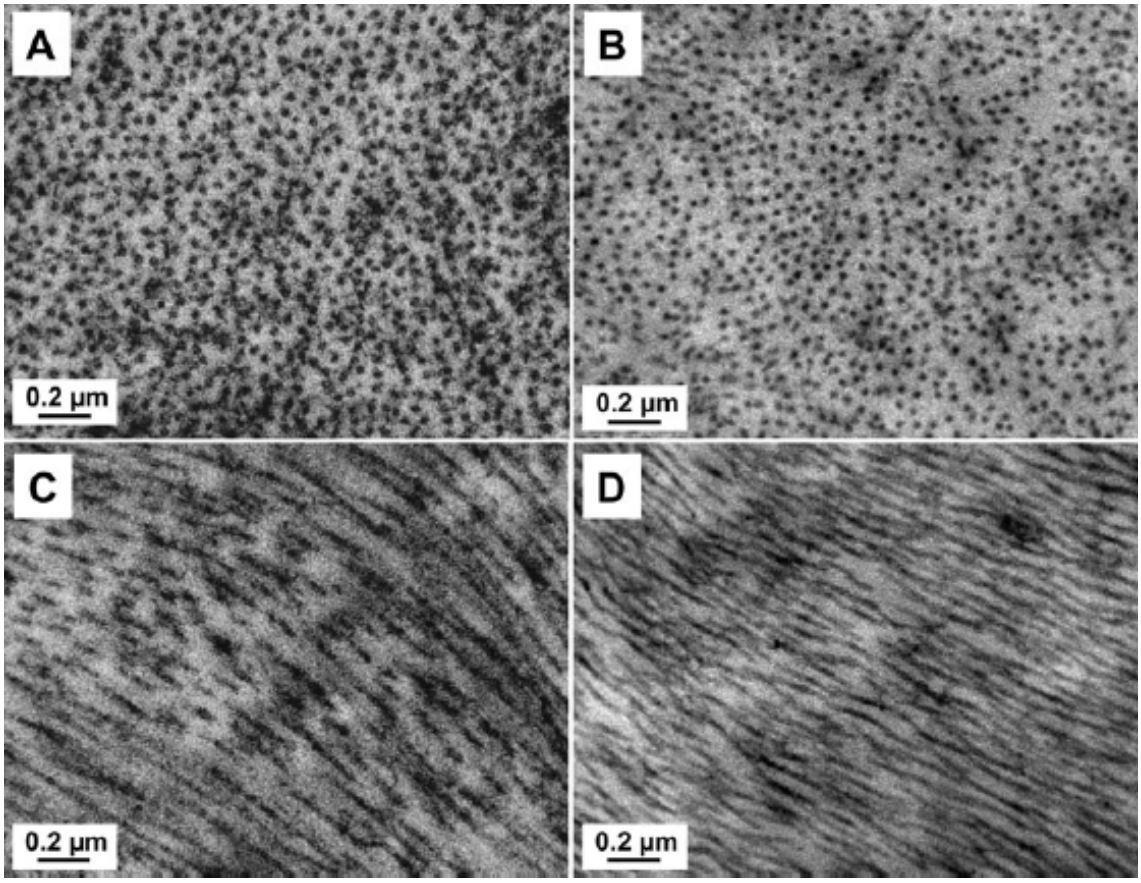

Figure 4.22 Transmission electron micrographs (TEM) of the stromal lenticule showing collagen fibrils. A, C: Fresh lenticule. B, D: Cryopreserved lenticule. A, B: Transversal section of collagen fibrils. C, D: Longitudinal section of collagen fibrils. Magnification, 50,000×. (Courtesy of Noriega et al. (171)).

The mean (+/- SD) CFD was 15.75±1.56 and 12.05±0.62 for the fresh and cryopreserved group, respectively. The mean (+/- SD) number of collagen fibrils was 728.33±38.19 and 795.33±33.84 in the fresh and cryopreserved groups respectively. There was no significant change in the number of collagen fibrils (P=0.09), but a significant decrease in CFD (P=0.02) was observed after cryopreservation.

4.3.5.2 TUNEL ASSAY

Analysis of apoptotic keratocytes in fresh (n=3) and cryopreserved (n=3) groups was

performed using a TUNEL assay, and cell nuclei were counterstained using DAPI (Figure 4.23).

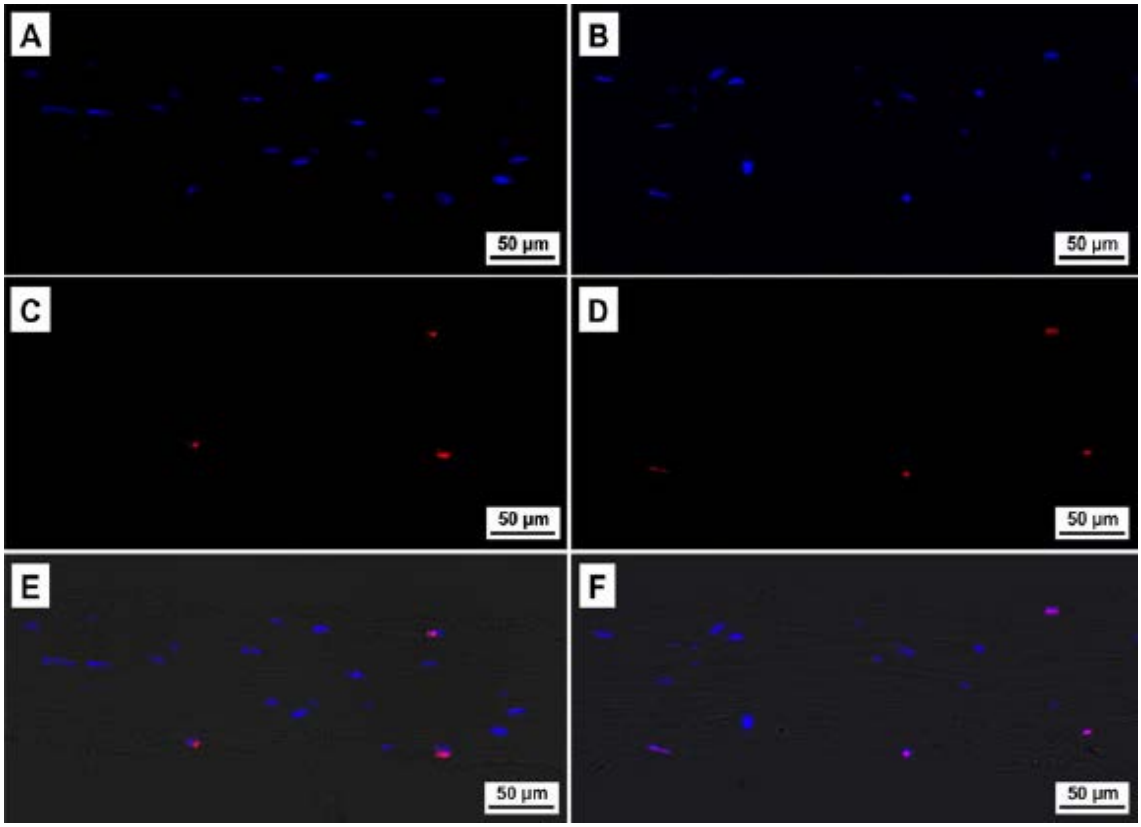

Figure 4.23 TUNEL-positive (deoxynucleotidyl transferase-mediated nick end labeling assay) cells in fresh and cryopreserved human lenticules. A, C, E: Fresh samples. B, D, F: Cryopreserved samples. A, B: DAPI-stained (4',6-diamidino-2-phenylindole stain) cells. C, D: TUNEL positive cells. E, F: Composite image of DAPI, TUNEL and Bright-field. Magnification, 200×. (Courtesy of Noriega et al. (171)).

Quantification of TUNEL-positive and DAPI-stained cells is described in Table 4.7. We observed TUNEL-positive cells in both the groups.

Location area	Peripheral		Central		Total	
Staining	DAPI	TUNEL	DAPI	TUNEL	DAPI	TUNEL
Fresh lenticules						
Total cells	147	54	427	34	574	88
Mean cells	7.0	2.6	20.3	1.6	27.3	4.2
SD	2.73	1.18	7.48	2.28	8.02	2.28
Max - Min	14–2	5–1	35–9	7–0	42–13	9–1
Percentage	73.1	26.9	92.6	7.4	86.7	13.3
Cryopreserved lenticules						
Total cells	137	59	242	37	378	96
Mean cells	6.5	2.8	11.5	1.8	18.0	4.6
SD	2.82	1.22	6.22	1.74	6.77	1.62
Max - Min	14–3	5–1	31–1	6–0	42–9	7–1
Percentage	69.9	30.1	86.7	13.3	79.7	20.3

TUNEL: deoxynucleotidyl transferase-mediated nick end labeling assay, DAPI: 4',6-diamidino-2-phenylindole, ReLEx: Refractive Lenticule Extraction procedure, SD: Standard Deviation.

Table 4.7 TUNEL and DAPI positive cells in peripheral, central and total area of fresh and cryopreserved ReLEx lenticules. (Courtesy of Noriega et al. (171)).

However, there was an increase in the number of TUNEL-positive cells and a proportional reduction in the number of DAPI-stained cells after cryopreservation. These findings were significant in the centre (P=0.007), but not in the periphery (P=0.419) of the lenticule (Figure 4.24 and Table 4.7).

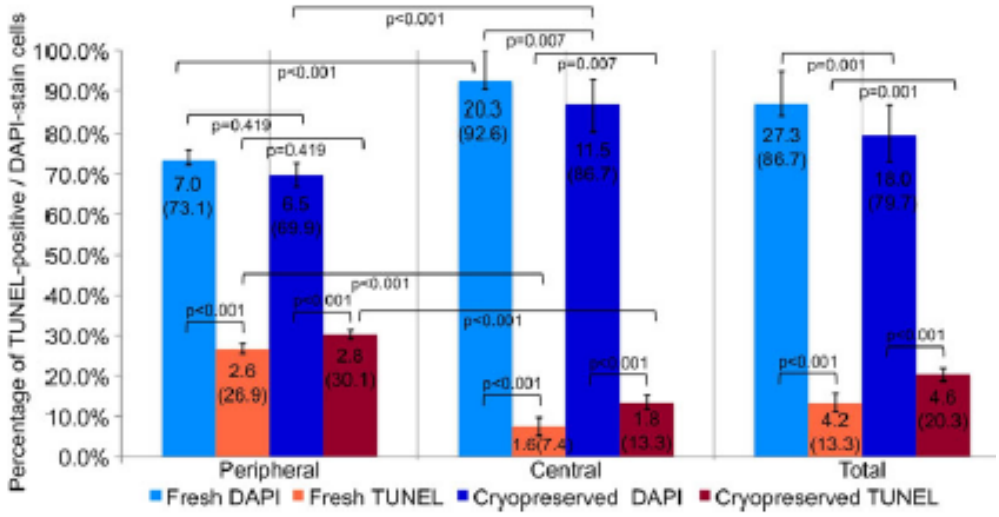

Figure 4.24 Mean number (%) of TUNEL (deoxynucleotidyl transferase-mediated nick end labeling assay) positive cells and DAPI (4',6-diamidino-2-phenylindole) stain cells in fresh and cryopreserved lenticules extracted from a ReLEx (Refractive Lenticule Extraction) procedure. It was considered a significant difference when $p<0.05$. (Courtesy of Noriega et al. (171)).

Altogether, there were more TUNEL-positive cells located in the periphery than in the centre of the lenticules, in fresh ($P<0.001$) and cryopreserved ($P<0.001$) groups. The number of DAPI-stained cells was higher in the centre than in the periphery, in fresh ($P<0.001$) and cryopreserved ($P<0.001$) groups (Figure 4.24 and Table 4.7).

4.3.5.3 Cell Culture

We were able to culture viable keratocytes from fresh (n=3) and cryopreserved (n=3) lenticules. After stromal digestion with collagenase, isolated keratocytes were cultivated in medium containing serum (FBS). The keratocytes adopted typical elongated morphology of fibroblastic phenotype within two days in culture and rapidly proliferated to reach confluence in one week, in both the groups. We did not notice any difference in cellular morphology or proliferation rates between the groups (Figure 4.25).

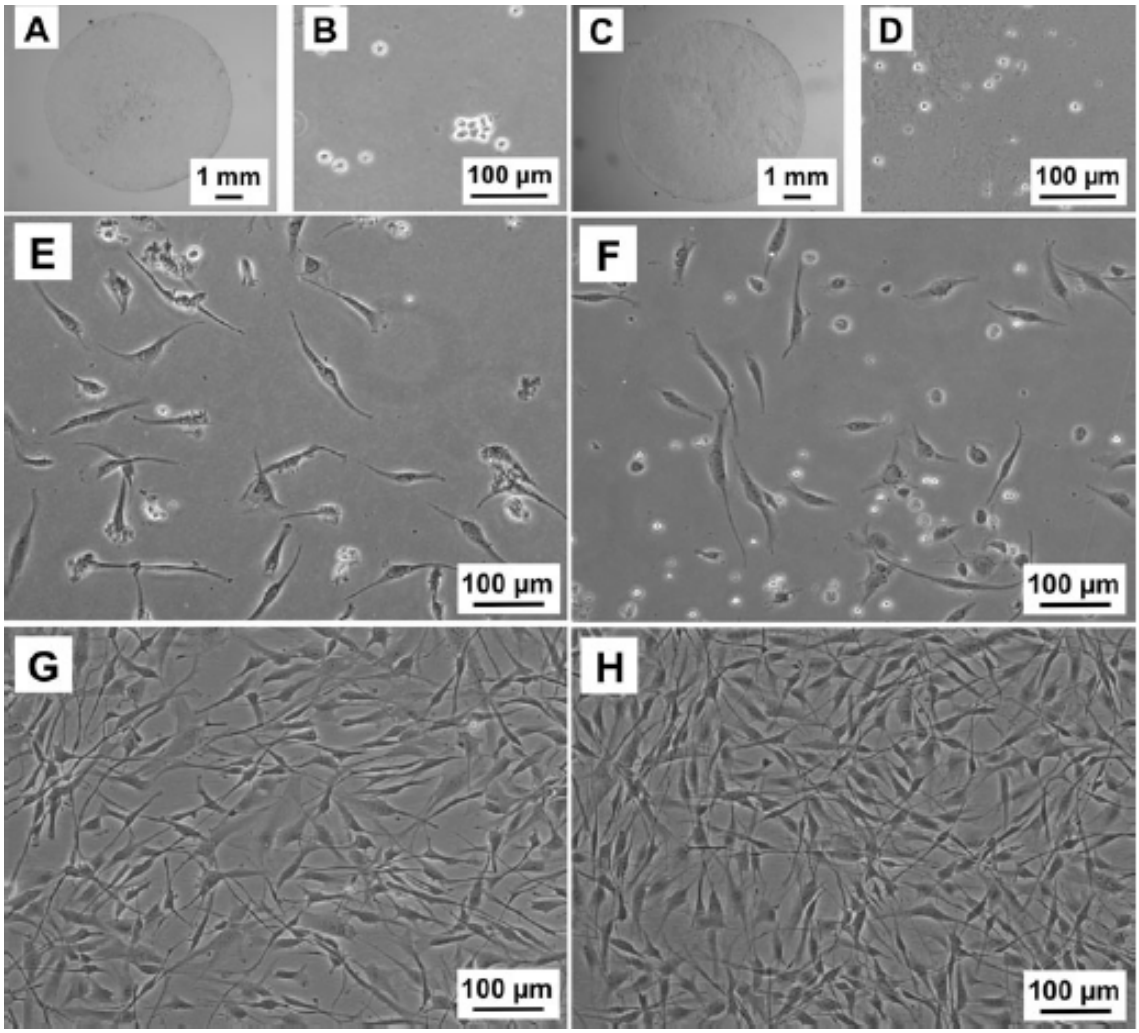

Figure 4.25 Representative images of cultured keratocytes from ReLEx (Refractive Lenticule Extraction) lenticules. A, B, E, G: Fresh samples. C, D, F, H: Cryopreserved samples. A, C: ReLEx lenticule. B, D: Free floating stromal keratocytes following enzymatic digestion for at least 4 h in collagenase. E, F: Attached keratocytes beginning to elongate into spindle-like fibroblastic cells by Day 2 in culture. G, H: Confluent stromal fibroblasts after 7 days in culture. (Courtesy of Noriega et al. (171)).

4.3.5.4 RT-PCR

Gene expression analysis of fresh and cryopreserved lenticules showed expression of keratocytes specific genes KERA and ALDH3A1 (Figure 4.26).

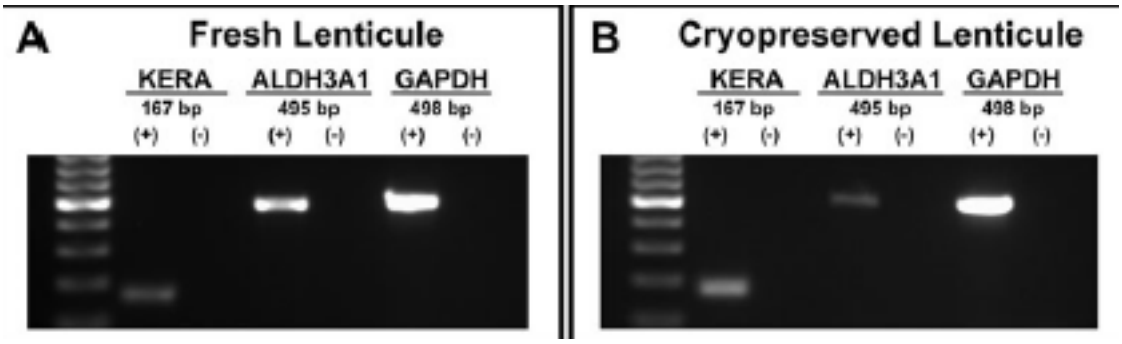

Figure 4.26 Expression of keratocyte specific markers in isolated cells from ReLEx (Refractive Lenticule Extraction) lenticules. Fresh (A) and cryopreserved (B) lenticules. Human keratocan (KERA) with 167 bp, aldehyde dehydrogenase 3A1 (ALDH3A1) with 495 bp and the housekeeping gene glyceraldehyde 3-phosphate dehydrogenase (GAPDH) with 498 bp. (+): Lenticule sample. (-): Negative control. (Courtesy of Noriega et al. (171)).

4.3.6 Lenticule Re-Implantation Proof of Concept-Rabbit Study

4.3.6.1 Slit Lamp Photography

Slit lamp photographs showed that corneal clarity progressively improved from day 3 to 28 following lenticule reimplantation with minimal stromal inflammation, infiltration, or diffuse lamellar keratitis (DLK) (Figure 4.27A, upper panel). Retro illumination photography revealed irregularities or microstriae within the lenticule on postoperative day 3. These were predominantly seen at the periphery of the lenticule (Figure 4.27A, bottom panel). These irregularities had disappeared by day 14 after re implantations, and by day 28, the re-implanted corneas were comparable to unoperated control corneas in terms of clarity (Figure 4.27A, bottom panel). Corneal clarity gradually improved from post re-implantation day 3 (2.20 ± 0.45) to day 28 (0.20 ± 0.27) (Figure 4.27D). There was a statistical significant difference in corneal clarity between day 3 and pre-operative corneas ($P < 0.001$), and between day 14 and pre-operative corneas ($P < 0.05$). The corneal clarity on day 28 was comparable to before the ReLEx (FLEx) surgery.

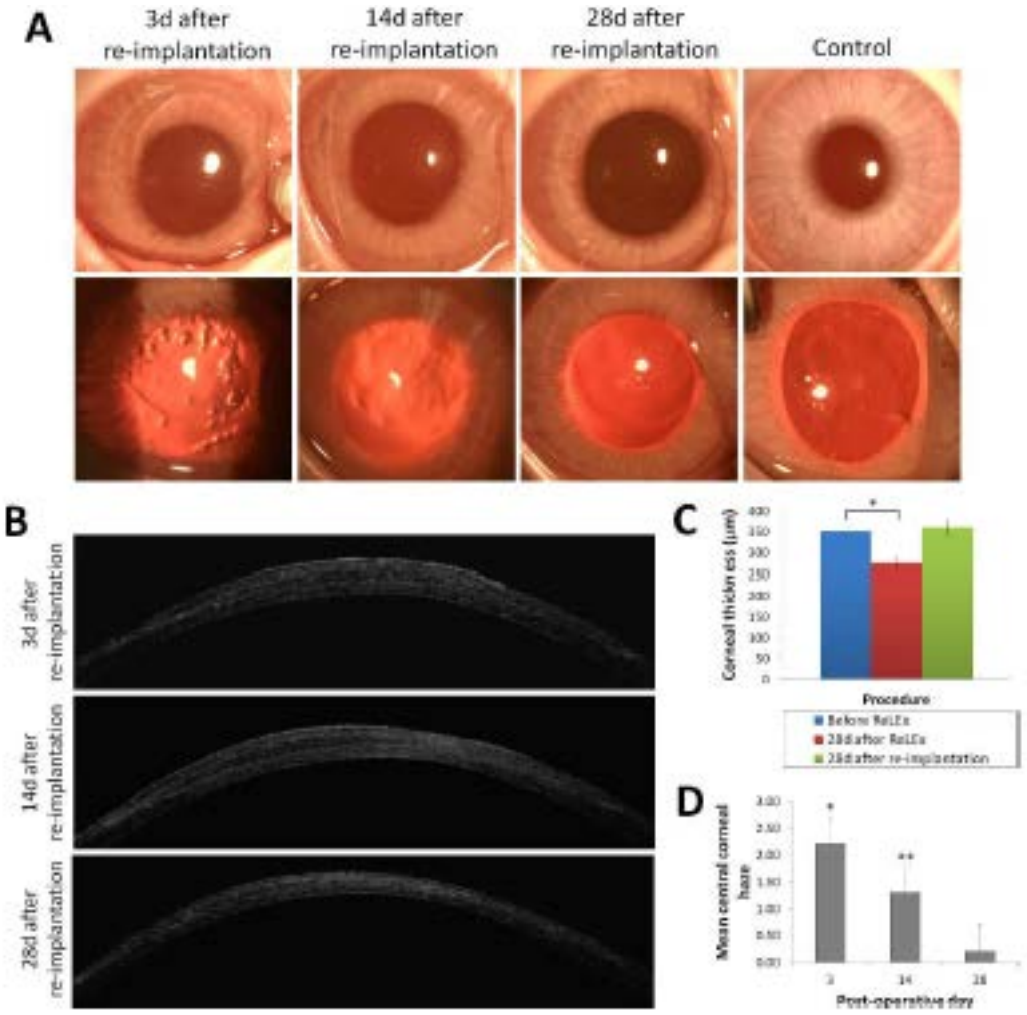

Figure 4.27 Slit lamp microscopy, AS-OCT, and pachymetry of the postoperative corneas. (A) The top panel shows slit lamp photographs of the non operated cornea (control) and cornea on day 3, 14, and 28 after lenticule re-implantation. The bottom panel shows retro illumination photographs of the control and postoperative corneas. (B) Temporal AS-OCT images of postoperative corneas shows resolving tissue edema over time. (C) Bar graph showing the corneal thickness before ReLEx procedure, 28 days after ReLEx, and 28 days after lenticule re-implantation. (D) Quantification of central corneal haze on day 3, 14, and 28 after lenticule re-implantation. Corneal clarity or haze is graded on a scale of 0–4 (from 0 being completely clear to 4 being completely obscured). Statistical significance was obtained by comparing postoperative to pre-operative corneal clarity. Error bars represent +/- 1 SD. *P < 0.001, and **P < 0.05. (Courtesy of Angunawela et al. (172)).

4.3.6.2 Stromal Volume Restoration

On AS-OCT, corneas appeared edematous compared with control eyes on day 3 after re-implantation, but returned to normal at subsequent time points (Figure 4.27B). The anterior and posterior borders of the lenticule were easily discernible on postoperative

day 3. AS-OCT corneal pachymetry before ReLEx (FLEx), 28 days after ReLEx (FLEx), and 28 days after reimplantation was measured at 351.67 +/- 11.90 microns, 274.73 +/- 11.64 microns, and 361.00 +/- 18.13 microns, respectively (Figure 4.27C).

4.3.6.3 In Vivo Confocal microscopy

The anterior border (top panel), lamellae (middle panel), and posterior border (bottom panel) of the re-implanted corneal lenticule on postoperative days 3, 14, and 28 were clearly identifiable on confocal microscopy (Figure 4.28).

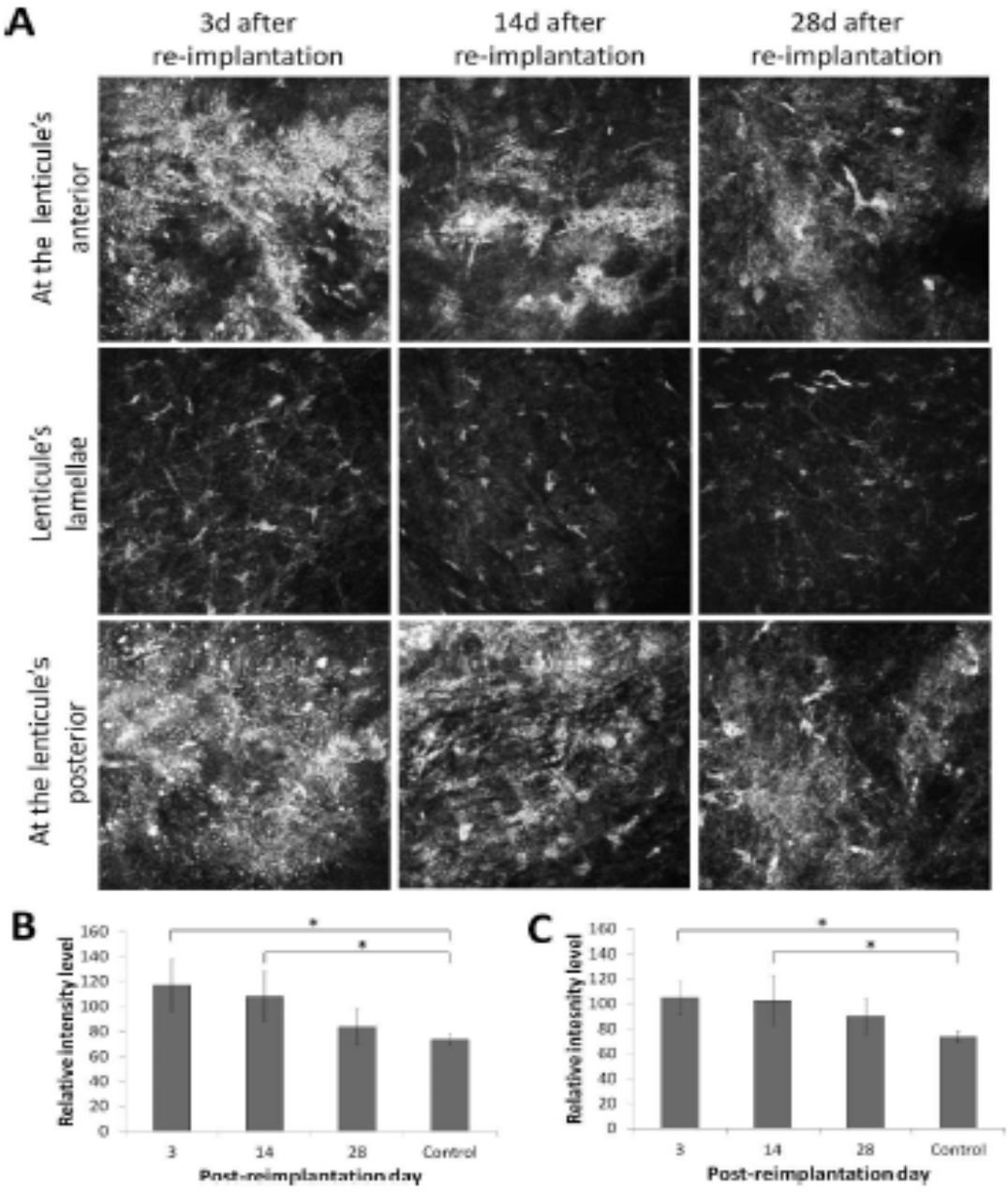

Figure 4.28 In vivo confocal micrographs of the corneas on day 3, 14, and 28 after lenticule re-implantation. (A) The top panel shows the anterior border of the lenticule within the re-implanted cornea. The middle panel shows the presence of quiescent keratocytes within the lenticule's lamellae. The bottom panel shows the posterior interface of the lenticule. Repopulation of anterior and posterior borders of the lenticule occurs by day 28. (B) Bar graph showing the mean reflectivity level of the lenticule's anterior interface on day 3, 14, and 28 after lenticule re-implantation. (C) Bar graph showing the mean reflectivity level of the lenticule's posterior plane on day 3, 14, and 28 after lenticule re-implantation. Error bars represent SD. *P < 0.05. (Courtesy of Angunawela et al. (172)).

The anterior and posterior border of the lenticule showed increased light reflectance and was acellular on day 3 after re-implantation. Interspersed small particles with variable size and reflectivity were observed at the lenticule's anterior and posterior border, which were likely to be post surgical debris. On day 14, the reflective layer at both interfaces was less prominent and keratocytes were visible, particularly at the posterior interface of the lenticule. Increased numbers of keratocytes had appeared at the anterior border of the lenticule on day 28. The keratocytes within the centre of the lenticule remained quiescent and did not seem to change in terms of their morphology and activity from postoperative day 3 to 28. Quantification of the relative reflectivity level of the lenticule's anterior and posterior borders are shown in Figures 4.28A and 4.28B respectively, and were seen to decrease over the duration of the study. The intensity of the reflective layer at the lenticule's anterior decreased from 117.09 +/- 20.67 on post re-implantation day 3 to 83.73 +/- 14.15 on day 28, and reduced from 105.15 +/- 12.87 on day 3 to 90.09 +/ 14.10 on day 28 at the lenticule's posterior. Significant difference ($P < 0.05$) was observed between day 3 and control, and between day 14 and control at both interfaces.

4.3.6.4 Corneal Topography and keratometry

Corneal topographic maps (Figure 4.29) showed obvious flattening consistent with the -6.00 D treatment 28 days after the initial ReLEx (FLEx) procedure.

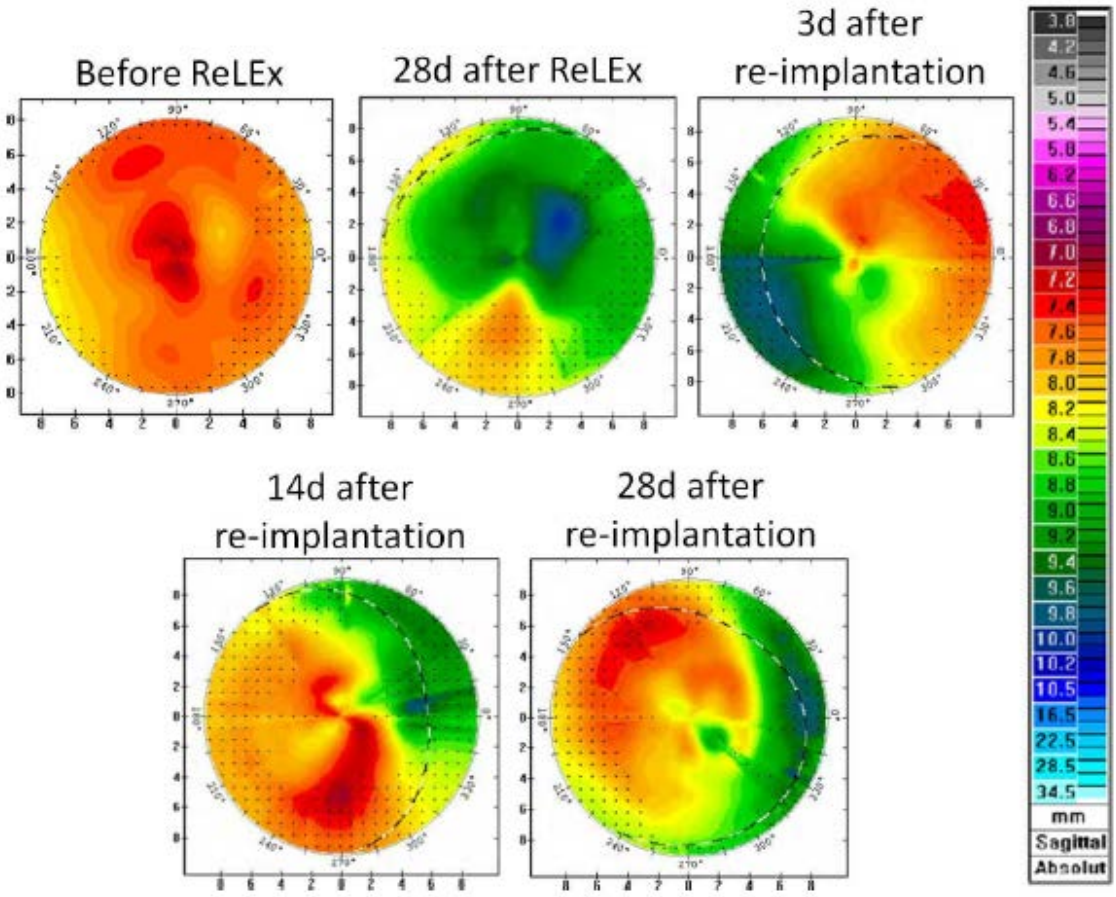

Figure 4.29 Corneal topography before ReLEx procedure, 28 days after ReLEx, and 3, 14, and 28 days after lenticule re-implantation. There is initial flattening of the cornea consistent with the 6.00 D ReLEx correction initially, however, by day 28 post lenticule re-implantation topographic indices are similar to the unoperated state. (Courtesy of Angunawela et al. (172)).

Twenty eight days after lenticule reimplantation, corneas were steepened centrally in all cases, and topographic maps appeared similar to corneas before ReLEx (FLEx). Mean keratometry values for operated eyes were as follows: 48.0 +/- 2.3 D before ReLEx (FLEx), 42.0 +/- 2.0 D 28 days after ReLEx (FLEx), and 45.6 +/- 1.8 D 28 days after lenticule re-implantation. Based on these values, the mean keratometry after re-implantation was 2.4 +/- 0.7 D less than the unoperated keratometry before ReLEx (FLEx). When the keratometry of the control non-operated fellow corneas was measured, we found a baseline mean keratometry of 48.6 +/- 1.9 D. The mean keratometry at the final time point in control eyes (28 days after lenticule re-

implantation in the fellow eye) was 46.7 +/- 1.3 D. These measurements demonstrated an overall flattening and commensurate reduction in the mean keratometry of -1.9 ± 1.0 D in control eyes over the 56 day time course of this study. This is a previously documented natural aging phenomenon that occurs as the rabbit matures. When this natural reduction in keratometry was compensated for in the operated eyes, the final keratometry following re-implantation was -0.6 +/- 0.8 D from the preoperative correction.

4.3.6.5 IMMUNOHISTOCHEMISTRY

On day 28 after re-implantation, fibronectin was expressed along the anterior and posterior border of the lenticule (Figure 4.30, top panel).

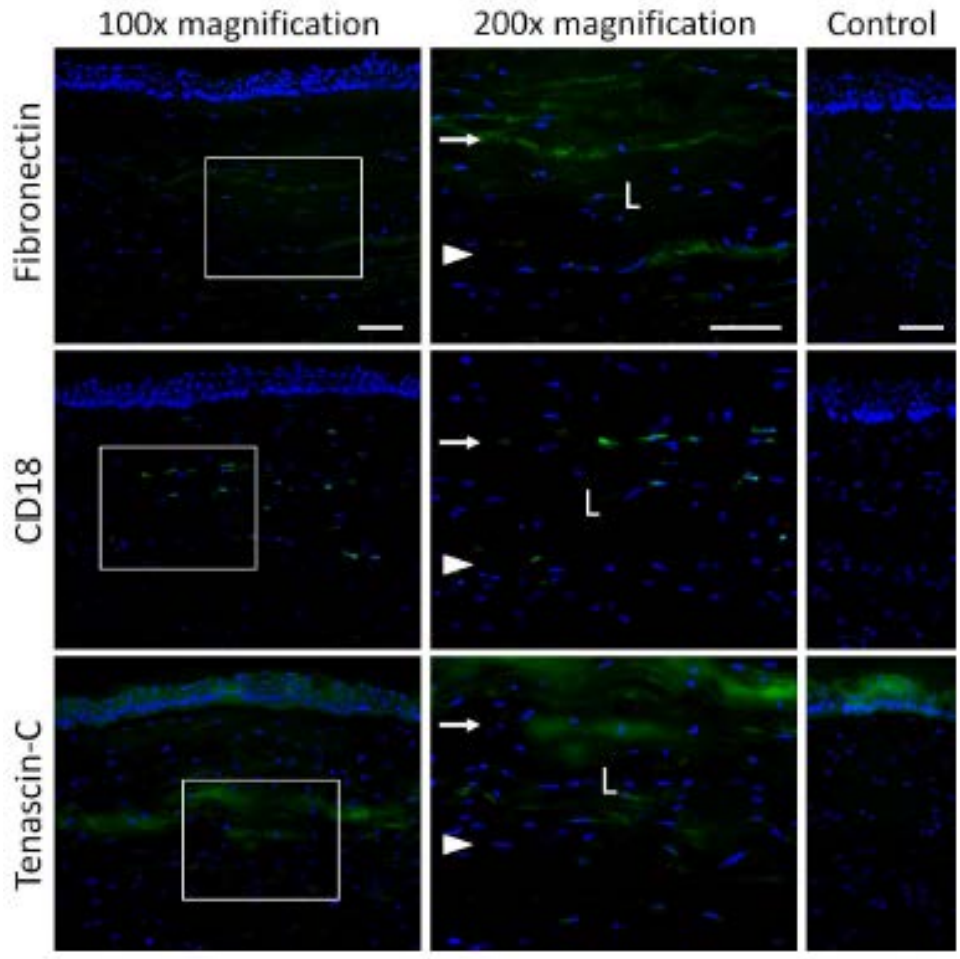

Figure 4.30 Expression of fibronectin, CD18, and tenascin-C in the corneas on day 28 after lenticule re-implantation. Images in the middle column are the magnified images within the white boxes found in the left column. Staining of the non-operated corneas (control) is shown in the right column. Arrowheads show the lenticule's posterior interface and arrows show the lenticule's anterior interface. L indicates the re-implanted lenticule within the corneal stroma. Sections were counterstained with DAPI, which stained the nuclei (blue). Scale bars: 50 micron. (Courtesy of Angunawela et al. (172)).

Leukocyte integrin b2 (CD18), an inflammatory marker and mediator of polymorphonuclear leukocyte (PMN) migration within the corneal stroma, was seen expressed only by a few cells and predominantly found at the interfaces of the lenticule (Figure 4.30, middle panel). Tenascin-C could be detected within the lenticule, and was mainly expressed along lenticule's anterior interface (Figure 4.30, bottom panel).

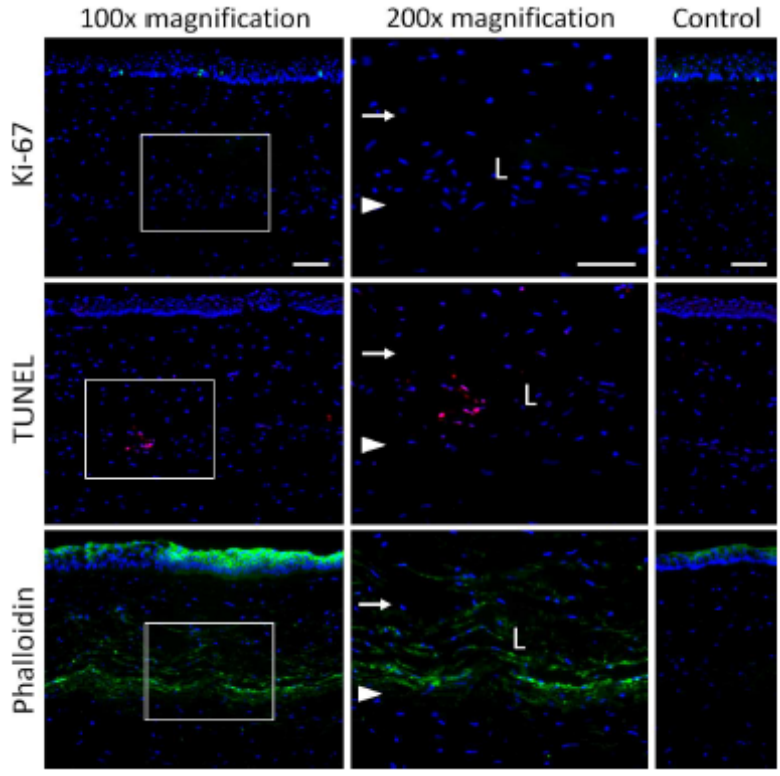

Figure 4.31 Fluorescent staining of Ki67, TUNEL, and phalloidin in the corneas on day 28 after lenticule re-implantation. Images in the middle column are the magnified images within the white boxes found in the left column. Staining of the nonoperated corneas (control) is shown in the right column. Arrowheads show the lenticule's posterior interface and arrows show the lenticule's anterior interface. L indicates the re-implanted lenticule within the corneal stroma. Sections were counterstained with DAPI, which stained the nuclei (blue). Scale bars: 50 microns. (Courtesy of Angunawela et al.

(172)).

No proliferating Ki67-positive cells were observed within the lenticule and corneal stroma (Figure 4.31, top panel), and only a few apoptotic TUNEL-positive cells were found within the lenticule of the re-implanted cornea (Figure 4.31, middle panel). No apoptotic epithelial cells were present in the cornea after reimplantation (Figure 4.31 middle panel). Cell migration, indicated by the relatively strong staining of phalloidin indicating the intracellular assembly of filamentous actin, could be seen within the re-implanted lenticule (Figure 4.31, bottom panel). This was more abundant in the posterior portion of the lenticule.

There were no myofibroblasts detected in the re-implanted cornea, which was indicated by the absence of α-SMA (Figure 4.32, top panel). Thy-1–positive fibroblasts were also only scarcely present in the operated cornea, and were typically found within the lenticule (Figure 4.32, bottom panel).

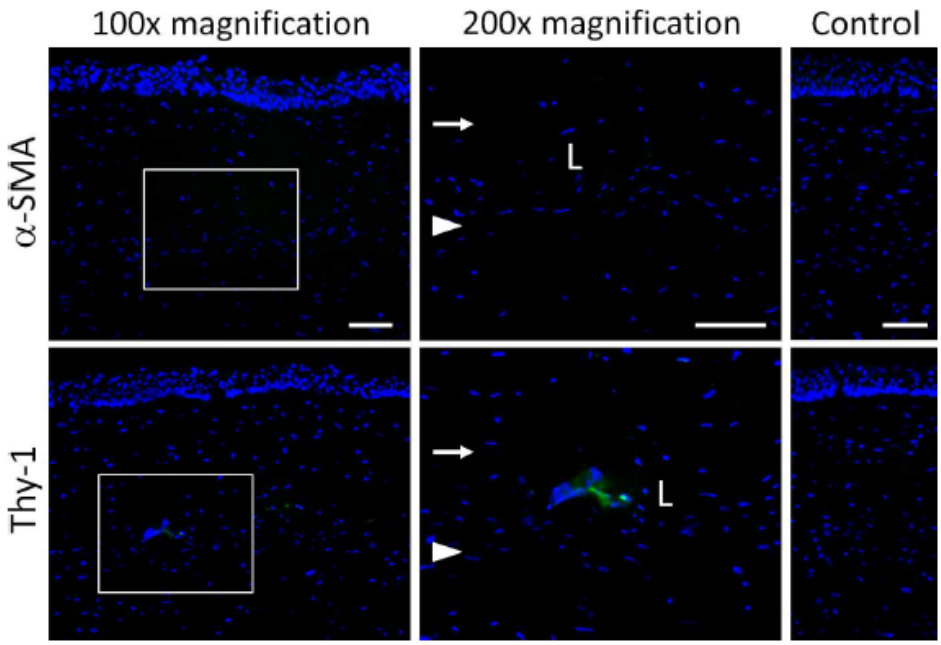

Figure 4.32 Expression of a-SMA and Thy-1 in the corneas on day 28 after lenticule re-implantation. Images in the middle column are the magnified images within the white boxes found in the left column. Staining of the nonoperated corneas (control) is shown in the right column. Arrowheads show the lenticule's posterior interface and arrows show the lenticule's anterior interface. L indicates the re-implanted lenticule within the corneal stroma. Sections were counterstained with DAPI, which stained the nuclei (blue). Scale bars: 50 micron. (Courtesy of Angunawela et al. (172)).

4.3.7 Lenticule Re-Implantation Proof of Value NHP Study

4.3.7.1 Slit Lamp Evaluation

Slit lamp examination with direct light and retro-illumination showed clear corneas at week 8 and 16 following ReLEx surgery with no stromal inflammation, epithelial ingrowth or diffuse lamellar keratitis (Figure 4.33A). Similar results were observed in the corneas at 8 and 16 weeks after RL re-implantation (Figure 4.33A). Corneal clarity was noted to progressively improve from 2.43 +/- 0.53 at day 3 after reimplantation, to 2.00 +/- 0.58 at week 2, to 1.07 +/- 0.73 at week 4, stabilizing to 0.21+/- 0.27 and 0.14 +/- 0.24 at weeks 8 and 16, respectively (Figure 4.33D). There was no significant difference in the clarity of re-implanted corneas at weeks 8 and 16 compared to the pre-operated corneas ($p=0.9$).

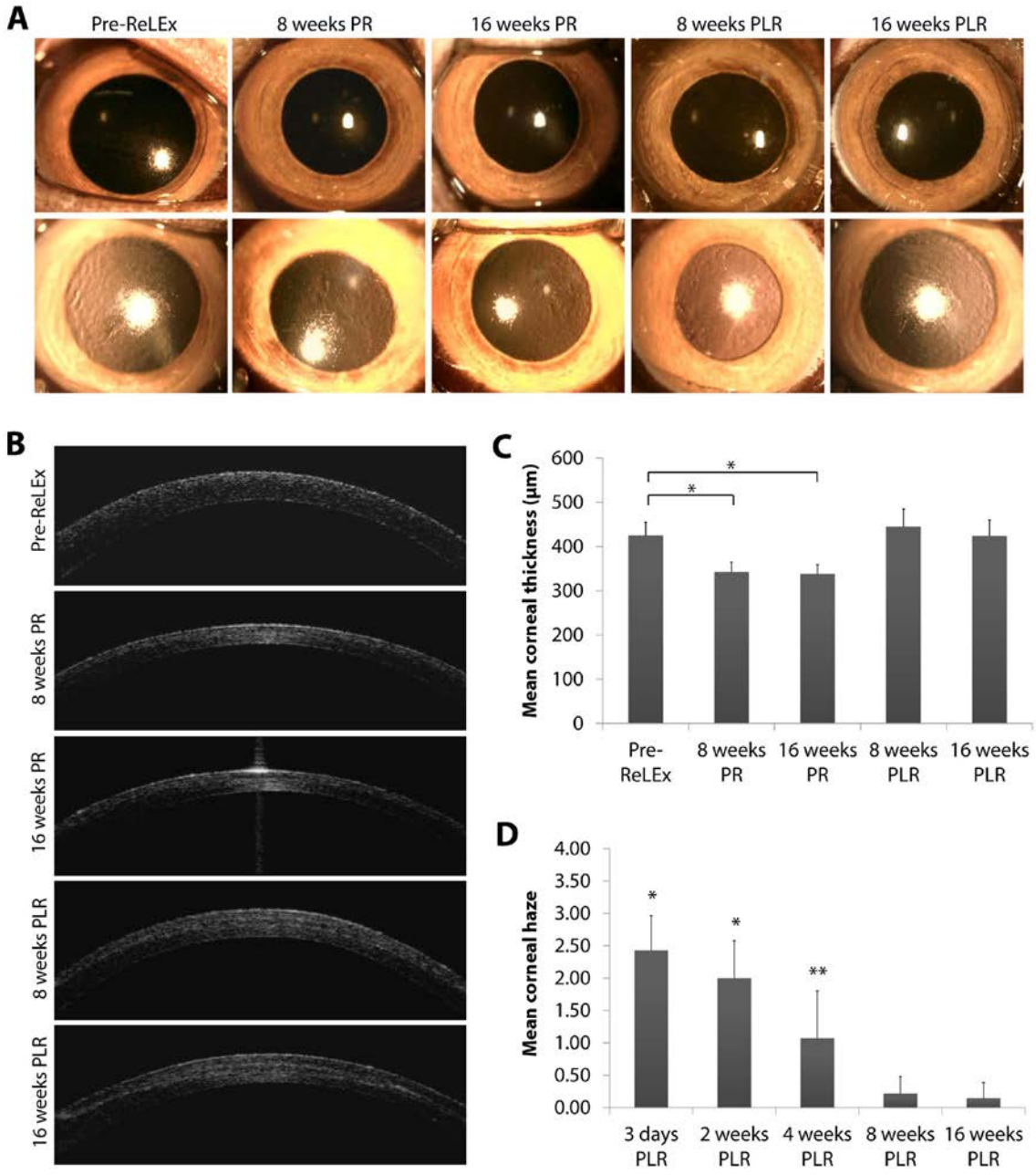

Figure 4.33 Slit lamp microscopy and anterior segment optical coherence tomography (AS-OCT) images of pre- and postoperative corneas. (A) Slit lamp (top panel) and retro illumination photographs (bottom panel) of the cornea before ReLEx and on week 8 and 16 after ReLEx and refractive lenticule re-implantation. (B) Temporal AS-OCT images of postoperative corneas shows thinning of the cornea after ReLEx and restoration of corneal thickness after lenticule re-implantation. (C) Mean corneal thickness before ReLEx and 8 and 16 weeks after ReLEx and lenticule re-implantation. (D) Post-reimplantation corneal haze graded based on observation of the slit lamp photographs found in Figure S3. Corneal clarity or haze was graded on a scale of 0–4 (from 0 being completely clear to 4 being completely obscured). Statistical significance was obtained by comparing post-operative to pre-operative corneal clarity. Error bars in the bar graphs represent standard deviation. Asterisk (*) and double asterisk (**) denote

P<0.001 and P<0.05, respectively. PR: post-ReLEx, PLR: post-lenticule re-implantation. (Courtesy of Riau et al. (173)).

4.3.7.2 ASOCT

Anterior segment-optical coherence tomography (AS-OCT) scans showed thinner corneas after ReLEx surgery as expected, but the thickness was restored after RL re-implantation (Figure 4.33B). The anterior and posterior interface of the lenticule was visible at weeks 8 and 16 after re-implantation (Figure 4.33B). Central corneal thickness before surgery, 16 weeks post-ReLEx, and 16 weeks after RL re-implantation was measured at 425.05 +/- 30.25 mm, 338.33 +/- 20.41 mm, and 423.76 +/- 36.67 mm (n= 7), respectively (Figure 4.33C). There was a statistically significant difference in corneal thickness (P=0.001) between the corneas pre- and post- ReLEx surgery, but no significant difference between the corneas pre-ReLEx and post-lenticule reimplantation.

4.3.7.3 Restoration of Corneal Curvature and Spherical Error

Corneal curvature (keratometry) measurements suggested an obvious flattening of the cornea consistent with the -6.00D myopia treatment at weeks 8 and 16 after ReLEx procedure. At weeks 8 and 16 after re-implantation of the RL, corneas were steepened centrally and the keratometry values were similar to the pre-operative corneas. Similar observations were made in relation to changes in corneal spherical error. There were no significant differences in the spherical error values in the pre-ReLEx and post-re-implantation corneas (Table 4.8).

	Keratometry (D)[c]	p value[d]	Spherical error (D)[c]	p value[e]
Pre-ReLEx	58.6±2.1		−1.64±0.56	
8 weeks PR[a]	54.5±1.3	0.001	+4.43±0.87	<0.001
16 weeks PR[a]	54.1±2.4	0.003	+4.29±0.86	<0.001
8 weeks PLR[b]	57.9±0.8	0.438	−1.61±0.43	0.895
16 weeks PLR[b]	58.0±1.2	0.506	−1.64±0.35	0.891

[a]PR = post-ReLEx.
[b]PLR = post-lenticule re-implantation.
[c]D = diopter.
[d]p values relative to the keratometry before ReLEx.
[e]p values relative to the spherical error before ReLEx.
doi:10.1371/journal.pone.0067058.t001

Table 4.8 Mean Corneal curvature measured by keratometer and mean SEQ measured by refractometer (N=7). (Courtesy of Riau et al. (173)).

4.3.7.4 IN VIVO CONFOCAL MICROSCOPY

In vivo confocal photographs showed appearance of a light reflective layer or haze in the femtosecond laser incision or stromal injury plane. Post-ReLEx surgical regions were marked by interspersed small particles with variable size and reflectivity, which were likely to be mixture of post-surgical debris, inflammatory cells and disrupted extracellular matrix. The reflectivity level was gradually decreased in the subsequent follow ups (Figure 4.34A) and quantified (Figure 4.34C). The intensity level of the reflective layer decreased from 120.9 +/- 611.57 pixels on post-operative day 3 to 92.11+/-17.52 pixels on week 4, and to 78.79+/-11.54 pixels on week 16. There were significant differences observed between post-operative day 3 and pre-operative corneas (P=0.001), as well as between week 2 and pre-operative corneas (P=0.001) and between post-operative week 4 and pre-operative corneas (P=0.05). In addition, keratocyte re-population was seen on week 8 and 16 at the flap interface of post-ReLEx corneas (Figure 4.34A). Similar to post-ReLEx corneas, the anterior (top panel) and posterior border (bottom panel) of the RL showed a higher level of light reflectance and was

acellular in the earlier time points after re-implantation. The reflectivity level was progressively reduced in the subsequent follow-ups (Figure 4.34B) and is depicted in bar graphs (Figure 4.34D and 4.34E). The intensity levels of the reflective layer or haze at the lenticular anterior border decreased from 103.93 ± 20.71 pixels on post-reimplantation day 3 to 83.84+/-16.27 pixels on week 4, and to 80.57 ±12.78 pixels on week 16. Similarly, the reflectance at the lenticular posterior interface reduced from 92.63+/-15.32 pixels on day 3 to 78.03+/-14.08 pixels on week 4, and to 78.20+/-9.31 pixels on week 16. There were statistically significant differences observed between day 3 and control corneas (P=0.05), and between week 2 and control corneas (P=0.05) at both interfaces. Keratocytes were visible at both interfaces of the re-implanted lenticule on week 8 and 16 (Figure 4.34B). Activated and elongated keratocytes within the centre of the lenticule were observed at week 8 (Figure 4.34B, middle panel). At week 16, most of the keratocytes appeared normal and quiescent (Figure 4.34B, middle panel), and resembled those found in the pre-operative corneal stroma (Figure 4.34A, control).

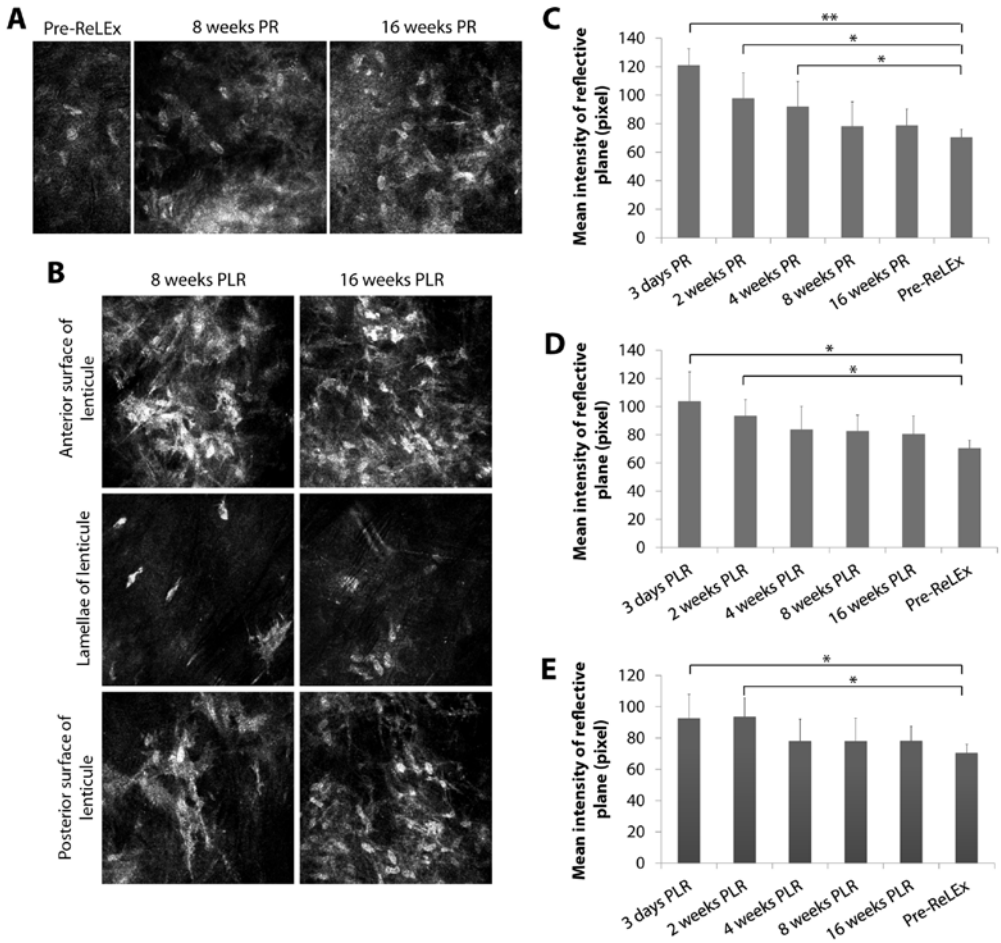

Figure 4.34 In vivo confocal micrographs of pre- and post-operative corneas. (A) Horizontal surgical plane between the flap and stromal bed on week 8 and 16 after ReLEx. This region is normally indicated by a relatively higher light reflective layer. Keratocyte repopulation could be observed on week 8 and 16. (B) The top panel shows the anterior interface of the re-implanted lenticule. The middle panel shows the presence of keratocytes within the lamellae of the lenticule and the bottom panel shows the posterior interface of the lenticule. Keratocyte repopulation of anterior and posterior borders of the lenticule occurred by week 8 after lenticule re-implantation. (C) Mean reflectivity level of the laser incision site on day 3, and 2, 4, 8 and 16 weeks after ReLEx. The representative in vivo confocal images of the cornea at the stated time point can be found in Figure S4A. (D) Mean reflectivity level of the re-implanted lenticule's anterior interface on day 3, and 2, 4, 8 and 16 weeks. (E) Mean reflectivity level of the lenticule's posterior interface post-reimplantation. The representative in vivo confocal images of the cornea at the stated time point in panes D and E can be found in Figure S4B. Error bars in the bar graphs represent standard deviation. Asterisk (*) and double asterisk (**) indicate $P<0.05$ and $P<0.001$, respectively. PR: post-ReLEx, PLR: post-lenticule re-implantation. (Courtesy of Riau et al. (173)).

4.3.7.5 IMMUNOHISTOCHEMISTRY ANALYSIS

On week 8 post-ReLEx surgery, expression of fibronectin was observed along the laser

incision site (Figure 4.35A) and which was weaker on week 16 (Figure 4.35B).

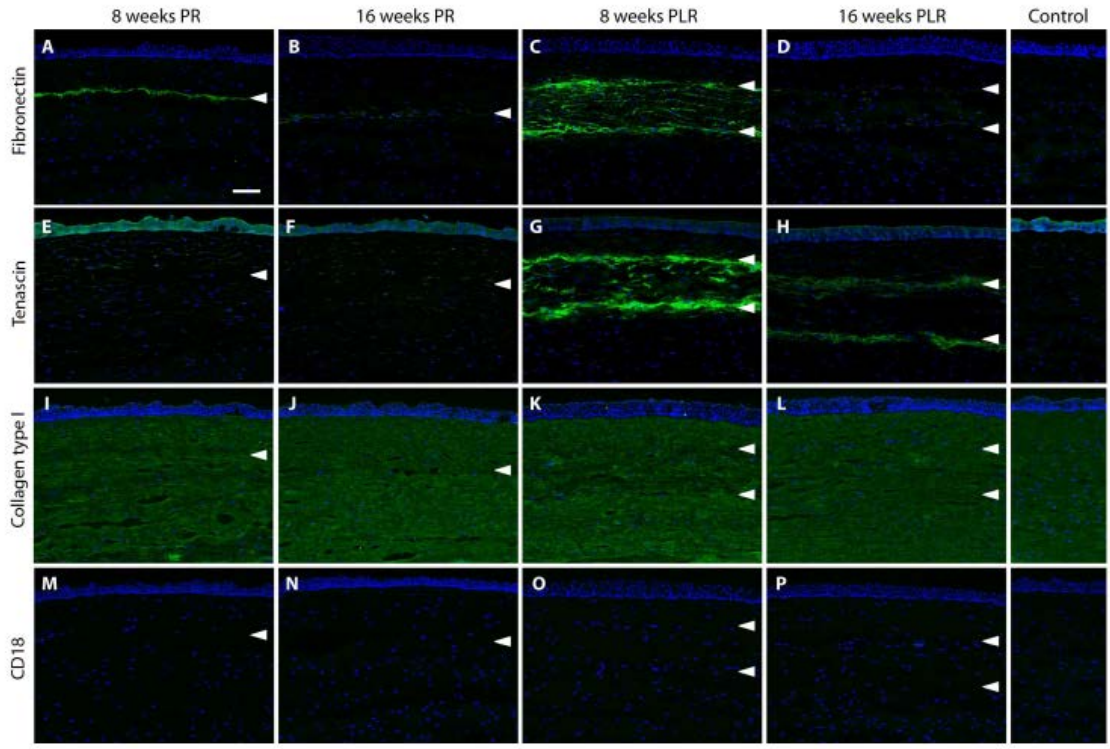

Figure 4.35 Expression of fibronectin, tenascin, collagen type I and CD18 in post-operative central corneas. (A–D) Fibronectin predominantly appeared along the laser incision site or lenticular interface. The expression was reduced over time after either ReLEx or refractive lenticule re-implantation. (E–H) Tenascin was absent along the flap interface on week 8 and 16 following ReLEx, but was present along the borders of the stromal lenticule after re-implantation. The intensity of the staining was attenuated over time. (I–L) Collagen type I was expressed uniformly in the full thickness of corneal stroma. No significant anomaly in collagen arrangement was observed in the corneas post-ReLEx and post-reimplantation. (M–P) CD18-positive cells were not seen in all post-operative corneas. Unoperated corneas were used as control. Arrowheads indicate the location of the laser incision site or lenticular interface. PR: post-ReLEx, PLR: post-lenticule re-implantation. Scale bar: 50 microns. (Courtesy of Riau et al. (173)).

Similar phenomenon could be seen in the corneas after refractive lenticule re-implantation. Fibronectin was predominantly present along the anterior and posterior interface of the re-implanted lenticule on week 8 (Figure 4.35C). Its expression was reduced over time and weaker staining was detected on week 16 (Figure 4.35D). Tenascin is normally found in the corneal epithelial cells and only found in the corneal

stroma after an injury. On week 8 and 16 after ReLEx, tenascin was no longer expressed along the laser injury plane (Figure 4.35E and 4.35F). Similar to fibronectin, tenascin was predominantly present along the anterior and posterior interface of the re-implanted lenticule on week 8 (Figure 4.35G) and its expression was diminished by week 16 (Figure 4.35H). Collagen type I, the predominant collagen type present in the cornea stroma, was uniformly expressed in full thickness of the stroma of control corneas and all the samples in the postoperative corneas. No significant alteration to the collagen expression was observed after either ReLEx procedure (Figure 4.35I and 4.35J) or RL re-implantation (Figure 4.35K and 4.35L). Leukocyte integrin b2 (CD18), an inflammatory marker and mediator of polymorphonuclear leukocyte (PMN) migration within the corneal stroma, was not expressed in post-ReLEx (Figure 4.35M and 4.35N) and post-re-implantation corneas (Figure 4.35O and 4.35P).

In all post-ReLEx and RL re-implanted corneas, no proliferating Ki-67-positive cells were observed within the stroma (Figure 4.36A–4.36D) and no apoptotic TUNEL-positive cells were found within the lenticule or stroma (Figure 4.36E–4.36H). Cell migration, indicated by the relatively strong staining of phalloidin suggest the intracellular assembly of F-actin in the earlier time points, which later decreased after ReLEx surgery (Figure 4.36A,B and 4.36E,F).

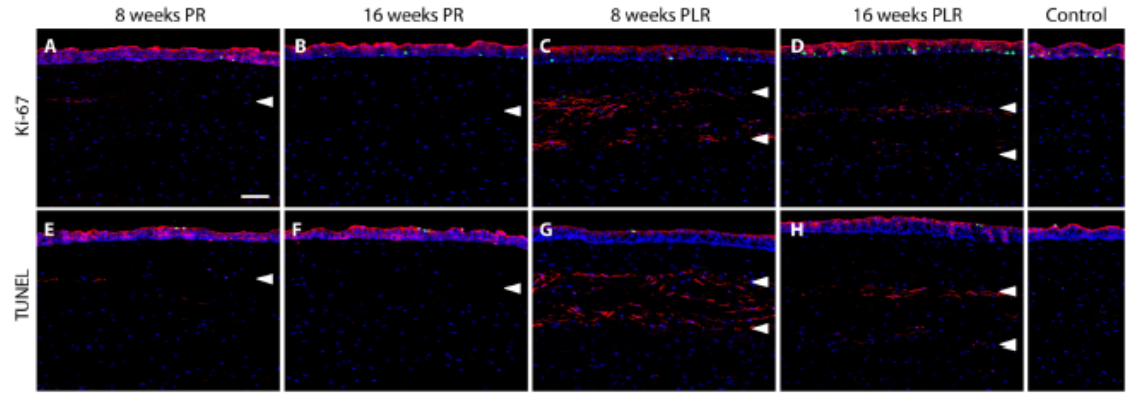

Figure 4.36 Immunofluorescent staining of Ki-67, TUNEL and phalloidin in post-operative central corneas. (A–D) Ki-67-positive cells (green) were not found in the corneal stroma on week 8 and 16 after ReLEx and refractive lenticule re-implantation. (E–H) Similarly, presence of TUNEL-positive cells (green) was also not detected in the corneal stroma. In pane A–H, F-actin marker (red), phalloidin, was observed in the laser incision site or lenticular interface. Its presence was attenuated over time. Nuclei were counterstained using DAPI (blue). Unoperated corneas were used as controls. Arrowheads indicate the location of the laser incision site or lenticular interface. PR: post-ReLEx, PLR: post-lenticule re-implantation. Scale bar: 50 microns. (Courtesy of Riau et al. (173)).

However, presence of phalloidin could be seen within the re-implanted lenticule and was abundant in the anterior and posterior portion of the lenticule at week 8 post-re-implantation (Figure 4.36C and 4.36G), although the presence of F-actin became less abundant at week 16 (Figure 4.36D and 4.36H). There were no myofibroblasts detected at the central cornea on week 8 and 16 after ReLEx (Figure 4.37A and 4.37B) and RL reimplantation (Figure 4.37C and 4.37D), which was indicated by the absence of α-smooth muscle actin (α-SMA) expression.

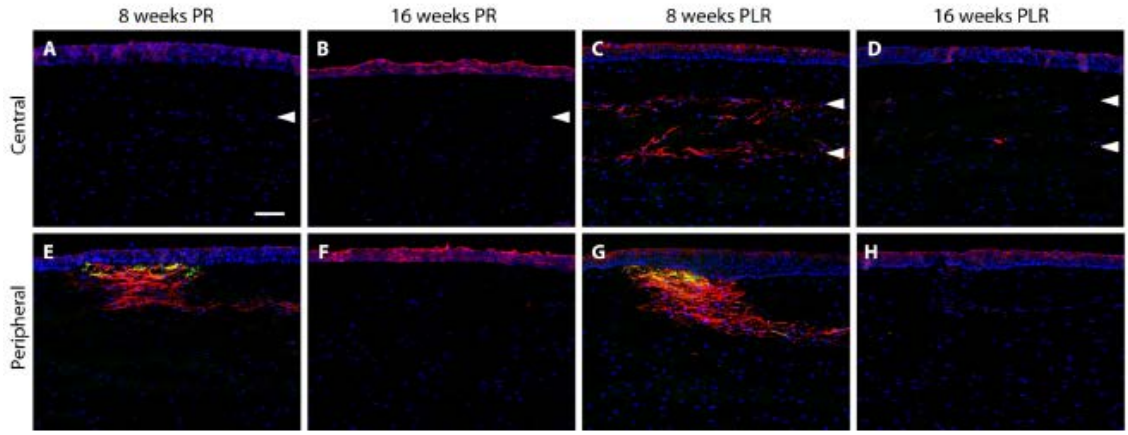

Figure 4.37 Expression of α-smooth muscle actin (α-SMA) in the post-operative central corneas and peripheral flaps. (A–D) α-SMA (green), a marker of myofibroblasts, was not present in the central corneas on week 8 and 16 after both ReLEx and refractive lenticule re-implantation. (E–H) α-SMA (green) was expressed at the flap periphery and co-localized with F-actin (red) subepithelially on week 8 post-ReLEx and lenticule reimplantation, but was absent 16 weeks after both surgical procedures. In pane A–H, α-SMA (green) was double immunostained with F-actin marker (red), phalloidin. Nuclei were counterstained using DAPI (blue). Arrowheads indicate the location of the laser incision site or lenticular interface. PR: post-ReLEx, PLR: post-lenticule reimplantation. Scale bar: 50 microns. (Courtesy of Riau et al. (173)).

α-SMA, which has been reported to be present at the LASIK flap margin due to the incision of the epithelial basement membrane, was detected only subepithelially and co-localized with the F-actin at the corneal flap edge on week 8 following ReLEx (Figure 4.37E) and RL re-implantation (Figure 4.37G). At week 16, myofibroblasts were absent in post-ReLEx (Figure 4.37F) and RL re-implantation groups (Figure 4.37H).

4.4 DISCUSSION

4.4.1 EFFECT OF FIRING PATTERN ON COLLAGEN DISRUPTION

Refractive lenticule extraction with the Visumax femtosecond laser represents an alternative to conventional LASIK. The femtosecond laser system enables users to alter the laser-firing pattern during creation of the lenticule's anterior and posterior surfaces so that the laser pulses can be delivered centripetally or centrifugally. We have shown in this study that variations in the firing pattern of the laser may result in differences to collagen disruption and corneal ultrastructure, which may in turn affect postoperative results.

Shah et al. (105) found that patients who had laser pulse delivery from the periphery in (for the lenticular posterior surface) and from the centre out (for the lenticular anterior surface) showed better clinical results with respect to visual recovery, efficacy, safety, and refractive outcomes when compared with those who had laser delivery from the centre out (posterior surface) and from the periphery in (anterior surface). The authors suggest that the disparity in the results was perhaps due to the distorted stromal layer adjacent to the lenticule's anterior incision plane.

In our study, we assessed the biological and ultrastructural impact of 4 combinations of laser firing patterns in ReLEx surgery using a rabbit model. We studied the wound-healing responses 18 hours after surgery and focused our findings on the central and anterior aspect of the refractive lenticule because these areas are more likely to be visually significant. The posterior incision of refractive lenticules is always initiated in normal and undisrupted stromal layers regardless of the type of treatment; hence, the outcome of the laser delivery was not significantly different. We did not find any difference in the intensity level of the reflective surface at the keratotomy site of any treated cornea on in vivo confocal microscopy regardless of the laser-delivery

pattern.

We found a relatively weak expression of fibronectin along the anterior incision site and no inflammatory cells in the stroma of all corneas treated with firing patterns (A, B, C, and D). We saw a difference in the expression of collagen type I, the predominant collagen type in the cornea composing the stromal fibrils, between eyes treated with patterns A, B, and C compared with those treated with pattern D. In the pattern D treated corneas, a stronger and discontinuous collagen type I staining pattern was observed along the anterior incision plane, suggesting disruption in the collagen arrangement.

On TEM, we observed the appearance of an electron dense surface uniformly along the anterior incision site, suggesting disruption of collagen fibrils caused by the laser delivery. The separation between the laser affected area and the undisrupted collagen fibrils was easily discernible in corneas treated with firing pattern A and B. In corneas treated with firing pattern C (posterior surface centripetal, anterior surface centripetal), the border between the laser disrupted tissue and the unaffected collagen fibrils became more difficult to discern because of the increased disruption of the fibrils. In the corneas in the pattern D treatment group (posterior surface centrifugal, anterior surface centripetal), the collagen fibrils appeared even more disrupted. The border between the disrupted and undisrupted tissue was completely indiscernible. This collagen fibril derangement at the incision plane correlated with the distribution of more intense staining of collagen type I observed on immunohistochemistry.

A limitation of this study is that the lenticular anterior incision– flap interface

was created at the depth of approximately 120 microns. In the rabbit corneas of 400 microns thickness on average, this means that after lenticule (- 6.00 D correction) formation, the cornea would maintain a residual stromal bed thickness of approximately 200 microns. Because the anatomy of the more posterior cornea is less organized, it may have affected some of our results. However, the depth of the lenticular anterior incision in all types of laser treatment was maintained at 120 microns so that this experimental variable could be minimized.

The observed differences in terms of disruption to collagen architecture reported here may be explained by our proposed theory based on critical differences in the timing of pulse delivery to central and peripheral areas of the anterior cornea. We suggest that the lamellar arrangement of collagen fibres are displaced and distorted on a submicron scale when plasma expansion and cavitation bubbles are formed by the laser pulses as posterior dissection of the lenticule progresses. In firing pattern A (centripetal followed by centrifugal), the central anterior surface of the lenticule is created immediately after completion of the central posterior surface of the lenticule. Thus, there is little delay between the creation of the central posterior and anterior surfaces of the lenticule. In contrast, there is a greater delay (6 to 8 seconds) between treatment of the central posterior and the central anterior surface of the lenticule in firing pattern D because the pulse pattern is initially centrifugal and then centripetal. This delay may allow increased displacement and distortion of the anterior stromal collagen lamellae (more wavy collagen fibres) to occur as a result of tissue edema and coalescence of cavitation bubbles at the central posterior lenticular interface. This displacement of stroma and disruption of collagen lamellar architecture, even on a submicron scale, could then lead to imprecise delivery of femtosecond laser pulses when creating the

anterior lenticular surface, which may account for the greater irregularity of this surface observed on TEM in pattern D-treated corneas.

Clinically, although pattern B-treated corneas had minimal histochemical and ultrastructural changes similar to those with pattern A-treated corneas, the initiation of the lenticule's posterior incision from the centre outward would mean that the patient would find it difficult to maintain focus on the fixation light from the outset of the procedure. It may increase the risk for suction loss due to degrading visual perception and resultant excessive eye movement during the procedure.

4.4.2 Early Wound Healing and Inflammatory Response after ReLEx

Little has been known about the immediate inflammatory and wound healing responses after ReLEx. Increased reflectivity can be easily detected along the laser-ablated site using in vivo confocal microscopy. The localization of the lenticule’s anterior cut and lenticule’s posterior cut was noticeable in each of the post-ReLEx eyes in which the flap was left undisturbed, where reflective particles were evident. The intensity of the reflectivity remained similar after the removal of the lenticule. This may imply that there was relatively similar level of apoptotic cells or denatured collagen before and after the lenticule removal, and that the lenticule manipulation and removal action did not induce more wounding to the underlying stroma. Interestingly, a different phenomenon was observed in the post-LASIK eyes where there was an increase in light reflecting particles as we increased the degree of refractive correction. Because the reflectivity was not that different between the post-ReLEx corneas with intact flaps and those with lenticules removed, we can speculate that the excimer laser may have caused

more damage to the stroma with greater attempted corrections (compare -3.00 D and -9.00D correction). Greater levels of correction require more tissue to be ablated and longer exposure to the excimer laser, hence delivering more energy to the cornea. For -3.00 D correction, a total energy of approximately 4.10 J is delivered to the cornea, and it increases to approximately 8.07 J and approximately 11.94 J for -6.00 D and -9.00 D correction, respectively (data were obtained from Bausch & Lomb). In contrast, with the ReLEx procedure, the laser simply cuts a different shaped lenticule, requiring an energy of only about 0.58 J (data were obtained from Carl Zeiss Meditec) and the energy levels do not differ significantly between attempted corrections.

Through in vivo confocal microscopy, the deposited acellular and amorphous stromal layer at the keratotomy level showed an elevated light-scattering. Fibronectin was consistently expressed along the incision line on immunohistochemistry, including weak expression along the lenticule's posterior and anterior cut in post-ReLEx eyes with intact flap. The removal of the lenticule and increment of the refractive correction did not seem to alter the fibronectin expression. However, treatment with the excimer laser in LASIK caused an elevated intensity of fibronectin staining when compared with the eye in the same group where the corneal flap remained intact. The little accumulation of fibronectin in the central area of the flap interface suggests a reduced wound healing reaction after ReLEx if compared with that after LASIK, especially at higher refractive correction. We also found that fibronectin was expressed at a higher level at the flap margin of LASIK compared with ReLEx, which could be ascribed to the wider treatment zone in LASIK, which normally includes a 1.0-mm blend zone in addition to the optical zone. A conventional blend zone is not necessary in ReLEx as the lenticule is shaped accordingly to allow a smooth transition between the laser-treated

zone and the untreated area of the cornea.

Monocytes that expressed CD11b were used as a marker for inflammatory infiltration in this study. There was a significant increase of the number of CD11b-positive cells along the centre of the laser-ablated site as the power of refractive correction was increased after LASIK compared with after ReLEx: 24.07 ± 3.39 vs. 2.96 ± 2.57 ($P < 0.001$) after -6.00 D correction and 31.48 7 ± 3.39 vs. 3.33 7 ± 3.33 ($P < 0.001$) after -9.00 D correction. Inflammatory infiltration was almost negligible even after -9.00 D ReLEx correction. In the corneas with non-lifted flap, there were no inflammatory cells seen after ReLEx, which suggests that the excimer laser treatment in LASIK stimulates a higher degree of inflammation, by releasing more cytokines and chemokines that recruit the inflammatory cells to the injury site. Inflammatory cells were abundant in the periphery of the flap in post-ReLEx eyes. Similar findings in post-LASIK eyes have been reported in the literature (108). This is understandable as both techniques create an incision through the epithelium and basement membrane at the flap edge. In the healthy and intact cornea, the basement membrane can function to bind cytokines, suggesting that it may act as a physical barrier for signaling molecules that are produced by the epithelial cells or tear fluid. Thus, when the barrier is compromised, the underlying stroma is exposed to the signaling molecules and the inflammatory cell infiltration is augmented. In more advanced ReLEx techniques such as SMILE, with a much reduced incision size, these may be reduced further due to less epithelial disruption.

Cell proliferation was only detected at the flap margin and occurred primarily in the epithelial cells at and surrounding the epithelial plug. This staining pattern was seen

both after ReLEx and LASIK procedures, as well as before and after the flap was lifted. Our observation in post-LASIK eyes is similar to those previously reported by Meltendorf et al. (108) and Netto et al. (109). Cellular apoptosis observed after ReLEx in this study was comparable to the cell death previously reported after LASIK. Apoptosis has been suggested to be the initiator of the subsequent corneal wound healing cascade. Apoptosis of keratocytes underlying the ablation zone has been proposed to be caused by the release of IL-1, TNF-α, and Fas ligand from the injured corneal epithelium. However, in the absence of epithelial damage or displacement, femtosecond laser-assisted LASIK and ReLEx still induce keratocyte cell death. Femtosecond laser-induced reactive oxygen radicals has been proposed as a contributor to the keratocyte apoptosis. Therefore, it is not surprising that DNA fragmentation was detected along the posterior and anterior cut of the lenticule in the cornea with intact flap after ReLEx. These TUNEL-positive cells were possibly located at both the direct anterior and posterior of lenticule anterior cut, as well as the lenticule posterior incision line. The cell death seen after lenticule removal might be the residual apoptotic keratocytes, which were not removed along with the lenticule or might be from the combination of apoptotic cells at the direct front of the lenticules anterior incision and directly at the back of the lenticules posterior incision.

We also investigated the keratometric changes after ReLEx. The difference after -3.00 D LASIK and ReLEx treatments was minimal. However, the differences became more significant as we increased the degree of correction. The differences in topographic changes observed in this study may be due to less tissue being ablated or perhaps an under-correction after ReLEx surgery compared with LASIK.

4.4.3 FLEx: Clinical Results, Interface Evaluation and IOP Variation

The clinical results of this prospective study of FLEx for the correction of myopia and myopic astigmatism reveal results that are comparable, in terms of safety, stability, predictability, as well as efficacy, to that reported in other studies of this technique (105). The experimental components of this study reveal comparable increase in IOP during FLEx and FS-LASIK using the VisuMax laser, which would be expected—and are considerably lower than reported in other femtosecond lasers and microkeratome LASIK. Eyes undergoing FLEx had almost twice the duration of exposure to suction and increased IOP compared with the eyes that underwent FS-LASIK, but given the relatively low pressures, this is unlikely to have clinical consequences. Finally, an objective grading system of flap and bed surfaces imaged with SEM for both FLEx and FS-LASIK revealed comparably smooth surfaces with both procedures. In the case of the FLEx stromal bed, morphology was independent of the attempted correction and depth of the FS laser ablation.

In FLEx, preparation of the superficial flap relies on a low pressure (approximately 35 mm Hg) suction cone to stabilize the globe and a curved lens attached to the laser delivery system to grasp the cornea. Sufficient suction must be achieved to fixate the docking cone during the laser firing. The advantage of this FS laser system is that the resultant increase in IOP from the suction is low, as the suction is applied to the edge of the cornea and limbus. This reduces the likelihood of reported complications associated with the sudden increase in IOP during suction. We found no significant differences in peak IOP increase for both procedures and the IOP level remained stable throughout the FLEx procedure, indicating no instability of the anterior

chamber during the lenticule formation. However, eyes that underwent FLEx endured elevated IOP levels for a significantly longer time compared with FS-LASIK ($P < 0.001$). This might not be of significance, given the relatively low suction pressure with the VisuMax laser. However, there is potentially a higher risk of suction loss with the longer duration of the FLEx procedure at this low pressure and this occurred in one patient in our series. We have also previously shown that with the VisuMax laser, suction breaks can be immediately re-treated in the same sitting by reapplication of the interface cone and resuming laser ablation from the start, as the lamellar ablation did not involve the visual axis.

Scanning electron microscopy analysis demonstrated a few significant observations. First, a smooth corneal bed surface was observed in pre-lenticule-extracted (anterior lenticule surface) FLEx corneas, which were not discernibly different from those that underwent FS-LASIK. The surface quality of the anterior lenticule surface in our study for both FLEx and FS-LASIK was qualitatively comparable to a similar study by Kunert et al. (110). Second, we observed that the anterior lenticule surface was qualitatively smoother compared with the stromal bed, after the lenticule was removed at all myopic corrections. This rougher surface (mean irregularity scores, range, 8.7 to 10.3) was likely the result of the deeper plane of posterior cut and the trauma from manual removal of the lenticule as it is peeled from the stromal bed, which emphasizes the need for gentle dissection. Third, we compared the smoothness of the stromal beds at different treatment depths (mean depth: A, 189 ± 7.5 μm; B, 205 ± 5.5 μm; C, 225 ± 3.5 μm) after lenticule removal and found that there was no significant, quantitative difference in stromal bed quality between the three refractive groups (mean surface irregularity scores in group A, 8.8 ± 0.6; B, 10.3 ± 0.4; and C, 8.7 ± 0.6; P

=0.88). This suggests that the smoothness of the lenticule extracted stromal bed is reliant on careful manual peeling of the lenticule. When we compared the visual recovery in our patients divided into the same myopic corrective treatment groups as our human cadaver eye study, we found no significant differences in percent eyes with UCVA 20/25 at 1 week between groups (A, 75% vs. B, 73% vs.C, 80%; P = 0.53) and 1 month (A, 82% vs. B, 75% vs. C, 87%; P =0.55). As visual outcomes correlate with smooth optical surfaces, these clinical results taken in consideration with the SEM data suggest that the early visual outcomes for FLEx are independent of attempted correction and treatment depth and more dependent on careful lenticule extraction.

The results of FLEx from our clinical study are promising. UCVA 20/25 was achieved in 94% of eyes at 3 months postoperatively; and 81.8% were within ±0.5 D while 95.5% were within ±1.0 D of the intended refractive target. Refractive stability in our patients was achieved within 1 month (P = 0.001). In other similar studies on FLEx, 90% and 98.1% of eyes treated were within ±1.0 D, and 40% and 74.8% of eyes were within ±0.5 D of the intended correction respectively (105, 111). Overall, they showed that 97.1% of patients were satisfied with the visual result and 90% of eyes had a UCVA of 20/40 or better. The progressively improving results with each published study suggest that there is a learning curve and an improvement in FLEx techniques.

There have been minor complications previously reported including non-progressive epithelial ingrowths, tears at the incision edge, epithelial defects, and incomplete incision opening for lenticule extraction. In our study, we did not observe any of these complications although one case experienced suction loss during the procedure where >10% of the lenticule cut was completed. In such cases, it was

previously recommended to restart the entire procedure. However, we believe that by continuing the ablation this led to induced astigmatism (-2.0 D) due to laser misalignment; it is now recommended to abort the procedure and perform LASIK instead. Current recommendations for suction loss during each stage are now as follows: Stage 1 (lenticule cut <10%): re-start; Stage 2 (lenticule cut >10%): switch to LASIK; Stage 3 (lenticule side cut): repeat lenticule side with decreased size; Stage 4 (flap cut): repeat flap cut; and Stage 5 (flap side cut): repeat flap side cut with decreased size.

The main limitation of our study is that ideally, the experimental studies such as SEM examination and in vivo IOP measurements should be made in our patients from the clinical study. However, these techniques are invasive and not possible to be performed on our patients. Therefore, we evaluated these parameters using the same technique in both a human cadaveric model and an animal model. We did not compare our SEM results from FLEx to a complete LASIK procedure (i.e., FS flap and excimer ablation). There have been several prior publications on this topic (110) and the aim of our study was to examine the comparative effect of different ablations after FLEx.

4.4.4 Comparison of Four Circle patterns for Flap Creation after SMILE

In this study, we assessed four new VisuMax Circle patterns (Carl Zeiss Meditec) that are programmed to create a series of intrastromal incisions, leading to the creation of a corneal flap for SMILE re-treatment. Overall, based on the ease of flap lift and the resultant flap bed quality, we found that Circle pattern D, a lamellar ring at the same depth as the cap to meet the cap cut in the clearance zone with the help of a junction cut, was the most optimal approach for SMILE enhancement.

In pattern A, where no lamellar ring was formed, the side cut had to be made within the clearance zone of the cap cut, which results in a suboptimal reduction in retreatment area. In addition, a hyperopic enhancement limited by the smaller flap diameter would be more prone to result in an undercorrection. Flaps formed by Circle pattern A were easy to lift, with difficulty similar to femtosecond laser-created flap. On SEM, the resulting flap bed was smooth and undisrupted both centrally and peripherally. Different from pattern A, pattern D places a lamellar ring adjacent to and at the same depth as the cap cut. The resultant flaps were as easy to lift as those created by pattern A and SEM revealed similar stromal bed quality as pattern A treated corneas and indiscernible transition between lamellar ring and original cap cut.

A significant difference in intrastromal dissection resistance was experienced when manipulating the lamellae in an attempt to access the cap cut from the lamellar ring, which was placed either posteriorly in pattern B or anteriorly in pattern C. Flaps created by pattern B were the most difficult to lift compared to the other patterns. Furthermore, the tissue damage resulted from the flap lifting process, as observed by SEM, suggests that the pattern B approach should not be attempted for SMILE re-treatment. Although no tissue damage was inflicted on the stromal bed, the flap lift after pattern C was not as easy and straightforward as after pattern D. Due to the difference in the depths of lamellar ring and cap cut, the barely visible transition between these planes could still be seen on SEM. The measurement of the actual depth of the original interface is necessary to determine the parameters of the Circle patterns to attempt to ensure that the femtosecond laser incisions intersect the intended cap cut and thus create an easy to lift corneal flap. However, on day 28 after SMILE in rabbits we could hardly

detect the original cap cut using AS-OCT, which normally appears as a highly reflective layer at the flap interface. We have noticed that with time, the original interface also becomes more difficult to differentiate in human patients; at early measurements (ie, those at 1 month), the interface is more defined than that at 1 year (112). This should not be a concern because many studies have shown that the measured thickness of flaps created by VisuMax femtosecond laser system is not significantly different than the programmed value. When the flap interface has become indiscernible and its depth is not measurable, the programmed depth of cap cut from the initial SMILE procedure can be used to configure the circle patterns.

We have previously reported that the standard deviation of the measured thickness of the corneal caps ranged between 9.5 and 10.9 μm (112). This range is still within the span of the junction cut (set at 20 μm in depth in our study and could be increased further if necessary), which further ensures the lamellar ring would intersect the original cap cut. The junction cut also ensures the presence of postoperative epithelial hyperplasia, does not pose any problem in selecting the depth of the lamellar ring.

Depending on the time between refractive enhancement and the initial SMILE, lifting of circle-created flaps may become more challenging over time. If circle created flap lift is difficult and the surgeon decides not to proceed because of concern that the flap will be torn or damaged, surface ablation with mitomycin C may become the next viable option. Prior studies have shown the efficacy and safety of this treatment strategy, despite patient discomfort and longer visual recovery (113, 114). The other possible option for SMILE re-treatment would be insertion of an implantable contact

lens or creation of refractive lenticule anterior to the original cap–stromal bed interface. Insertion of an implantable contact lens would not be a common technique used for re-treatment because the residual refractive error is generally small. Performing another SMILE after the primary refractive procedure could be another viable option. This technique bears resemblance to the re-cutting of flap technique for LASIK enhancement. Several studies have demonstrated similar refractive outcome, safety, and effectiveness between re-treated eyes that underwent flap re-lift and flap re-cutting (115, 116). A study on the feasibility and effectiveness of performing another SMILE for enhancement after primary SMILE is currently underway in our institution.

Alternatively, LASIK could possibly be performed anterior to the previous SMILE cap if the patient seeks re-treatment in an eye centre that does not operate a VisuMax femtosecond laser system. Because of the relatively small sample size (n = 3 in each treatment group), we were unable to perform an extensive and meaningful statistical analysis. It would be of great value to present the mean value of the grading of the flap lift difficulty or the percentage of cases presenting each grading. However, we found that the degree of flap lift difficulty was consistent in all 3 eyes in every treatment group, which means the standard deviation of the grading would be 0. Our SEM, ASOCT, and in vivo confocal microscopy results were also consistent in all 3 eyes in every treatment group.

4.4.5 Lenticule Viability and Integrity

In the present study, we evaluated the viability of human cornea lenticules extracted following ReLEx procedure and one month after storage using a developed

cryopreservation technique. Our TEM findings showed a similar pattern of apoptotic and quiescent keratocytes within a well preserved and well aligned collagen structure in fresh and cryopreserved lenticules. Similarly, TUNEL-positive cells were mainly localized in the periphery of the lenticule in both groups. However, there was a significant increase in the TUNEL positive cells in the centre of the lenticule following cryopreservation. We were able to verify the presence of keratocyte-specific gene expression of KERA and ALDH3A1 by RT–PCR in the cells isolated from the lenticules both pre and post cryopreservation.

The viability of the cells in fresh and cryopreserved lenticules was also confirmed by cell culture. The differences in donor age, time from death to tissue harvest and time from death to surgery in our sample should not significantly affect our findings. It has been reported previously that there is no correlation between the donor age, death to preservation time or total storage time of the corneas and the percentage of dead keratocytes when stored in Optisol (117). International donor sharing and air-transportation of corneas stored in Optisol is as safe and effective as using local tissue (118, 119).

The cryopreservation of the extracted stromal lenticule was achieved using a cryopreservation procedure that involved gradual cooling of the stromal lenticule (in a cryocontainer) to −80 °C in the presence of a cryoprotectant, DMSO, before being transferred into liquid nitrogen for longterm storage. This approach is known to lessen the damage caused by intracellular ice formation (120). In this study, viable keratocytes were isolated from the cryopreserved stromal lenticule, and expanded into healthy stromal fibroblasts. Similar cryopreservation techniques have been successfully used in

the storage of cornea and other human tissues (121). However, standard cryopreservation and freeze–thaw techniques (e.g., liquid nitrogen (122, 123), freezing at −80 °C, nitrogen (N2) gas, and cryoprobe at −80 °C) have been shown to induce apoptosis and necrosis in keratocytes (121, 124). Differential inter-species variation with respect to collagen fibril damage has also been shown following cryopreservation (122).

In the present study, TEM analysis showed a decrease in CFD after cryopreservation without a significant change in the number of collagen fibrils. This change is due to the swelling of tissues that takes place after cryopreservation. However, overall collagen integrity and structure was maintained in the cryopreserved lenticules. Collagen fibrils remained well preserved and well aligned, similar to the freshly extracted lenticules after ReLEx procedure. These observations confirm that our cryopreservation technique with the lenticules is reliable in maintaining the collagen structure of the lenticule. Regular collagen architecture is one of the key factors to maintain cornea transparency (125). Therefore, if the lenticule is to be considered for re-implantation, maintenance of regular corneal collagen architecture is vital following cryopreservation.

TUNEL positive cells were detected mainly in the periphery of the fresh lenticules. These results are similar to our previous report on ReLEx in rabbits, where there was large amount of TUNEL-positive cells in the periphery of unextracted lenticules (126). This result implied that the peripheral damage was produced by the FS laser and not by the manual removal of the lenticule. However, there was an increase in the amount of TUNEL-positive cells in the centre of the lenticules following

cryopreservation but no significant increase in the periphery. Our results suggest that the cells located in the centre of the lenticule are more susceptible to damage during cryopreservation and thawing process.

Transmission electron microscopy (TEM) showed more necrotic than apoptotic keratocytes in both the fresh and cryopreserved groups. Several reports have shown mixed necrotic or apoptotic keratocytes following liquid nitrogen cryopreservation (122, 123). One of the limitations of TUNEL assay is that it detects fragmented DNA, which is not entirely specific for apoptotic cells (127-130). In fact, keratocytes undergoing necrosis after FS laser have been recognized by TUNEL assay (109). In addition, we noted a significant decrease in the number of DAPI positive, TUNEL negative cells in the centre of the lenticule following cryopreservation. This maybe due to the following mechanisms: 1) TUNEL assay is less sensitive to the single-strand DNA breaks in late stage necrosis than the double stranded DNA fragmentation in apoptosis (130) and 2) DAPI visualize cells by specifically staining the nuclei and in late necrosis some nuclei may not stain. Hence we hypothesise that the reduction in number of DAPI positive (TUNEL negative cells) and the main mode of keratocyte death in fresh and cryopreserved lenticules following ReLEx is most likely to cell necrosis as opposed to apoptosis.

Isolated cells from fresh and cryopreserved lenticules showed a positive expression of KERA and ALDH3A1. KERA, a small leucine-rich proteoglycan, is a specific marker for keratocytes and highly expressed in the corneal stroma (131). It is associated with the production of extracellular matrix and aids in corneal transparency (125). The corneal crystallin, ALDH3A1 is a water-soluble protein highly

expressed in quiescent keratocytes, and is associated with maintenance of corneal transparency (132, 133). Thus, the expression of these specific keratocyte markers in the fresh and cryopreserved lenticules showed that they contain viable and quiescent keratocytes.

Keratocytes isolated and cultured from both fresh and cryopreserved lenticules showed similar growth dynamics, taking on a fibroblastic phenotype and proliferating rapidly after growth in serum containing culture medium. More importantly, our results suggests that although dead keratocytes were seen using TEM and TUNEL assay, there were enough viable keratocytes within the cryopreserved lenticules that could be isolated and propagated following 1-month storage. Similar findings have also been previously described following cryopreservation of whole human corneas and freeze–thaw injury in pig corneas (134, 122).

There are several clinical implications of our study. The viability of long-term lenticule storage by cryopreservation after ReLEx surgery may offer an added dimension to corneal refractive laser surgery, that of potential reversibility. Lenticules may be stored for individual ReLEx patients for a prolonged period of time, and could conceivably be reimplanted at a later date in the event of keratectasia, or even as a means of treating presbyopia several years later, by restoring myopia in the non-dominant eye to create a state of monovision, or as an autologous presbyopic lenticular inlay. In addition, with appropriate informed consent, as well as serology clearance, these lenticules could be used as allograft refractive lenticules in other patients who develop post-LASIK keratectasia, in other forms of keratectasia, such as keratoconus, and also may be used as allograft presbyopic inlays, as it is well known

that minimal risks of immune-mediated allograft rejection occur in anterior lamellar keratoplasty (135).

4.4.6 Lenticule Re-implantation Proof of Concept-Rabbit Study

This study, for the first time, demonstrates the potential of stromal volume restoration following FSL refractive surgery using autologous stromal tissue stored at the time of initial surgery. We have previously demonstrated, using human corneal tissue that cells within these extracted lenticules remain viable and are capable of proliferation under culture conditions following storage at -80°C for a prolonged period of time (136). This would allow the patient to augment the volume of their own stroma with tissue containing autologous cells, thereby circumventing the risk of immune rejection of the transplanted tissue. The technique is applicable at present only to ReLEx (FLEx, SMILE, and pseudo-SMILE), which utilize the Visumax FSL to correct ammetropia by intrastromal lenticular extraction.

In this study, we utilized DMSO, a ubiquitous and nontoxic cryoprotectant, often used in the cryostorage of embryonic and haematopoietic stem cells, to prevent intralenticular cell damage during freezing in liquid nitrogen (137). We used FBS in the cryoprotectant solution, and alternatives may need to be explored if this technique were to be adopted for human use to avoid the use of xeno-derived products and risk of zoonosis.

The technique of lenticular storage described here, which utilized a simple rigid gas permeable lens with an orientation mark to indicate the 12 o'clock position of the

lenticule on the eye, would also need to be optimized for clinical use especially in patients with toric lenticules, with the development of dedicated cryopreservation lenticular cases, which maintain the anatomical curvature of the lenticules and the appropriate axial orientation of the lenticules. Lenticular orientation is more critical if a spherocylindrical ReLEx treatment is applied, where correct repositioning of the lenticule would be required if the pre-operative refraction were to be restored.

However, the true importance of precise lenticular re-implantation remains to be seen, as one potential application of this technique could be the opportunity for further laser refractive surgery to provide a presbyopic patient with monovision, in which case, orientation may not be as critical as induced astigmatism may be corrected at the time of further surgery. Despite initial tissue edema and microstriae within the first few days of lenticule implantation, corneas were clear and comparable to un-operated fellow eyes by day 28.

Corneal thickness before ReLEx (FLex) was restored in all eyes after the lenticule was replaced. The very slight increase in thickness at the end of the study period could be due to mild residual edema, but was not statistically significant and may normalize over a longer observation period. Another explanation of the slight increase in corneal thickness would be the mild epithelial hyperplasia (138) that usually takes place after central flattening of the cornea either by FSL refractive surgery or resection. Clarity of the re-implanted cornea returned to control levels by 28 days after lenticule replacement and was matched by a commensurate reduction in interface reflectivity based on confocal microscopy measurements.

Myofibroblasts and fibroblasts, both cell types implicated in scarring and haze formation in the cornea, were largely absent on immunohistochemical staining. Temporal confocal cellular analysis demonstrated resident keratocytes within the lenticule body and repopulation of the anterior and posterior lenticular borders by day 28 after implantation. Repopulation of the lenticular borders appears to occur through migration of adjacent keratocytes, rather than by keratocyte proliferation as indicated by a relative absence of Ki67 staining cells (a marker of cell proliferation), together with positive staining for cellular actin (phalloidin staining), a contractile cytoskeletal element within the cell body. The lack of a proliferative keratocyte response is probably partly as a result of the fact that the lenticule itself contains a viable resident population of cells.

We observed sparse inflammatory cell presence, even following lenticule re-implantation (CD18). This weak healing stimulus, probably also explains why there is very little extracellular matrix deposition following lenticule re-implantation (i.e., fibronectin and tenascin). This relative lack of inflammation and wound healing response will clearly be advantageous with regards to maintenance of corneal clarity and refractive accuracy in refractive stromal reimplantation procedures.

Current methods for stromal volume restoration, particularly in cases of corneal ectasia after refractive surgery, are mainly limited to various techniques of anterior lamellar keratoplasty (ALK) involving the removal of part or all of the host stroma and replacement with donor stromal tissue. These techniques are technically and surgically demanding, time consuming, and are usually performed by corneal transplant surgeons, necessarily limiting their applicability to specific indications. In addition, use of donor

corneal tissue involves some risk of graft rejection (135). Epikeratophakia, a technique in vogue in the 1990s, was another method for stromal volume restoration used in the treatment of keratoconus. The epikeratophakia technique involved the removal of host corneal epithelium and fixation by suture of a cryolathed donor corneal lenticule on to the anterior stroma, over which the host epithelium would heal (139). The failure to widely adopt this technique resulted from a number of postoperative complications including interface scarring between the lenticule and host cornea, and poorly predictable astigmatic outcomes. In contrast to these methods, the technique of refractive stromal lenticule re-implantation described here clearly has significant advantages in terms of lamellar accuracy and refractive correction. Significantly, it respects many of the benefits of corneal wound healing by allowing the lenticule to be placed under a stromal flap without undue epithelial injury.

Risk of epithelial ingrowth, which we did not observe in any study cases, is likely to be no greater than with conventional LASIK. If keratectasia occurs in a patient who underwent a ReLEx procedure, the use of the patient's own autologous tissue also circumvents the risk of tissue rejection and the need for prolonged topical immunosuppression postoperatively. In patients who develop post LASIK keratectasia, stored lenticules that are not personally reserved by the original ReLEx patients could be donated to these patients (with appropriate informed consent from the donor, and also appropriate serological testing) to restore corneal volume under the LASIK flap. Being allogeneic, there would be a small risk of stromal rejection, similar to immunological risk after an ALK procedure. Unlike ALK or deep ALK (DALK), however, the intrastromal insertion technique is surgically easier and could be done by any surgeon experienced with LASIK or ReLEx surgery.

Temporal topographic indices during our study demonstrated post implantation mean keratometry values that were within -0.6 - 0.8 D of values before ReLEx (FLEx). While this is promising and shows that pre-operative corneal topography can be largely restored after lenticule implantation, there are a number of potential sources of inaccuracy in our data. Significantly, although handheld topography scans were captured at the corneal centre, actual ReLEx (FLEx) treatments were difficult to centre accurately and consistently on the pupil centre of the anaesthetized rabbit due to a tendency for the rabbit eye to roll eccentrically when applanated with the treatment cone of the Visumax FSL. Even though attempts were made to fixate the globe with forceps while applying suction, it was not fully possible to control eye position, resulting in slightly eccentric treatments. This is unlikely to pose a problem in a conscious patient focused on the fixation light during actual ReLEx.

Lenticule storage and re-implantation is a novel technique for stromal volume restoration that may be utilized in a number of potential clinical situations. In cases of post refractive surgery corneal ectasia, the technique offers the possibility to restore corneal stromal volume with autologous tissue, theoretically any time after surgery, and may also be combined with collagen cross-linking for added structural re-enforcement. A more ubiquitous clinical scenario is that of a previously myopic patient who has undergone refractive surgery to near emmetropia, and then finds, with time, that near visual tasks become more difficult as accommodation is lost through presbyopia. Current excimer-based refractive surgeries result in permanent stromal tissue loss, thereby, limiting the possibility of further corneal surgery; however, lenticule replacement could restore the patients previous refractive state, and would offer the

possibility of reimplantation of an autologous lenticule reshaped to a -1.5 or -2.0 D power, in the nondominant eye, thus, enabling monovision. An alternative approach here could be the use of these stored lenticules as an autologous biological intrastromal inlay in the same manner as synthetic inlays, thus, obviating biocompatibility and nutritional issues.

4.4.7 Lenticule Re-Implantation Proof of Value NHP Study

This study addressed two aspects of ReLEx surgery, namely, the medium-term corneal tissue response to the ReLEx procedure, and the medium-term feasibility of ReLEx lenticule reimplantation.

With regards to the long-term evaluation of the tissue responses to ReLEx surgery, we observed only a mild corneal wound healing reaction, with minimal inflammatory cellular and myofibroblast responses, and normal collagen type I expression in the monkeys up to 16 weeks post-ReLEx. In addition, slit lamp examination and in vivo confocal microscopy revealed virtually no corneal haze formation. We have further demonstrated the medium-term feasibility of RL re-implantation post-ReLEx surgery in an in-vivo non-human primate model. The effectiveness of this technique in reversing the refractive procedure was demonstrated by the restoration of corneal thickness, curvature and refractive error indices to near pre-operative values following RL re-implantation. There was similarly minimal inflammatory response, myofibroblastic formation, and wound healing reaction, or no abnormal collagen type I expression after 8 weeks. In addition, we noted keratocyte re-population along the re-implanted RL interfaces.

With regards to corneal morphology, evaluation of the 3 ocular biometrics of

corneal thickness (Figure 4.33), corneal curvature (keratometry; Table 4.7) and refractive state measured before and after ReLEx surgery, and after the RL reimplantation confirmed that restoration of all 3 parameters were achieved after RL re-implantation. Corneal thickness was restored to near pre-operative values after the RL re-implantation. Similarly, refraction and topography were restored after RL re-implantation. Corneal keratometry pre-ReLEx was 58D and became flatter 16 weeks after ReLEx, but was restored to 58D at week 16 after RL re-implantation ($p= 0.506$). This result was comparable to that reported in patients 3 months post-FLEx in our earlier study.

These data, which show that lenticule re-implantation can indeed lead to full restoration of the anatomical changes which occurred after ReLEx surgery, confirms that clinical reversibility of the refractive procedure is possible. The keratometric values being 0.6D less than pre-operative values were possibly due to the formation of a corneal flap. This may be obviated when reversing a SMILE procedure.

Slit lamp examination in the re-implanted corneas showed mild haze in the first 2 weeks after surgery, but transparency progressively improved at subsequent follow-up time points. These observations were matched by a commensurate reduction in the levels of interface reflectivity seen during in vivo confocal microscopy. The absence of myofibroblasts (α-smooth muscle actin expressing cells) in the central cornea further confirms our results obtained with slit lamp and in vivo confocal microscopy in terms of haze, usually attributed to these cells. In vivo confocal analysis also showed quiescent keratocytes within the lenticular lamellae and later, re-population of the anterior and posterior lenticular interface by week 4 after re-implantation, suggesting the cornea's

attempt to return to a quiescent state.

In the present study, the re-population appeared to occur through migration of adjacent keratocytes as indicated by F-actin staining, rather than by cell proliferation, as indicated by the absence of Ki-67-positive cells in the stroma. This is markedly different from pathological responses seen after excimer laser ablation in PRK and LASIK where the keratocytes are vapourised. Keratocytes, seen within the re-implanted lenticule, were probably cells that have survived the process of cryopreservation. In addition, keratocytes have been shown to be responsible in modulating extracellular matrix synthesis and cytoskeleton organization, which contribute to the mechanical strength of a collagen-based biomaterial (140).

This finding presents the fundamental implication of the ReLEx reversal technique, particularly in treating biomechanically compromised ectatic corneas. The RL re-implantation didn't appear to induce any significant alteration in wound healing reaction (low level of fibronectin) or incite an inflammatory (absence of CD18 expression) response. In addition, the uniform presence of collagen type I throughout the full-thickness of post-re-implanted corneal stroma indicates normal collagen expression, maintaining corneal transparency.

A reversible refractive procedure described in the present study has significant advantages in terms of accurate FSL lamellar excision and precise refractive correction. The RL insertion technique is also relatively easier to perform surgically and could potentially be performed by refractive surgeons experienced in LASIK or ReLEx surgery.

4.5 SUMMARY

In conclusion, we have shown ultrastructurally that corneas treated with laser scanning from the centre of the cornea out for posterior incisions and from the periphery in for the anterior incisions results in more disrupted collagen arrangement, in particular at the centre of the lenticule's anterior plane. This disruption may result in slower postoperative visual recovery. Therefore, the application of firing pattern from the peripheral cornea in for the posterior surface of the lenticule and from the centre out for the anterior surface of the lenticule during ReLEx surgery is the most optimum clinically and ultrastructurally. In addition, these findings of ultrastructural changes in the cornea after femtosecond laser ablation may provide us with a better understanding of laser– stromal interactions, leading to improved outcomes in laser-assisted corneal refractive surgery.

We have shown that there is a less reactive wound healing response and inflammatory infiltration, early on after ReLEx in comparison with LASIK, suggesting that ReLEx using just the femtosecond laser may result in less corneal inflammation, which may impact favorably on visual results and outcomes. These disparities were only significant at higher refractive corrections, and may be related to marked differences in energy delivery to the cornea with each treatment. This may also explain the higher variability in efficacy and predictability with LASIK for high myopia. In addition, eyes having ReLEx at higher corrections showed less corneal flattening compared with similar levels of correction with LASIK. This may represent less tissue loss to achieve the same refractive correction with ReLEx.

Our clinical study presents encouraging visual outcomes in patients that underwent FLEx. Our in vivo animal studies support the early clinical results and safety of this procedure; while in vitro human eye bank cornea revealed that stromal bed irregularity was independent of treatment and ablation depth.

We have shown the stromal bed quality and difficulty in lifting flaps created with four circle patterns for SMILE enhancement. We found that pattern D, which created the lamellar ring at the same depth as the original cap–stromal bed interface, appears to be the most optimal for clinical use. Accessing the correct plane (the cap–stromal bed interface) from the lamellar ring was uneventful, and the subsequent lifting of the flap was relatively straightforward and akin to lifting a femtosecond laser-created LASIK flap. In addition, the resultant flap bed was undisrupted, and the transition between the lamellar ring and the cap–stromal bed interface was smooth and indiscernible.

The stromal lenticules extracted following ReLEx maintain keratocyte viability and overall collagen structural integrity in pre- and post- cryopreserved tissue samples. Keratocytes have been shown to be an important contributor for the maintenance of corneal transparency and this may be important if the lenticule is to be re-implanted in future e.g., in the treatment of corneal ectasia following myopic correction. However, the maintenance of the collagen architecture is probably the most important finding since corneal stromal buttons decellularized of keratocytes have been shown to be viable following host keratocyte migration. Future work evaluating the viability of these lenticules following reimplantation is currently being investigated using an in vivo

animal model of ReLEx.

This study demonstrates proof of principle of reversibility of an FSL corneal refractive procedure. Up until now, excimer-based refractive surgeries, such as LASIK, have offered excellent visual results, albeit with permanent loss of stromal tissue and without any possibility of reversibility. The potential option of stromal lenticule storage after ReLEx offers patients the unique opportunity to bank their tissue in case of future need, or to donate their tissues to others in need.

We have also demonstrated the reversibility of a FSL assisted myopia treatment (ReLEx) using a non-human primate model of refractive surgery. This study for the first time demonstrates that a laser refractive corneal procedure can be safely and effectively reversed. The potential option of RL cryostorage after ReLEx allows refractive patients to preserve their tissue for subsequent re-implantation in the event of keratectasia, or a change in their refractive state, including presbyopia, or to donate their RLs for other patients to treat these same conditions and other forms of keratectasia, including keratoconus.

CHAPTER 5

5.0 CONCLUSIONS AND FUTURE WORK

The use of femtosecond lasers in corneal surgery has increased over the last few years, but its increased use for full thickness keratoplasty has been tempered by changes in keratoplasty techniques (135). The shift to more lamellar surgery has had a significant effect on the type of corneal transplantation being performed, with more work focused on using the laser for lamellar surgery as opposed to full thickness penetrating keratoplasty. However, following our work other authors have also shown the superiority of femtosecond laser use in penetrating keratoplasty compared standard trephination (141,142). Work has also gone on further to assess the effect of different inicisional profiles on clinical outcomes, showing better wound construction with novel femtosecond laser profiles (143).

For endothelial keratoplasty the surgery has progressed to ultrathin Descemet's Stripping endothelial keratoplasty (DSEK) to Descemet's Membrane endothelial keratoplasty (DMEK). The ability to cut ultrathin tissue has been challenging with current lasers and this has been demonstrated in clinical trials (144). Following our work documented in this thesis, we continued our focus, but tried to tackle the problem from lasering from the endothelial side of the donor tissue (145). This approach improved the quality of the interface in a single pass, but did require gentle applantation of the laser head to the corneal endothelium (145). However, with the advent of femtocataract, liquid interfaces that are now available, this may circumvent the later problem, especially in conjunction with newer generation femtosecond laser, for example Ziemer, offering energy in the 1-5nJ as opposed to older lasers such as the IntraLase (800nJ) and VisuMax (160nJ).

For Deep ALK (DALK), this still remains a challenge to perform with a femtosecond laser. One of the issues has been to replicate a smooth, even optical interface. However, the superior wound contruction of the femtosecond laser can be applied to DALK as well (143). Keratoconus is a leading indication for DALK surgery, and the issue with using a laser, for the lamellar cut, has been to cut an even resection depth, with respect to Descemet's membrane. Ideally if the laser could track the posterior curvature it could then produce a lamellar depth of equal uniformity. In contrast, the accuracy of the vertical cut with DALK has been evaluated for the recipient and donor and has been shown to be accurate clinically (146). Future work will be to enable the laser to create a channel, 150-200 microns from the DM, in which a canula maybe directly passed in order to obtain a 'Big bubble' separation of the stroma, from DM or linking the laser to a topography machine so that it may track the posterior surface of the cornea, while performing the lamellar cut.

Our work comparing different femtosecond lasers, highlighted the importance of patient experience without compromising on clinical outcomes. We were able to show the benefits of the lower energy VisuMax laser system over the IntraLase with respect to not only patient experience but also achieving a superior ocular surface postoperatively. The ultrastructural analysis showed the advantages of a large numerical aperture laser over a small one, and also the lower IOP rise due to the different suction between the two laser systems, which also affected the patient's choice of laser system. The clinical refractive outcomes were not significantly different as might be anticipated but the ocular surface data was an interesting finding. We have also collected tear samples from these patients and in future will analyse them using mass spectrometry

(147). The use of eye trackers on excimer lasers is now commonplace but initially, due to the opaque bubble layer formation with femtosecond lasers, there was a fear that the trackers may not work. The second clinical trial dispelled this myth.

The ability to cut a lenticule with a femtosecond laser offered the possibility of a new refractive procedure. We were able to show the optimal firing sequence required to create the lenticule and also compared wound healing to LASIK. The main advantage of ReLEx seemed to be its superior wound healing response in moderate to high myopia. This was seen in our laboratory experiments and also in our initial clinical study. This has subsequently shown by other in clinical series (148). Since the lenticule had to be removed by gentle dissection, it was important to ascertain the quality of the interface. All the results pointed to the use of a good dissecting instrument being the key. I have subsequently customized special instruments for this procedure (www.asico.com). FLEx offered few other advantages over LASIK, since there was a flap creation in both procedures, but SMILE offered the added advantage of a flapless procedure. The lenticule being taken out through a small incision. This could potentially offer advantages with respect to ocular surface recovery following refractive surgery, but also the eye could be potentially biomechanically stronger. However, this could also cause a problem in how enhancement would be performed. Further work by our group (149) and others (150) have shown the superiority of SMILE over LASIK with respect to better corneal innervation and ocular surface disease. The biomechanical assessment has been equivocal primarily due to the limitations of current investigative equipment i.e the ORA or Corvis (151).

During the studies, one method of enhancement that converted the flap to a

pocket was optimised. This would allow the use an excimer laser to enhance the correction. We have conducted further work studying the wound healing effects of different enhancement procedures (152) as well as risk factors for enhancement in a clinical series that would guide clinicians as to the best option (153). To really show the efficacy and safety of SMILE, a randomized contralateral clinical study should be performed (similar to the LASIK study above), if this procedure is to truly become more widespread (154). We have currently finished such a study.

The concept of lenticule re-implantation was also shown to be a feasible option in both rabbit and monkey models. This approach has several potential advantages and following these papers, patients have already undergone lenticule implantation for the correction of hyperopia, stromal volume enhancement in patients with keratconnus, and also for the treatment of presbyopia in both India and China (155, 156, 157). The concept of lenticule banking for future use is therefore important and requires further research in the future.

CHAPTER 6

6.0 REFERENCES

1. Zewail, A.H. (2000) 'Femtochemistry: Atomic-Scale Dynamics of the Chemical Bond Using Ultrafast Lasers (Nobel Lecture) The Nobel Foundation 2000', *Angew Chem Int Ed,* 39(15), pp. 2586-2631.
2. Eigen, M. (1972). *Immeasurable Fast Reactions: in Nobel Lectures (Chemistry),* Elsevier.
3. Shank, C.V., Ippen, E.P. & Bersohn, R. (1976). 'Time-resolved spectroscopy of haemoglobin and its complexes with subpicosecond optical pulses', *Science*, 193(4247), pp. 50-51.
4. Spence, D.E., Kean, P.N. & Sibbett, W. (1991) '60-fsec pulse generation from a self-mode locked Ti:Sapphire laser', *Opt Lett*. 16(1), pp. 42-44.
5. Stern, D., Schoenlein, R.W., Puliafito, C.A., Dobi, E.T., Birngruber, R., Fuijmoto, J.G. (1989) 'Corneal Ablation by Nanosecond, Picosecond and Femtosecond Lasers at 532 and 625nm', *Arch Ophthalmology,* 107(4), pp. 587-592.
6. Trokel, S.L., Srinivasan, R. & Braren, B. (1983) 'Excimer Laser Surgery of the cornea', *American Journal of Ophthalmology,* 96, pp. 710-715.
7. Marshall, J., Trokel, S., Rothery, S., Krueger, R.R. (1986) 'Photoablative re-profiling of the cornea using an excimer laser: photorefractive keratectomy', *Lasers Ophthalmology,* 1, pp. 21-48.

8. Seiler, T., Bende, T., Wollensak, J., Trokel, S. (1988) 'Excimer laser keratectomy for correction of astigmatism', *American Journal of Ophthalmology*, 105, pp. 117-124.

9. Seiler, T., Marshall, J., Rothery, S., Wollensak, J. (1986) 'The potential of an infrared hydrogen fluoride (HF) laser (3.0 μm) for corneal surgery', *Lasers Ophthalmology*, 1, pp. 49-60.

10. Loertscher, H., Mandelbaum, S., Parrish, R.K., Parel, J.M. (1986) 'Preliminary report on corneal incisions created by a hydrogen fluoride laser', *American Journal of Ophthalmology*, 102, pp. 217-221.

11. Kurtz, M.D., Horvath, C., Liu, H.-H., Krueger, R.R., Juhasz, T. (1998) 'Lamellar refractive surgery with scanned intrastromal picosecond and femtosecond laser pulses in animal eyes', *J Refractive Surgery*, 14, pp. 541-548.

12. Holger, L., Maatz, G., Heisterkamp, A., Hetzel, U., Drommer, W., Welling, H., Ertmer, W. (2000) 'Application of ultrashort laser pulses for intrastromal refractive surgery', *Graefe's Arch Clin Exp Ophthalmol*, 238, pp. 33-39.

13. Ratkay, I.R., Juhasz, T., Horvath, C., Suarez, C., Kiss, K., Ferincz, I., Kurtz, R. (2001) 'Ultra-short pulse (femtosecond) laser surgery: Initial use in LASIK flap creation', *Ophthalmology Clinics of North America*, 14(2), pp. 1-10.

14. Juhasz, T., Kastis, G.A., Suarez, C., Bor, Z., Bron, W.E. (1996) 'Time-resolved observations of shock waves and cavitation bubbles generated by femtosecond laser pulses in corneal tissue and water', *Lasers in Surgery and Medicine*, 19, pp. 23-31.

15. Knox. W.H., Downer, M.C., Fork, R.L., Shank, C.V. (1984) 'Amplified femtosecond optical pulses and continuum generation at 5-kHz repetition rate', *Opt Letters*, 9, pp. 552-554.

16. Habib, M.S., Speaker, M.G., Kaiser, R., Juhasz, T. (1995) ‘Myopic intrastromal photorefractive keratectomy with Nd:YLF picosecond laser in the cat cornea’, *Arch Ophthalmology*, 113, pp. 499-503.

17. Gimbel, H., Coupland, S., Ferensowisc, M. (1997) ‘Review of intrastromal photorefractive keratectomy with the Hd:YLF laser’, *Int Ophthalmol Clin*, 37, pp. 95-102.

18. Ito, M., Quantock, A., Malhan, S., Schanzlin, D.J, Krueger, R.R. (1996) ‘Picosecond laser in situ keratomileusis with a 1053-nm Nd:YLF laser’, *J Refractive Surgery*, 12, pp. 721-728.

19. Kurtz, R.M., Liu, X., Elner, V.M., Squier, J.A., Due, D., Mourou, G.A. (1997) ‘Plasma mediated ablation in human cornea as a function of laser pulse width’, *J Refract Surgery*, 13, pp. 653-658.

20. Zysset, B., Fujimoto, J.G. & Deutsch, T.F. (1989) ‘Time resolved measurements of picosecond optical breakdown’, *Appl Phys B*, 48, pp. 139-147.

21. Vogel, A., Hentschel, W., Holzfuss, J., Lauterborn, W. (1986) ‘Cavitation bubble dynamics and acoustic transient generation in ocular surgery with pulsed Neodymium:YAG laser’, *Ophthalmology*, 93, pp. 1259-1269.

22. Vogel, A., Capon, M.R., Ayso-Vogel, M.N., Birngruber, R. (1994) ‘Intraocular photodisruption with picosecond and nanosecond laser pulses: Tissue effects in cornea, lens and retina’, *Investigative Ophthalmology and Visual Science*, 35, pp. 3022-3044.

23. Juhasz, T., Hu, X.H., Turi, L., Bor, Z. (1994) ‘Dynamics of shock waves and cavitations generated by picosecond laser pulses in corneal tissue and water’, *Lasers Surg Medicine*, 15, pp. 91-98.

24. Niemz, M.H., Hoppeler, T., Juhasz, T., Bille, J.F. (1993) ‘Intrastromal ablations for refractive corneal surgery using picosecond infrared laser pulses’, *Lasers Light Ophthalmology*, 5, pp. 145-152.

25. Doukas, A.G., Zweig, A.D., Frisoli, J.K., Birngruber, R., Deutsch, T.F. (1991) ‘Non-invasive determination of shock wave pressure generated by optical breakdown’, *Appl Phys B*, pp. 237-245.

26. Braun, A., Liu, H., Horvath, C., Liu, X., Juhasz, T., Mourou, G. (1997) ‘All solid-state, directly diode-pumped chirped-pulse amplification laser system’, *OSA Technical Digest*, 11, pp. 323-324.

27. Sletten, K.R., Yen, K.G., Sayegh, S., Loesel, F., Eckhoff, C., Horvath, C., Meunier, M.S., Juhasz, T., Kurtz, R.M. (1999) ‘An in vivo model of femtosecond laser intrastromal refractive surgery’, *Ophthalmic Surg Lasers*, 30, pp. 742-749.

28. Nordan, L.T., Slade, S.G., Baker, R.N., Suarez, C., Juhasz, T., Kurtz, R. (2003) ‘Femtosecond Laser Flap Creation for Laser in situ Keratomileusis: Six-month follow-up of initial U.S Clinical Series’, *J Refractive Surgery*, 19(1), pp. 8-14.

29. De Medeiros, F.W., Kaur, H., Agrawal, V., Chaurasia, S.S., Hammel, J., Dupps, W.J. Jr., Wilson, S.E. (2009) ‘Effect of femtosecond laser energy level on corneal stromal cell death and inflamation’, *J Refractive Surgery*, 25(10), pp. 869-874.

30. Montés-Micó, R., Rodríguez-Galietero. A., Alió, J.L. (2007) ‘Femtosecond laser versus mechanical keratome LASIK for myopia’, *Ophthalmology*, 114, pp. 62–68.

31. Kezirian, G.M., Stonecipher, K.G. (2004) ‘Comparison of the IntraLase femtosecond laser and mechanical keratomes for laser in situ keratomileusis’, *J Cataract Refract Surg*, 30, pp. 804–811.

32. Kim, J.Y., Kim, M.J., Kim, T.I., Choi, H.J., Pak, J.H., Tchah, H. (2006) ‘A femtosecond laser creates a stronger flap than a mechanical microkeratome’, *Invest Ophthalmol Vis Sci*, 47, pp. 599–604.

33. Netto, M.V., Mohan, R.R., Medeiros, F.W., Dupps, W.J. Jr., Sinha, S., Krueger, R.R., Stapleton, W.M., Rayborn, M., Suto, C., Wilson, S.E. (2007) ‘Femtosecond laser and microkeratome corneal flaps: comparison of stromal wound healing and inflammation’, *J Refract Surg*, 23, pp. 667–676.

34. Meltendorf, C., Burbach, G.J., Buhren J., et al. (2007) ‘Corneal femtosecond laser keratotomy results in isolated stromal injury and favourable wound healing response’, *Invest Ophthalmol Vis Sci*., 48, pp. 2068–2075.

35. Holzer, M.P., Rabsilber, T.M., Auffarth, G.U. (2006) ‘Femtosecond laser-assisted corneal flap cuts: morphology, accuracy, and histopathology’, *Invest Ophthalmol Vis Sci*., 47, pp. 2828–2831.

36. Seitz, B., Langenbucher, A., Hofmann-Rummelt, C., et al. (2003) ‘Nonmechanical posterior lamellar keratoplasty using the femtosecond laser (femto-plak) for corneal endothelial decompensation’, *Am J Ophthalmology*, 136, pp. 769–772.

37. Meltendorf, C., Schroeter, J., Bug, R., et al. (2006) ‘Corneal trephination with the femtosecond laser’, *Cornea*, 25, pp. 1090–1092.

38. Kurtz, R.M., Sarayba, M.A., Juhasz, T. (2003) ‘*Ultrafast Lasers: Technology and Applications*’, Marcel Dekker.

39. Sarayba, M.A., Maguen, E., Salz, J., et al. (2007) ‘Femtosecond laser keratome creation of partial thickness donor corneal buttons for lamellar keratoplasty’, *J Refract Surg*., 23, pp. 58–65.

40. Sarayba, M.A., Juhasz, T., Chuck, R.S., et al. (2005) ‘Femtosecond laser posterior lamellar keratoplasty: a laboratory model’, *Cornea*, 24, pp. 328–333.

41. Soong, H.K., Mian, S., Abbasi, O., et al. (2005) ‘Femtosecond laser-assisted posterior lamellar keratoplasty: initial studies of surgical technique in eye bank eyes’, *Ophthalmology*, 112, pp. 44–49.

42. Sarayba, M.A., Ignacio, T.S., Tran, D.B., et al. (2007) ‘A 60kHz Intralase femtosecond laser creates a smoother LASIK stromal bed surface compared to Zyoptix XP mechanical microkeratome in human donor eyes’, *J Refract Surg*., 23, pp. 331–337.

43. Fine, B.S., Yanoff, M. (1979) ‘*Ocular Histology; A Text and Atlas*’, Harper and Row.

44. Kim, J.-H., Lee, D., Rhee, K.-I. (2008) ‘Flap thickness reproducibility in laser in situ keratomileusis with a femtosecond laser: optical coherence tomography measurement’, *J Cataract Refract Surg*., 34, pp. 132–136.

45. Cheng, Y.Y.Y., Pels, E., Nuijts, R.M.M.A. (2007) ‘Femtosecond-laser-assisted Descemet’s stripping endothelial keratoplasty’, *J Cataract Refract Surg*., 33, pp. 152–155.

46. Mehta, J.S., Por, Y.M., Cajucom-Uy, H., Parthasarathy, A., Tan, D.T. (2007) ‘Femtosecond laser for endothelial keratoplasty’, *J Cataract Refract Surg*., 33, pp. 1141.

47. Tan, C.S., Au Eong, K.-G., Lee, H.-M. (2007) ‘Visual experiences during different stages of LASIK: Zyoptix XP microkeratome v Intralase femtosecond laser’, *Am J Ophthalmology*, 143, pp. 90-96.

48. Flaxel, C.J., Choi, Y.H., Sheety, M., Oeinck, S.C., Lee, J.Y., McDonnell, P.J. (2004) ‘Proposed mechanism for retinal tears alters LASIK: an experimental model’, *Ophthalmology*, 111, pp. 24–27.

49. Chateris, D.G., Cooling, R.J., Lavin, M.J., McLeod, D. (1997) ‘Retinal detachment following excimer laser’, *Br J Ophthalmol*., 81, pp. 759–761.

50. Hu, J., Zeng, J., Huang, L., Qin, B. (2007) ‘Retinal detachment after laser in situ keratomileusis in myopic eyes’, *Am J Ophthalmol*., 144, pp. 921–923.

51. Cameron, B.D., Saffra, N.A., Strominger, M.B. (2001) ’Laser in situ keratomileusis - induced optic neuropathy’, *Ophthalmology*, 108, pp. 660–665.

52. Arevalo, J.F., Mendoza, A.J., Velez-Vazquez, W., et al. (2005) ‘Full-thickness macular hole after LASIK for the correction of myopia’, *Ophthalmology*, 112, pp. 1207–1212.

53. Ruiz-Moreno, J.M., Perez-Santonja, J.J., Alio, J.L. (2001) ‘Choroidal neovascularization in myopic eyes after laser-assisted in situ keratomileusis’, *Retina*, 21, pp. 115–120.

54. Maden, A., Yilmaz, S., Yurdakul, N.S. (2008) ‘Nonarteritic ischemic optic neuropathy after LASIK with femtosecond laser flap creation’, *J Neuro-Ophthalmol*., 28, pp. 242–243.

55. Bushley, D.M., Parmley, V.C., Paglen, P. (2000) ‘Visual field defect associated with laser in situ keratomileusis’, *Am J Ophthalmol*., 129, pp. 668–671.

56. Bissen-Miyajima, H., Suzuki, S., Ohashi, Y., Minami, K. (2005) ‘Experimental observation of intraocular pressure changes during microkeratome globe suction in laser in situ keratomileusis’, *J Cataract Refract Surg*., 31, pp. 590–594.

57. Kasetsuwan, N., Pangilinan, R.T., Moreira, L.L., et al. (2001) ‘Real time intraocular pressure and lamellar corneal flap thickness in keratomileusis’, *Cornea*, 20, pp. 41–44.

58. Hernandez-Verdejo, J., Teus, M.A., Roman, J.M., Bolvar, G. (2007) ‘Porcine model to compare real-time intraocular pressure during LASIK with a mechanical microkeratome and femtosecond laser’, *Invest Ophthalmol Vis Sci*., 48, pp. 68 –72.

59. Jue, B., Maurice, D.M. (1986) ‘The mechanical properties of the rabbit and human cornea’, *J Biomech*., 19, pp. 847–853.

60. Nahen, K., Vogel, A. (2002) ‘Plume dynamics and shielding by the ablation plume during Er:YAG laser ablation’, *J. Biomed. Opt*., 7, pp. 165.

61. Noack, J., Vogel, A., (1998) ‘Single-shot spatially resolved characterization of laser-induced shock waves in water’, *Appl. Opt.*, 37, pp. 4092.

62. Scipioni, L., Stern, L., Notte, J., Sijbrandij, S., Griffin, B. (2008) ‘Helium ion microscope’, *Adv. Mater. Proc.*, 166, pp. 27.

63. Morgan, J., Notte, J., Hill, R., Ward, B. (2006) ‘An introduction to the helium ion microscope’, *Microsc. Today*, 14, pp. 24.

64. Provenzano, P.P., Vanderby, R. Jr. (2006) ‘Collagen fibril morphology and organization: implications for force transmission in ligament and tendon’, *Matrix Biol.*, 25, pp. 71.

65. Durrie, D.S., Kezirian, G.M. (2005) ‘Femtosecond laser versus mechanical keratome flaps in wavefront-guided laser in situ keratomileusis: prospective contralateral eye study’, *J Cataract Refract Surg*., 31, pp. 120–126.

66. Patel, S.V., Maguire, L.J., McLaren, J.W., Hodge, D.O., Bourne, W.M. (2007) ‘Femtosecond laser versus mechanical microkeratome for LASIK; a randomized controlled study’, *Ophthalmology*, 114, pp. 1482–1490.

67. Montes-Mico, R., Rodrıguez-Galietero, A., Alio, J.L. (2007) ‘Femtosecond laser versus mechanical keratome LASIK for myopia’, *Ophthalmology*, 114, pp. 62–68.

68. Lim, T., Yang, S., Kim, M.J., Tchah, H. (2006) ‘Comparison of the IntraLase femtosecond laser and mechanical microkeratome for laser in situ keratomileusis’, *Am J Ophthalmol*, 141, pp. 833–839.

69. Kezirian, G.M., Stonecipher, K.G. (2004) ‘Comparison of the IntraLase femtosecond laser and mechanical keratomes for laser in situ keratomileusis’, *J Cataract Refract Surg*, 30, pp. 804–811.

70. Yao, P., Xu, Y., Zhou, X. (2011) ‘Comparison of the predictability, uniformity and stability of a laser in situ keratomileusis corneal flap created with a VisuMax femtosecond laser or a Moria microkeratome’, *J Int Med Res*, 39, pp. 748–758.

71. Zhou, Y., Tian, L., Wang, N., Dougherty, P.J. (2011) ‘Anterior segment optical coherence tomography measurement of LASIK flaps: femtosecond laser vs microkeratome’, *J Refract Surg*, 27, pp. 408–416.

72. Yuen, L.H., Chan, W.K., Koh, J., Mehta, J.S., Tan, D.T., for the SingLasik Research Group (2010). ‘A 10-year prospective audit of LASIK outcomes for myopia in 37,932 eyes at a single institution in Asia’, *Ophthalmology*, 117, pp. 1236–1244.

73. Blum, M., Kunert, K., Gille, A., Sekundo, W. (2009) ‘LASIK for myopia using the Zeiss VisuMax femtosecond laser and MEL 80 excimer laser’, *J Refract Surg*, 25, pp. 350–356.

74. Stonecipher, K., Ignacio, T.S., Stonecipher, M. (2006) ‘Advances in refractive surgery: microkeratome and femtosecond laser flap creation in relation to safety, efficacy, predictability, and biomechanical stability’, *Curr Opin Ophthalmol*, 17, pp. 368–372.

75. Fares, U., Otri, A.M., Al-Aqaba, M.A., Faraj, L., Dua, H.S. (2012) ‘Wavefront-optimized excimer laser in situ keratomileusis for myopia and myopic astigmatism:

Refractive outcomes and corneal densitometry', *J Cataract Refract Surg*, 38, pp. 2131–2138.

76. Chayet, A., Bains, H.S. (2012) 'Prospective, randomized, double-blind, contralateral eye comparison of myopic LASIK with optimized aspheric or prolate ablations', *J Refract Surg*., 28, pp. 112–119.

77. Montes-Mico, R., Rodrıguez-Galietero, A., Alio, J.L., Cervino, A. (2007) 'Contrast sensitivity after LASIK flap creation with a femtosecond laser and a mechanical microkeratome', *J Refract Surg*., 23, pp. 188–192.

78. Reinstein, D.Z., Carp, G.I., Archer, T.J., Gobbe, M. (2012) 'LASIK for presbyopia correction in emmetropic patients using aspheric ablation profiles and a micro-monovision protocol with the Carl Zeiss Meditec MEL 80 and VisuMax', *J Refract Surg*, 28, pp. 531–539.

79. Chaurasia, S.S., Luengo Gimeno, F, Tan K, Yu S, Tan DT, Beuerman RW, Mehta JS. (2010) 'In vivo real-time intraocular pressure variations during LASIK flap creation', *Invest Ophthalmol Vis Sci*, 51, pp. 4641–4645.

80. Eisenlohr, J.E., Langham, M.E., Maumenee, A.E. (1962) 'Manometric studies of the pressure-volume relationship in living and enucleated eyes of individual human subjects', *Br J Ophthalmol*, 42, pp. 536–548.

81. Stefansson, E., Pedersen, D.B., Jensen, P.K., la Cour, M., Kiilgaard, J.F., Bang, K., Eysteinsson, T. (2005) 'Optic nerve oxygenation', *Prog Retin Eye Res*, 24, pp. 307–332.

82. Pillunat, L.E., Anderson, D.R., Knighton, R.W., Joos, K.M., Feuer, W.J. (1997) 'Autoregulation in human optic nerve head circulation in response to increased ocular pressure', *Exp Eye Res*, 64, pp. 737–744.

83. Riva, C.E., Harino, S., Petrig, B.L., Shonat, R.D. (1992).' Laser Doppler flowmetry in the optic nerve', *Exp Eye Res*, 55, pp. 499–506.

84. Bragheeth, M.A., Dua, H.S. (2005) 'Corneal sensation after myopic and hyperopic LASIK: clinical and confocal microscopic study', *Br J Ophthalmol*., 89(5), pp. 580–585.

85. Nassaralla, B.A., McLeod, S.D., Nassaralla, J.J. Jr. (2003) 'Effect of myopic LASIK on human corneal sensitivity', *Ophthalmology*, 110(3), pp. 497–502.

86. Lee, S.J., Kim, J.K., Seo, K.Y., Kim, E.K., Lee, H.K. (2006) 'Comparison of corneal nerve regeneration and sensitivity between LASIK and laser epithelial keratomileusis (LASEK)', *Am J Ophthalmol*., 141(6), pp. 1009–1015.

87. Patel, S.V., McLaren, J.W., Kittleson, K.M., Bourne, W.M. (2010) 'Subbasal nerve density and corneal sensitivity after laser in situ keratomileusis: femtosecond laser vs mechanical microkeratome', *Arch Ophthalmol*., 128(11), pp. 1413–1419.

88. Ang, R.T., Dartt, D.A., Tsubota, K. (2001) 'Dry eye after refractive surgery', *Curr Opin Ophthalmol*., 12(4), pp. 318–322.

89. Donnenfeld, E.D., Solomon, K., Perry, H.D., et al. (2003) 'The effect of hinge position on corneal sensation and dry eye after LASIK', *Ophthalmology*, 110(5), pp. 1023–1029.

90. Barequet, I.S., Hirsh, A., Levinger, S. (2008) 'Effect of thin femtosecond LASIK flaps on corneal sensitivity and tear function', *J Refract Surg*., 24(9), pp. 897–902.

91. Tanaka, M., Takano, Y., Dogru, M., et al. (2004) 'Effect of preoperative tear function on early functional visual acuity after laser in situ keratomileusis', *J Cataract Refract Surg*., 30(11), pp. 2311–2315.

92. Kalyvianaki, M.I., Katsanevaki, V.J., Kavroulaki, D.S., Kounis, G.A., Detorakis, E.T., Pallikaris, I.G. (2006) 'Comparison of corneal sensitivity and tear function

following Epi-LASIK or laser in situ keratomileusis for myopia', *Am J Ophthalmol*., 142(4), pp. 669–671.

93. Lee, J.B., Ryu, C.H., Kim, J., Kim, E.K., Kim, H.B. (2000) 'Comparison of tear secretion and tear film instability after photorefractive keratectomy and laser in situ keratomileusis', *J Cataract Refract Surg*., 26(9), pp. 1326–1331.
94. Nejima, R., Miyata, K., Tanabe, T., et al. (2005) 'Corneal barrier function, tear film stability, and corneal sensation after photorefractive keratectomy and laser in situ keratomileusis', *Am J Ophthalmol*., 139(1), pp. 64–71.
95. Yu, E.Y., Leung, A., Rao, S., Lam, D.S. (2000) 'Effect of laser in situ keratomileusis on tear stability', *Ophthalmology*, 107(12), pp. 2131–2135.
96. Wilson, S.E. (2001) 'Laser in situ keratomileusis-induced (presumed) neurotrophic epitheliopathy', *Ophthalmology* ,108(6), pp. 1082–1087.
97. Mian, S.I., Shtein, R.M., Nelson, A., Musch, D.C. (2007) 'Effect of hinge position on corneal sensation and dry eye after laser in situ keratomileusis using a femtosecond laser', *J Cataract Refract Surg*., 33(7), pp. 1190–1194.
98. Mian, S.I., Li, A.Y., Dutta, S., Musch, D.C., Shtein, R.M. (2009) 'Dry eyes and corneal sensation after laser in situ keratomileusis with femtosecond laser flap creation Effect of hinge position, hinge angle, and flap thickness', *J Cataract Refract Surg*., 35(12), pp. 2092–2098.
99. Goto, T., Zheng, X., Klyce, S.D., et al. (2004) 'Evaluation of the tear film stability after laser in situ keratomileusis using the tear film stability analysis system', *Am J Ophthalmol*., 137(1), pp. 116–120.
100. Rodriguez-Prats, J.L., Hamdi, I.M., Rodriguez, A.E., Galal, A., Alio, J.L. (2007) 'Effect of suction ring application during LASIK on goblet cell density', *J Refract Surg*., 23(6), pp. 559–562.

101. Linna, T.U., Vesaluoma, M.H., Pérez-Santonja, J.J., Petroll, W.M., Alió, J.L., Tervo, T.M. (2000) 'Effect of myopic LASIK on corneal sensitivity and morphology of subbasal nerves', *Invest Ophthalmol Vis Sci*., 41(2), pp. 393–397.

102. Rodriguez, A.E., Rodriguez-Prats, J.L., Hamdi, I.M., Galal, A., Awadalla, M., Alio, J.L. (2007) 'Comparison of goblet cell density after femtosecond laser and mechanical microkeratome in LASIK', *Invest Ophthalmol Vis Sci*., 48(6), pp. 2570–2575.

103. McGhee, C.N.J., Craig, J.P., Sachdev, N., Weed, K.H., Brown, A.D. (2000) 'Functional, psychological, and satisfaction outcomes of laser in situ keratomileusis for high myopia', *J Cataract Refract Surg*., 26, pp. 497–509.

104. Hammond, S.D. Jr., Puri, A.K., Ambati, B.K. (2004) 'Quality of vision and patient satisfaction after LASIK', *Curr Opin Ophthalmol*, 15, pp. 328–332.

105. Shah, R., Shah, S., Sengupta, S. (2011). 'Results of small incision lenticule extraction: All-in-one femtosecond laser refractive surgery', *J Cataract Refract Surg.,* 37, pp. 127–137.

106. Du, Y., Roh, D.S., Funderburgh, M.L., Mann, M.M., Marra, K.G., Rubin, J.P., Li, X., Funderburgh, J.L. (2010) 'Adipose-derived stem cells differentiate to keratocytes in vitro', *Mol Vis*, 16, pp. 2680-9.

107. Fantes, F.E., Hanna, K.D., Waring, G.O. 3rd., Pouliquen, Y., Thompson, K.P., Savoldelli, M. (1990) 'Wound healing after excimer laser keratomileusis (photorefractive keratectomy) in monkeys', *Arch Ophthalmol*., 108, pp. 665–675.

108. Meltendorf, C., Burbach, G.J., Buhren, J., Bug, R., Ohrloff, C., Deller, T. (2007) 'Corneal femtosecond laser keratotomy results in isolated stromal injury and favorable wound-healing response', *Invest Ophthalmol Vis Sci*., 48, pp. 2068–2075.

109. Netto, M.V., Mohan, R.R., Medeiros, F.W., et al. (2007) 'Femtosecond laser and microkeratome corneal flaps: comparison of stromal wound healing and inflammation', *J Refract Surg*., 23, pp. 667–676.

110. Kunert, K.S., Blum, M., Duncker, G.I., Sietmann, R., Heichel, J. (2011). 'Surface quality of human corneal lenticules after femtosecond laser surgery for myopia comparing different laser parameters', *Graefes Arch Clin Exp Ophthalmol*. 249, pp. 1417–1424.

111. Blum, M., Kunert, K., Schroder, M., Sekundo, W. (2010) 'Femtosecond lenticule extraction for the correction of myopia: preliminary 6-month results', *Graefes Arch Clin Exp Ophthalmol.*, 248, pp. 1019–1027.

112. Hall, R.C., Mohamed, F.K., Htoon, H.M., Tan, D.T., Mehta, J.S. (2011). 'Laser in situ keratomileusis flap measurements: comparison between observers and between spectral-domain and time-domain ante- rior segment optical coherence tomography', *J Cataract Refract Surg.*, 37, pp. 544-551.

113. Srinivasan, S., Drake, A., Herzig, S. (2008). 'Photorefractive keratectomy with 0.02% mitomycin C for treatment of residual refractive errors after LASIK', *J Refract Surg.*, 24, S64-S67.

114. Neira-Zalentein, W., Moilanen, J.A., Tuisku, I.S., Holopainen, J.M., Tervo, T.M. (2008). 'Photorefractive keratectomy retreatment after LASIK', *J Refract Surg*., 24, pp. 710-712.

115. Domniz, Y., Comaish, I.F., Lawless, M.A., Rogers, C.M., Sutton, G.L. (2001) 'Recutting the cornea versus lifting the flap: comparison of two enhancement techniques following laser in situ keratomileusis', *J Refract Surg.*, 17, pp. 505-510.

116 Davis, E.A., Hardten, D.R. , Lindstrom, M., Samuelson, T.W., Lindstrom, R.L. (2002). ' LASIK enhancements: a comparison of lifting to re- cutting the flap', *Ophthalmology*, 109, pp. 2308-2314.

117 Komuro, A., Hodge, D.O., Gores, G.J., Bourne, W.M. (1999) 'Cell death during corneal storage at 4 C', *Invest Ophthalmol Vis Sci*., 40, pp. 2827-32.

118 Halberstadt, M,, Athmann, S., Winter, R., Hagenah, M. (2000) 'Impact of transportation on short-term preserved corneas preserved in Optisol-GS, Likorol, Likorol-DX, and MK-medium', *Cornea,* 19, pp. 788-791.

119 Shimazaki, J., Shinozaki, N., Shimmura, S., Holland, E.J., Tsubota, K. (2004) 'Efficacy and Safety of International Donor Sharing: A Single-Centre, Case-Controlled Study on Corneal Transplantation', *Transplantation*, 78, pp. 216-20.

120 Hunt, C.J. (2011) 'Cryopreservation of Human Stem Cells for Clinical Application: A Review', *Transfus Med Hemother*, 38, pp. 107-23.

121 Baust, J.G., Gao, D., Baust, J.M. (2009) 'Cryopreservation: An emerging paradigm change', *Organogenesis*, 5, pp. 90-6.

122 Oh, J.Y., Kim, M.K., Lee, H.J., Ko, J.H., Wee, W.R., Lee, J.H. (2009) 'Comparative observation of freeze–thaw-induced damage in pig, rabbit, and human corneal stroma', *Vet Ophthalmol*.,12, pp. 50-6.

123 Villalba, R., Peña, J., Luque, E., Villalba, J.M., Gómez-Villagrán, J.L. (2004) 'Keratocyte injury in human corneas cryopreserved under standard conditions', *Cell Tissue Bank*, 5, pp. 201-4.

124 Baust, J.M. (2002) 'Molecular mechanisms of cellular demise associated with cryopreservation failure', *Cell Preserv Technol*., 1, pp. 17-31.

125 Hassell, J.R., Birk, D. (2010) 'The molecular basis of corneal transparency', *Exp Eye Res.,* 91, pp. 326-335.

126 Riau, A.K., Angunawela, R.I., Chaurasia, S.S., Lee, W.S., Tan, D.T., Mehta, J.S. (2011) 'Early corneal wound healing and inflammatory responses following Refractive Lenticule Extraction (ReLEx)', *Invest Ophthalmol Vis Sci*, 52, pp. 6213-21.

127 Loo, D.T. (2011) 'In situ detection of apoptosis by the TUNEL assay: an overview of techniques', *Methods Mol Biol*., 682, pp. 3-13.

128 Kumari, S., Rastogi, R.P., Singh, K.L., Singh, S.P., Sinha, R.P. (2008) 'DNA damage: detection strategies', *Excli Journal*, 7, pp. 44-62.

129 Grasl-Kraupp, B., Ruttkay-Nedecky, B., Koudelka, H., Bukowska, K., Bursch, W., Schulte-Hermann, R. (1995) 'In situ detection of fragmented DNA (TUNEL assay) fails to discriminate among apoptosis, necrosis, and autolytic cell death: a cautionary note' Hepatology', 21, pp. 1465-8.

130 Hewitson, T.D., Bisucci, T., Darby, I.A. (2006) 'Histochemical localization of apoptosis with in situ labeling of fragmented DNA', *Methods Mol Biol*, 326, pp. 227-34.

131 Carlson, E.C., Liu, C.-Y., Chikama, T.-i., Hayashi, Y,. Kao, C.W.-C., Birk, D.E., Funderburgh, J.L., Jester, J.V., Kao, W.W. (2005) 'Keratocan, a cornea-specific keratan sulfate proteoglycan, is regulated by lumican', *J Biol Chem*., 280, pp. 25541-7.

132 Pei, Y., Reins, R.Y., McDermott, A.M. 'Aldehyde dehydrogenase (ALDH) 3A1 expression by the human keratocyte and its repair phenotypes', *Exp Eye Res*, 83, pp. 1063-73.

133 Jester, J.V., Moller-Pedersen, T., Huang, J., Sax, C.M., Kays, W.T., Cavangh, H.D., Petroll, W.M., Piatigorsky, J. (1999) 'The cellular basis of corneal transparency: evidence for 'corneal crystallins', *J Cell Sci*., 112, pp. 613-22.

134 Borderie, V.M., Lopez, M., Lombet, A., Carvajal-Gonzalez, S., Cywiner, C., Laroche, L. (1998) ‘Cryopreservation and culture of human corneal keratocytes’, *Invest Ophthalmol Vis Sci*., 39, pp. 1511-9.

135 Luengo-Gimeno, F., Tan, D.T., Mehta, J.S. (2011) ‘Evolution of deep anterior lamellar keratoplasty (DALK)’, *Ocul Surf* , 9, pp. 98-110.

136 Mohamed-Noriega, K., Toh, K.P., Poh, R., et al. (2011) ‘Cornea lenticule viability and structural integrity after refrective lenticule extraction (ReLEx) and cryopreservation’, *Mol Vis*., 17, pp. 3437–3449.

137 Hayakawa, J., Joyal, E.G., Gildner, J.F., et al. (2010) ‘5% dimethyl sulfoxide (DMSO) and pentastarch improves cryopreservation of cord blood cells over 10% DMSO’, *Transfusion*, 50, 2158–2166.

138 Ivarsen, A., Moller-Pedersen, T. (2005) ‘LASIK induces minimal regrowth and no haze development in rabbit corneas’, Curr Eye Res., 30, pp. 363–373.

139 Kaminski, S.L., Biowski, R., Koyuncu, D., Lukas, J.R., Grabner, G. (2003) ‘Ten year follow-up of epikeratophakia for the correction of high myopia’, *Ophthalmology*, 110, pp. 2147–2152.

140 Vrana, N.E., Elsheikh, A., Builles, N., Damour, O., Hasirci, V. (2007) ‘Effect of human corneal keratocytes and retinal pigment epithelial cells on the mechanical properties of micropatterned collagen films’, *Biomaterials*, 28, pp. 4303–4310.

141 Maier, P., Bohringer, D., Birnbaum, F., Reinhard, T. (2012) ‘Improved wound stability of top-hat profiled femtosecond laser-assisted penetrating keratoplasty in vitro’, *Cornea*, 31**,** pp. 963-966.

142 Kamiya, K., Kobashi, H., Shimizu, K., Igarashi, A. (2014) ‘Clinical Outcomes of Penetrating Keratoplasty Performed with the VisuMax Femtosecond Laser

System and Comparison with Conventional Penetrating Keratoplasty', *PLoS One,* 9**,** pp. e105464.

143 Farid, M., Steinert, R. F., Gaster, R. N., Chamberlain, W., Lin, A. (2009) 'Comparison of penetrating keratoplasty performed with a femtosecond laser zig-zag incision versus conventional blade trephination', *Ophthalmology,* 116**,** pp. 1638-43.

144 Heinzelmann, S., Maier, P., Bohringer, D., Auw-Hadrich, C., Reinhard, T. (2013) 'Visual outcome and histological findings following femtosecond laser-assisted versus microkeratome-assisted DSAEK', *Graefes Arch Clin Exp Ophthalmol.,* 251**,** pp. 1979-1985.

145 Liu, Y.C., Teo, E.P., Adnan, K.B., Yam, G.H., Peh, G.S., Tan, D.T., Mehta, J.S. (2104) 'Endothelial approach ultrathin corneal grafts prepared by femtosecond laser for descemet stripping endothelial keratoplasty', *Invest Ophthalmol Vis Sci.*, 55(12), pp. 8393-8401.

146 Price, F. W., Jr., Price, M. O., Grandin, J. C., Kwon, R (2009) 'Deep anterior lamellar keratoplasty with femtosecond-laser zigzag incisions', *J Cataract Refract Surg.,* 35**,** pp. 804-808.

147 D'Souza, S., Petznick, A., Tong, L., Hall, R.C., Rosman, M., Chan, C., Koh, S.K., Beuerman, R.W., Zhou, L., Mehta, J.S. (2014) 'Comparative analysis of two femtosecond LASIK platforms using iTRAQ quantitative proteomics', *Invest Ophthalmol Vis Sci*., 55(6), pp. 3396-3402.

148 Ivarsen, A., Asp, S., Hjortdal, J. (2014) 'Safety and complications of more than 1500 small-incision lenticule extraction procedures', *Ophthalmology,* 121(4), pp. 822-828.

149 Mohamed-Noriega, K., Riau, A.K., Lwin, N.C., Chaurasia, S.S., Tan, D.T., Mehta, J.S. (2014) 'Early corneal nerve damage and recovery following small incisionlenticule extraction (SMILE) and laser in situ keratomileusis (LASIK)', *Invest Ophthalmol Vis Sci*., 55(3), pp. 1823-1834.

150 Denoyer, A., Landman, E., Trinh, L., Faure, J.F., Auclin, F., Baudouin, C. (2015) 'Dry eye disease after refractive surgery: comparative outcomes of small incision lenticule extraction versus LASIK', *Ophthalmology*, 122(4), pp. 669-76.

151 Yang, E., Roberts, C.J, Mehta, J.S. (2015) 'A Review of corneal biomechanics after LASIK and SMILE and the Current methods of Corneal Biomechanical Analysis', *J of Clinical & Exp Ophthalmology*, 507, pp. doi:10.4172.

152 Riau, A.K., Liu, Y.C., Lim, C.H., Lwin, N.C., Teo, E.P., Yam, G.H., Tan, D.T., Mehta, J.S. (2017) 'Retreatment strategies following Small Incision Lenticule Extraction (SMILE): in vivo tissue responses', *PLoS One*, 12(7), pp. e0180941.

153 Liu, Y.C., Koh, J.C., Rosman, M., Mehta, J.S. (2017) 'Enhancement following small incision lenticule extraction (SMILE): Incidence, risk factors and outcomes', *Ophthalmology*, 124(6), pp. 813-821.

154 Ang, M., Tan, D., Mehta, J.S. (2012) 'Small incision lenticule extraction (SMILE) versus Laser in-situ keratomileusis (LASIK): A randomized, non-inferiority trial', *Trials*, 13, pp. 75-80.

155 Pradhan KR, Reinstein DZ, Carp GI, Archer TJ, Gobbe M, Gurung R. (2013) 'Femtosecond laser-assisted keyhole endokeratophakia: correction of hyperopia by implantation of an allogeneic lenticule obtained by SMILE from a myopic donor', *J Refract Surg*., 29(11), pp. 777-782.

156 Sun, L., Yao, P., Li, M., Shen, Y., Zhao, J., Zhou, X. (2015). 'The Safety and Predictability of Implanting Autologous LenticuleObtained by SMILE for Hyperopia', *J Refract Surgery*, 31(6), pp. 374-379.

157 Jacob S, Kumar DA, Agarwal A, Agarwal A, Aravind R, Saijimol AI. (2017) 'Preliminary Evidence of Successful Near Vision Enhancement With a New Technique: PrEsbyopic Allogenic Refractive Lenticule (PEARL) Corneal Inlay Using a SMILE Lenticule', *J Refract Surg*., 33(4), pp. 224-229.

APPENDIX A

158. Mehta, J.S., Parthasarthy, A., Por, Y.M., Cajucom-Uy, H., Beuerman, R.W., Tan, D.,T. (2008) 'Femtosecond laser-assisted endothelial keratoplasty a laboratory model', *Cornea*, 27(6), pp. 706-712.

My role in this paper was the design and conception of the work. To perform all the experiments on the donor corneas, to perform the histology and the preparation of tissue for SEM. To acquire and analyse and interpret all the data. I also drafted and wrote the paper and critically revised it before submission and after revision before publication.

159. Mehta, J.S., Shilbayeh, R., Por, Y.M., Cajucom-Uy, H., Beuerman, R.W., Tan, D.T. (2008) 'Femtosecond laser creation of donor cornea buttons for descemet's stripping endothelial keratoplasty', *Journal of Cataract & Refractive Surgery,* 34(11), pp. 1970-75.

My role in this paper was the design and conception of the work. To perform the all the experiments on the donor corneas, and to perform the assessment of the ablation. I also acquired, analysed and interpreted all the data. I also critically revised the paper before submission and after revision before publication.

160. Por, Y.M., Cheng, J., Parthasarthy, A., Mehta, J.S., Cajucom-Uy, H., Tan, D.T. (2008) 'Outcomes of femtosecond laser assisted penetrating keratoplasty', *AJO,* 145(5), pp. 772-774.

My role in this paper was the design and conception of the work. To acquire, analyse and interpret all the data, I also drafted and critically revised the paper before submission and after revision before publication.

APPENDIX B

161. Chaurasia, S.S., Gimeno, F.L., Tan, K., Yu, S., Tan, D., Beuerman, R.W., Mehta, J.S. (2010) 'In vivo real-time intraocular pressure variations during LASIK flap creation', *Investigative Ophthalmology and Visual Science*, 51(9), pp. 4641-5.

My role in this paper was the design and conception of the work. To perform all the experiments on the rabbits. To acquire and analyse and interpret all the data. I also critically revised the paper before submission and after revision before publication.

162. Riau, A.K., Poh, R., Pickard, D.S., Park, C.H., Chaurasia, S.S., Mehta, J.S. (2014) 'Nanoscale analysis of human corneal collagen lamellae following femtosecond laser dissection using helium ion microscopy', *J Biomed Nanotech*, 10(8), pp. 1552-62.

My role in this paper was the design and conception of the work. To perform all the experiments on the donor corneas. To analyse and interpret all the data. I also critically revised the paper before submission and after revision before publication.

163. Rosman, M., Hall, R.C., Chan, C., Ang, A., Koh, J., Htoon, H.M., Tan, D., Mehta, J.S. (2013) 'Comparison of efficacy and safety of femtosecond LASIK using two different femtosecond laser platforms in contralateral eyes', *JCRS*, 39(7), pp. 1066-73.

My role in this paper was the design and conception of the work. I performed the majority of cases in the RCT (over 80%). I analysed and interpreted all the data and also critically revised the paper before submission and after revision before publication.

164. Hall, R.C., Rosman, R., Chan, C., Tan, D.T., Mehta, J.S. (2014) 'Patients and surgeons experiences during LASIK using two different femtosecond laser systems', *JCRS*, 40(3), pp. 423-9.

My role in this paper was the design and conception of the work. I performed the majority of cases in the RCT (over 80%). I analysed and interpreted all the data and also critically revised the paper before submission and after revision before publication.

165. Petznick, A., Chew, A., Hall, R.C., Chan, C.M.L., Rosman, M., Tan, D., Tong, L., Mehta, J.S. (2013) 'Comparison of corneal sensitivity, tear function and corneal staining following laser in situ keratomileusis with two femtosecond laser techniques', *Clin Ophthal.*, 7, pp. 591-8.

My role in this paper was the design and conception of the work. I performed the majority of cases in the RCT (over 80%). I analysed and interpreted all the data and also critically revised the paper before submission and after revision before publication.

166. Gimeno, F., Chan, C., Lim, L., Tan, D.T., Mehta, J.S. (2011) 'Comparison of eye tracking success in LASIK after flap creation with two different femtosecond lasers', *JCRS*, 37(3), pp. 538-43.

My role in this paper was the design and conception of the work. I performed the majority of cases in the RCT (over 80%). I analysed and interpreted all the data and also critically revised the paper before submission and after revision before publication.

APPENDIX C

167. Riau, A.K., Angunawela, R.I., Chaurasia, S., Tan, D.T., Mehta, J.S. (2012) 'Effect of differential femtosecond laser firing patterns on collagen disruption during refractive lenticule extraction (ReLEx) procedure', *JCRS*, 38(8), pp. 1467-75.

My role in this paper was the design and conception of the work. To perform all the experiments on the animals of the differential firing pattern. To assist in the follow up

of the animals in the form of in vivo confocal microscopy. I assisted in the tissue sectioning and the immunofluorescence. I acquired and analysed and interpreted all the data. I also critically revised the paper before submission and after revision before publication.

168. Riau, A.K., Angunawela, R.I., Chaurasia, S.S., Lee, W.S., Tan, D.T., Mehta, J.S. (2011) 'Early corneal wound healing and inflammatory responses following refractive lenticule extraction (ReLEx)', *Investigative Ophthalmology and Visual Science*, 52(9), pp. 6213-21.

My role in this paper was the design and conception of the work. To perform all the experiments on the animals, both LASIK and ReLEx. To assist in the follow up of the animals in the form of Slit lamp photography, optical coherence tomography, corneal topography and in vivo confocal microscopy. I assisted in the tissue sectioning and the immunofluorescence. I acquired and analysed and interpreted all the data. I also critically revised the paper before submission and after revision before publication.

169. Ang, M., Chaurasia, S.S., Angunawela, R.I., Poh, R., Riau, A., Tan, D., Mehta, J.S. (2012) 'Femtosecond lenticule extraction (FLEx): Clinical results, interface evaluation and intraocular pressure variation', *IOVS*, 53(3), pp. 1414-21.

My role in this paper was the design and conception of the work. To perform the surgery on the patients in the clinical study. To perform procedures on the human cadaver eyes. To prepare the tissue for SEM. To perform the surgical procedures on the animals. To assist in the follow up of the patients. I acquired and analysed and interpreted all the data. I also critically revised the paper before submission and after revision before publication.

170. Riau, A.K., Ang, H.P., Lwin, N.C., Chaurasia, S.C., Tan, D.T., Mehta, J.S. (2013) 'Comparison of four different sets of circle patterns for flap creation after small incision lenticule extraction', *JRS*, 29(4), pp. 236-44.

My role in this paper was the design and conception of the work. To perform all the SMILE surgery on all the animals. I then performed all the circle surgey on all the animals. I did all the grading of the flap lifts. I assisted in the follow up of the animals in the form of optical coherence tomography and in vivo confocal microscopy. I acquired and analysed and interpreted all the data. I also critically revised the paper before submission and after revision before publication.

171. Noriega, K., Toh, K.P., Poh, R., Balehosur, D., Riau, A., Htoon, H., Peh, G.S., Chaurasia, S., Tan, D., Mehta, J.S. (2011) 'Cornea lenticule viability and structural integrity after refractive lenticule extraction (ReLEx) and cryopreservation', *Mol Vision*, 17, pp. 3437-49.

My role in this paper was the design and conception of the work. I performed all the ReLEx surgery on the donor corneas that provided the lenticules for the study. I acquired and analysed and interpreted all the data. I also critically revised the paper before submission and after revision before publication.

172. Angunawela, R.I., Riau, A.K., Chaurasia, S.S., Tan, D.T., Mehta, J.S. (2012) 'Refractive lenticule storage and re-implantation after myopic refractive lenticule extraction (ReLEx): a feasibility study of stromal restoration after refractive surgery in a rabbit model', *IOVS*, 53(8), pp. 4975-85.

My role in this paper was the design and conception of the work. To perform all the surgery on all the animals. I then performed all the lenticule re-implantation. I assisted in the follow up of the animals in the form of optical coherence tomography, in vivo

confocal microscopy and ASOCT. I assisted in the tissue sectioning and the immunofluorescence. I acquired and analysed and interpreted all the data. I also critically revised the paper before submission and after revision before publication.

173. Riau, A.K., Angunawela, R.I., Chaurasia, S.S., Lee, W.S., Tan, D.T., Mehta, J.S. (2013) 'Reversible femtosecond laser-assisted myopia correction: A non-human primate study of lenticule re-implantation after refractive lenticule extraction', *PLoS ONE*, 8(6), pp. e67058.

My role in this paper was the design and conception of the work. To perform all the surgery on all the animals. I then performed all the lenticule re-implantation. I assisted in the follow up of the animals in the form of optical coherence tomography, in vivo confocal microscopy and ASOCT. I assisted in the tissue sectioning and the immunofluorescence. I acquired and analysed and interpreted all the data. I also critically revised the paper before submission and after revision before publication.